UNIVERSITY OF NOTTINGHAM

DEPARTMENT OF CIVIL ENGINEERING

THE PREDICTION OF PERMANENT DEFORMATION IN FLEXIBLE PAVEMENTS

by

C. A. BELL B.Sc.

Thesis submitted to the University of Nottingham for the degree of Doctor of Philosophy

September 1978

C O N T E N T S

A B S T R A C T

At the present time (1978) new roads in the United Kingdom are designed empirically. However, over approximately the last twenty years pavement technologists throughout the world have been advocating fundamentally based procedures. Such procedures, when applied to flexible pavements, require a detailed knowledge of the two main modes of failure, fatigue of the bituminous bound layers and excessive permanent deformation of the pavement as a whole.

The research described herein was aimed at improving knowledge of the permanent deformation behaviour of flexible pavements, and at developing a technique for predicting this deformation which could be incorporated in a fundamental design procedure. Three laboratory experimental pavements were trafficked with a rolling wheel facility under conditions of constant temperature, load and speed, and the resulting deformations were monitored. These deformations were compared with predictions using models developed from the results of repeated load characterisation tests on the pavement materials and utilising a digital computer.

A review of previous work is presented in two parts, the first considering the resilient and permanent deformation response of pavement materials, the second considering proposals for the predic-:tion of permanent deformation in pavements.

The development of the wheel loading facility, and the construction, instrumentation and measurements from the pavements are described briefly. More attention is given to the theoretical

approach, materials characterisation testing and the prediction of resilient and permanent deformation response of the pavements.

The prediction techniques and their accuracy are assessed, the problems involved in the development of such procedures are discussed, and the conclusions which can be drawn from the work are presented. A number of suggestions regarding further work in this field are made.

Finally, an Appendix considers an alternative to the method of modelling permanent deformation presented in the main part of the text.

ACKNOWLEDGEMENTS

The author wishes to express his thanks to all those who assisted in this research programme and in the preparation of this thesis, including:

Professor R.C. Coates, Head of Department, for providing all the facilities of the Department.

Dr. S.F. Brown for his expert supervision.

Professor P.S. Pell for his interest and advice.

Mr. B.V. Brodrick, who developed the wheel loading facility and carried out the pavement tests and was always willing to help with other aspects of the work.

Messrs. A. Leyko, D. Lockyer, W. Robinson and G. Stokes who provided technical assistance.

Miss R. Allen who prepared a large number of the diagrams for this thesis.

Miss J.L. Clerbaut for her secretarial skills throughout the period of the research at Nottingham University.

Tarmac Roadstone Holdings Ltd. who supplied and laid the bituminous material.

Professor R.W. Kirwan, Trinity College, Dublin for making the DEFPAV computer program available, and Drs. M.S. Snaith and T.E. Glynn for advice on its use.

and to all other members of staff in the Department and in the Faculty Workshop who have willingly given advice and assistance.

The financial support for the research was provided by the European Research Office of the United States Army, and is gratefully acknowledged.

Finally, special thanks to Mrs. Isobel Gordon for her expert typing of this thesis, and endless patience when I frequently changed my mind over minor details. And, to my wife who alone has withstood my temper and changing moods during the inevitable difficult patches.

CHAPTER ONE

INTRODUCTION

At the time of the cuts in public expenditure by the British Government in December, 1976, the Secretary of State for Transport addressed the Institution of Highway Engineers. He said:

"All of us here are aware of firm evidence of the industrial value of roads. We have the results of the detailed cost benefit work which is carried out for all trunk road investment. Over half the benefits identified for the average scheme are savings in working time. If a road is improved, the lorry driver can make one more delivery, the salesman one more call, raw materials and components can arrive at the factory on time. All these are as potentially worthwhile as any direct industrial investment designed to speed up output. In this sense, road building is a vital part of total industrial investment. It is not simply icing on the cake."

Unfortunately, his views were not reflected in the 1977/78 Public Expenditure White Paper, which contains figures for the actual expenditure for the last five years, and planned expenditure for the next four years (1). Roads and Transport made up 5.4 per cent of public expenditure in 1975/76 (£2,811 million), but this will fall to 4.7 per cent in 1977/78 (£2,368 million) while total public expenditure rises. During this period, the actual expenditure on road construct-:ion and maintenance will have fallen from 74 per cent of the total to 47 per cent, while subsidies for transport will have risen from 8 per cent to 31 per cent.

Clearly expenditure on roads has suffered heavily in these times

of economic hardship. Significantly, during the seventies, the vast increase in the price of oil has meant a consequent rise in the cost of bitumen (more than threefold between 1973 and 1976). As a result motorway construction in 1976 was at the same level, in terms of miles, as in the mid sixties, and has followed an almost steady decline since a boom year in 1970. Meanwhile, planned construction has remained at virtually the same level (2).

The facts outlined above clearly indicate the highly significant role that economics play in road construction and maintenance. Highway engineers have a responsibility to develop and adopt rigorous and economic design procedures, so that the optimum use may be made of both material and financial resources. Even small improvements in design can produce vast savings in construction costs.

At the present time (1978) new roads in the United Kingdom are designed according to Road Note No. 29 (3), and the materials to be used are selected from the "Specification for Road and Bridge Works" (4). This procedure is typical of the "subgrade protection" methods of design which have developed from the California Bearing Ratio (CBR) method, which was instituted in California in 1938. These methods attempt to provide an adequate thickness of pavement material to protect the subgrade from excessive stress that might lead to shearing, or excessive permanent deformation of the subgrade. They are based largely on experience, which, in the case of Road Note No. 29, was provided by the Transport and Road Research Laboratory full scale experiments such as those at Alconbury Hill (5).

The limitation of the CBR method, and other empirically based methods, is that they cannot be applied to situations outside current experience. Such situations are changes in subgrade conditions, environment, loading and new materials. Only a design system based

on theory is capable of application outside current experience, and able to predict behaviour of a pavement under conditions which have not existed before. To this end a research effort, spanning more than two decades, has been proceeding, mainly in America and Europe, but also other areas, resulting in a wealth of ideas and co-operation (6, 7, 8, 9). Consequently, analytical or structural design approaches have evolved (10, 11, 9), although they are not yet adopted in the United Kingdom.

An analytical or structural design approach to pavement design is similar in concept to the traditional engineering approach to design of other structures. The pavement is proportioned so that the stresses, strains and displacements produced by critical loading conditions are within permissible limits for the material in the various layers. Such permissible levels need to be established by laboratory testing of the materials, and in-situ measurements. The primary aim of the approach is to ensure that the riding quality of the pavement remains acceptable throughout the design life, with the most economic use of materials.

Experience in various countries has indicated that there are three principal distress mechanisms which appear to be most significant in contributing to a loss in riding quality of pavements. These are permanent deformation, load induced cracking and thermal cracking. In the United Kingdom, permanent deformation is generally accepted as being the major contributor to loss in riding quality, with a potential for occasional load associated (fatigue) cracking, but thermal cracking is a low temperature phenomenon generally not experienced. Thus, any pavement design approach should be aimed at limiting the potential for permanent deformation and fatigue to acceptable limits, so that riding quality will remain acceptable.

Due to the fact that the bulk of pavement research has been

carried out in the U.S.A., where the cracking problem is of major importance, the state of knowedge at present is such that the cracking problem is better understood than that of deformation.

Fatigue cracking can be found only in the bituminous layers of a pavement and by definition is caused by repeated loading of the pavement. The criterion for cracking is tensile strain (12), the maximum value of this parameter generally occurring at the bottom of the bituminous layer. The allowable value for this criterion is determined from the fatigue curve relating tensile strain to service life of the material.

Permanent deformation can occur in all layers of a pavement as a result of traffic loading, in association with environmental factors. For bituminous materials, permanent deformation depends largely on temperature, and to a lesser extent on stress level and loading time. Granular materials and clays are also sensitive to stress and to moisture conditions. Lister (13) has outlined some aspects of permanent deformation in British roads, utilising inform-:ation from full scale experiments, and in-situ measurements from in service roads. He emphasises the complexity of the variation of conditions to which a road is subject and the difficulty of relating these transient conditions to observed long term behaviour. He concluded that the maximum rate of deformation in the whole pave-:ment occurs in the late spring, when the onset of high temperatures coincides with a high water table.

It should also be noted that permanent deformation can be caused by swell or shrinkage of a subgrade soil, by consolidation settlement of a compressible material, or by heave of a frost susceptible material. These forms of deformation can be avoided by careful construction technique and selection of materials.

Load associated permanent deformation accruing in the various layers of a pavement results in the formation of ruts at the pave-:ment surface, corresponding to the wheel tracks in each traffic lane. On motorways, the inside wheel track of the inside traffic lane, where the heaviest and slowest vehicles are most numerous, shows most susceptibility to deformation. This occurs since drivers tend to keep to an almost constant distance from the kerbside, whereas the width of vehicles varies, thus a greater density of loads occurs at a particular point in the inside track. The effect of this phenomenon, rutting, is often exaggerated because of the tendency to neglect this area somewhat when compacting during construction (14).

Excessive rutting affects riding quality of a pavement by inducing drivers to follow the path of the rut and attempts to leave the path may cause difficulties with steering. Perhaps more import-:antly, in wet conditions, water in the ruts can cause aquaplaning and also presents a serious spray hazard. Should ice be formed the possibility of skidding also occurs. Additionally, large deformations can result in cracking of the pavement which will eventually lead to the breaking up of the surface.

It is virtually impossible to prevent deformation occurring, but it is clearly necessary to limit rut depth to a safe and acceptable level. British practice defines a critical level as a 10mm rut depth measured below a 1.8m straight edge, with failure as 20mm (15). The former condition can be remedied by an overlay, whereas failure would require reconstruction. As an example of the difference in cost, it was estimated by Derbyshire County Council in 1976 (16), that the cost of overlaying a 1km strip of road would be £2,540 whereas reconstruction would cost £7,950. Obviously, it is essential that a road should be designed to limit permanent deformation to an acceptable level for as long as possible, but, once a critical level is reached, resurfacing

is essential to prevent great expense should failure be reached.

The above discussion highlights the need for an economic design procedure, capable of limiting both fatigue cracking and deformation to acceptable levels for as long as possible. At the present time, there is sufficient information available to provide a "fatigue sub-system", but a "permanent deformation sub-system" is still in the development stage.

The work described in this thesis has been aimed at improving knowledge of the permanent deformation behaviour of flexible pave-:ments, and at developing a prediction technique which can be incorporated in a sub-system. The philosophy adopted was that deformation should be measured in laboratory pavements which would be trafficked by a rolling wheel facility under conditions of constant temperature, load and speed. The measured deformations would be compared with predictions based on the characterisation of the pavement materials by well established repeated load triaxial testing techniques, combined with theoretical models to be developed utilising a digital computer. If agreement could be achieved between measurements and predictions, under these controlled conditions, then perhaps the prediction of deformation under more transient in-situ conditions would be possible.

The construction, instrumentation and trafficking of the pavements, and the development of the rolling wheel facility were in the main carried out by a colleague (17, 18). However, a description of these aspects is included in this thesis to provide essential background to the characterisation tests and subsequent development of the predict-:ion techniques.

The general approach adopted for the prediction of permanent deformation was that suggested by Romain (19) and Barksdale (20). They suggested that a suitable linear or non-linear elastic analysis

be carried out to determine the stress distribution in a pavement. The vertical permanent strain at various locations within the structure should then be determined from characterisation tests, and surface permanent deformation evaluated by integration with depth. This approach separates the calculation of elastic strains from that of permanent strains, which is justified by the fact that under a single application of load, the latter will generally be much smaller than the former.

Previous research workers who have adopted this approach have tended to concentrate on the stress and strain distributions with depth on the axis of symmetry of the wheel load in order to calculate the maximum permanent deformation or rut depth. The approach to predicting permanent deformation described herein, has been aimed at predicting permanent strain at any point in the pave-:ment relative to the position of the wheel load , and, it will be shown that for certain locations, the maximum permanent strain was found to occur at a position away from the axis of symmetry.

A major problem in prediction of permanent deformation, part-:icularly in the bituminous layers, is the availability of results from characterisation tests covering the whole range of possible stress conditions. Characterisation tests using a repeated load triaxial machine can only produce directly the stress conditions occurring on the axis of symmetry of the load where the principal stresses are vertical and horizontal and the horizontal stresses are equal and compressive. Off the load axis, two of the principal stresses are inclined, all three principal stresses are different, and even if their vertical and horizontal components can be approx-:imated, the resulting shear stresses have to be ignored. Tensile stresses exist in the lower part of the bituminous layer and these cannot be reproduced directly in the triaxial cell.

An approach suggested by Brown (21) was utilised, in the prediction procedure described herein, which considers the principal stresses in the pavement. The stress invariants at all positions in a pavement were calculated from the principal stresses, and it was found possible to reproduce a much wider range of stress conditions by reproducing these invariants in the triaxial cell. Measurement of deformations on the test specimens enabled corresponding strain invariants to be calculated which could then be used to predict vertical deformations.

A total of three pavements were tested, which were all full depth constructions with a layer of dense bitumen macadam (DBM) laid directly on a silty clay subgrade of Keuper marl. The DBM and clay used in all pavements were nominally the same. The approach to prediction of permanent deformation could be extended to pavements with more than two layers providing adequate characterisation tests were carried out. The characterisation tests should include both measurements of permanent strains and resilient strains, so that the resilient properties of the materials can be determined and used as input for the elastic analysis of the pavement, an approach which was adopted here. In the case of the pavement experiments, in addition to measurements of permanent strains, stresses and resilient strains were measured in order that the validity of the elastic analyses could be checked.

CHAPTER TWO

REVIEW OF PREVIOUS WORK - STRESS-STRAIN BEHAVIOUR OF FLEXIBLE PAVEMENT MATERIALS

2.1 INTRODUCTION

The previous Chapter outlined the general approach adopted herein for the prediction of permanent deformation (19, 20), which consists of analysing the pavement by linear or non-linear elastic theory, to determine the stress distribution, and then determination of the vertical permanent strain, at suitable locations, from characterisation tests. Analysis of the pavement requires the resilient properties of the pave-:ment materials, and determination of permanent deformation requires the permanent strain characteristics. This Chapter will review relevant research which has investigated both of these aspects using repeated load triaxial testing.

An alternative test to the repeated load triaxial test is the simple uniaxial creep test. The most important research using this test has been in conjunction with prediction procedures, hence, the review of research with this type of test is included in the next Chapter.

2.2 REPEATED LOAD TESTING OF BITUMINOUS MATERIALS

Repeated load triaxial tests were carried out by Snaith (22) on a dense bitumen macadam (DBM). Experimental details, and a description of the equipment, have been summarized by Brown and Snaith (23). This work was intended to provide general information on the deformation characteristics of the material which could be broadly applied to similar materials. The effect of six variables was investigated: vertical stress, confining stress, temperature, frequency of the vertical stress pulse, rest periods and binder content.

Snaith found that at vertical stress pulse frequencies above 1 Hz,

i.e. corresponding to in-situ speeds greater than 1 kph, the rate of permanent strain was time dependent, and that the effect of rest periods was negligible. However, both these variables do affect the stiffness of the material, which is time dependent. Thus, for a mix with a particular binder content, the effects of the other three variables on the permanent strain behaviour of the material were determined by three sets of tests. The results are summarized in Figures 2.1 and 2.2.

It can be seen that, generally, the relationships in the log log plots of Figures 2.1 and 2.2 are straight lines; these were represented by equations of the form:

$$\log \varepsilon_{vp} = a + b \log_{10} t \qquad (2.1)$$

where, ε_{vp} is the permanent vertical strain, "a" is the intercept of the straight line produced with the ε_{vp} axis, "b" is the slope of the line, and "t" is the elapsed time. It was found possible to produce two equations such that "a" and "b" were predicted for any values of vertical stress, confining stress, and temperature within the experimental range, and thus, a value for the vertical permanent strain was derived. Snaith applied this method to predicting the permanent deformation of a bituminous layer in a pavement, based on a linear elastic analysis.

However, since his test conditions were not specifically related to in-situ stress, their range of applicability was small, and they could only be applied safely to situations on the centre-line of the load and where the in-situ confining stress was compressive and in the range 0 to 200 kN/m^2. Therefore, this method could predict only the permanent strain in the compressive zone of the bituminous layer.

Kirwan and Snaith (24) updated the representation of Snaith's (22) results to a single equation where the induced permanent strain (ε_{vp}) is proportional to a power of the induced stress:

$$\varepsilon_p(\%) = \{0.00015 \left[(0.68 + 0.0008T^2) \log_{10} N\right]^{1.9\nabla}\}^{1.75} \qquad (2.2)$$

where, N is the elapsed time, T is the temperature, and ∇ is a function

of the stress conditions. The equation can be used to give an approx-:imate value of permanent strain when the confining stresses are tensile, i.e. where the stress conditions are different to those from which the equation was developed.

The following conclusions were drawn from Snaith's (22) repeated loading tests, with respect to the permanent strain behaviour of DBM:

1. An increase in temperature caused a significant increase in strain.
2. An increase in vertical stress caused an increase in strain.
3. An increase in confining stress caused a decrease in strain.
4. The level of constant confining stress which gave the same strain as the dynamic confining stress was approximately equal to the mean level of that stress.
5. Realistic changes in the relative lengths of vertical and confining stress pulses did not affect the strain.
6. The rate of strain was time dependent at frequencies above 1 Hz.
7. Rest periods between vertical stress pulses had negligible effects on strain.
8. An optimum binder content existed for maximum resistance to strain, depending on the temperature.

The following conclusions were drawn from Snaith's results with respect to the resilient behaviour of the DBM:

1. The resilient modulus was linearly elastic within the range of vertical stress, when unconfined at $20^{o}C$.
2. The resilient modulus decreased with an increase in the temperature of the material.
3. The resilient modulus increased with an increase in the frequency of the dynamic vertical stress.
4. The resilient modulus increased slightly with an increase in confining pressure.
5. Poisson's ratio was decreased by an increase in the confining pressure

and increased by an increase in the temperature of the material.

6. Poisson's ration was little affected by the magnitude of the dynamic stress level, the frequency, or the binder content of the material.

Most of these conclusions are typical of a visco-elastic material and have been substantiated by other researchers. However, conclusion 4, with respect to the permanent strain could considerably simplify experimentation, and also conclusion 7, since the inclusion of rest periods considerably lengthens testing. These have not been substant-:iated by other researchers. The information on the resilient behav-:iour of the material is extremely useful, particularly with respect to the Poisson's ratio where information is scarce. However, the range of stresses employed in the testing was not comprehensive, since only vertical stresses of 150, 400, 650 and 900 kN/m^2 were investigated. In-situ stress conditions usually involve higher confining stresses, which may be tensile, and all three principal stresses may be different. Snaith's results can only be applied with confidence to conditions where two of the principal stresses are equal and all three are compressive, i.e. on the centre line of the loaded area.

Snaith's (22) method of predicting permanent deformation in the bituminous layers was limited because it could not deal with situations where the lateral and longitudinal in-situ stresses are tensile. This zone was dealt with in a preliminary way by Morris et al (25) and by McLean and Monismith (26) by applying a tensile axial stress in the triaxial test. The test conditions used were selected from the in-situ principal stresses occurring below the centre line of the loaded area in typical pavements.

Morris et al carried out two series of repeated load tests on labor-:atory manufactured speciments of asphaltic concrete similar to that occur-:ring in the Brampton test road (27). These were compression tests and tension tests, both utilising cyclic confining stress combined with cyclic

axial compressive and tensile stresses respectively. Both vertical and lateral permanent deformations were measured, the former being of interest for the compressive zone, and the latter for the tensile zone. To predict permanent deformation in the Brampton test road, the asphaltic layer was divided into a number of sub-layers, and the pavement analysed by a finite element technique assuming non-linear elastic behaviour for the asphaltic concrete. Good agreement between predictions and measure-:ments was obtained, with the majority of the deformation occurring in the tensile zone.

McLean and Monismith(26) also tested an asphaltic concrete in repeated loading. Three types of tests were used: triaxial extension (cycling lateral stress only), confined compression (cycling vertical stress only), and triaxial tension (cycling vertical stress in tension and lateral stress in compression). Their prediction technique utilised a linear elastic approach based on layer theory. They analysed a pavement structure similar to that tested by Hofstra and Klomp (28), with 200mm of asphaltic concrete and a sand subgrade. Allowing for the difference in their bituminous mixes, good agreement was obtained. The results of their elastic analysis and the prediction of permanent strain are shown in Figure 2.3, showing that the elastic strain versus depth relationships is similar in form to that for permanent strain. Both Heukelom and Klomp (29) and Brown (30) had prev-:iously suggested that the elastic strain might be a significant parameter.

Figure 2.3 also shows that the maximum permanent strain predicted by McLean and Monismith occurs in the upper part of the asphaltic layer in contrast to the findings of Morris et al. Brown and Bell (31) have shown that this difference can be explained due to the differences in the resilient properties of the structure. It seems likely that distributions such as that obtained by Morris et al are typical when an asphaltic layer is relat-:ively stiff in comparison to the underlying layers, and those such as obtained by McLean and Monismith are more typical where the asphaltic layer is relatively soft.

Similar conclusions about permanent strain distributions were

drawn by Aussedat and Azibert (32) using the approach to prediction of permanent deformation developed by the Esso laboratories in France. They carried out predictions for two overlays of identical thickness but of different materials, grave-bitume and asphaltic concrete. Figure 2.4 shows the stress distribution with depth for each overlay, the stiffer grave-bitume showing horizontal tensile stresses at the bottom, whereas the less stiff asphaltic concrete shows a completely compressive distribution. The resulting strain rate versus depth predictions have remarkable similarities to those obtained by Morris et al and McLean respectively.

Aussedat and Azibert also demonstrated the effect, on the predicted permanent strain rate, of increasing the depth of each overlay. With the grave-bitume, a depth of overlay existed which produced a maximum strain rate, a greater or lesser depth producing lower strain rates. This was attributed to the form of the stress distribution in that material, which became markedly less severe at the bottom of the layer where the strain rate was highest, as the depth increased. However, with the asphaltic concrete the strain rate increased almost linearly with an increase in thickness, and, although no explanation was provided, this was probably due to the fact that the stress distribution produces the maximum strain rate at the top of that layer.

Hofstra and Klomp (28) measured the deformation occurring in four pavements with asphaltic concrete layers of 5, 10, 14.2 and 20 cm. thickness on a sand sub-grade of 18% CBR. They found little difference in the measurements of total deformation, which occurred entirely in the asphaltic concrete except when that layer was 5 cm. thick. They concluded that the deformation was independent of layer thickness, a conclusion supported by McLean and Monismith.

In discussing their own predictions of rut depth for two pave-:ments of different thickness, Morris et al noted that the consider-

:able decrease with the thicker pavement was in agreement with a postulation advanced by Klomp and Dorman (33) some years ago. They suggested that strains occurring above some "elastic limit" were plastic (non-recoverable), therefore increasing the thickness to a point where the strains were below this limit would reduce permanent strains to negligible proportions. In the light of the more recent work described above such a general statement seems incorrect.

The Esso approach is also interesting because it utilises the Mohr's circle representation of stress for various locations within the pavement on the axis of symmetry of the wheel. When superimposed on iso-creep lines, which are developed from laboratory characterisation tests, these give the permanent strain rate at each location. Only compression tests were conducted for the characterisation, therefore, extrapolation is required when considering locations in the tension zone.

2.3 REPEATED LOAD TESTING OF FINE GRAINED SOILS

The repeated load behaviour of cohesive soils was first studied, with respect to pavement design, by Seed et al (34). This study, and subsequent ones, by Professor Seed and his associates at the University of California (35, 36, 37) showed that deformation characteristics determined by normally accepted tests are not necessarily indicative of soil deformation under repeated loading conditions. Their early work (34) indicated that the resilient modulus was stress dependent increasing with increasing deviator stress, and was considerably greater than the static modulus. However, their later work (37) showed that the resilient modulus decreased with increasing deviator stress, which is the usual finding of subsequent researchers.

Seed et al (34) found that the repeated stress required to reach a given permanent strain was lower than the static stress required. Later work (38, 39) found that when a confining pressure was cycled in

phase with the deviator stress, the permanent strain accruing was greater than when a constant confining pressure was used. Seed and Chan (35) examined the effects of loading history on the permanent strain behaviour. They found that by applying a series of 10,000 small conditioning stress pulses to specimens, then applying a larger repeated stress, the permanent strain was reduced compared with applying only a few conditioning stress pulses. It was claimed that this was due to a structural rearrangement of the particles.

Recent work at the University of California by Monismith et al (40) was directed at the permanent deformation characteristics of sub-grade soils, due to repeated loading with respect to the effect of compaction, stress magnitude and stress sequence. A silty clay was tested at dry densities from 90 to 95 per cent of the maximum obtained in the modified AASHO compaction tests, and at moisture contents from 16 to 20 per cent. Static compaction was used because it was thought to induce particle orientations, at high degrees of saturation, similar to those obtained under field conditions, by compacting the specimen on the dry side of optimum and subsequently soaking it (36). They found that the rate of strain increased with increasing deviator stress. The results also showed that specimens compacted near the maximum dry density tended to deform less. The stress history investigations confirmed the earlier findings of Seed and Chan (35). Logarithmic plots of the permanent axial strain versus the number of stress applications were found to approximate to straight lines, and it was also found that the permanent strain, after a part-:icular number of applications could be related to the applied stress by a hyperbolic relationship.

These two findings were similar to those of Snaith (22) for DBM, and Barksdale (20) for granular materials, respectively, and were used to develop constitutive relationships for the permanent strain

behaviour of the material.

Monismith et al (40) also outlined two alternative cumulative procedures to deal with the application of stresses of different magnitudes in different sequences, such as would occur in the field. These were the time hardening and strain hardening procedures. The former was utilised in the development of the prediction technique described herein and both procedures will be explained in a later Chapter.

Most of the work outlined above was with compacted, and hence partially saturated, silty clay, a situation relevant to California with which Seed was primarily concerned. However, in the United Kingdom subgrades occurring in "cut" are likely to be saturated, and, in addition, most naturally occurring fine grained soils are overconsolidated to various degrees (42). With this in mind, and also so that results could be assessed in terms of effective stress, research on a reconstituted saturated silty clay (Keuper Marl) was carried out at the University of Nottingham.

Lashine (43) carried out work on a normally consolidated material under undrained conditions with pore pressure measurements. He related the behaviour of the material under dynamic conditions to its behaviour under single loading by a stress ratio, D, as follows:

$$D = \frac{\text{maximum cyclic shear stress}}{\text{undrained shear strength}}$$

It was found that there was a critical range of cyclic shear stress between 75 and 80 per cent of the undrained shear strength. Applied stresses below this range did not cause failure; stresses above it did, and within the range there was a 50 per cent chance of failure. Failure was defined as the point where the rate of deformation started to increase.

Lashine's results for permanent strain measurements are shown in Figure 2.5a for a range of stress ratios, and the three phases defined

above may be seen. When these results were replotted on a logarithmic scale it was found that the logarithm of the permanent strain was approx-:imately proportional to the logarithm of the number of cycles, for the duration of the test. Lashine also found that, for all stress ratios, the logarithm of the strain rate was proportional to the logarithm of the number of cycles before failure occurred, or, for sub-failure stresses, for a substantial part of the test.

The critical range of stress ratio of 75 - 80 per cent found by Lashine was, in effect, a threshold stress. Glynn and Kirwan (44) had postulated the existence of both a lower yield stress (threshold stress) below which no plastic deformation develops, and an upper yield or critical stress above which failure rapidly occurs.

In his analysis of resilient strains, Lashine also confirmed the stress softening effect noted by Seed et al (36), based on the deviator stress amplitudes. However, he also found that a stiffening effect resulted with increasing the mean level of the deviator stress.

Further work on an overconsolidated reconstituted clay was carried out by Hyde (45). Some of the important aspects of the work on the repeated load behaviour were reported by Brown et al (42). Although few failures occurred, it appeared that failure in repeated loading occurred at lower stress levels than in the single load tests. Under comparable stress conditions the resulting permanent strains from repeated load tests were greater than in the single load tests. This could be compared with the findings of Seed et al (34), for a compacted material, that the repeated stress required to reach a certain level of permanent strain was lower than the static stress. Generally, permanent strain tended to build up at a significant rate throughout the tests, up to the maximum number of 10^6 cycles applied. In contrast, for the normally consolidated material, failure was more easily defined. However, when deviator stress and pore pressures were the same for both types of tests, the resulting permanent strains were similar. In both types of

test, pore pressures levelled out after approximately 10^4 seconds, larger values (both positive and negative) being found in the repeated load tests with comparable shear stress conditions.

Hyde found that the resilient modulus decreased during tests, the effect being less marked as the over-consolidation ratio increased. The value was uniform after 10^5 cycles (at 10 Hz) and was shown to be a function of the ratio of cyclic deviator stress (q_r) to initial effective confining stress (σ_3') after that number of cycles. The resilient modulus was non-linear, of the stress softening type, being particularly sensitive at values of (q_r/σ_3') less than 1.5. The relationship was hyperbolic, similar to those of Monismith et al (40) and Barksdale (20), of the form:

$$E_r = K/(q_r/\sigma_3')^n \qquad (2.3)$$

Hyde found that, for sub-failure stresses, the logarithm of the permanent strain rate was directly proportional to the logarithm of the elapsed time and that the slope could be defined as a decay constant λ. For samples on the "dry" side* of critical state (46) λ was equal to -1; for the wet side* it was equal to -0.87. The decay constant λ was dependent on the stress history and the level of applied stress. Thus, the strain rate after a given time could be expressed by an equation of the form:

$$\dot{\varepsilon}_p = e^{\alpha} T^{-\lambda} \qquad (2.4)$$

where $\dot{\varepsilon}_p$ = strain rate
T = elapsed time
λ = decay constant
α = function for the strain rate after unit time.

Hyde used equations of this form to represent his results, which could then be integrated between limits to predict accumulated permanent strain.

* Samples on the "dry" side of critical state develop negative pore pressures during testing; samples on the "wet" side develop positive pore pressures. In this case lightly over-consolidated samples were on the "wet" side.

Lashine (47) had arrived at a similar prediction equation, and found that λ varied with the applied repeated stress to sample strength ratio.

Hyde's permanent strain versus cycles relationships were all curved (Figure 2.6), but when these are replotted on a completely logarithmic basis (Figure 2.7) it can be seen that the logarithm of perm-:anent strain is proportional to the logarithm of the number of cycles. Thus the results of Monismith et al (40), Lashine (43), and Hyde all indicate this form of relationship which was also found by Snaith (22) for bituminous materials.

2.4 REPEATED LOAD TESTING OF GRANULAR MATERIALS

Relatively little attention has been given to this type of material. Early work by Williams (48) was directed at defining the stiffness of granular material in order to be able to calculate stresses in the overlying bituminous layers. Williams established a relation-:ship for a sand of the form:

$$E_r = K_1 + K_2(\sigma_3)^{\frac{1}{3}} \qquad (2.5)$$

He also found that the rate of loading had little effect on the resilient modulus.

Subsequent workers have all found that the stiffness increased with an increase in the confining or mean normal stress (p) level. Brown and Pell (49) determined a relationship of the form:

$$E_r = K_1(p)^{K_2} \qquad (2.6)$$

This was established from measurements taken in a model pavement study, and was similar to that developed by Hicks (50) and by Barksdale (20).

Hicks found that there was a higher correlation when the resilient modulus was expressed in this way, in comparison to express-:ing it as a function of confining stress (σ'_3). Hicks concluded that the degree of saturation affected K_1. In all his tests, K_1 was lower for a partially saturated sample than for a corresponding dry sample

but for saturated samples, K_1 (based on effective stresses) was almost the same as for the dry samples. These tests used a constant confining stress (σ_3) and a repeated axial stress (σ_1). Hicks found that the resilient Poisson's ratio (ν_r) varied with the stress ratio (σ_1/σ_3). When his results were plotted by Boyce (55) in terms of the ratio of the stress invariants (q/p), ν_r was directly proportional to (q/p), for both dry and partially saturated samples. A measure of agreement between the relationships for the two conditions was achieved when a reasonable value of suction was assumed for the partially saturated material. It would therefore seem likely that the material is affected by soil suction.

In measuring resilient strains, Hicks concluded that one specimen could be used at all reasonable stress levels and that the stress levels could be applied in any order. The measurements of strains were taken after 50 to 100 load applications at each stress level.

Lashine et al (51) carried out repeated load tests on a partially saturated material in drained and undrained conditions. Brown (52) has also reported some of the important features of the work. They found a similar relationship for the resilient modulus to those of other researchers (20, 49, 50). However, this was only applicable when the mean deviator stress (q_m) was equal to half the repeated deviator stress (q_r). A more complex relationship applied when q_m was greater than $q_r/2$, and indicated that the resilient modulus was dependent on the levels of q_m and q_r. The former case was that employed by Hicks. It was also found that frequency, in the range 1 to 10 Hz., had little effect on the resilient modulus.

Lashine et al also found that, for drained tests both the resilient and permanent strains reached equilibrium values, after approximately 10^4 cycles, in all but a few tests with high deviator

stress. Before this equilibrium value was reached the permanent strain was approximately proportional to the logarithm of the number of cycles. The equilibrium value was assumed to be due to the dissipation of pore pressures. The permanent strain at equilibrium was related to the applied stresses by the equation:

$$\varepsilon_p = 0.01 \ (q_{max}/\sigma_3) \qquad (2.7)$$

However, all the tests were carried out at an approximately constant value of p_m/σ_3, where p_m is the mean value of the mean normal stress. A marked increase of permanent strain was noted in those tests using undrained conditions, which was probably due to the development of pore pressures.

The majority of tests carried out by Lashine et al were drained with constant confining pressure. However, preliminary tests were carried out with cyclic confining pressure, and were used as a guide for subsequent tests by Hyde (45) on an identical material. The results of these tests were also reported by Brown and Hyde (52). This work confirmed the conclusion of Hicks, that one specimen could be used to determine the resilient behaviour under differing conditions, providing sub failure stresses were involved. However, Brown and Hyde concluded that stress history had a considerable effect on permanent strain, and, therefore, each specimen could be treated at only one stress condition. Hyde compared the resilient modulus (Er) and permanent strain (εp) obtained in tests with cyclic confining stress and those with a constant confining stress equal to the mean of the cyclic value, and obtained similar results. However, the compatibility did not occur in the determination of Poisson's ratio; much higher values resulting from the tests with constant confining stress. Brown and Hyde concluded that Poisson's ratio is affected by the amptitude of the mean normal stress (which is smaller with constant confining pressure) as well as p_m, but Er and εp are only

affected by p_m.

Thus Hyde's results indicated that the much simpler test with constant confining stress could not be used to determine Poisson's ratio. However, he found that by plotting volumetric strain versus p_r/p_m and shear strain versus q_r/p_m, two unique relationships described the resilient behaviour for both the types of test. The only exception to this was when dilation occurred. Thus, expressions, for bulk and shear moduli, could be developed, which described the resilient behaviour more adequately under the non-linear conditions, for which the constant confining stress tests were applicable.

Hyde found that relationships developed by Lashine et al (51) for permanent strain:

$$\varepsilon_p = 0.01\ (q_{max}/\sigma_3) \qquad (2.8)$$

could be applied to tests with cyclic confining stress, provided that the mean level of confining stress was used in the expression.

Barksdale (20) carried out repeated load test on ten different base course materials, specifically to evaluate permanent deformation behaviour. He found that the permanent axial strain was proportional to log (N) (N is the number of load cycles) after a settling down period of about 10 cycles:

$$\varepsilon_p = K.\ \log_{10}N \qquad (2.9)$$

The constant (K) was related to the stress ratio q_r/σ_3 by a complicated hyperbolic law, although the results exhibited a large degree of scatter. This was in contrast to the relatively simple expression obtained by Lashine et al (51) and Hyde (45).

Barksdale's results showed that density, degree of saturation, and amount and type of fines, all affect permanent strain behaviour. Generally, low density, high fines content, and high saturation, increased permanent strain.

Allen and Thompson (54) carried out repeated load tests, with

both constant and cyclic confining pressure, on a variety of granular materials, to compare resilient behaviour. The value of the constant confining pressure was equal to the maximum of the cyclic value; thus, their conclusion that the former tests overestimated Poisson's ratio agreed with Brown and Hyde (53), whereas, their conclusion that those tests also generally over-estimated the resilient modulus, did not agree.

Boyce (55) carried out repeated load tests, with both constant and cyclic confining pressures on a dry crushed limestone. Thus, all the measured stresses were effective stresses, and pore pressure measurement was unnecessary. He tested the material under a much wider range of stress conditions than those used by other researchers, in order to obtain the resilient characteristics. In a preliminary investigation of stress history effects he found, similar to Hyde (45) and Hicks (50), that the resilient strain reached a steady value after a relatively small number of stress applications. However, two distinct effects were observed:

1. Under stress conditions which did not cause any substantial permanent strain, the resilient strain reached a steady value after 200 - 1000 cycles, and was usually reduced by 0 - 10%, as it approached that value.
2. If permanent strain did occur, no clear pattern emerged of the effect of permanent strain on resilient behaviour; increases and decreases of up to 30% were observed.

Boyce reduced these effects by taking resilient strain readings during only four cycles of stress. The effect of large numbers of load cycles and permanent strain on the resilient behaviour was investigated in his permanent strain tests.

Another preliminary investigation confirmed that resilient strains were not dependent on frequency in the range 0.2 to 20 Hz.,

similar to Lashine et al (51), who found the same for the range 1 to 10 Hz.

Boyce performed subsequent tests at 1 Hz. He tested nine specimens during the main resilient strain tests, three with negative deviator stresses applied, and six with the usual positive deviator stress. The former were hitherto unused in testing granular materials, but their inclusion widened considerably the range of stress conditions used. In each of the latter tests, approximately 200 different stress paths were applied to each specimen, but not in the same order, and it was found that the order was not significant.

Boyce determined an expression which summarised the total range of resilient behaviour obtained in his tests:

$$W_r = (P_m/K)^n \sinh [2T_r/T_m + 1] \qquad (2.10)$$

where $K = 6.8 \times 10^{-6}$ kN/m^2, $n = 0.33$, and W_r has units of microstrain. W_r is an expression for the strain, and is a function of the volumetric strain, v_r, and the shear strain, ε_r. T_r and T_m are functions of p_m and q_m.

Under restricted conditions, where q_m, q_r and p_r are small in comparison to p_m, he showed that this relationship agreed with the much simpler one derived by Hicks and other researchers, namely:

$$E_r = K_1 (p_m)^{K_2} \qquad (2.11)$$

However, these conditions are applicable when the material is well away from failure, as had been noted by the other workers, and by no means covered the range of stresses which might occur in-situ. He also found that within these conditions, Poisson's ratio was constant at a value of 0.29. When stresses outside these restrictions were employed, the simpler model considerably under-predicted strains.

The data which Boyce obtained with respect to the permanent

strain behaviour was much more limited than for the resilient strain tests, since only one stress path could be used for each specimen. Only seven different stress paths were used, in comparison to two hundred in the resilient strain tests. However, he found that under certain stress conditions, behaviour such as that reported by Lashine et al (51) and Hyde (45) occurred; viz., after a large number of cycles the permanent strain reached an almost constant value. Before this stage was reached the development of permanent strain was approximately proportional to the logarithm of the number of cycles, following a large initial strain which occurred in the first few cycles. This relationship was common to the results of Lashine, Hyde, Barksdale and Boyce. Where failure of a specimen occurred, the permanent shear strains were much greater than in the tests described above, and there was a tendency for dilation to occur. The maximum stress ratio used in tests where failure occurred was 2.25 in comparison to the maximum of 2.18 reached in the single loading tests that he had carried out. It could, therefore, be postulated, since the results were by no means conclusive, that under repeated loading the material was capable of sustaining higher stress ratios than under single loading.

Boyce postulated that the mechanism of permanent deformation in a granular material may be one of "shakedown" with a possibility of "incremental strain collapse", at high stresses. Those tests where the permanent strain had stabilised at a fairly low value could be judged to have undergone shakedown, and the particles of the specimen could have become more densely packed, thus strengthening the specimen and causing resistance to further deformation. However, failure could occur by incremental collapse, if the first few load cycles caused rearrangement of the particles such that dilation occurred and weakened the specimen. A difficulty encountered in a repeated load test, is in achieving the stress path required in the first few cycles

of a test. If a mechanism such as described above does occur, then successively larger stress paths applied while approaching the required one (which potentially may cause failure) may strengthen the specimen and inhibit failure. Thus, the inherent variability in repeated load tests on granular material, and possibly other pavement materials, can be explained.

Boyce found that the logarithm of the permanent axial strain was directly proportional to the stress ratio q_{max}/σ_{3mean}. He found quite good comparison with the results of a crushed granite tested at optimum moisture content by Barksdale (20). Hyde (45) has shown, by combining his results with those of Lashine et al (51), that the natural value of the axial permanent strain was directly proportional to q_{max}/σ_{3mean}. Neither Boyce's results nor those of Hyde and Lashine resulted in linear relations when plotted completely logarithmically.

It was also found that anistropy occurred as a result of permanent strain developing, although no relationship could be obtained, and was attributed to the random arrangement of the particles in each specimen. The anisotropy was always biased in the same sense, which could have been due to the mode of testing and of specimen preparation, and, if so, it may not occur in-situ, although compaction of the material in-situ can cause orientation of the particles and introduce anisotropy.

Concluding, Boyce emphasises the considerable non-linear behaviour of the material, and necessity to use an appropriate analysis if a realistic assessment of the behaviour in-situ is to be obtained. Such analysis would be by employing a finite element technique and to use the model of resilient behaviour determined by Boyce. However, this has been attempted and found to be extremely difficult (56).

2.5 SUMMARY OF THE ESSENTIAL PROPERTIES OF FLEXIBLE PAVEMENT MATERIALS

2.5.1 Resilient Properties

It is well established that for bituminous materials, the resilient modulus is time and temperature dependent. Snaith (22) showed that at 20°C DBM behaved linearly. He also showed that Poisson's ratio increased with temperature.

For fine grained (subgrade) soils the resilient modulus is non-linear and decreases as deviator stress increased (37, 42), it is also independent of loading time (43). There is very little definitive information on variation of Poisson's ratio.

The resilient behaviour of granular materials is non-linear and complex. Boyce considered that the resilient modulus and Poisson's ratio could not adequately describe the behaviour of a crushed lime-:stone. Other researchers (20, 49, 50) found relationships of the type:

$$E_r = K_1(p)^{K_2} \qquad (2.12)$$

Boyce found that Hicks' results indicated a linear relationship between Poisson's ratio and q/p.

2.5.2 Permanent Strain Behaviour

The accumulation of permanent strain in the three types of material is independent of the frequency of loading, but time dependent. Generally, increasing q increases the rate of deform-:ation, and increasing p decreases the rate. Only bituminous materials are affected by temperature.

Permanent strain versus time relationships for bituminous materials are approximately linear when plotted logarithmically (22). A similar relationship was found for a compacted fine grained soil

by Monismith et al (40), and also, for a normally consolidated and overconsolidated silty clay, when the results of Lashine (43) and Brown et al (42) were replotted. For sub-failure conditions, for the compacted and normally consolidated clays, permanent strain is approximately proportional to log time. For granular materials there appears to be a linear relationship between permanent strain and log cycles before an equilibrium value is reached. The results were not linear when plotted completely logarithmically.

The linear relationships between permanent strain and log time, and log permanent strain and log time, have great potential for application in prediction procedures. Similar relationships were found for the materials' characterisations connected with the research for this thesis, and were readily incorporated into a prediction procedure.

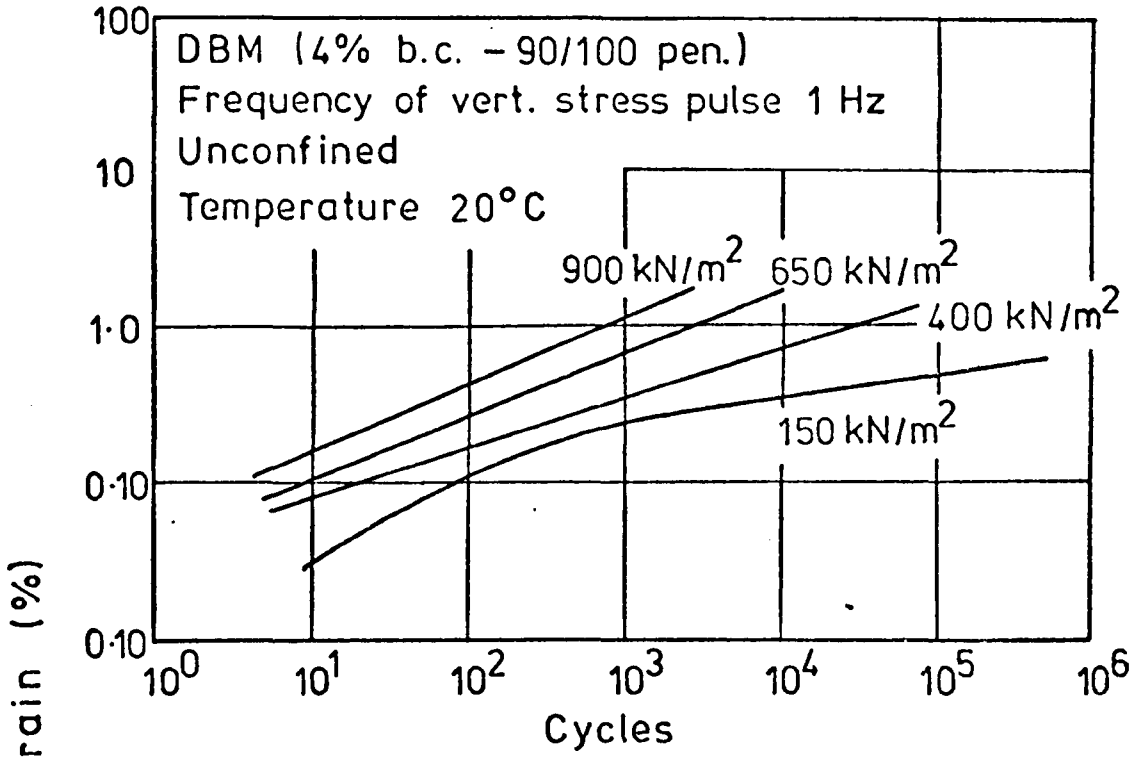

(a) Effect of vertical stress pulse on vertical permanent strain.

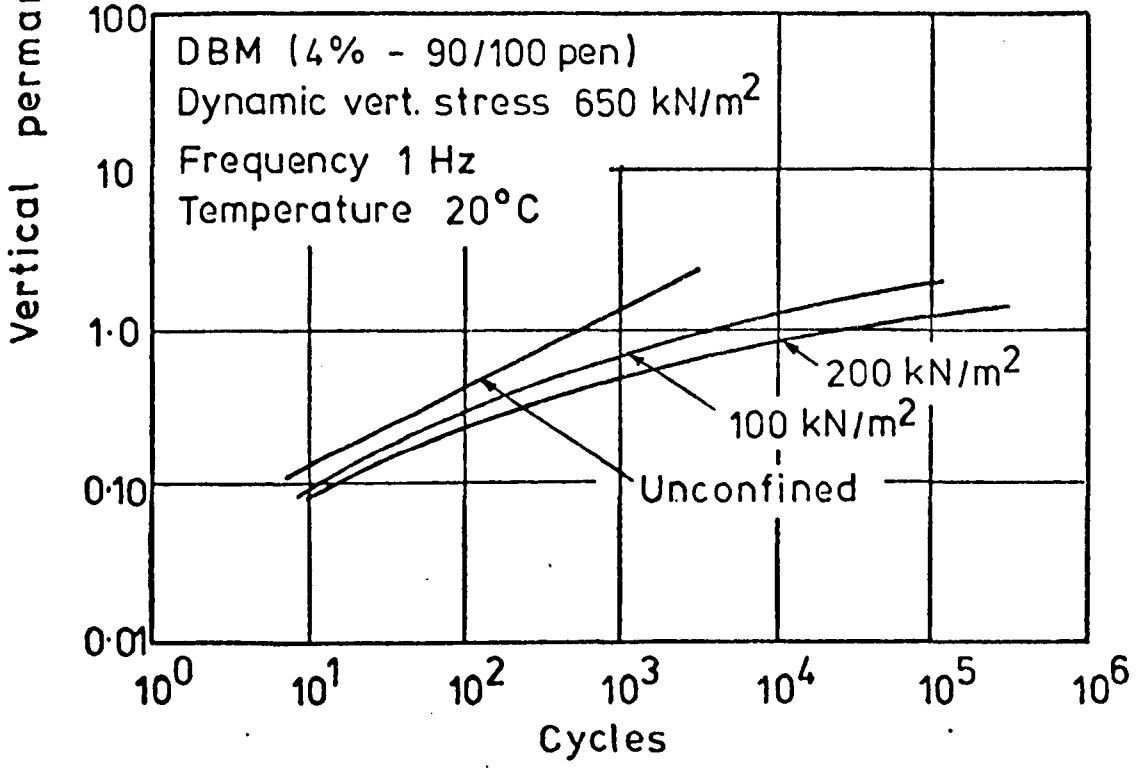

(b) Effect of confining pressure on vertical permanent strain.

FIGURE 2.1 PERMANENT STRAIN BEHAVIOUR OF DBM (AFTER SNAITH (22))

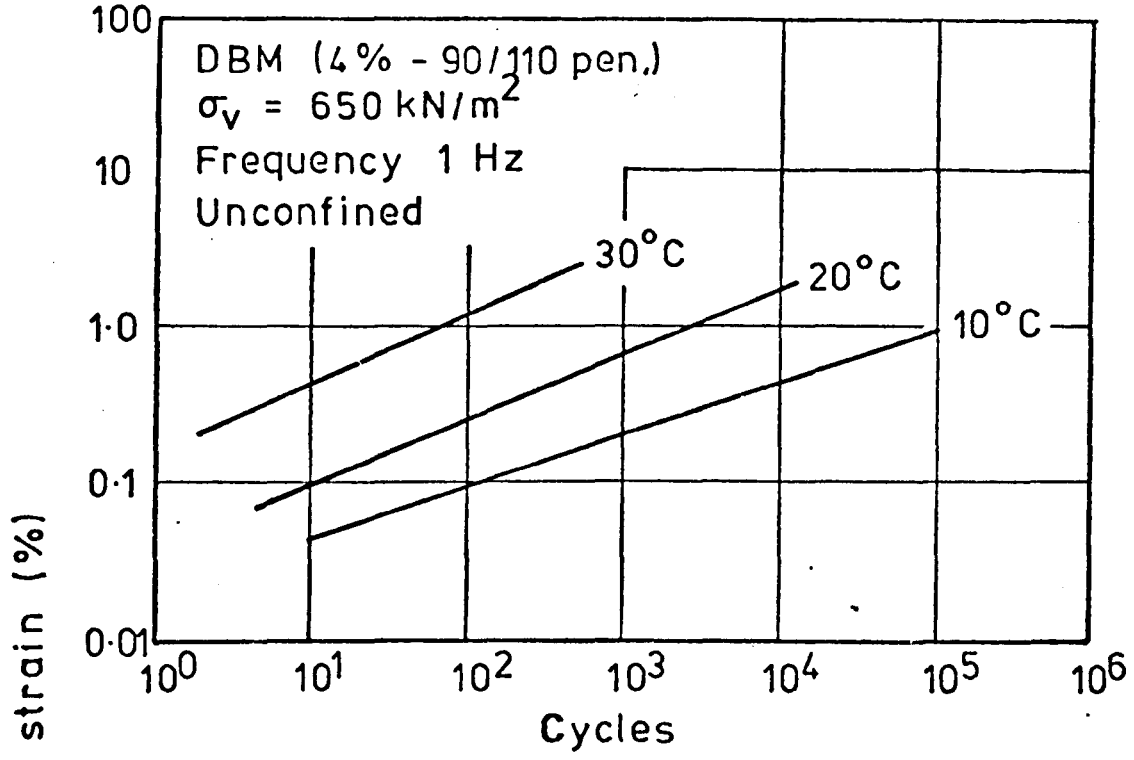

(a) Effect of temperature on vertical permanent strain

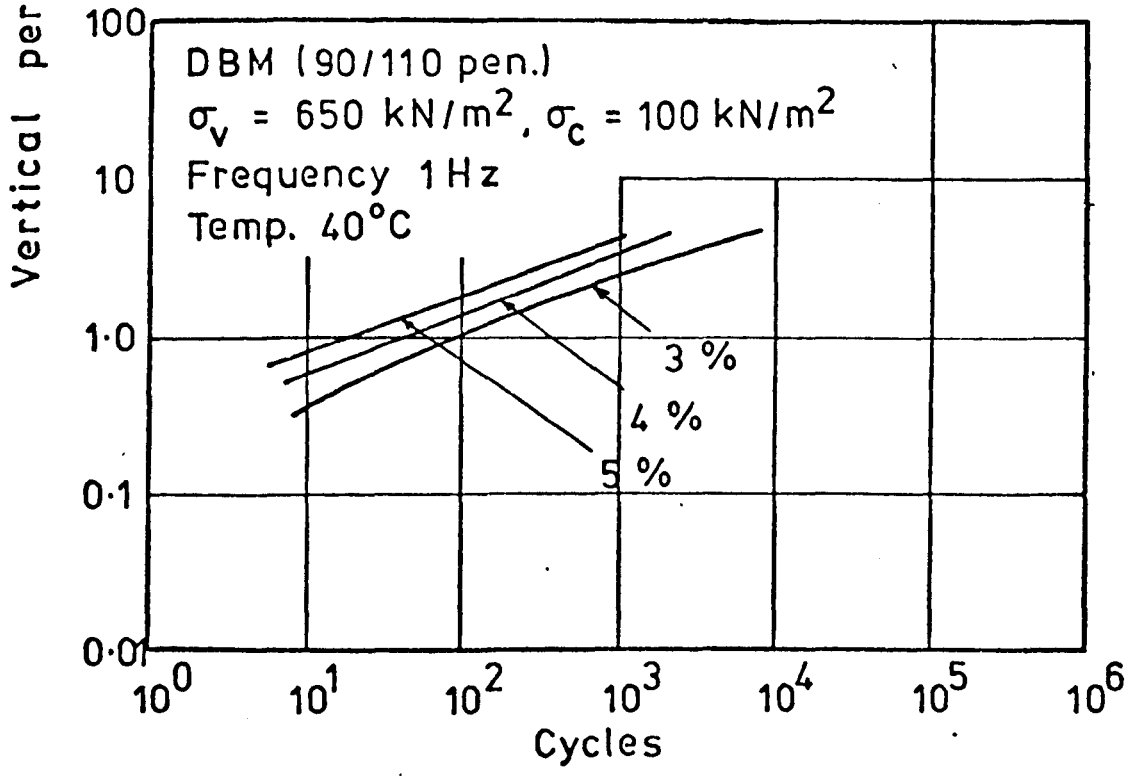

(b) Effect of binder content on vertical permanent strain

FIGURE 2.2 PERMANENT STRAIN BEHAVIOUR OF DBM (AFTER SNAITH (22))

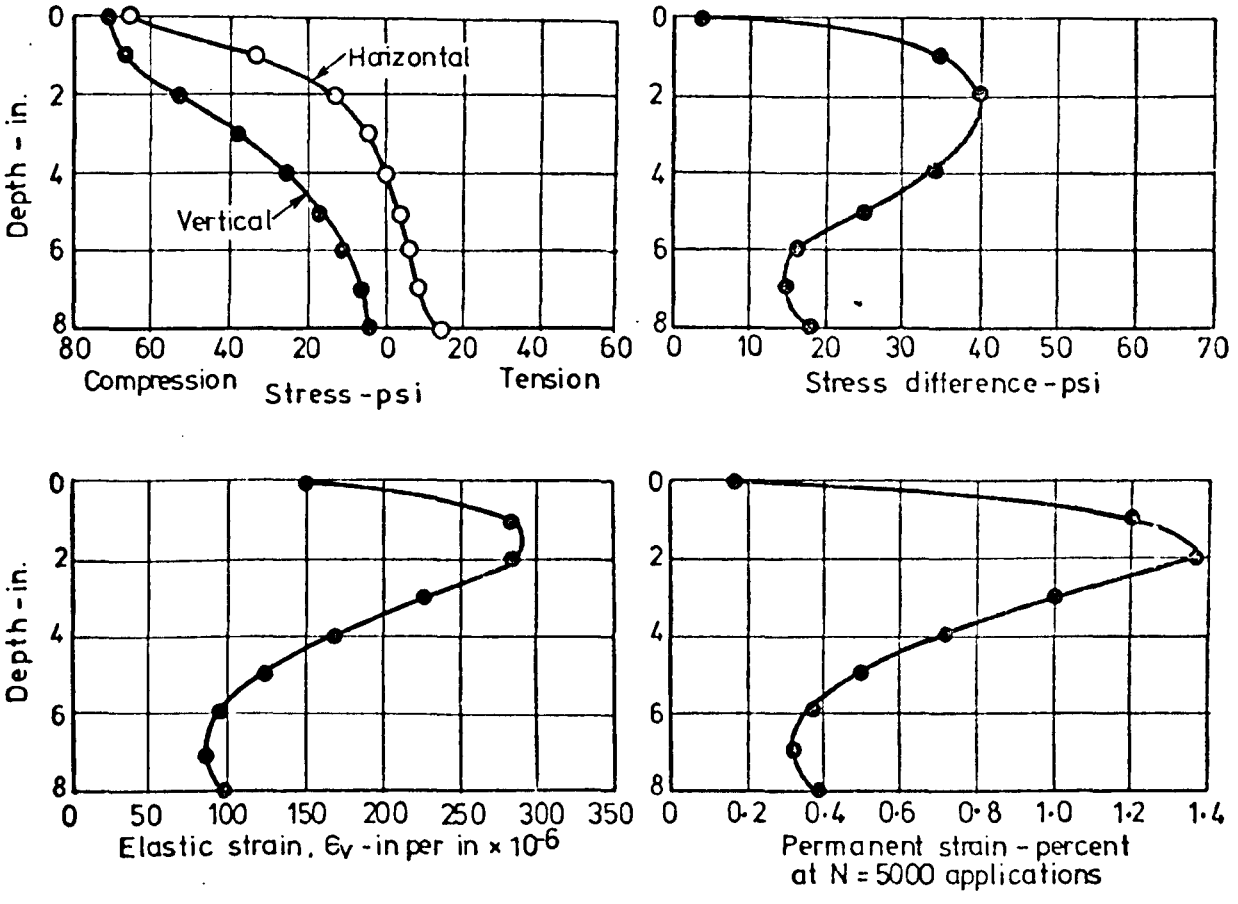

FIGURE 2.3 STRESS AND STRAIN DISTRIBUTIONS IN AN 8 INCH THICK ASPHALTIC CONCRETE LAYER SUBJECT TO A 1500 LB. WHEEL LOAD WITH A 70 PSI CONTACT PRESSURE (AFTER McLEAN AND MONISMITH (26))

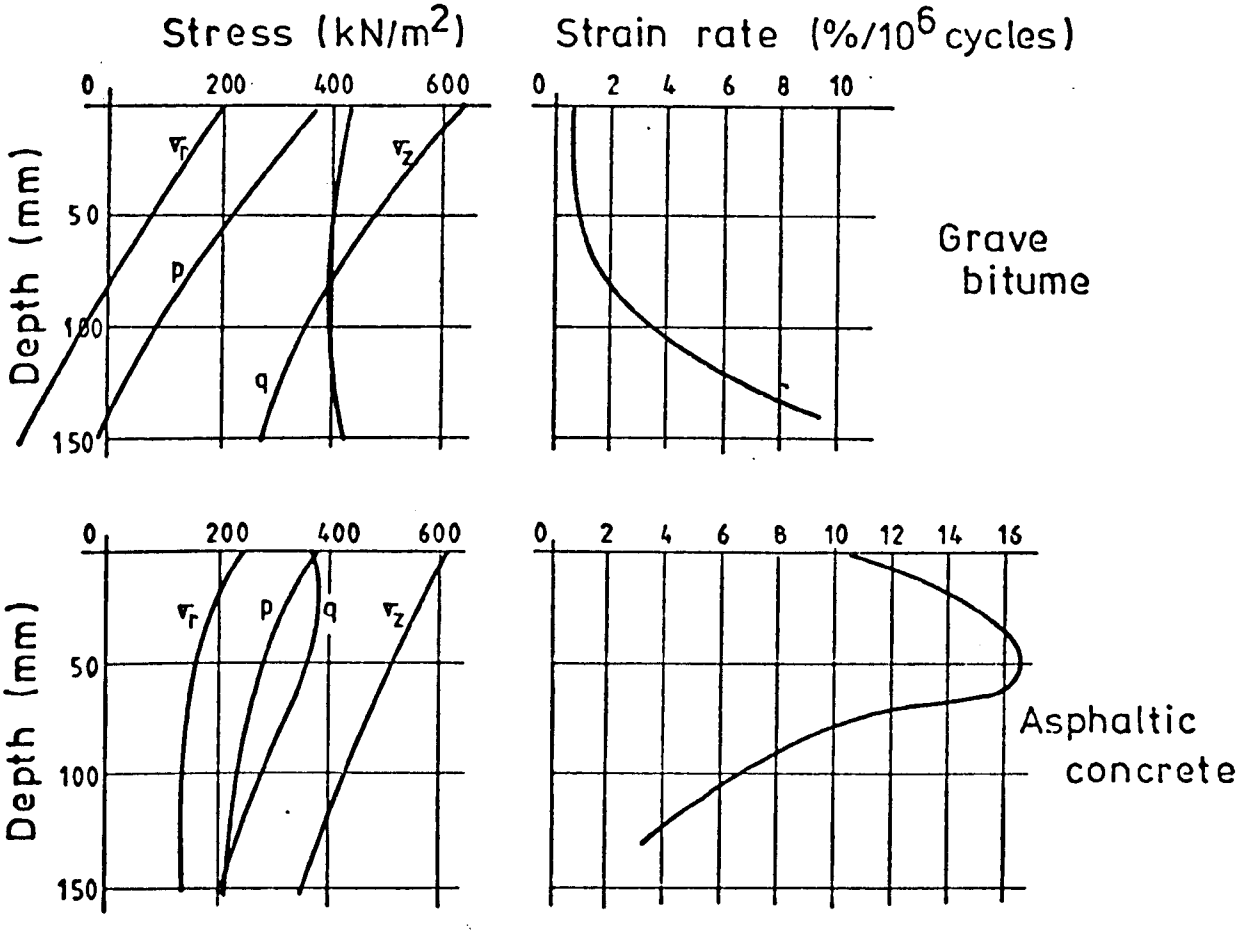

FIGURE 2.4 STRESSES AND PERMANENT STRAIN RATES FOR TWO BITUMINOUS OVERLAYS (DERIVED FROM AUSSEDAT and AZIBERT (32))

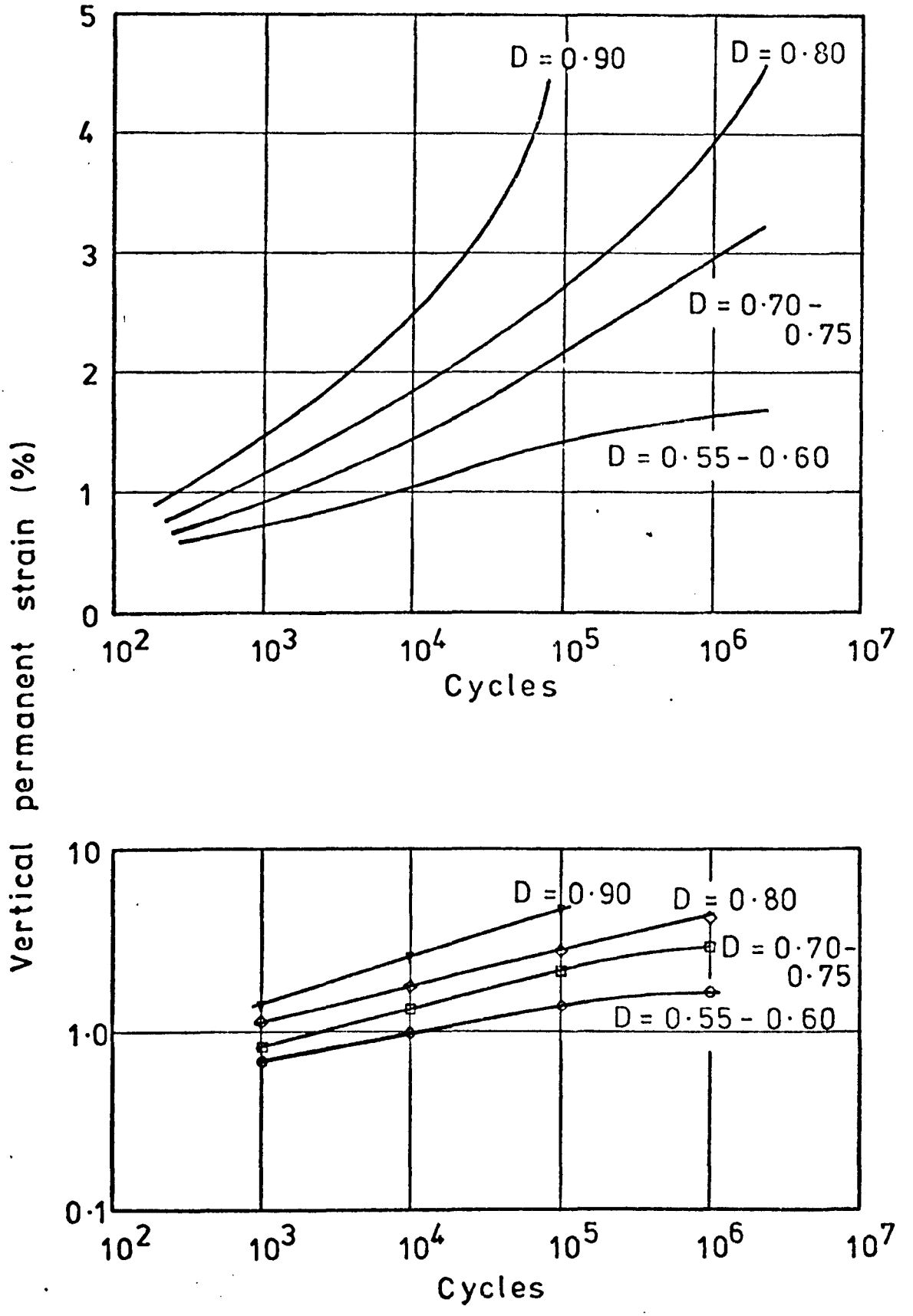

FIGURE 2.5 PERMANENT STRAIN BEHAVIOUR OF NORMALLY CONSOLIDATED KEUPER MARL (AFTER LASHINE (43))

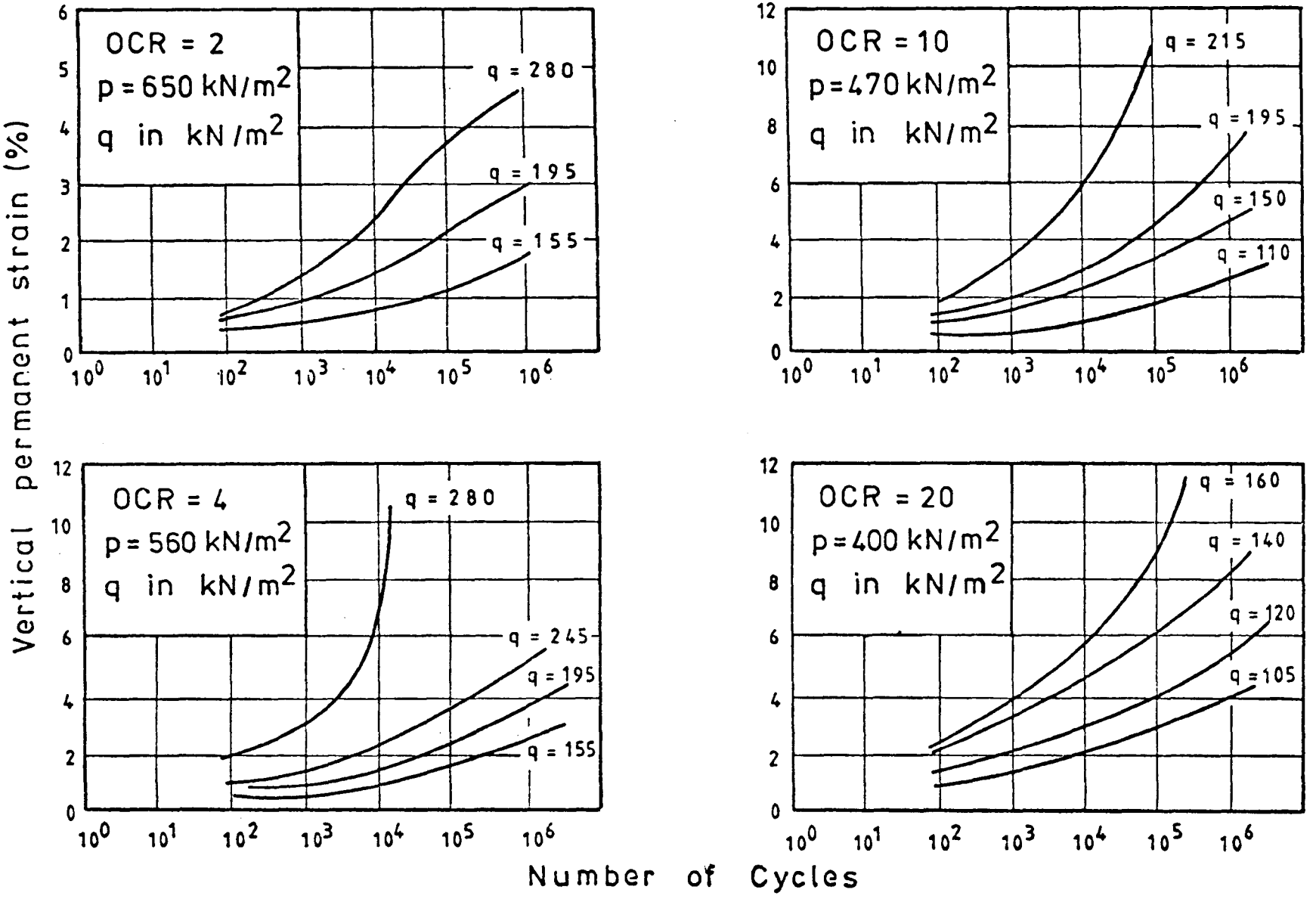

FIGURE 2.6 PERMANENT STRAIN BEHAVIOUR OF OVERCONSOLIDATED KEUPER MARL (AFTER BROWN ET AL (42))

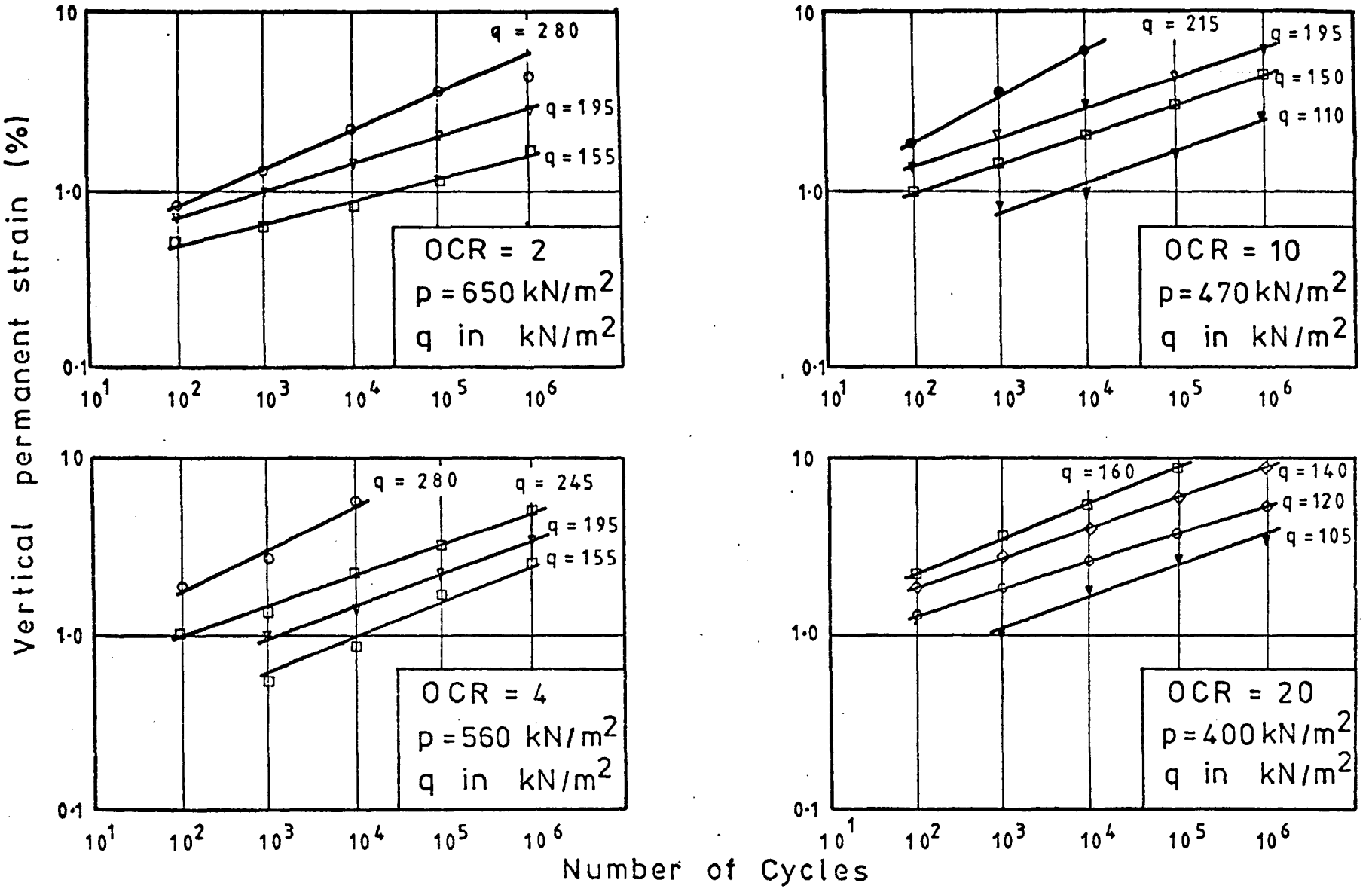

FIGURE 2.7 LOGARITHMIC PLOT FOR PERMANENT STRAIN BEHAVIOUR OF OVERCONSOLIDATED KEUPER MARL

CHAPTER THREE

REVIEW OF PREVIOUS WORK - PROPOSALS FOR PREDICTION OF PERMANENT DEFORMATION

3.1 METHODS BASED ON CREEP TESTING OF BITUMINOUS PAVEMENT MATERIALS

A recent research effort by Shell (56, 57, 58) has led to the development of a method of predicting permanent deformation (59) based on unconfined creep testing of bituminous materials. The method depends heavily on empirically derived correction factors to achieve predictions accurate to within a factor of two.

The deformation in the underlying layers of a pavement is assumed to be negligible, which is certainly not the case for British roads (13), unless, perhaps, the road has a rigid base. The method also assumes that the rut depth observed at the surface of a pavement amounts to 1.5 times the reduction in layer thickness, based on observations in test track experiments. However, it will be shown herein that this was not the case with the experiments carried out in this project, and it should also be noted that such a situation infers virtually zero volume change, whereas under repeated loading, realist-:ically compacted pavement materials invariably undergo volume change.

This method has the advantage of being based on a simple creep test, which need not involve sophisticated measurements or loading devices. Also, some analysis of the in-situ stresses is carried out, although this is by linear elastic analysis (60), and may be an over-:simplification.

The Shell method (59) involves the plotting of a stiffness of the mix (S_{mix}) versus stiffness of bitumen (S_{bit}) curve, for the bituminous material of the pavement in question. This is achieved from the results of the creep tests where axial strain is measured with

increasing time, under an applied stress of 0.100 MN/m^2. The stiffness of the mix after a particular time is obtained by dividing the applied stress by the total strain at that time; the stiffness of the bitumen is obtained from van der Poel's nomograph (61) which requires the penetration index and ring and ball temperature of the bitumen.

A S_{mix} versus S_{bit} curve, for cores taken from the first pave-:ment tested in connection with this project (62) is shown in Figure 3.1. Shell correlate this type of curve with the in-situ behaviour by assuming that only the viscous component of the bitumen stiffness ($S_{bit,\ visc}$) contributes to rutting. This is calculated from:

$$S_{bit,\ visc} = 3\eta/t \qquad (3.1)$$

where η is the viscosity of the bitumen, obtained from a nomograph, and t is the total elapsed time, obtained from the product of the time for one load application and the total number of applications. The in-situ value of S_{mix} is read off from the curve by inputting $S_{bit,\ visc}$.

The change in thickness of the bituminous layer is then determined by:

$$\delta_H = C_M H_o(\sigma_{av}/S_{mix}) \qquad (3.2)$$

where C_M is a correction factor, H_o is the original layer thickness, and σ_{av} is the average stress in the pavement. The average stress is obtained from:

$$\sigma_{av} = Z.\sigma_o \qquad (3.3)$$

where σ_o is the contact stress, and Z is a factor relating the elastic strain which would occur in the bituminous layer in-situ (calculated by linear elastic analysis) to that which would occur in an unconfined specimen of the material subject to the stress σ_o. Finally, as discussed above, the change in thickness is

multiplied by 1.5 to obtain the rut depth.

The outline above indicates the method used to obtain a rut depth for a simple situation of constant temperature, constant tyre pressure, and constant wheel path. Van der Loo (59) presented methods of dealing with variations in these quantities, which appear to be sound, apart from the method of dealing with a lateral distrib-:ution of wheel loads, which seems to assume that deformation is proportional to the number of load applications, whereas this relation-:ship is, in fact, exponential.

Snaith (22) carried out some creep tests on the same material that he used for his repeated load tests, and compared the results. Figure 3.2 shows a comparison of the two tests, which were both uniaxial, where the strains after 100 and 500 seconds are plotted against the applied stress. It was concluded that stresses of about 65 per cent of the dynamic levels would be required to produce the same levels of permanent strain in creep tests. Plots of S_{mix} versus S_{bit} for the two types of test were discussed by Brown and Snaith (23). These indicated lower mix stiffnesses for the dynamic tests, where the mean stress level had been used to calculate S_{mix}. However, if 65 per cent of the stress level was used for this calculation the comparison was very good.

Kirwan et al (63) have proposed that the level of static stress equivalent to a dynamic stress should be taken as the root mean square (rms) value of that dynamic value. This is 61 per cent for sinusoidal loading, and by replotting Snaith's (22) results for a DBM, they found good agreement between the dynamic test results and interpolated results from the creep tests. Snaith had also carried out some tests with a triangular stress pulse and observed that there was less deformation than in comparable tests with sinusoidal pulses. A triangular pulse has a smaller rms value than a sinusoidal one, and hence these results

support the concept of using an equivalent stress based on rms values.

Brown and Cooper (64) applied a numerical procedure to Snaith's results to determine the creep stress equivalent to the sinusoidal stress pulse. For the four dynamic stress levels used by Snaith they found that the average ratio of equivalent creep stress to dynamic stress was 0.59. They also determined equivalent creep test values based on the rms concept of Kirwan et al, taking into account the value of dead load that Snaith had used, and found an average ratio of 0.63. Brown and Cooper carried out repeated load tests on a DBM, similar to that tested by Snaith, under triaxial conditions with square wave pulses. The permanent strain levels resulting were found to be higher than those from equivalent creep tests, where the stress level was the same as the peak stress in the repeated load tests. The reason for the discrep-:ancy is not clear, but could be associated with the "overshoot" result-:ing from the sudden load application in a square wave. This form of loading does not simulate that occurring in-situ which resembles the sinusoidal form more closely, where the load is gradually applied.

Hence, the value of creep stress producing the same permanent strain behaviour as a uniaxial repeated load test, using a sinusoidal wave form, is approximately 60 per cent of the peak sinusoidal stress. The value is close to the rms value for a sine wave, which may be used providing a significant dead load is not applied in the repeated load test. Clearly, it should be established that this approach can be applied to bituminous materials other than the DBM roadbase discussed above, and for other waveforms. The approach appears to be inapplicable for square wave loading under triaxial conditions, but should be investigated for other waveforms under these more realistic conditions.

Snaith tested mixes with three different binder contents, and found that the creep curves were substantially different, as were the values of S_{mix} at corresponding loading times and stress levels. A similar

effect had been noted from the Shell results from tests of various mixes (56), particularly those with different aggregates.

Brown and Snaith focused attention on the fact that the Shell method of predicting permanent deformation does not take account of confining pressure, which Snaith found to have a considerable effect on permanent strains in dynamic tests. The S_{mix} calculation could take account of the confining stress, but the determination of S_{bit} by van der Poel's nomograph does not consider stress level. Clearly, confined creep tests could better represent the in-situ stress conditions, and perhaps better prediction of permanent deformations could be obtained with the Shell method if such tests could be incorporated into that method.

Huschek (65) has also proposed a method for predicting the permanent deformation in bituminous layers, based on creep testing carried out at the Federal Institute of Technology, Zurich. The method has many similarities to the Shell method (the creep test apparatus is identical, linear elastic layer theory is used to analyse pavements, and a viscosity value is used in the prediction), but is more fundamental in its approach.

Huschek's method differs from the Shell approach in that the deformation behaviour of the bituminous material is idealised by a Maxwell model, as shown in Figure 3.3a, and the permanent or irreversible deformation is due to the viscous element of the model. Mathematical treatment of the model behaviour yields an expression for the irreversible strain for each wheel pass:

$$\varepsilon_{irr} = (\sigma/\eta) \cdot \Delta t \qquad (3.4)$$

where, η is the viscosity, σ the applied stress, and Δt is the time of loading.

Presumably, total deformation after an accumulated loading time is given by:

$$\varepsilon_{irr} = (\sigma/\eta) \cdot t \qquad (3.5)$$

The application of a Maxwell model should be questioned since the response would be as shown in Figure 3.3b with instantaneous elastic response, constant creep, and instantaneous elastic recovery. A more appropriate model is Burger's, shown in Figure 3.4, together with the response, which provides an essential feature of bituminous material behaviour, namely delayed elastic response and recovery. Such a model is more difficult to represent mathematically.

Huschek also utilises a relationship given by van der Loo (59), based on the results of the Shell creep tests (55):

$$\varepsilon_{irr} = c \cdot \sigma \cdot t^{A} \qquad (3.6)$$

where c and A are experimental constants obtained from plots such as Figure 3.5, and t is the total time of loading. Equating equations (3.5) and (3.6) eliminates σ and leaves an expression for the viscosity:

$$\eta = t^{1-A}/c \qquad (3.7)$$

Hence, the viscosity is obtained from a creep test.

The creep tests are only conducted at one value of applied stress (0.100 MN/m^2), which is the same as that used in the Shell tests. The use of this value was justified by the Shell investigators for their prediction procedure by confirmation that different stress levels did not affect their S_{mix} versus S_{bit} relationships. However, in Huschek's case, one value of applied stress is used to obtain representative values of viscosity for different pavement layers where stress levels vary. This may introduce error since the materials will probably respond in a non-linear manner (non-Newtonian) under the loading and environmental conditions which produce permanent deformation.

The results of Snaith (22) for both dynamic tests and creep tests are similar to equation (3.6), as are those found by the Author, which are presented in this thesis. Snaith, and the Author, found results of the form:

$$\varepsilon_{irr} = C\, t^{A} \qquad (3.8)$$

where the constants C and A depend on the stress level, and the actual stress level does not occur in the relationship, since the values of C and A differ considerably with the stress level.

Huschek's prediction of permanent deformation in a pavement layer (j) is determined by:

$$\delta_j = (\Delta H_j \cdot E_j)/(\eta_j \cdot v) \qquad (3.9)$$

where H_j is the elastic deformation in the layer determined by elastic analysis, E_j is the resilient modulus of the layer, and v is the average wheel speed. The resilient modulus is determined by interrupted creep tests, an interesting feature of Huschek's method. The standard creep test is interrupted at 10, 60 and 120 minutes and periods of rectangular repeated loads are applied.

The total deformation in the bituminous layers is obtained by summation of the deformations in all layers. It would appear that the deformation due to the total number of load applications for a particular temperature interval is obtained by multiplying by that number. As for the Shell approach, this would be incorrect due to the exponential form of the deformation versus time relationship. Huschek compared measured and predicted rut depths for the five sections of a test road and obtained favourable results. However, complete validation of the method will require comparisons for different types of construction and materials, and confirmation that the assumptions which are likely to cause errors are justified.

3.2 FUNDAMENTALLY BASED PROPOSALS FOR PREDICTING PERMANENT DEFORMATION

Romain (19) and Barksdale (20) have outlined procedures which are basically similar, but differ in detail. Barksdale proposed that the pavement layers should be divided into a number of sub-layers, and that the permanent deformation at the centre of each sub-layer should be

determined, the total deformation in all layers giving the surface deformation. This is achieved by calculating the stresses at the centre of each sub-layer, by suitable linear or non-linear elastic analysis, and determining the deformations from the results of laboratory tests carried out at a suitable range of stresses. Romain also proposed that each pavement layer should be divided into sub-layers, but also that each sub-layer should be divided into elements, the calculations of stresses and subsequent determination of permanent deformation being for the centre of each element.

These approaches separate the calculation of the resilient behaviour of the pavement from that of the permanent strain behaviour. The justification for this separation is that the permanent strain caused by one wheel passage is very small indeed compared to the elastic strain. Thrower (66) has discussed the relevance of this approach, which he terms "separative" and has concluded that such an approximate method is satisfactory, with the exception that the permanent strains will not, in general, satisfy compatability requirements. Thrower's work will be discussed, in more detail, later in this section.

Brown (21) suggested the use of stress invariants as a framework for determining the permanent deformation characteristics of bituminous materials, based on repeated load triaxial tests. Such an approach is readily adaptable to the proposal of Romain, where the pavement is divided into elements, since it has the advantage of being able to deal with situations where the principal stresses are not vertical and horizontal (positions off the load axis) and situations where one or more of the stresses aretensile (positions at the bottom of the bituminous layers). The invariant approach is also ideally suited to investigation of the resilient properties, and it can also be extended to cover other pavement materials.

The invariant approach was adopted for the prediction procedure in this thesis, and will be discussed further in a subsequent Chapter. However, a summary will be presented here to facilitate comparison with other suggested procedures.

Timoshenko and Goodier (67) defined the generally recognised stress invariants, I_1, I_2, and I_3, as the coefficients in the characteristic equation for the principal stresses:

$$\sigma^3 - I_1 \sigma^2 + I_2 \sigma - I_3 = 0 \qquad (3.10)$$

where the three roots of the equation are the three principal stresses, σ_1, σ_2 and σ_3.

and,
$$I_1 = \sigma_1 + \sigma_2 + \sigma_3$$
$$I_2 = \sigma_1\sigma_2 + \sigma_2\sigma_3 + \sigma_3\sigma_1 \qquad (3.11)$$
$$I_3 = \sigma_1\sigma_2\sigma_3$$

I_1, I_2 and I_3 completely define the principal stresses in magnitude, but not in direction. They can be replaced by any trio of symmetrical and homogeneous polynominals in the principal stresses of the first, second and third degree respectively; each member of such a trio can be expressed in terms of I_1, I_2, and I_3 and vice versa.

Brown's approach utilises two invariants, p and q, defined as:

$$p = I_1/3 \qquad (3.12)$$
$$\text{and} \quad q = 1/\sqrt{2}\ \left[\sqrt{(2I_1^2 - 6I_2)}\right]$$

hence
$$p = (\sigma_1 + \sigma_2 + \sigma_3)/3$$

and
$$q = 1/\sqrt{2}\ \left[\sqrt{(\sigma_1 - \sigma_2)^2 + (\sigma_2 - \sigma_3)^2 + (\sigma_3 - \sigma_1)^2}\right] \qquad (3.13)$$

p is the mean normal stress, σ_{oct}, and q is closely related to the octahedral shear stress, τ_{oct}

$$q = 3/\sqrt{2} \cdot \tau_{oct} \qquad (3.14)$$

A third invariant was not suggested, on the grounds that there is no evidence to suggest that I_3 could be significant, and it has no physical parallel, such as I_1 and I_2 have in σ_{oct} and τ_{oct}.

The first stage of Brown's approach is to calculate the in-situ principal stresses at the centre of each element, by a suitable linear or non-linear analysis. The second stage is to reproduce the invariants, corresponding to those principal stresses, in a triaxial test, within the restrictions that, in the test, two of the principal stresses are positive and equal. This is done for as large a range of values as possible, for an appropriate number of load applications, and the permanent and resilient strains continuously recorded. Thirdly, the values of two strain invariants, the permanent volumetric strain, v_p, and the permanent shear strain, ε_p, are calculated. These are defined as:

$$\begin{aligned} v_p &= \varepsilon_{p_1} + \varepsilon_{p_2} + \varepsilon_{p_3} \\ \varepsilon_p &= \sqrt{2}/3 \cdot \sqrt{[(\varepsilon_{p_1} - \varepsilon_{p_2})^2 + (\varepsilon_{p_2} - \varepsilon_{p_3})^2 + (\varepsilon_{p_3} - \varepsilon_{p_1})^2]} \end{aligned} \qquad (3.15)$$

where ε_{p_1}, ε_{p_2} and ε_{p_3} are the three principal strains.

Finally, the in-situ vertical permanent strain is obtained from equations (3.15) (the method will be described later) and integration of all such values in a particular column of elements provides the surface deformation.

Brown carried out a linear elastic analysis on some typical pavement structures and concluded that for conditions when permanent deformation is most likely to occur, viz, high temperature, the majority of stress conditions in the bituminous layer can be reproduced. For

these conditions a non-linear analysis would be more appropriate, but it is likely that the same conclusions would be reached.

Thrower (68) has also discussed the use of stress invariants as a framework for the testing of pavement materials. However, he considered three invariants defined as:

$$\chi_1 = I_1/3 = P \tag{3.16}$$

$$\chi_2 = (2I_1^2 - 6I_2)/9$$

$$= 1/9.\ (\sigma_1 - \sigma_2)^2 + (\sigma_2 - \sigma_3)^2 + (\sigma_3 - \sigma_1)^2 \tag{3.17}$$

$$= \tau_{oct}^2$$

$$\chi_3 = 2/27.I_1^3 - I_1 I_2/3 + I_3$$

$$= 1/27.(2\sigma_1 - \sigma_2 - \sigma_3)(2\sigma_2 - \sigma_3 - \sigma_1)(2\sigma_3 - \sigma_2 - \sigma_1) \tag{3.18}$$

$$= \tau_1^3$$

The first invariant is identical to that suggested by Brown (21), and the second is similar, in that it is related to τ_{oct}. The third invariant is a function of stress differences, similar to the second, and the cube root τ_1 has dimensions of stress. Thrower adopts p, τ_{oct}, and τ_1 as a set of invariants for reproduction in the triaxial test. For the test, as mentioned previously, two of the principal stresses are equal. Thrower assumes that these are σ_2 and σ_3 and rewrites equations (3.17) and (3.18) as follows:

$$\tau_{oct}^2 = 2(\sigma_1 - \sigma_3)^2/9$$

$$\tau_1^3 = 2(\sigma_1 - \sigma_3)^3/27 \tag{3.19}$$

He concludes that changes in material properties due to the deviator stress $q = (\sigma_1 - \sigma_3)$, will be related to both τ_{oct} and τ_1, that τ_{oct}^2 will always be positive, but τ_1^3 could be either positive or negative, and hence

indicates whether σ_3 is greater than σ_1. To obtain a complete picture of material behaviour under realistic in-situ stress conditions, the separate effects of τ_{oct} and τ_1 need to be established. If the sign of τ_1 is found to be insignificant, then there is justification in ignoring a third stress invariant.

By analysing a number of hypothetical pavements, Thrower concluded that his approach was applicable to a large number of stress situations in bituminous layers, with a severe restriction of reproducing those where stresses are tensile. For granular materials, he found that the approach was severely limited, and for subgrade type materials he found that the approach was particularly suitable. However, it should be noted that his analysis was linear elastic, which he admitted may not be appropriate for bituminous or granular materials.

Thrower also considered Boyce's (55) results, some of which gave an indication of the effect of the sign of τ_1. These indicated that the resilient properties may be affected by the sign. There were no results of permanent strains which could be considered. It should be noted that Boyce tested only a granular material and, as yet, nobody has supplied suitable experimental results to assess the effects on bituminous and subgrade materials.

Thrower suggested three additional tests to supplement the triaxial test, viz, to investigate stress conditions not reproducable in that test. These are:

a) Simple shear plus a normal stress on the same face.

b) Simple shear plus a normal stress on a different face.

c) Plane stress: normal stresses σ_1 and σ_3, on two faces of a cube, the third being free, i.e. biaxial stress conditions.

Experimentally, all three tests are more complex than the triaxial test, and their application may thus be prohibitive. However, Ansell (68) has tested a granular material in repeated simple shear, and his work may provide some guidelines for tests a) and b).

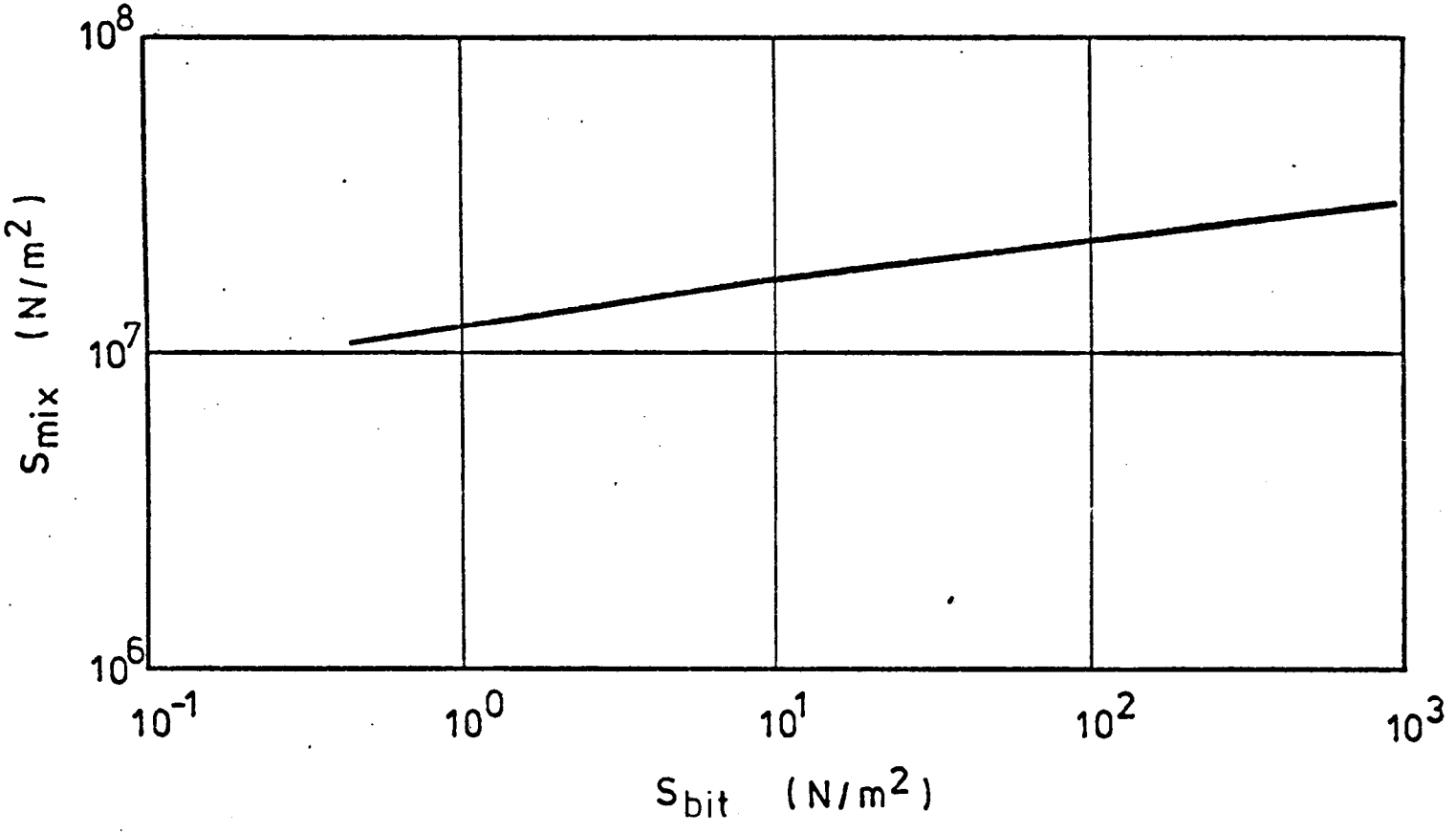

FIGURE 3.1 RESULTS OF CREEP TESTS CARRIED OUT BY SHELL ON CORES OF DBM FROM PAVEMENT 1

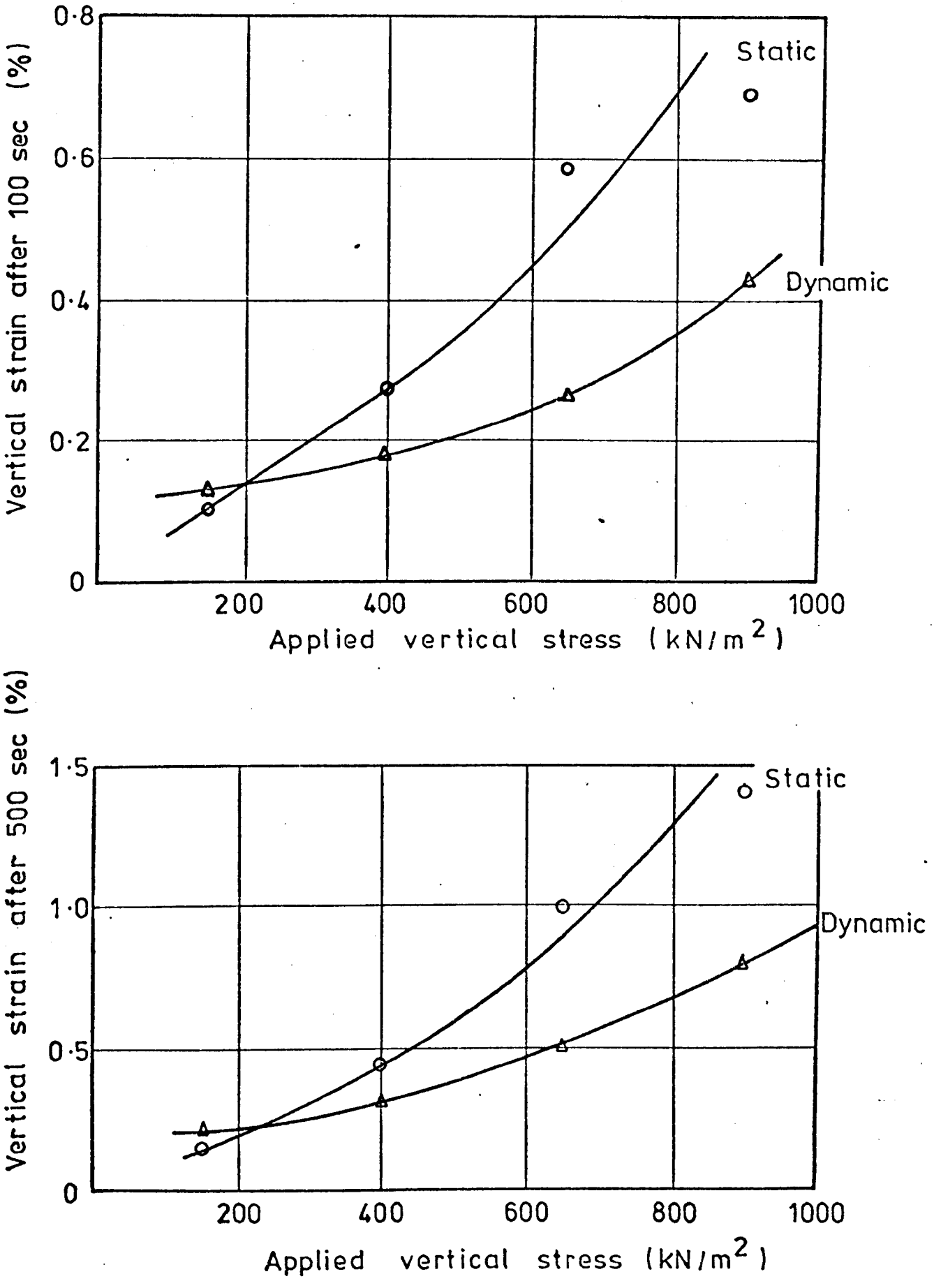

FIGURE 3.2 COMPARISON OF RESULTS FROM DYNAMIC TESTS AND CREEP TESTS AT 20°C (AFTER SNAITH (22))

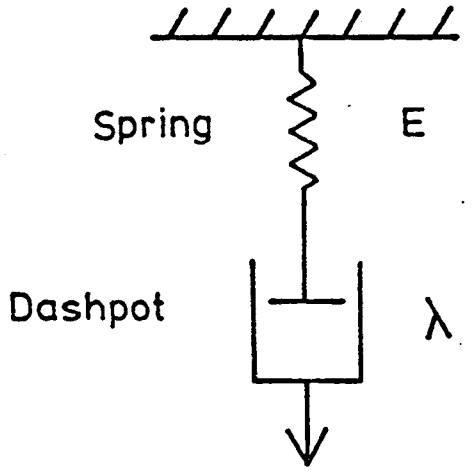

(a) Maxwell model

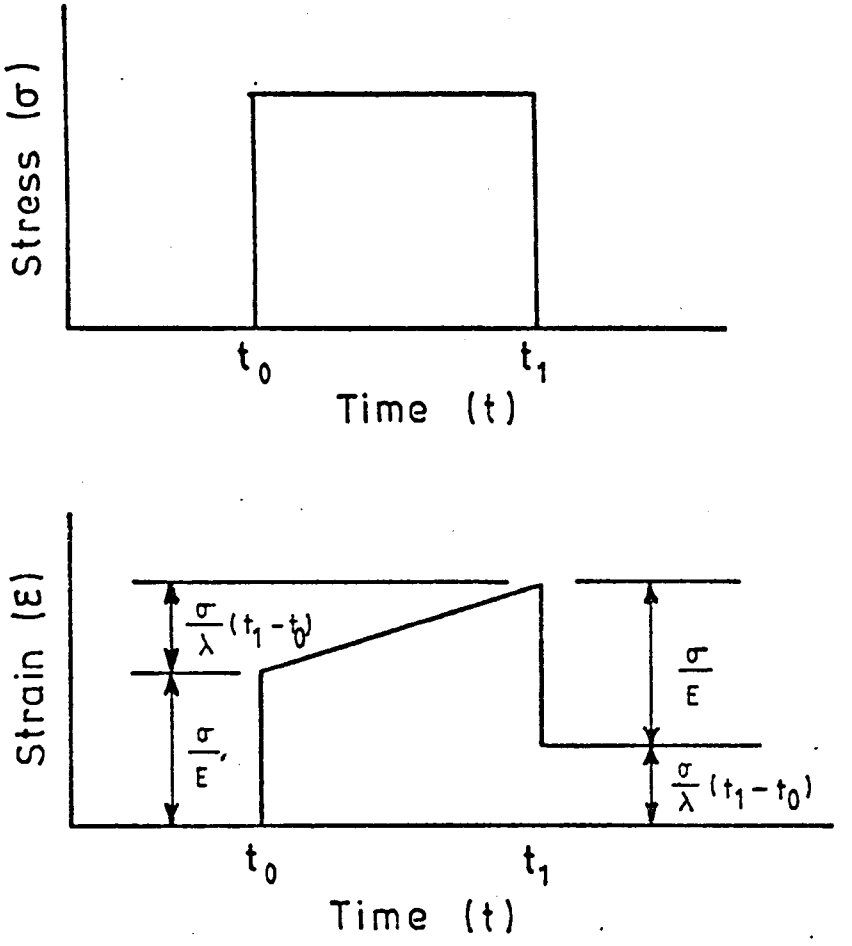

(b) Response

FIGURE 3.3 MAXWELL MODEL OF VISCO-ELASTIC BEHAVIOUR

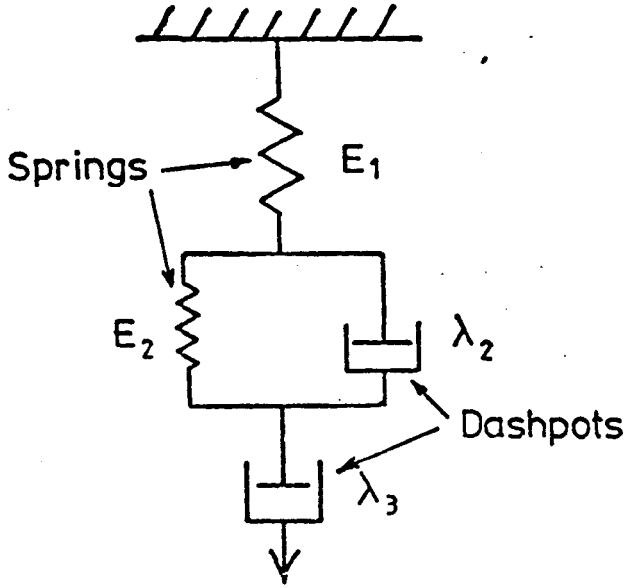

(a) Burgher model

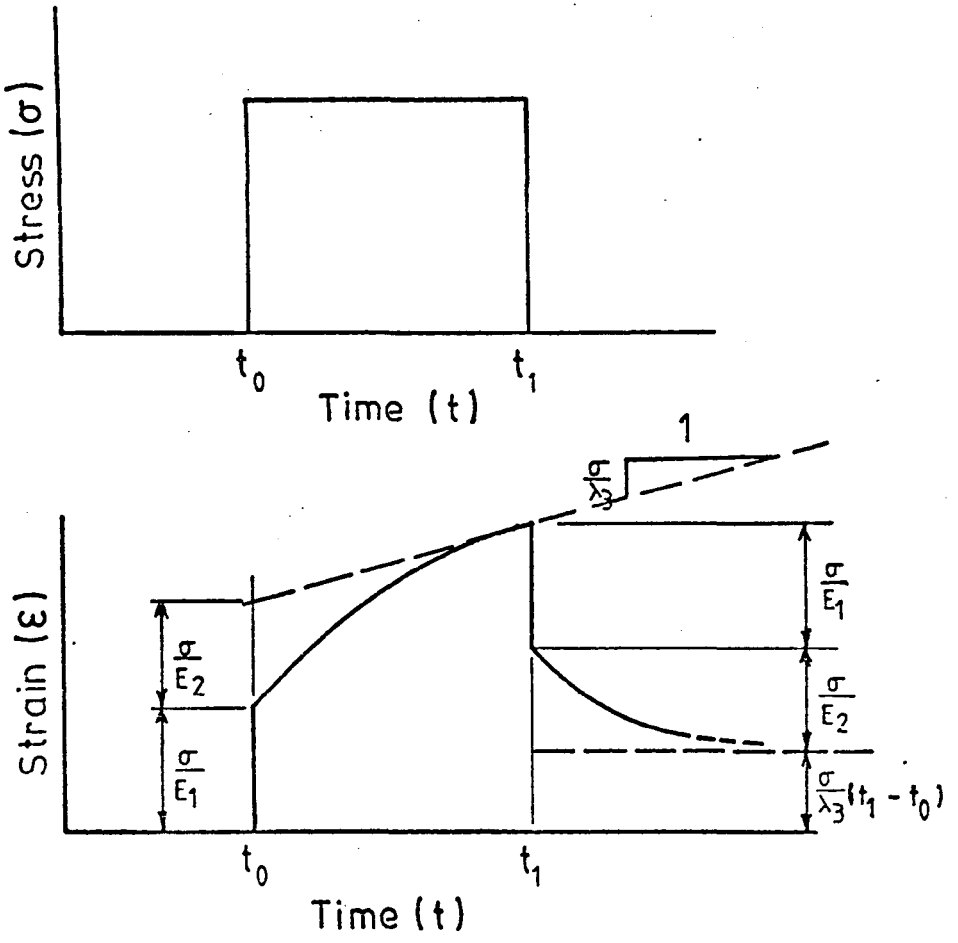

(b) Response

FIGURE 3.4 BURGHER MODEL OF VISCO-ELASTIC BEHAVIOUR

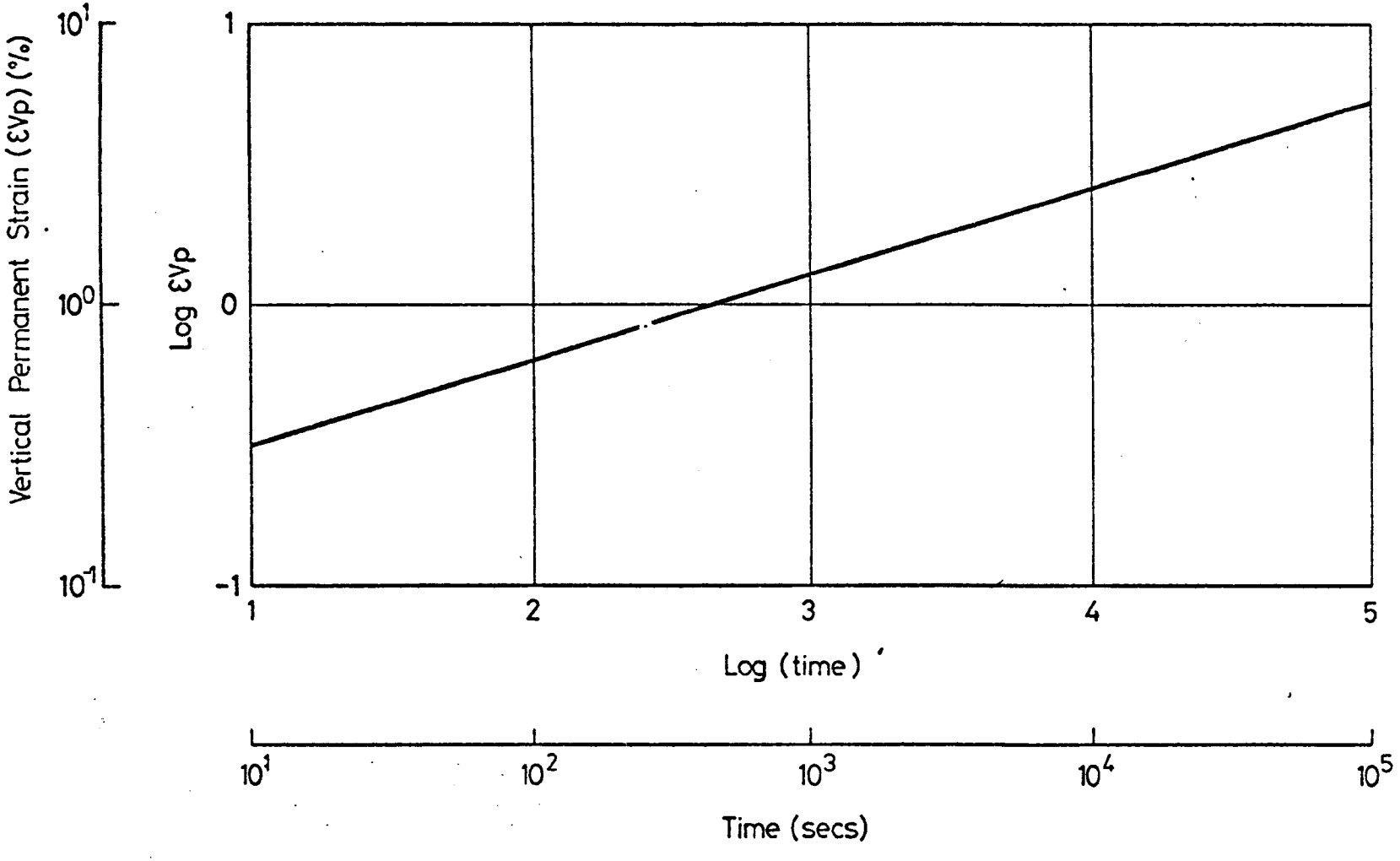

FIG. 3.5 IDEALISED LOGARITHMIC PLOT OF VERTICAL PERMANENT STRAIN VERSUS TIME

CHAPTER FOUR

THE PAVEMENT WHEEL LOADING FACILITY

4.1 INTRODUCTION

The loading facility was designed by a colleague (17, 18) to simulate a realistic loading of a pavement by moving vehicles. The reader is referred elsewhere (18) for more detail. The main part of the apparatus is shown in Figure 4.1. Also shown, as an insert, is a sketch plan of the facility, to show its position relative to the test pavement. A wheel was mounted on a loading carriage which travelled between two 'I' section guide beams, in the direction shown in the Figure. The whole assembly could be moved at right angles to this direction by a traversing facility, so that a lateral distribution of wheel passes could be simulated.

The assembly was located in a laboratory, 10m x 4.5m, which resulted in a maximum distance of travel of 6.7m in the longitudinal direction, consisting of 2.4m for acceleration, 1.9m at constant speed, and the remainder for deceleration before reversal. A constant speed of 14 km/hr was used for the experiments, although higher (and lower) speeds were attainable, with changes in the acceleration, deceleration and constant speed portions. A load of nominally 10 kN was applied through a heavy duty forklift truck tyre at an inflation pressure of approximately 600 kN/m^2, resulting in a contact area approximating to an ellipse 180mm x 130mm.

A false insulating ceiling was installed, to reduce the air volume around the facility, and the pavement temperature was maintained at $30^{o}C$, although higher temperatures could be achieved.

4.2 THE TEST PIT

The pavements were installed in a pit, 2.4m wide x 1.5m deep. For the first pavement the pit was 4.9m long, but for subsequent ones it was extended to 7.2m by excavating 300mm at each end. A 150mm layer of lean concrete was placed at each end, as shown in Figure 4.2. The pit was lined with concrete and waterproofed with a liquid sealant and overlapping strips of 'Bituthene'.

The first two pavements consisted of 150mm of DBM directly over the subgrade material, or the lean concrete, and the third pavement of 225mm of DBM directly over the subgrade (150mm over the lean concrete). The surface of the DBM was in each case level with the laboratory floor. Details of the instrumentation and the materials are given in the following Chapters.

The loading facility was dismantled following the testing of each pavement, and reassembled once the next pavement had been constructed. Improvements were made to the facility without interrupting the test programme and the final version is described briefly in the following sections.

4.3 THE LOADING CARRIAGE

A rectangular aluminium chassis carried the guide bearings and the wheel loading assembly (Figure 4.3). Vertically mounted bearings transmitted forces between the carriage and the lower flanges of the beams, and horizontally mounted ones maintained the alignment of the carriage between the webs of the beams.

A dual triangular lever arrangement was used to apply the wheel load, as shown in the Figure. The power for the rams in this system came from a self-contained hydraulic system (Figure 4.3b). The pressure required to produce a load of approximately 10 kN was set by the control valve, this having been checked against the output from

strain gauges mounted on the guide beams (Figure 4.1), which had been previously calibrated.

4.4 CABLE AND HYDRAULIC DRIVE SYSTEMS

A central plate was bolted across the top of the guide beams, which provided additional rigidity, but served as a mounting for the drive mechanism. A grooved drum was mounted in bearings on the plate with a cable passing at least four times around itself, around pulleys at the ends of the guide beams, and attached to the carriage via tensioning rods (Figures 4.1 and 4.3). Rotation of the drum caused the carriage to move between the beams.

The drum was driven by hydraulic power by means of an oil pump, hydraulic motor and a servo-valve. The motor and servo-valve were mounted on the central plate and linked to the drum with a flexible coupling, and to the pump with flexible pipes. The motor and servo-valve were connected with a distribution block. The precise action of the servo-valve controls the direction and rotational speed of the motor and hence the drum. Response was excellent due to the proximity of the components and the low inertia of the rotating parts.

The control of the electrical signals to the servo-valve, which controlled the movement of the carriage is discussed in the next section.

4.5 ELECTRONIC CONTROL SYSTEM

This consisted of a small control unit with both automatic and manual controls. The velocity of the carriage could be adjusted for the automatic mode, and the position for the manual mode. A gain control could be operated in both modes to provide a smooth response. A counter monitored the number of wheel passes and an emergency stop button could be used if necessary to cut out the pump. The unit continually compared output signals to the servo-valve, with input

signals from a tachogenerator which was connected to the motor shaft (giving the velocity), and from an LVDT position transducer, ensuring precise control.

Safety circuits were incorporated to cut out the hydraulic pump, and operated in the event of carriage over-travel, cable failure, excessive speed at each end of the travel, accidental engagement of both control modes, and loss of supply to the electronics system. Large springs welded at the ends of the guide beams prevented damage to the carriage in the event of over-shoot, with the possibility of rebounding it back into the operating range.

4.6 THE TRAVERSING FACILITY

This was incorporated to enable a realistic transverse distrib-:ution of wheel passes to be simulated, and was capable of controlling movement of the whole loading facility perpendicular to the direction of travel of the wheel, over a 900mm width of pavement. For the pavement multi-track experiments, a normal distribution of wheel passes was simulated over a 600mm width.

The transverse motion was produced by long stroke hydraulic rams connected to the bogies at each end of the guide rails (Figure 4.4). Movement was controlled by a unit which was pre-set so that any desired number of wheel passes (up to 9,999) could be produced in each of nine positions. Positional feedback of the facility was again through an LVDT.

The nine lateral positions could be set at various spacings within the total possible width. A spacing of 75mm was used for a 600mm width, and ensured approximately 50 per cent overlap of tyre contact areas in adjacent wheel paths. When each of the nine positions had been loaded, the carriage was stopped and a new programme pre-set on the control unit. This was repeated until the total number of wheel passes required

was achieved.

An operational disadvantage was that up to five passes could be completed when changing position, and this was significant in the early stages of a test when the number of passes required at each position was small (less than 30 at the outside positions). This problem could be overcome by operating the rams by a manual switch when the wheel was at the ends of its travel, away from the instrumented area of the pavement, viz, below the constant speed zone.

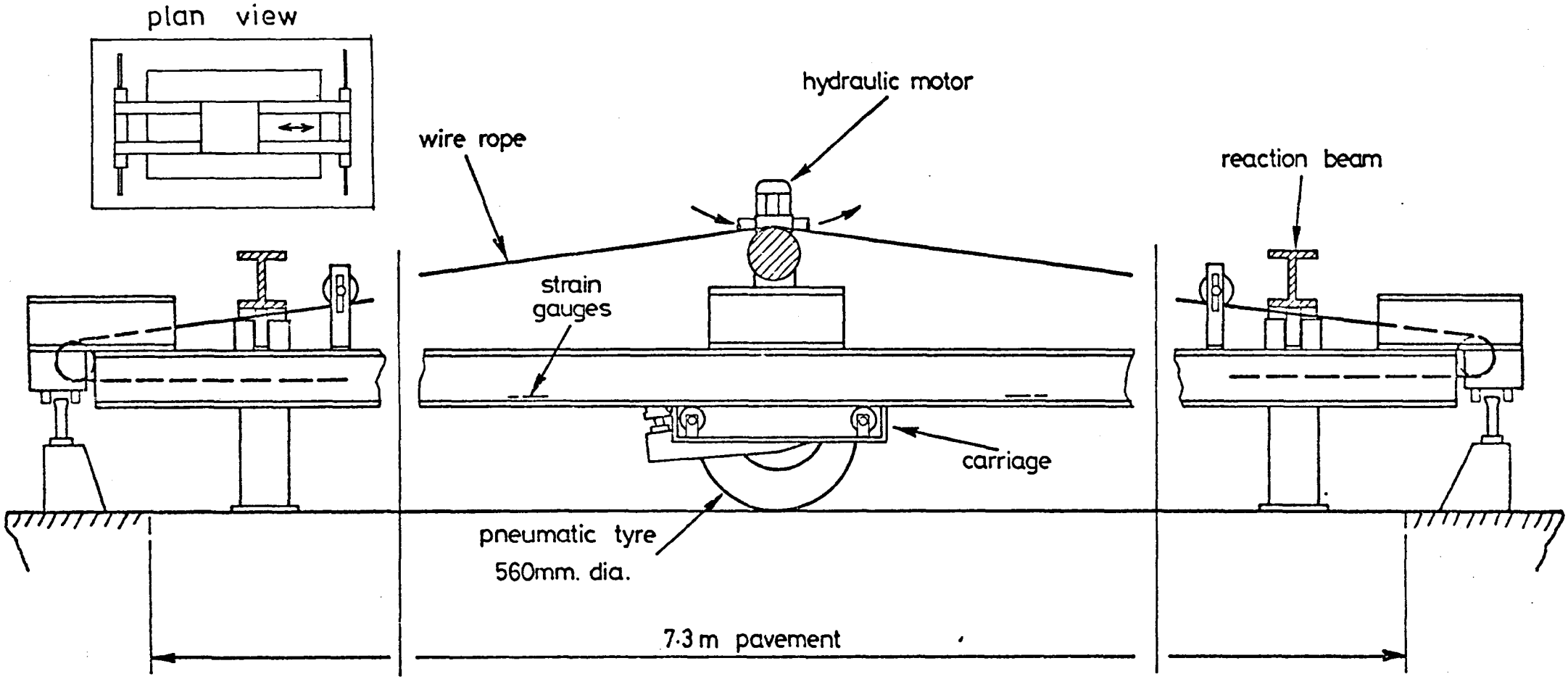

FIG. 4.1 SIDE VIEW OF PAVEMENT TESTING FACILITY

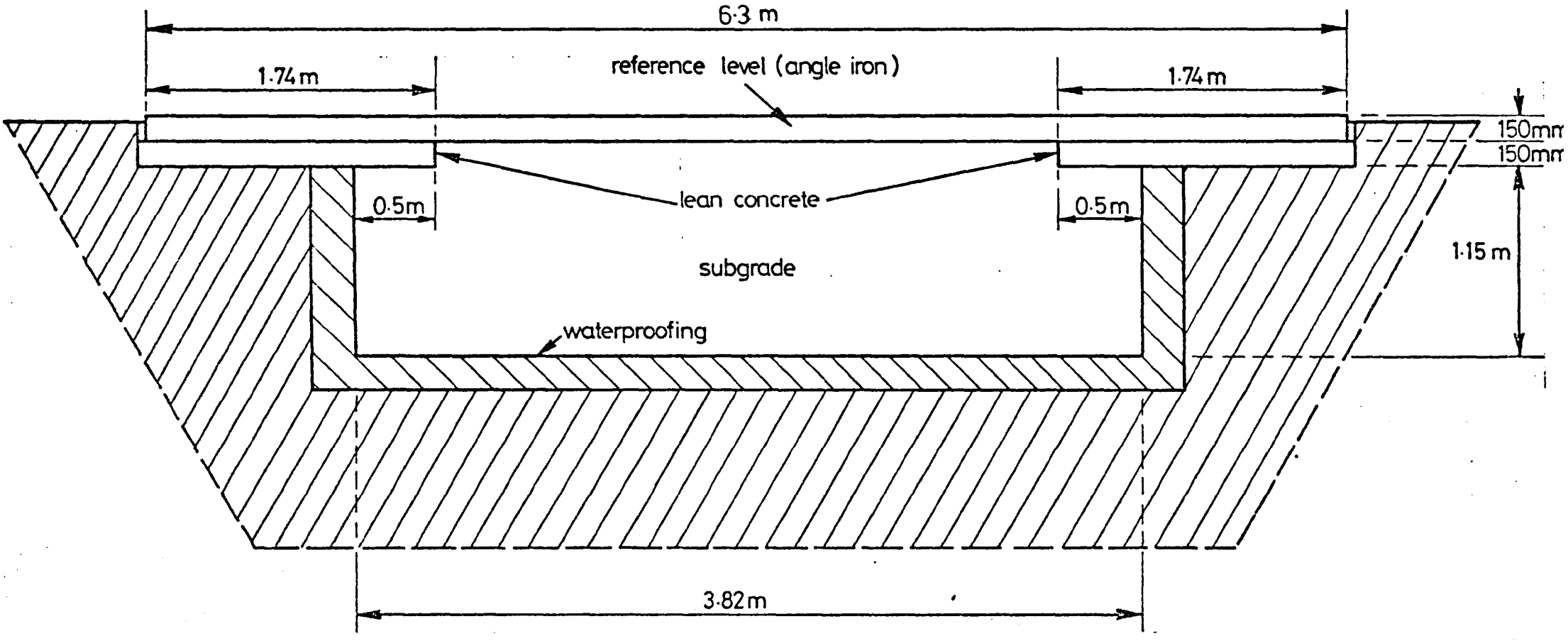

Note : pavement surface is at reference level

FIG. 4.2 SIDE VIEW OF EXTENDED PIT

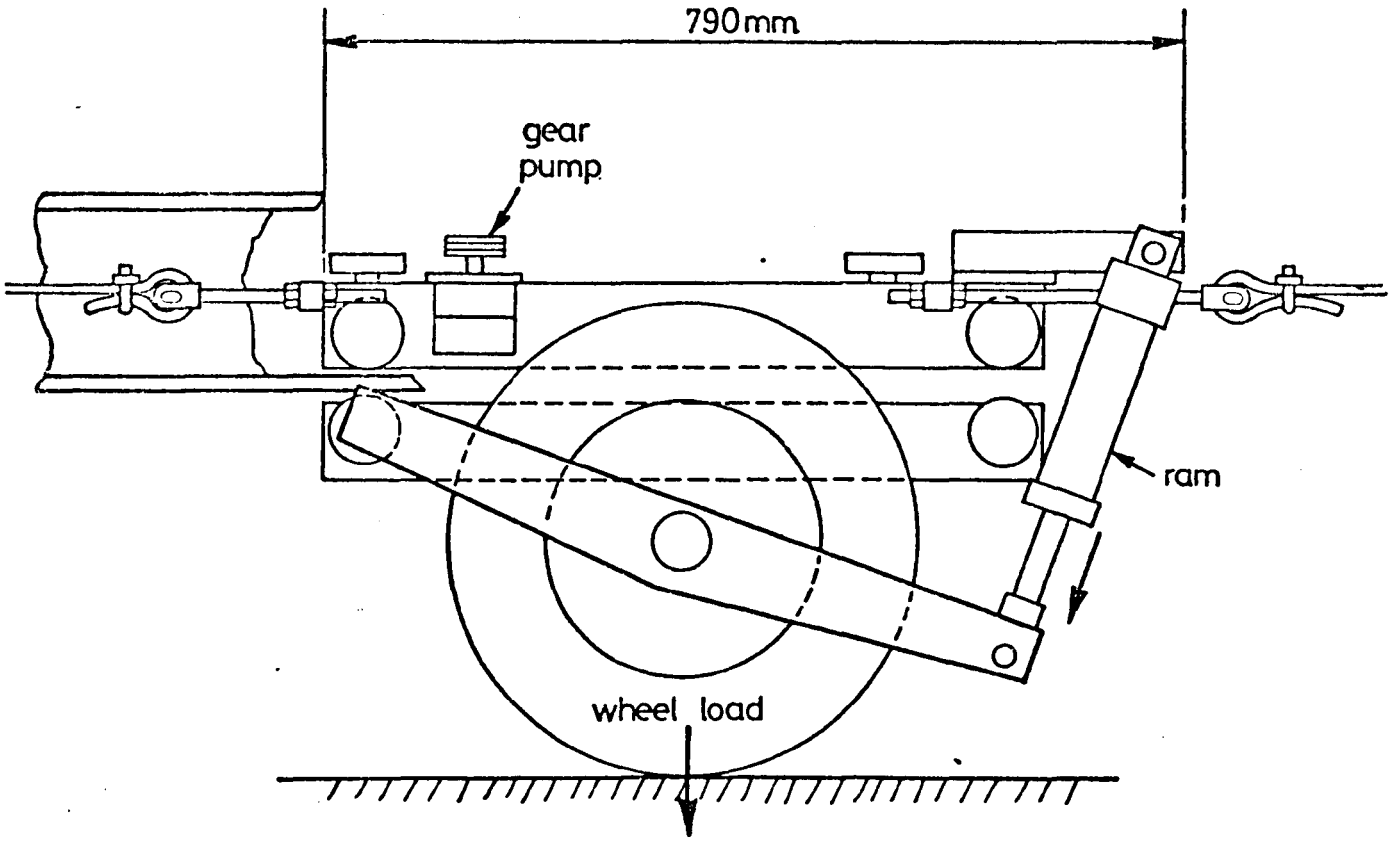

(a) LOADING SYSTEM

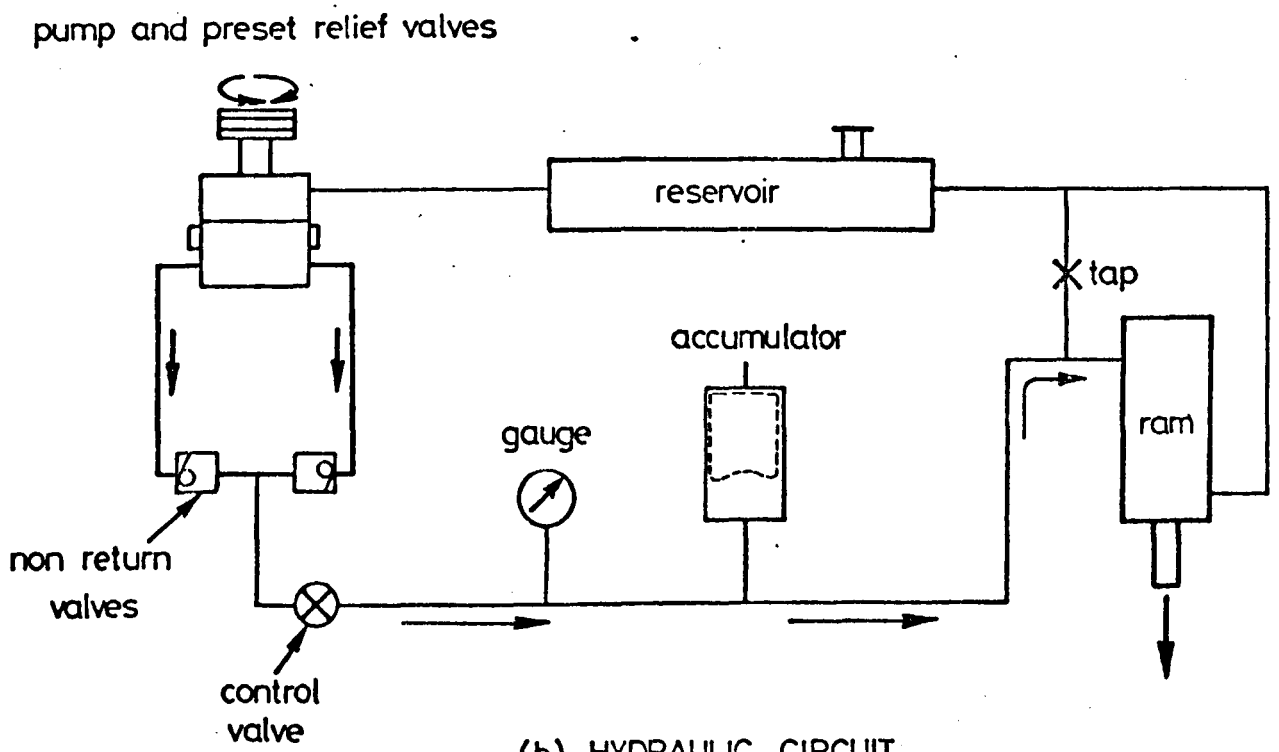

(b) HYDRAULIC CIRCUIT

FIG. 4.3 LOADING CARRIAGE

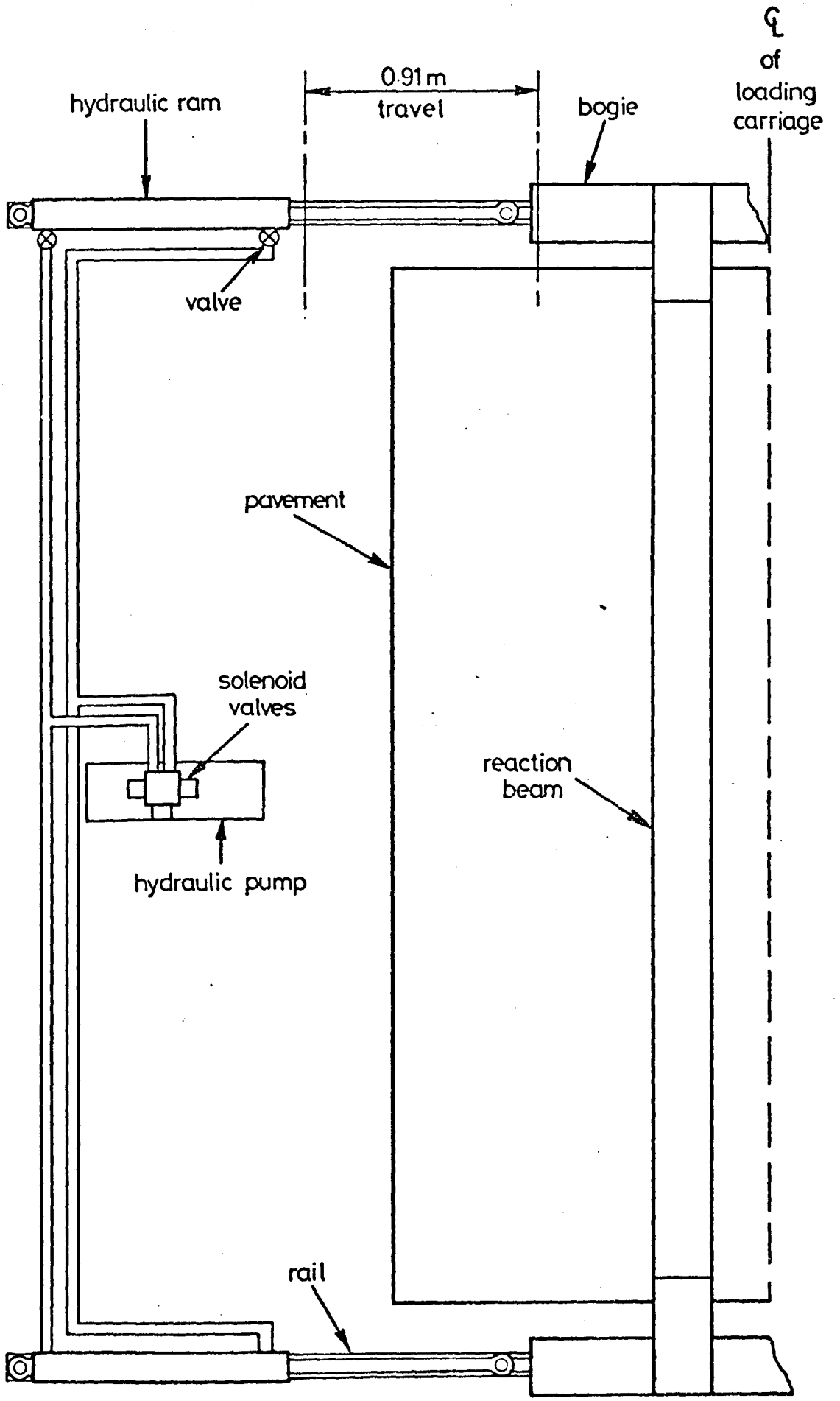

FIG. 4.4 TRAVERSING FACILITY

CHAPTER FIVE

PAVEMENT INSTRUMENTATION

5.1 INTRODUCTION

Stress and strain measuring instrumentation had been well investigated at Nottingham University in previous years (70, 71, 72). For the three pavements tested in connection with this work, the instruments that were installed are given in Table 5.1, together with their use and the material in which they are installed. The 'registration' for each instrument is also given, which gives a measure of the difference in readings obtained when the instrument was introduced into the material, compared to that obtained when it was calibrated mechanically in air.

The reader is referred elsewhere for details of instrument calibration (71, 72). Installation of the instruments in the pave-:ments will be described in the next Chapter.

The following parameters were measured:

Elastic strains.

Permanent strains.

Surface elastic deflection.

Surface permanent deformation.

Stresses.

Temperature.

5.2 STRAIN MEASUREMENT

Primarily, the permanent strain distribution with depth was required, so that the accuracy of prediction techniques could be assessed. The distribution was measured with continuous vertical stacks of strain coils. The contribution of each pair of coils was continuously monitored at frequent intervals during each test and

TABLE 5.1 APPLICATION OF PAVEMENT INSTRUMENTS

Instrument	Measurement	Material	Registration
Strain coils	permanent strains elastic strains	bituminous layer and subgrade	1.0
Strain gauge carrier blocks	elastic strains	bituminous layer	In situ calibration in material specimens
Strain cells	permanent strains elastic strains	subgrade	0.87 0.82
Pressure cells	stresses	bituminous layer and subgrade	0.94 0.92
Accelerometers (a) Servo type (b) Piezo-electric type	elastic vertical deflection	pavement surface	Manufacturer's calibration Bench calibration
Thermocouples	temperature	bituminous layer and subgrade	direct reading

recorded.

The strain coils also gave elastic strain measurements, which were supplemented by strain gauged carrier blocks in the DBM, and by Nottingham strain cells in the subgrade. The strain cells also measured permanent strains. The strain gauges could not be used to give permanent strains, because of inherent drift in their output.

Horizontal elastic and permanent strains were measured in the longitudinal and transverse directions, with a coplanar arrangement of strain coils, and with strain gauges on carrier blocks. These measurements were primarily at the DBM/subgrade interface but some were also taken within the DBM with strain gauged blocks.

5.3 SURFACE DEFLECTION AND DEFORMATION MEASUREMENT

Elastic deflections were measured with both a servo and a piezo-electric accelerometer. The manufacturer's calibration was used for the servo device, but the piezo-electric device was calibrated on a vibrator. The outputs from both were electronically double integrated, the resulting output being related to elastic deflection. This type of instrument and its related equipment had not been used before, and unfortunately meaningful results were not obtained.

Surface deformation was measured with a surveyor's level in the first pavement, but for subsequent pavements a profilometer was developed (Figure 5.1). This consisted of a displacement transducer attached to a sliding block which ran on a stiff guide rail. The dual wheel arrangement which was fixed to the sliding shaft of the transducer followed the profile of the pavement surface when traversed.

5.4 STRESS MEASUREMENT

Vertical and horizontal stresses were measured with Nottingham pressure cells, whose performance was well understood when placed in

a soil mass (72). These were used in the subgrade in the first two pavements and also in the DBM in the third pavement. A problem existed in obtaining a suitable value of cell registration for the latter application, since the cells were designed for a different type of material with a much lower stiffness, and theoretical considerations indicated that large under registration may occur in the stiffer bituminous material. A cell was calibrated in a 150mm diameter DBM specimen using the same installation technique employed in the pavement. The registration value obtained by this method was used to assess the results. Subsequent research (73) verified that the cells can be used in bituminous materials provided that a realistic calibration technique is used.

5.5 TEMPERATURE MEASUREMENT

Copper-constantan thermocouples were used to measure temperature in the DBM, where it was important to ensure minimal deviation from the chosen test temperature of 30°C. These were connected to a continuously sampling single point chart recorder, which also recorded output from a reference thermocouple which was immersed in a water bath at 30°C.

5.6 RECORDING EQUIPMENT

Permanent strains from the strain coils were obtained from a reading on the maker's balancing box. Elastic strains from the coils and strain cells, the stress measurement, and wheel load outputs from the strain gauging of the guide beams, were recorded on an Ultra-Violet recorder. Permanent strain from the strain cells was indicated on a digital voltmeter (DVM). A second UV recorder monitored outputs for the elastic strain from the strain gauges.

A storage oscilloscope was used for examining the response of

those instruments developing sufficient output. In particular, the velocity of the wheel could be examined, and the output from the accelerometer.

The profilometer output was monitored on a DVM and outputs compared with that obtained at a fixed reference point each time a set of readings was taken.

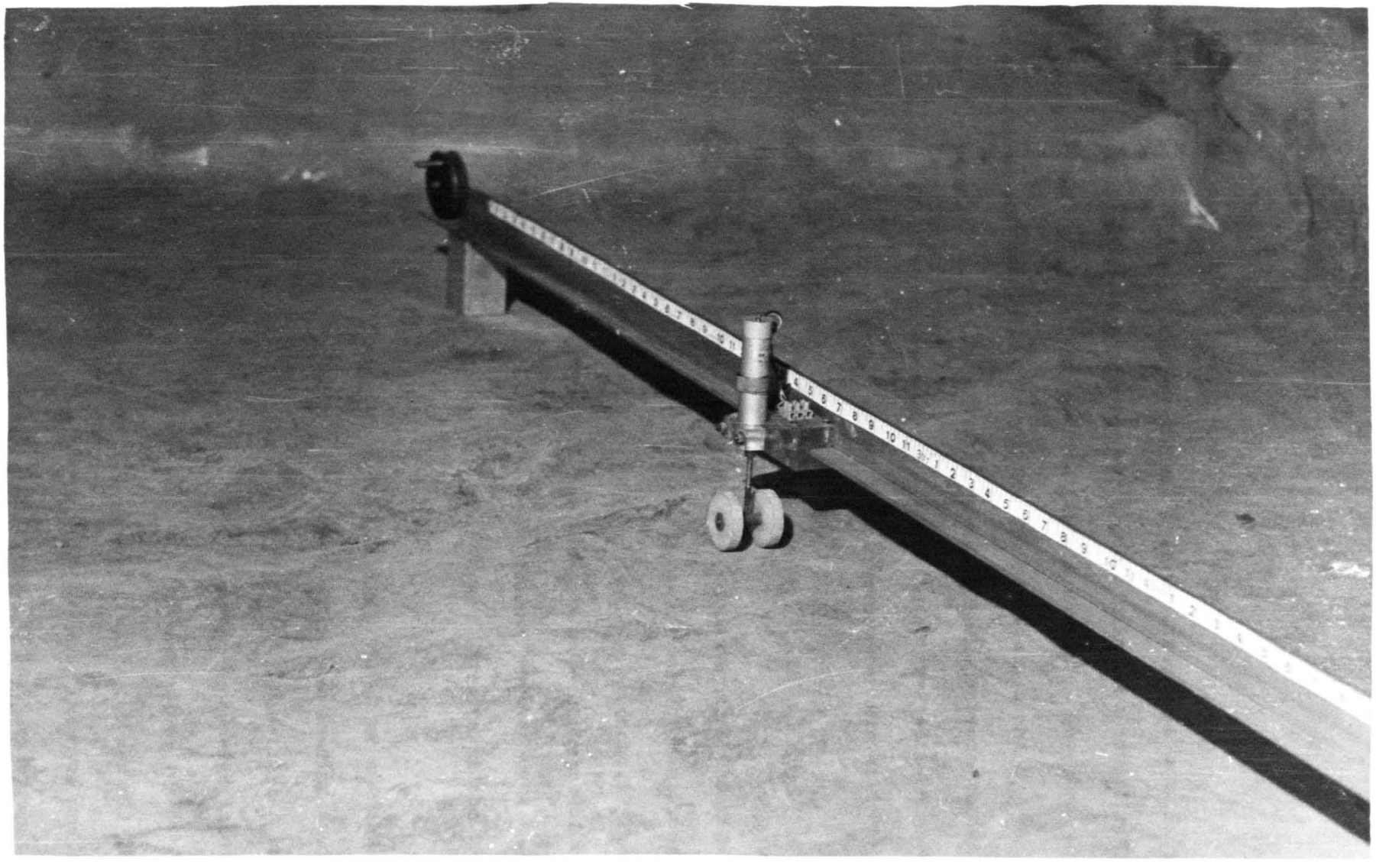

FIGURE 5.1 PROFILOMETER

CHAPTER SIX

THE PAVEMENT EXPERIMENTS

6.1 INTRODUCTION

The three test pavements were all 2-layer structures consisting of a silty clay subgrade of Keuper marl, and a main structural layer of dense bitumen macadam (DBM). The DBM was nominally the same mix in all cases, and nominally 150mm thick for pavements 1 and 2, and 230mm for pavement 3. A 150mm thick layer of lean concrete, 1.75m long was installed at each end of the test pit for the tests on pave-:ments 2 and 3. The composition of these three materials will be given in the next section.

All the pavements were tested at 30°C.

Two types of test were conducted on each pavement. The first and main test was a mul+i-track test, in which a 'normal distribution' of wheel passes was applied about the centre of the pavement. The second was a single track test, carried out on a separate part of the pavement, consisting of the same number of passes that had been applied along the central path in the multi-track test. Details of the test-:ing programme will be given in a subsequent section.

The wheel load was intended to be nominally 10 kN at a speed of 14 km/hr. However, during commissioning of the wheel loading facility, which included the tests on pavement 1, small bore pipes limited the response of the rams on the carriage, resulting in an average load of 15 kN. Subsequent modifications reduced the average load to 11 kN for pavements 2 and 3. The speed was consistently 14 km/hr for all three pavement experiments. The contact pressure between the tyre and the pavement surface for each pavement was determined from measurement of the contact area and the known value of the load. For the three pave-

:ments, the average values were 660 kN/m^2, 550 kN/m^2, and 550 kN/m^2 respectively.

Various measurements were taken throughout each test, using the instrumentation described in the previous Chapter. The locations of the instruments will be given in a subsequent section.

6.2 PAVEMENT MATERIALS

6.2.1 Dense Bitumen Macadam

This was a 28mm nominal size basecourse mix, and complied with the Specification for Road and Bridge Works (74)*. The aggregate was a crushed rock, and the bitumen 100 pen grade. Grading curves for the three pavements are shown in Figure 6.1, which also shows the specified grading limits. The curves are based on average values obtained from sieve analyses on several samples of aggregate obtained from cores of the material. Thus, the curves are not a true representation for the larger stones, a considerable number of which were reduced in size during the sawing of the core. Table 6.1 shows the average binder contents and void volumes measured from a number of cores, for each pavement.

Table 6.1

Pavement	Binder Content (%)	Void Content (%)
1	4.7	5.2
2	4.9	9.7
3	5.0	8.3

* The specification for coated macadams is now given by BS 4987 (75).

The DBM mix also complied with the specification (74) for a 28mm nominal size road base mix, which has an identical aggregate grading (binder content range 4.0 - 5.0% compared to 4.2 - 5.2% for a basecourse mix).

The material was supplied and laid by Tarmac Roadstone Holdings Ltd. Due to the limited access to the laboratory, and the small area to be paved, compaction was carried out with a small vibrating roller. A compaction trial had been carried out prior to the installation of the first pavement, and this had indicated that such a roller would be suitable. The variation in level of the finished surface depended to a large extent on the proficiency of men carrying out the work.

6.2.2 Keuper Marl

This was a silty clay with low to medium plasticity. Some basic properties are shown in Table 6.2. Approximately 35 tonnes of material was required to fill the test pit to the required level. The material was obtained in the form of unfired bricks, which had a moisture content slightly higher than the optimum. Compaction of the material was carried out in 125mm layers with a single headed and a triple headed pneumatic tamper.

The dry density versus moisture content relationship for the material, obtained from a British Standard Compaction Test (76) is shown in Figure 6.2. The Figure also shows four zones representing values obtained from 125mm x 100mm diameter cores, which were taken for the characterisation tests. Zone 1 represents those cores which were taken after the compaction of each 125mm layer. It was found that the clay lost moisture during the testing of a pavement and became more dense due to trafficking and compaction of the DBM (zones 2 and 4). Following the completion of the testing of a pavement, the central area of the DBM was removed in slabs by use of a saw, which required water as

a coolant. This operation caused saturation of the subgrade surface and necessitated the removal and replacement of 150mm of the material for pavement 2 (zone 3), but no replacement was necessary for pavement 3 where the thickness of DBM was greater.

Table 6.2 Results of Basic Tests on Keuper Marl

Liquid Limit	30%
Plastic Limit	16%
Plastic Index	14%
CBR	5%
Sieve Analysis:	
Percentage by weight retained on No. 200 sieve	52%
BS Compaction Test:	
Maximum Dry Density	1880 kg/m^3
Optimum Moisture Content	15.2%

6.2.3 Lean Concrete

This also complied with the Specification for Road and Bridge Works (74). An aggregate to cement ratio of 15:1 was used, with 40% of the aggregate passing a 5mm sieve, and a nominal maximum size of 19mm. The material was mixed and laid by the University laboratory staff, using a small vibrating roller and vibrating plates for compaction. Cubes were prepared from the mix, and the required 7 and 28 day strengths were well exceeded. Beams of the material were also prepared and tested non-destructively to give values of the dynamic modulus of elasticity, and Poisson's ratio. The 28 day values were 29,600 MN/m^2 and 0.24 respectively.

6.3 INSTRUMENTATION LAYOUT AND INSTALLATION

6.3.1 General

The layouts for each pavement are shown in Figures 6.3 to 6.5. An area of pavement approximately 1.4m x 0.6m was instrumented for each pavement to a depth of 300mm in pavements 1 and 2 and 344mm in pavement 3. The intensity of instruments increased from pavements 1 to 3. For all the pavements the emphasis was on strain measurement, with the majority of instruments, for strain measurement, concentrated along the centre line of the pavements. Stress measurement was limited to the subgrade for the first two pavements, but was attempted in pavement 3 by use of five pressure cells.

Where possible, the separation of pressure cells and strain cells was 300mm. The exception to this was for pavement 3 (Figure 6.5) where a separation of 150mm was necessary in order to position the cells in the space available. As many replicate measurements as possible were taken, which was governed by availability of instruments and the space available within the test section of the pavement. To eliminate disturbance to the electro-magnetic coupling of the strain coils, strain and pressure cells had to be isolated from the coils by at least three times their gauge length.

Instruments which were installed in the subgrade were placed in holes at the required depth and care was taken to replace the material at a similar compaction to the surrounding material. The cables for these instruments, and for those positioned at or near the interface between the subgrade and the DBM were buried just below the subgrade surface and channelled to an outlet at the edge of the test pit which was linked to the monitoring equipment. Instruments installed in the bituminous layers during construction were surrounded with fine material as were their cables, to avoid damage due to penetration of sharp stones. Some instruments were installed at the pavement surface after

construction, in which case they were placed in indentations (formed by blocks or bars of metal which had been rolled into the surface) and covered with a hot sandsheet mix. During construction of the DBM layer several passes of the roller were made before the vibrator was switched on, in order to achieve light compaction to stabilise the positions of the instruments, before heavy compaction was started.

6.3.2 Strain Coils

One vertical stack of 25mm diameter coils was installed in pave-:ment 1, nominally 25mm apart, and over a total depth of 300mm. In addition, two 50mm diameter coils were installed at the top and bottom of the DBM layer. The maximum theoretical spacing of strain coils in coaxial alignment is four diameters (77) and a practical minimum spacing is governed by the material. It was found that a 25mm spacing was too small, since some pairs of coils in pavement 1 became closer together during compaction of the DBM, and during the later stages of the pavement tests these became difficult to balance. Therefore, a spacing of 38mm was used in pavements 2 and 3, in each of which two vertical stacks were used. Similar to pavement 1, two 50mm coils were installed, at the top and bottom of the DBM layer, in pavements 2 and 3. Also, a 50mm coil was installed in the clay at the same depth as the lowermost 25mm coil.

For ease of installation of the 25mm diameter coils in the DBM, these were attached to carrier blocks of sandsheet or DBM (Figure 6.6). Sandsheet blocks were used in pavement 1 and DBM blocks, cut from the materials used in the previous pavement, were used for pavements 2 and 3. This change was made in order to try and match the deformation characteristics of the carriers with the surrounding material. The positions of the blocks can be seen in Figures 6.3 to 6.5. Those which were installed in the interior of the DBM were held in place with a small amount of sandsheet and subsequently surrounded with selected DBM,

without the larger stones.

The vertical stacks of 25mm coils provided a distribution of elastic and permanent strain with depth. The sum of the individual permanent deformations occurring between all these coils could be compared with the surface deformation measured with the profilometer or level. Additionally, the sum of the deformations measured by the 25mm coils in the DBM could be compared with that measured by the 50mm coils across the total depth. Similarly, in pavements 2 and 3 the total deformation in the subgrade could be measured by both the 25mm and the 50mm coils.

In addition to the coils measuring vertical strain, both 25mm and 50mm coils were included at the interface in pavements 2 and 3 to measure radial strains (Figures 6.4 and 6.5).

6.3.3 Strain Gauges

Strain gauges were installed only in the DBM. In pavement 1, gauges for measuring horizontal strains at the interface were mounted on sandsheet carrier blocks, whereas those for measuring vertical strains were mounted on DBM blocks. In pavements 2 and 3, DBM blocks were used throughout, since the sandsheet blocks were found to distort badly in pavement 1. Details of the carrier blocks are given in Figure 6.6. Two gauges were installed in a recess, at the surface of pavement 2, which had been formed by rolling a block of metal into the surface during construction. The recess was filled with selected reheated material from the same pavement. The same installation technique was used with the strain gauged carrier blocks as had been used with those carrying coils.

Dummy gauges were mounted on a 100mm diameter core of the DBM, which was sawn in half to give a flat surface for ease of attachment. The ungauged half was recessed to give clearance of the gauges and connections, and the two sections were bound together with adhesive

tape. The tape also served to prevent collapse of the core when replaced in the pavement, since it was no longer a tight fit and would otherwise be unsupported at the test temperature of 30°C.

6.3.4 Pressure Cells

Installation in the subgrade was achieved by cutting recesses or slots in the material, for cells measuring vertical and horizontal stresses respectively, and compacting carefully where necessary. For installation in the DBM, the cells were positioned with a hot sandsheet mix ensuring that the diaphragm was covered with fine material and therefore not subjected to larger stones which could produce stress concentrations.

6.4 PAVEMENT LOADING PROCEDURE

A reference grid was established for each pavement, Figure 6.7 showing that used for pavement 3. The main lines were the longitudinal and lateral centre lines. Once these had been marked, a comprehensive grid was marked out, with white road paint, composed mainly of 150mm and 300mm spacings. At each side of the pavement, a heavy steel angle section, which protected the edge of the pit, provided reference points for the levelling procedure and profilometer for the surface deformation measurements.

The unloaded wheel was then adjusted to run along the longitudinal centre line of the pavement, which was the central track of the multi-track test. This test comprised of another four track positions to each side of the centre line at 75mm spacings, resulting in nine positions in all covering a 300mm width of pavement. The 75mm spacings resulted in an overlap of approximately 55mm between adjacent wheel paths, since the tyre contact area was approximately 180mm x 130mm.

The distribution of wheel passes in the nine positions approx-:imated to a normal distribution, with a total of 100,000 passes.

This total was approached as randomly as possible. The first loading stage applied a total number of 100 passes, across the 300mm width of pavement, subdivided into nine discrete numbers which formed the basis of all subsequent totals, as shown in Table 6.3. Subsequent loading stages were such that the final total was approached in stages which were approximately evenly spaced on a logarithmic scale. This enabled surface deformation measurements to be taken at intervals compatible with the response of the pavement.

For pavement 1, the wheel was stopped after the required number of passes had been achieved in each wheel track, and moved to the adjacent track manually before loading was recommenced. This traversing was from position 9 to position 1 taken in order, for each loading stage. The number of passes applied in each loading stage was as shown in Table 6.3 until 10,000 were completed, and then the remaining passes were accumulated in stages of 5,000.

For pavements 2 and 3 traversing was mechanical and a more random loading could be applied than had been used for pavement 1, as may be seen in Table 6.3. The first 1,000 passes were achieved using a manual switch to control the traversing, but, complete automatic control was used for the remainder which was carried out in steps of 1,000 passes.

The wheel was unloaded and positioned away from the test area on completion of each loading stage, to permit complete freedom of movement for levelling or use of the profilometer. Readings were taken at all of the grid points shown in Figure 6.7.

On completion of the multi-track test, a single track test was performed on an untrafficked length of pavement, as indicated in Figure 6.7. The total number of passes was at least that which had been applied in the central position, 5, in the multi-track test, viz 22,000. In pavement 1, 44,000 passes were applied. Similar to the multi-track tests, surface deformation measurements were taken at approximately evenly spaced increments on a logarithmic scale.

6.5 READOUT PROCEDURE

The outputs from the pavement instruments were zeroed and readings of lateral and longitudinal profile were taken before the loading began and after a temperature equilibrium at 30°C. had been reached. Measurements of permanent strain and pavement profile were then taken at the intervals defined by the loading stages. The pavement surface was examined at each interval for possible cracking. Stress and elastic strain measurements were taken at regular intervals during loading for both situations when the wheel travelled in a track directly above the instrument (on-axis) or, when in a track laterally displaced from the instrument (off-axis). Since each pair of strain coils had to be balanced individually, due to different separations at installation, the acquisition of an elastic strain distribution from them was a lengthy procedure. Thus, in the early stages of a test when data acquisition time was minimal, only the more responsive coils in the subgrade and at the interface were monitored, with additional measurements from the DBM if time allowed. On completion of 5,000 passes it was possible to monitor the response of all the instruments within approximately 30 wheel passes.

TABLE 6.3 DISTRIBUTION OF WHEEL PASSES

Lateral total	Position								
	1	2	3	4	5	6	7	8	9
100	3	6	12	18	22	18	12	6	3
200	3	6	12	18	22	18	12	6	3
500	9	18	36	54	66	54	36	18	9
1000	15	30	60	90	110	90	60	30	15
2000	30	60	120	180	220	180	120	60	30
5000	90	180	360	540	660	540	360	180	90
10000	150	300	600	900	1100	900	600	300	150
20000	300	600	1200	1800	2200	1800	1200	600	300
50000	900	1800	3600	5400	6600	5400	3600	1800	900
70000	600	1200	2400	3600	4400	3400	2400	1200	600
100000	900	1800	3600	5400	6600	5400	3600	1800	900
Accumulated total =	3000	6000	12000	18000	22000	18000	12000	6000	3000

These passes were applied in the following order for pavements 2 and 3:

Sequence	9	6	7	3	1	4	2	5	8

All lateral totals were accumulated as multiples of the distribution required for 1000 passes during automatic traversing, e.g.

1000 - 2000	30	60	120	180	220	180	120	60	30

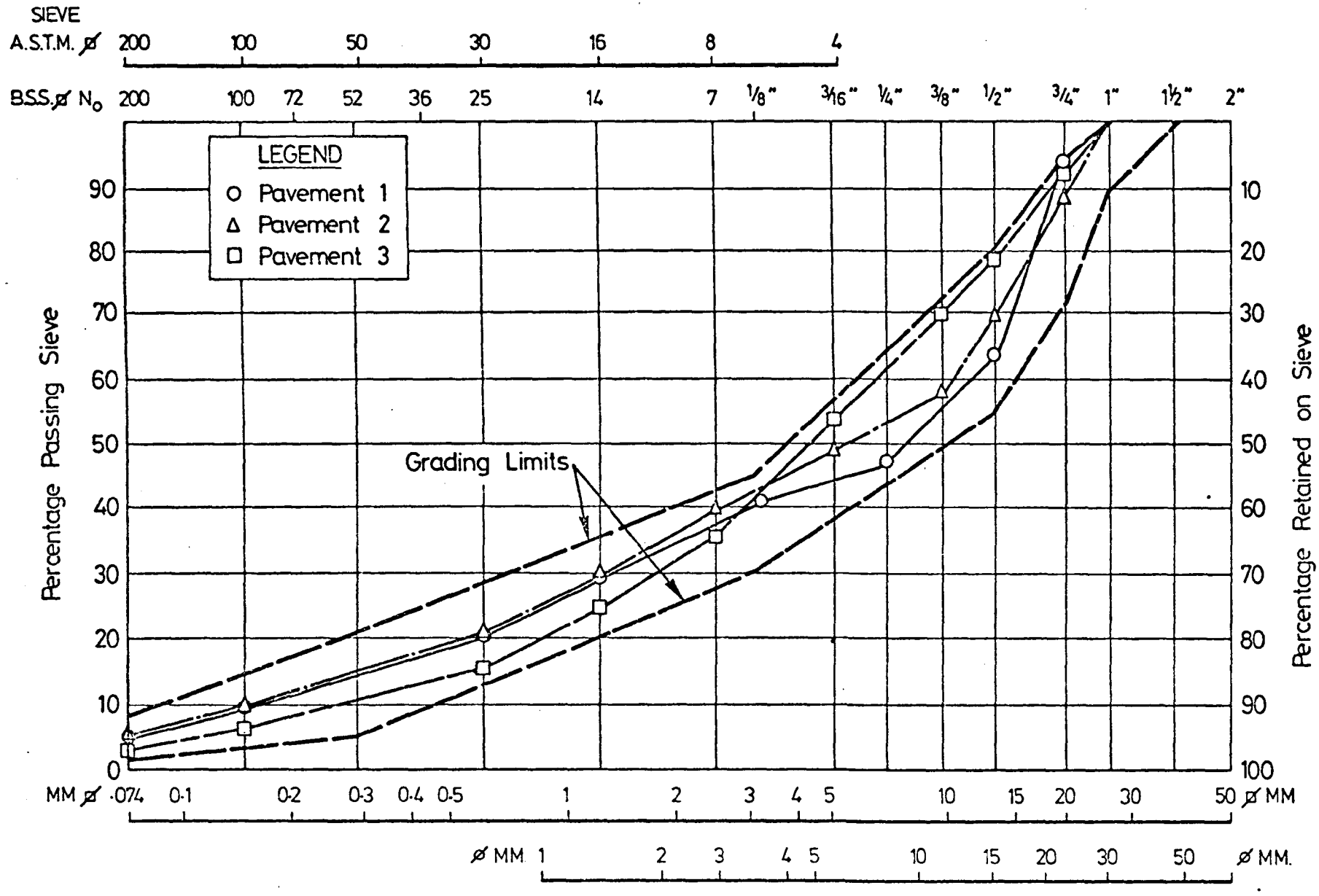

FIG. 6.1 GRADING CURVES FOR DBM FROM ALL THREE PAVEMENTS

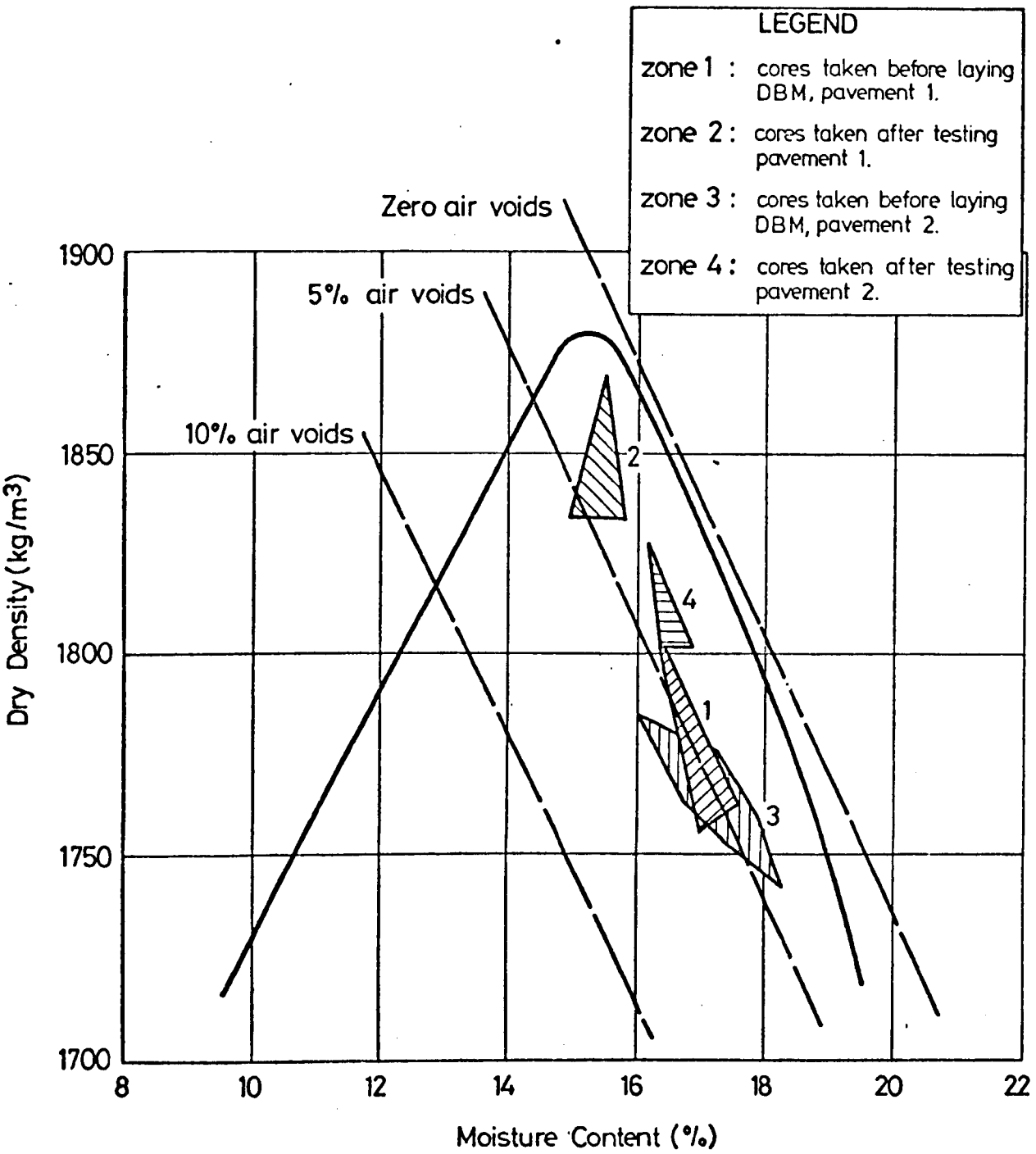

FIG. 6.2 DRY DENSITY VERSUS MOISTURE CONTENT RELATIONSHIP FOR KEUPER MARL, WITH RESULTS FROM CORES

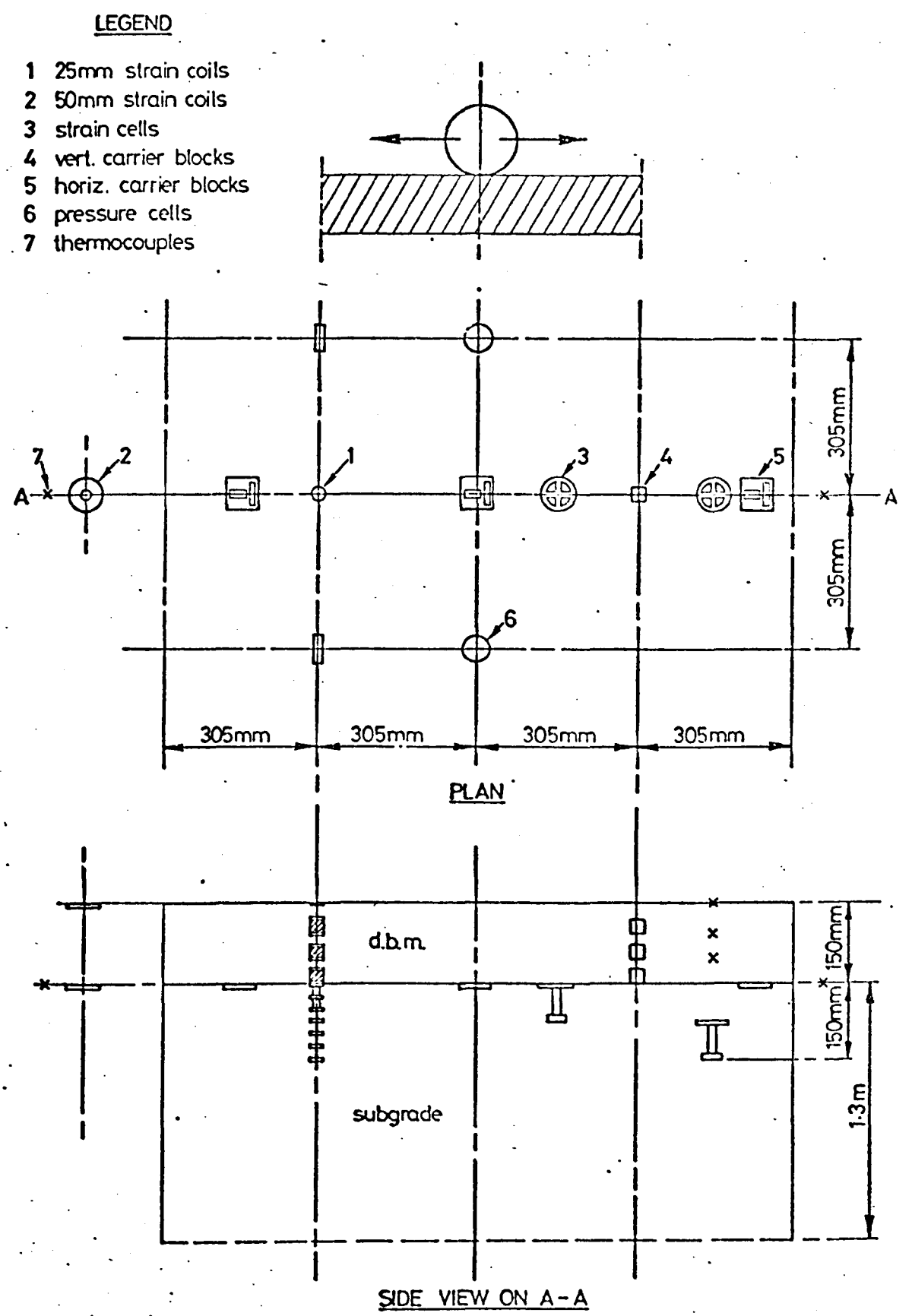

FIG. 6.3 INSTRUMENT LAYOUT, PAVEMENT NO. 1

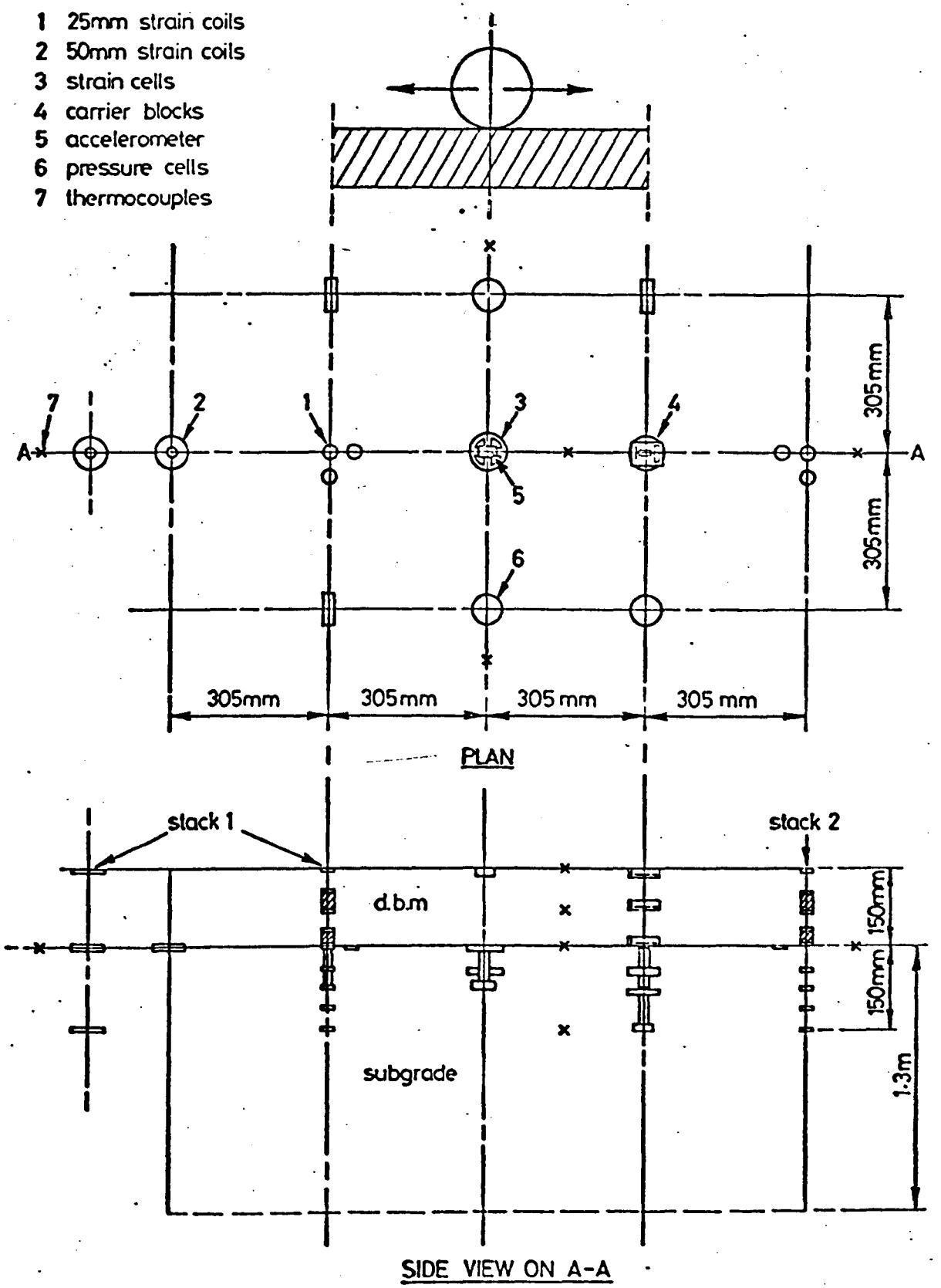

FIG. 6.4 INSTRUMENT LAYOUT, PAVEMENT NO. 2

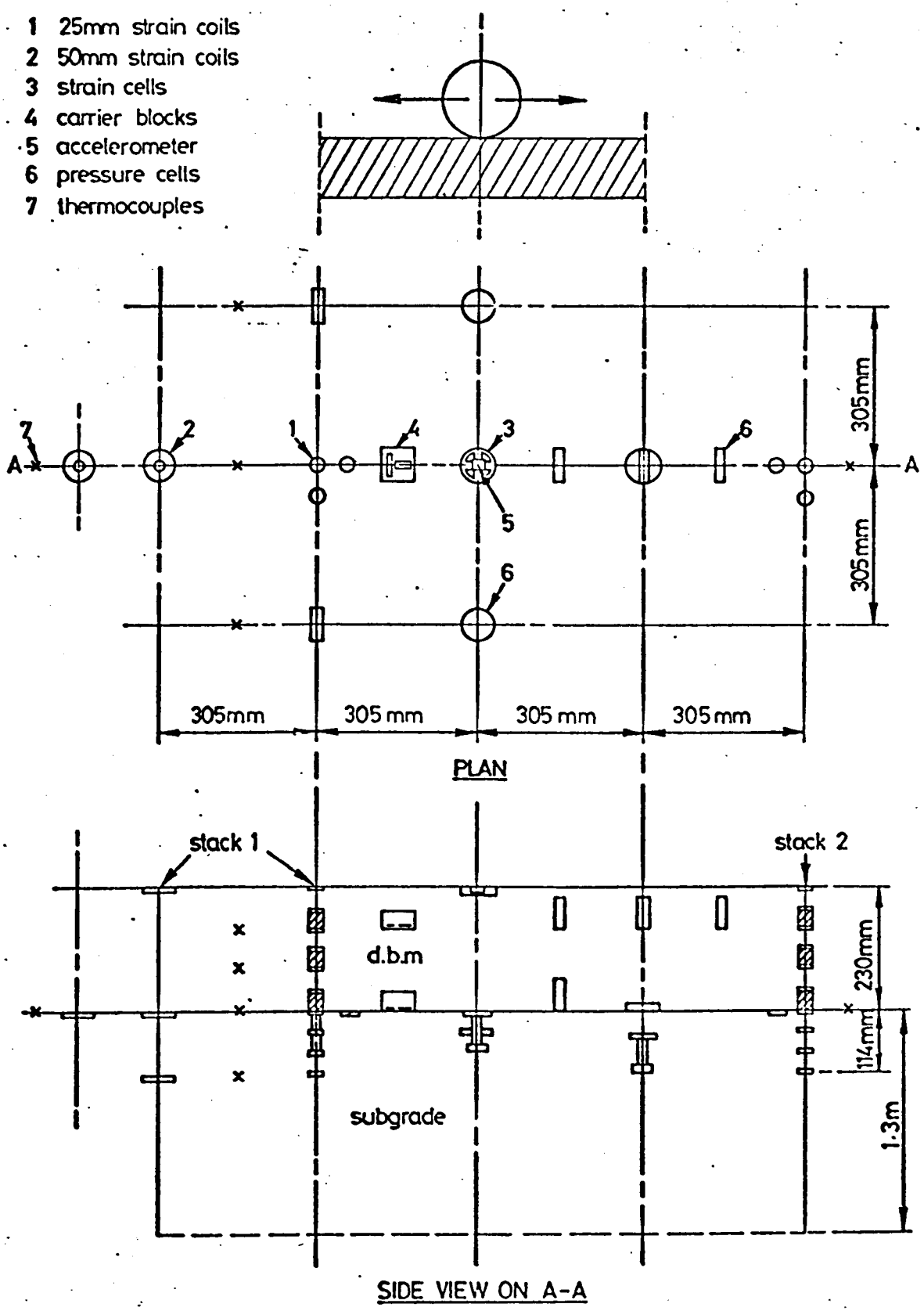

FIG. 6.5 INSTRUMENT LAYOUT, PAVEMENT NO. 3

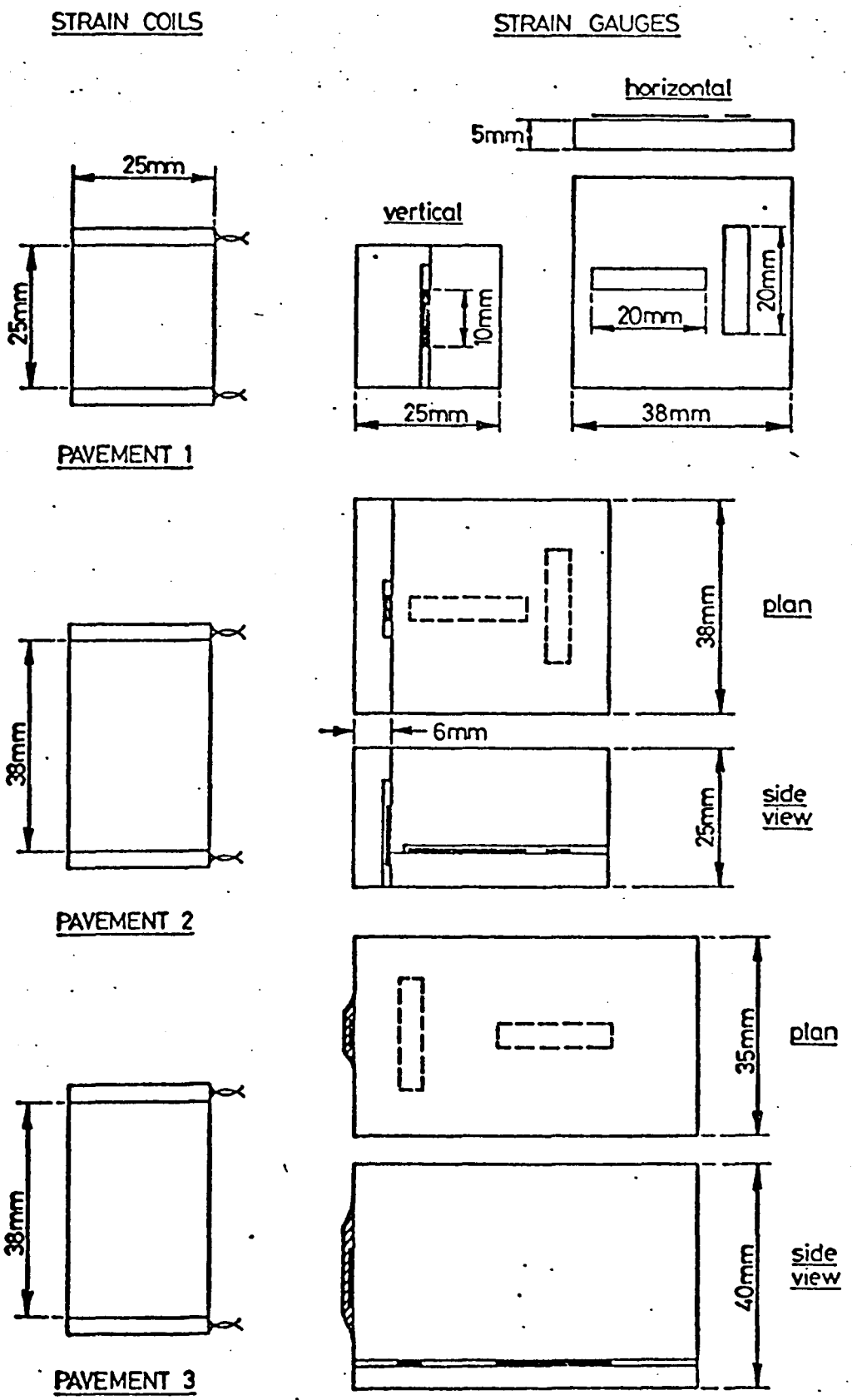

FIG. 6.6 DETAILS OF BITUMINOUS CARRIER BLOCKS

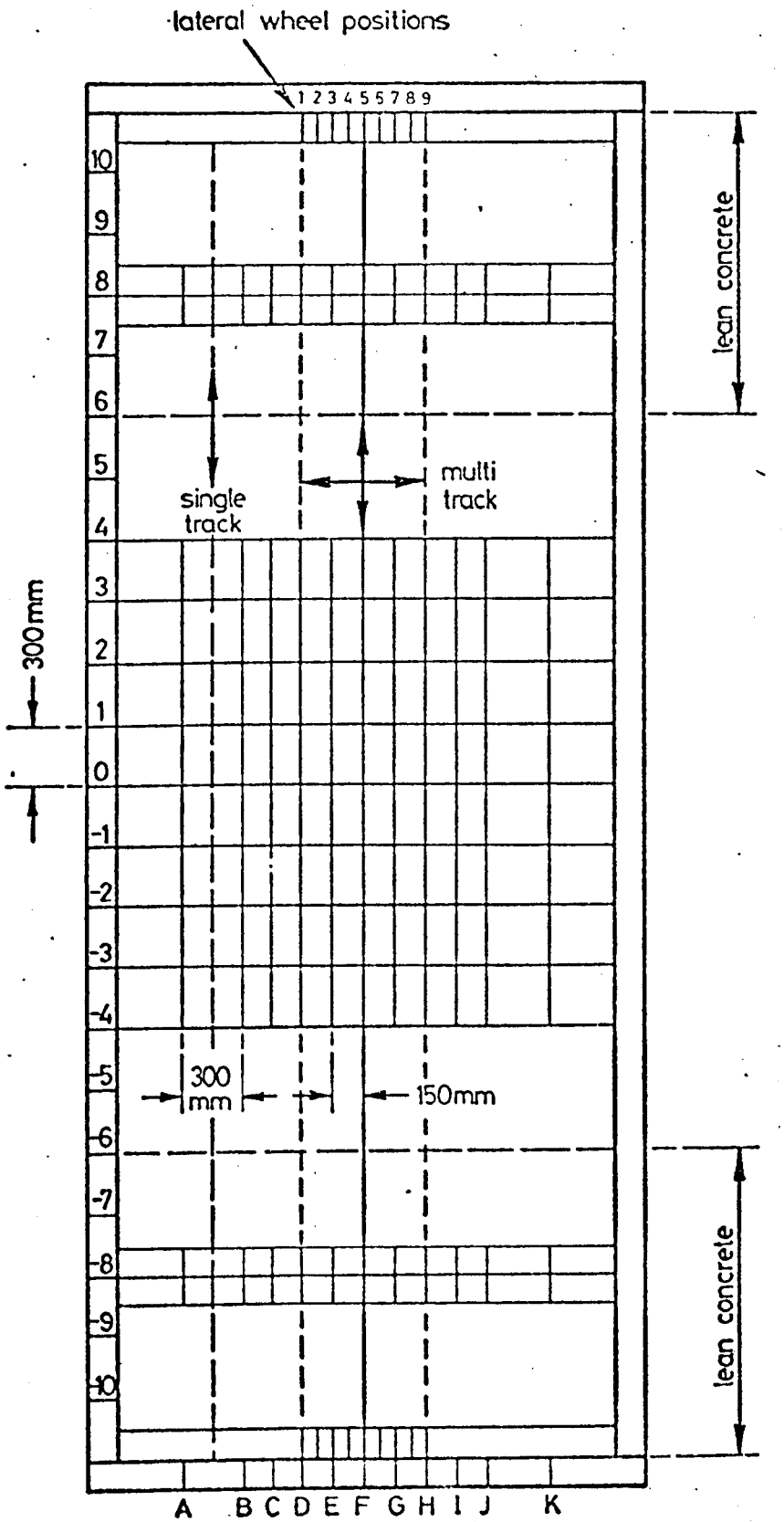

FIG. 6.7 PAVEMENT GRID

CHAPTER SEVEN

IN-SITU MEASUREMENTS

7.1 INTRODUCTION

This Chapter reviews the results of the measurements taken with instrumentation in both the bituminous layer and the subgrade, for the multi-track tests. Since the single-track tests were essentially supplementary, no instrumentation was installed to monitor pavement response during those tests, and only surface pavement deformation was measured.

As outlined in the previous Chapters, both elastic and permanent strains and stress were measured in each pavement, in addition to surface deformation measurements. Resilient measurements are compared with predictions using elastic theory in Chapter 10, to validate the theory. Similarly, Chapter 11 compares the permanent deformation measurements and predictions. The reader is referred elsewhere (17, 18) for a full presentation of the in-situ measurements, only a few examples will be included here. Since the accuracy of the measurements is of vital importance to the aims of this thesis, particular emphasis is given to the performance of the instrumentation.

7.2 PERMANENT DEFORMATION

7.2.1 Surface Deformation

The maximum surface deformation, viz at the rut centre, was measured with time. The plot for pavement 3 is shown in Figure 7.1, which also shows the deformation obtained by considering the stacks of 25mm strain coils, and the deformation measured above the layer of

lean concrete. For all pavements, the average deformation indicated by the strain coils was lower than that measured at the surface, suggesting a possible further contribution to the deformation at a greater depth in the subgrade, or, coil misalignment and reorientation which may have reduced the sensitivity of these instruments.

The contributions to the total deformation from the subgrade and DBM for each pavement are summarised in Table 7.1. Missing data is due to failure of certain critical strain coils either before or during a pavement test. It may be seen that the total deformation (rut depth) for pavements 1 and 3 are similar, but that the proportions of deform-:ation in each layer differ; the deformation in the DBM layer for pavement 3 is more significant due to its greater thickness, since the average strains for the two cases were similar. The total deform-:ation in pavement 2 is approximately twice that for pavements 1 and 3 due to the weaker DBM layer. Also, the proportion of deformation in the subgrade is higher since higher stresses would be transmitted to the subgrade.

The accuracy of the strain coil measurements can be assessed by comparing the thickness of the DBM layer measured by the coils with that measured directly after sawing and removal of sections of the DBM. The relevant data is summarised in Table 7.2. The discrepancy for the 25mm strain coil stack in pavement 1 is 15mm and is attributed to the possibility of a d.c. offset occurring as a result of an earth loop in the circuitry. The thickness measured with the 50mm coils is identical to the direct measurement, and therefore the deformation measured by these coils should be precise. Table 7.1 shows that this measurement agrees to within 25 per cent with that from the 25mm coils. For pavement 2, only stack 1 of the 25mm coils can be considered where a discrepancy of 6mm occurs due to the carrier block for the bottom pair of coils penetrating the subgrade by that amount, probably during

TABLE 7.1 COMPARISON OF IN-SITU DEFORMATIONS FROM STRAIN COILS AND RUT DEPTHS

Pavement No.	Stack No.	No. of wheel passes	Permanent deformation (mm)			
			Subgrade	DBM	Subgrade + DBM	Rut Depth
1	1	20,000	1.3	2.7	4.0	6.2
	50mm coils		-	3.6	-	
	1	100,000	-	6.3	-	12.4
	50 mm coils		-	7.4	-	
2	1	20,000	5.0	6.7	11.7	15.6
	2		6.2	-	-	
	1	100,000	9.9	11.4	21.3	23.4
	2		-	-	-	
3	1	20,000	1.7	8.2	9.9	9.2
	2		0.7	6.5	7.2	
	1	100,000	2.2	13.3	15.5	14.6
	2		0.9	11.0	11.9	

TABLE 7.2 THICKNESS MEASUREMENTS

Pavement No.	Thickness of bituminous layer (mm)			
	From excavated slabs at the rut centre		From final strain coil readings	
			Stack 1	Stack 2
1	136		151	136 (50mm coils)
2	121		127	-
3	226		215	220
3	From recovered carriers			
	Stack 1	Stack 2		
	-	39.9	-	top pair 40.1
	-	41.0	-	centre pair 41.3
	40.3	42.3	bottom pair 40.3	bottom pair 42.8

compaction. Comparison of measurements for pavement 3 was more comprehensive, since four of the six carrier blocks were removed intact, after the test, enabling a check to be made on the coil spacing; Table 7.2 shows a maximum error of 0.5mm.

No information was obtained from the 50mm coils in pavements 2 and 3 since the interface coil was damaged in the former and the surface coil remained just out of balance in the latter. Also, it was not possible to compare strain coil and direct measurements for the subgrade, since the material was soaked and disturbed during removal of the DBM.

Table 7.1 shows that the final surface deformations measured by strain coils directly agreed to within 20 per cent. Table 7.2 shows that slab thickness measured directly and by strain coils agreed quite closely, and any large discrepancies could be explained. Hence, the strain coils could be used with confidence for permanent strain measurements, if care was taken in installation.

7.2.2 Permanent Strain Distribution

The distributions of vertical permanent strain with depth, as measured by the 25mm strain coils, are given in Figures 7.2 to 7.4. For pavements 2 and 3 only the results from one stack of coils are shown, since those from stack 2 of pavement 2 were incomplete, and those from stacks 1 and 2 of pavement 3 are very similar. The Figures show the location of carrier blocks and out of balance or inoperative coils.

The distributions highlight the importance of selecting a material compatible with the DBM for the carrier blocks. Sandsheet blocks were used in pavement 1, and Figure 7.2 shows that the permanent strain distribution approximated to a smooth curve. DBM blocks were used in pavements 2 and 3, cut from the stiffer material

from pavement 1, and Figures 7.3 and 7.4 show that distorted distrib-:utions were obtained related to the positions of the carrier blocks. Since the overall measurements, discussed in the previous section, were of the right order, a line was projected through the measured strains based on the average between adjacent pairs of coils. It would seem advisable to use either an identical material to the surrounding one, or, one that is weaker, when choosing carrier blocks, and where possible, their use should be avoided.

The permanent strain distributions with depth in the subgrade are also shown in Figures 7.2 to 7.4. For pavement 1 the pattern is erratic and does not give the highest strains at the top of the sub-:grade as expected, since the stresses are greatest at that point. This could be because these coils had been made at Nottingham (for the first time), and possibly the compaction of the material during installation had been uneven. Much higher values of permanent strain were recorded at the subgrade surface in pavements 2 and 3, and the distributions were as expected, except that in pavement 3 the central pair of coils indicated a lower strain than the bottom pair. The bottom pair of coils in pavements 1 and 3 indicated a significant strain, supporting the view that the general underestimation of the rut depth from the coils was to some extent caused by deformation taking place below the lowest pair, possibly due to consolidation.

Some results relating to horizontal permanent strain measured at the interface were also obtained. This is a particularly difficult area to deal with, and insufficient replicate measurements were obtained to merit comparison with predicted values. Hence, these measurements are not presented.

7.3 RESILIENT BEHAVIOUR

7.3.1 Elastic Strain Measurements

The distributions of elastic strain with depth, as measured by the 25mm strain coils, are shown in Figures 7.5 to 7.7. The values shown are the averages of several readings taken after 50,000 passes for pavements 1 and 2, and from all the readings for pavement 3. There is no obvious correlation between the elastic and permanent strain distributions in the DBM for either pavements 1 or 2, a carrier block effect being apparent for the elastic distribution in pavement 1 which had not occurred for the permanent one, and vice versa for pave-:ment 2. However, a similarity does exist for pavement 3, both distributions exhibiting a carrier block effect. The distributions for the subgrade of all three pavements were similar and showed that significant strains occurred at greater depths than the instruments. Comparison of the elastic and permanent strain distributions for pave-:ment 1 is not possible, with only two definite values for the former, but similar distributions were obtained for pavements 2 and 3.

An assessment of the lateral variation of elastic strains was possible when readings were taken with the strain coils when the wheel travelled along each of the nine wheel tracks. These measurements were limited because of the shorter time available to take readings, not because of problems with the instruments. The majority of data of this type was obtained from pavement 3 and is presented in Chapter 10 where comparison with predicted distributions is made.

Generally, insufficient replicate measurements were available for elastic strain values, and although the results appear to be sensible, caution should be exercised when examining them quantitatively.

7.3.2 Stress Measurements

The maximum stresses measured in the subgrade of each pavement are summarised in Table 7.3. Those for pavement 1 decreased as the test progressed, possibly due to the subgrade undergoing additional compaction due to trafficking. Similar to the elastic strain measurements, lateral variation of stress could be obtained, although insufficient measurements were taken in pavement 1 to define this. The variations for pavements 2 and 3 are given in Chapter 10.

Table 7.3 Comparisons of maximum stresses measured in the subgrade

Pavement No.	Vertical Stress (kN/m^2)	Longitudinal radial stress (kN/m^2)
1	89.6 - 41.4	6.9 - 4.8, 34.5 - 27.6
2	66, 55, 40	25.4, 34.7, 22.1
3	60, 52	15, 17

The measurement of stresses in the DBM of pavement 3 was concentrated on measuring longitudinal radial stress at the top of the layer. A considerable variation in the results was obtained from the three pressure cells at this location. The single cell measuring the same parameter at the bottom of the layer indicated a significant compression and also tension (the cell was not designed to measure tension). A cell measuring vertical stress at the bottom of the layer gave a value of 77 kN/m^2, which, considered with the average value of 56 kN/m^2 in the subgrade, indicates equilibrium at the interface. The lateral variation in the stress levels measured are given in Chapter 10.

Summarising, more measurements were obtained for pavement 3 and those in the subgrade were considered reliable. A scatter of results was obtained for pavement 2, indicating less reliability. The

difference in readings of radial stress in pavement 1 indicates the possible variability and illustrates the need for at least three replicate measurements of each parameter, and preferably more.

7.3.3 Pulse Shapes

Typical pulses taken from high speed recorder traces are shown in Figures 7.8 and 7.9 for pavement 3. These show how the pulse lengths varied and also that the responses were, in general, smooth and symmetrical. Phase differences between peak readings are a function of the positions of the instruments and are not due to a material effect. However, pulse lengths did vary, which depended on the depth of the instrument. The readings for the pressure cells are to scale, but those for the strain coils are not, due to different sensitivity settings during the test.

The longitudinal radial stress in the bottom of the DBM layer indicated a compression tension-compression shape, but the tension part is truncated since the cells cannot respond completely to tension. A rough suggestion of the complete pulse shape has been drawn in. Stress measurements in the subgrade reveal compressive vertical stresses of long duration and compressive longitudinal radial stresses which decrease when the wheel is directly over the cell.

7.4 SUMMARY OF INSTRUMENT PERFORMANCE

The measurement of permanent and resilient strains with Bison strain coils was successful. The accuracy of the measurements depends on the success of the installation, and a series of calibrations in specimens of the in-situ material is recommended particularly if carrier blocks are to be used. The results of resilient strains measured by strain gauges in the DBM have not been reported, since they were very limited due to failures during installation of the pavements. Clearly

more work is required on installation technique before strain gauges can be used with confidence. The strain cells did not produce satisfactory results, and it is felt that these instruments are limited for this type of work, where numerous instruments are installed in a limited space, because of their large size.

The pressure cells performed well, particularly for pavement 3, and seemed entirely suitable for the clay subgrade used in all pave-:ments. The use of the cells in the DBM of pavement 3 indicated the potential of their use in bituminous material. However, the DBM stresses obtained should be considered only as a guide at this stage.

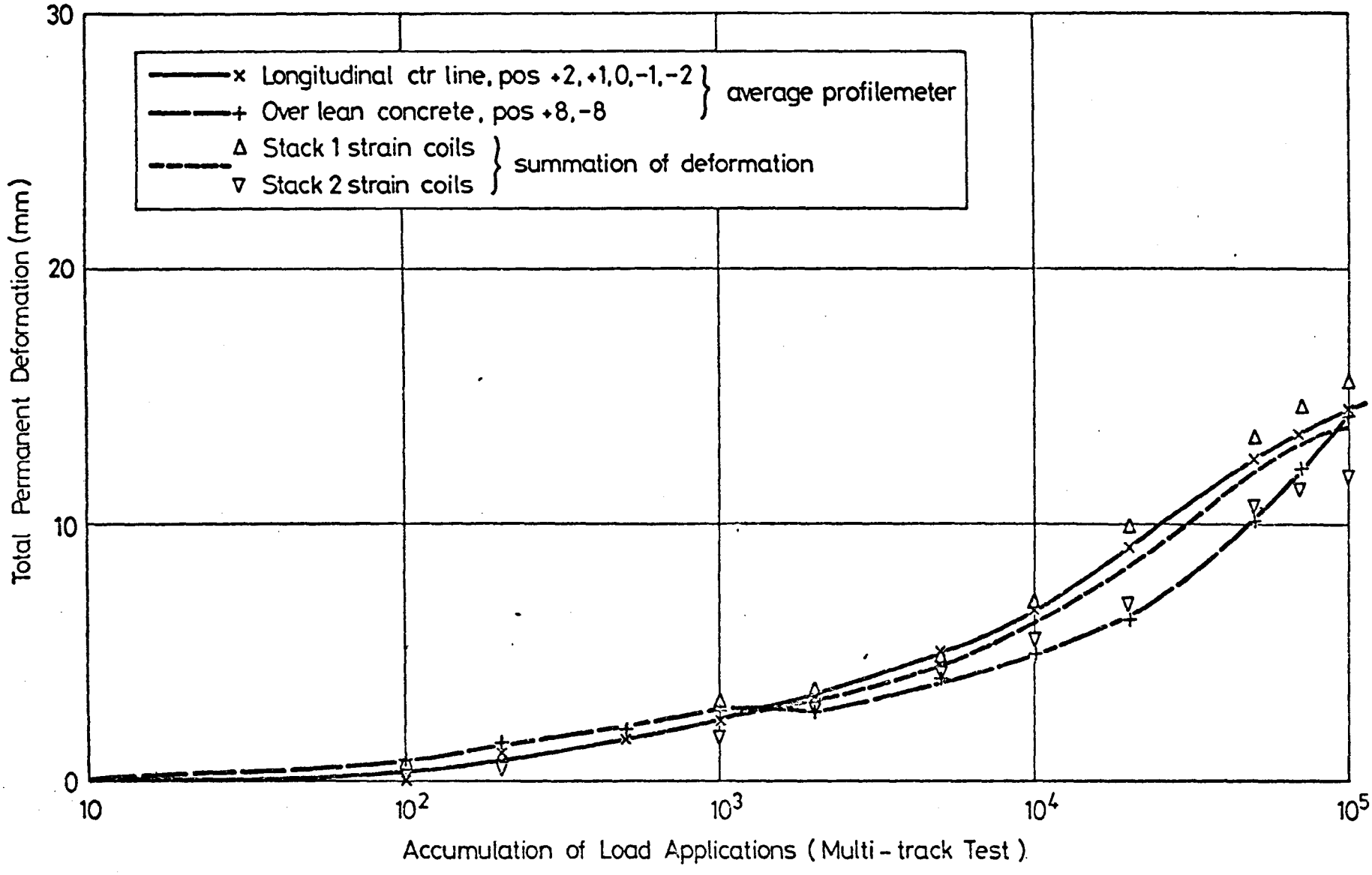

FIG. 7.1 ACCUMULATION OF PERMANENT DEFORMATION, PAVEMENT NO. 3

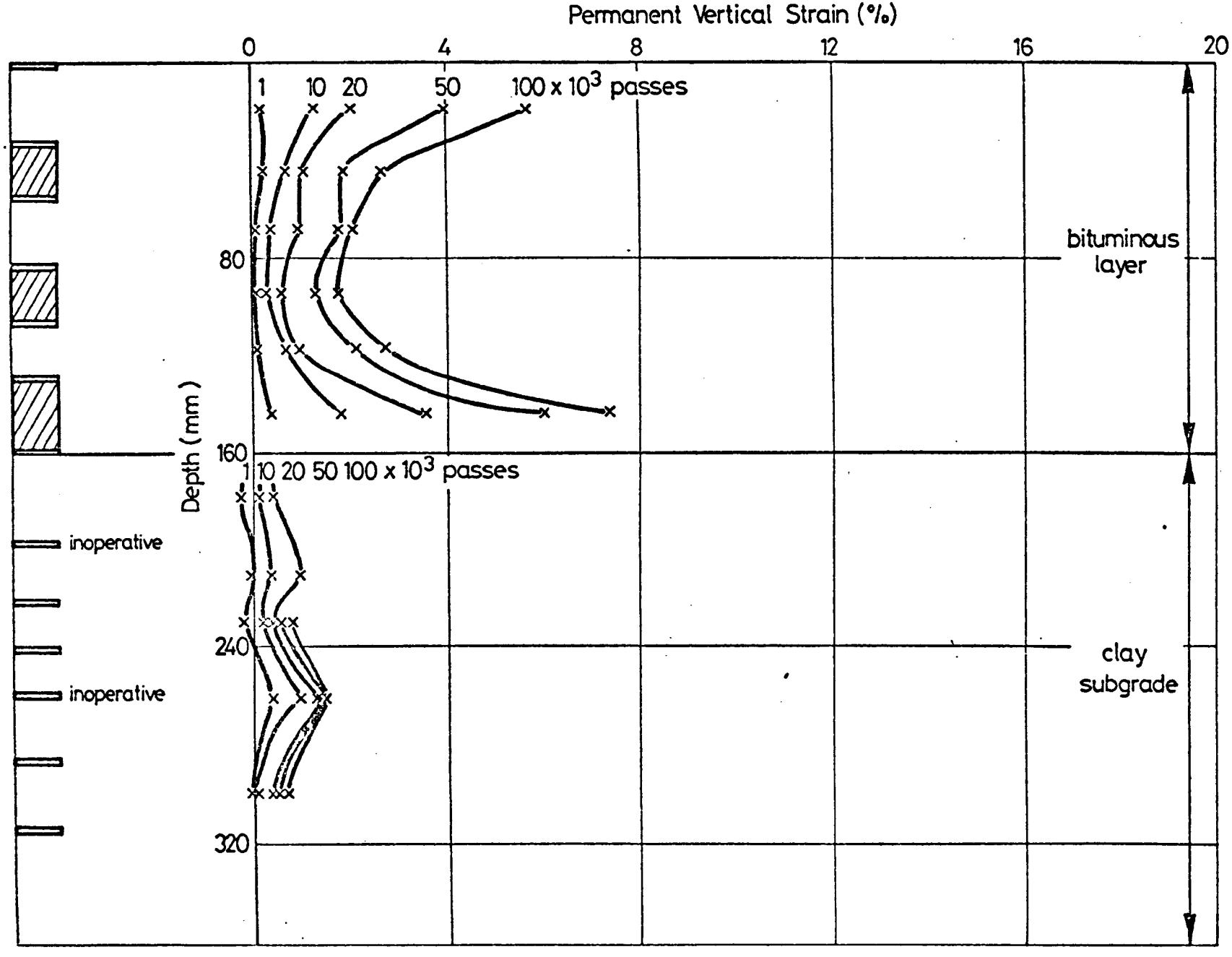

FIG. 7.2 VARIATION OF PERMANENT VERTICAL STRAIN WITH DEPTH, PAVEMENT NO. 1

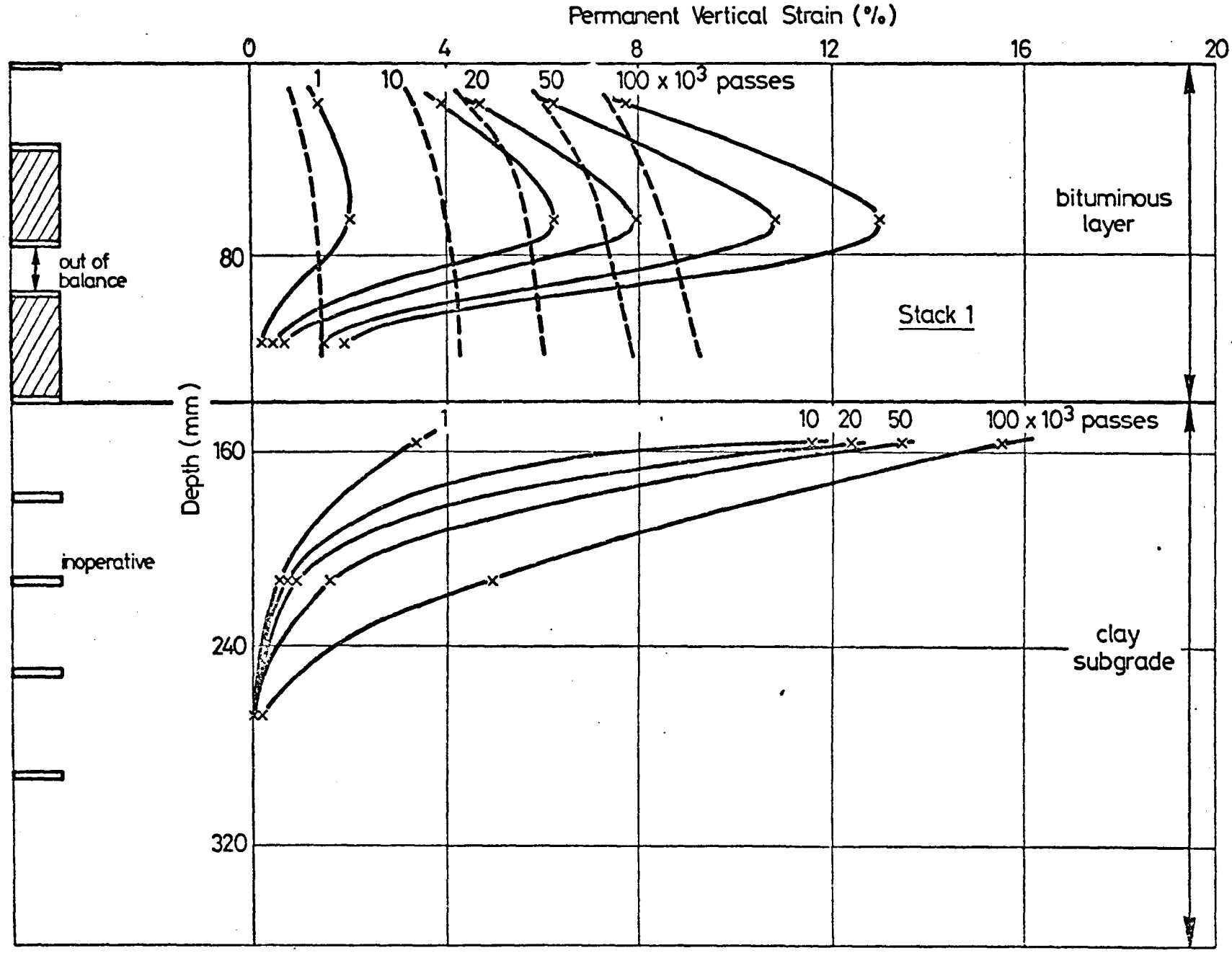

FIG. 7.3 VARIATION OF PERMANENT VERTICAL STRAIN WITH DEPTH, PAVEMENT NO. 2

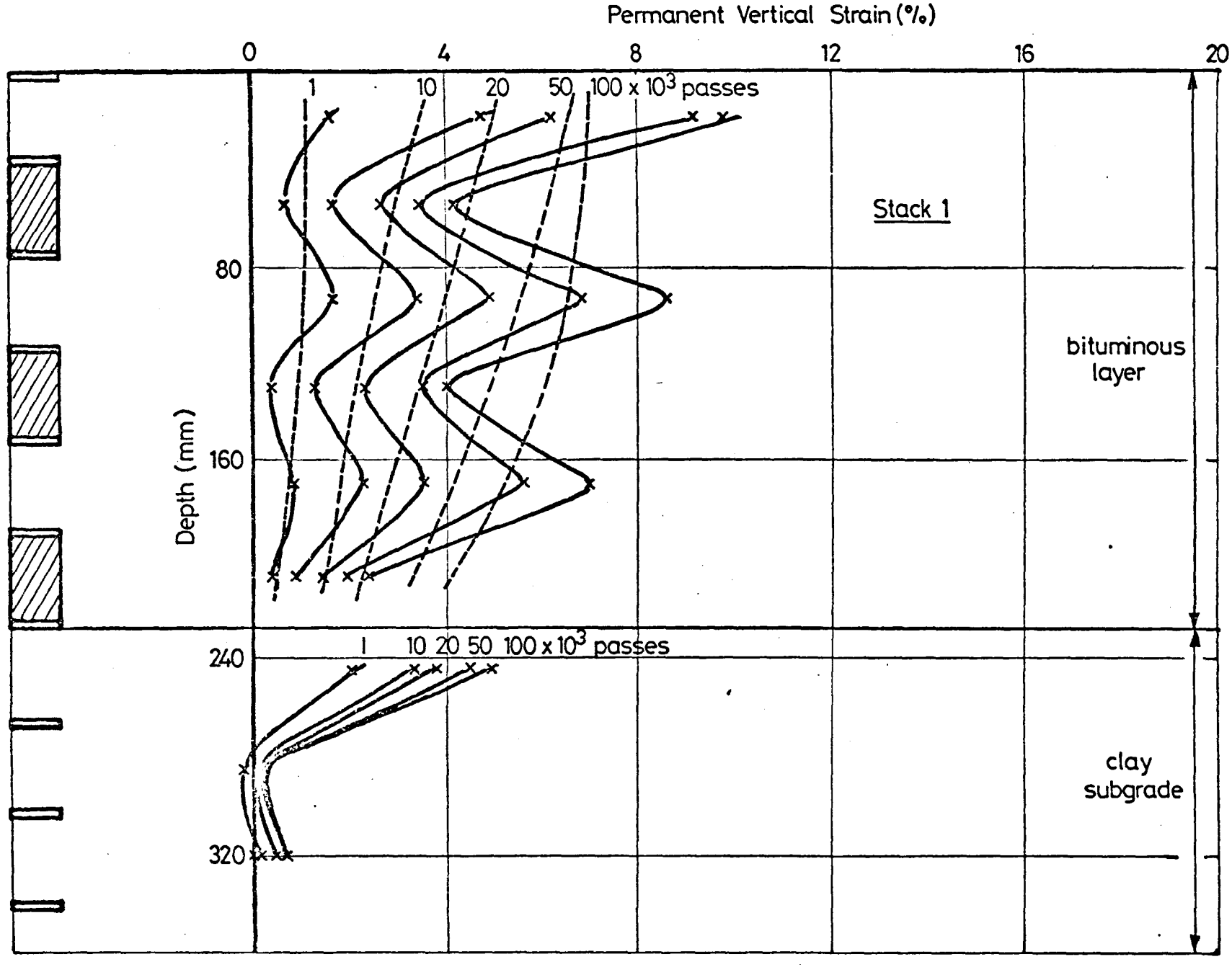

FIG. 7.4 VARIATION OF PERMANENT VERTICAL STRAIN WITH DEPTH, PAVEMENT NO. 3

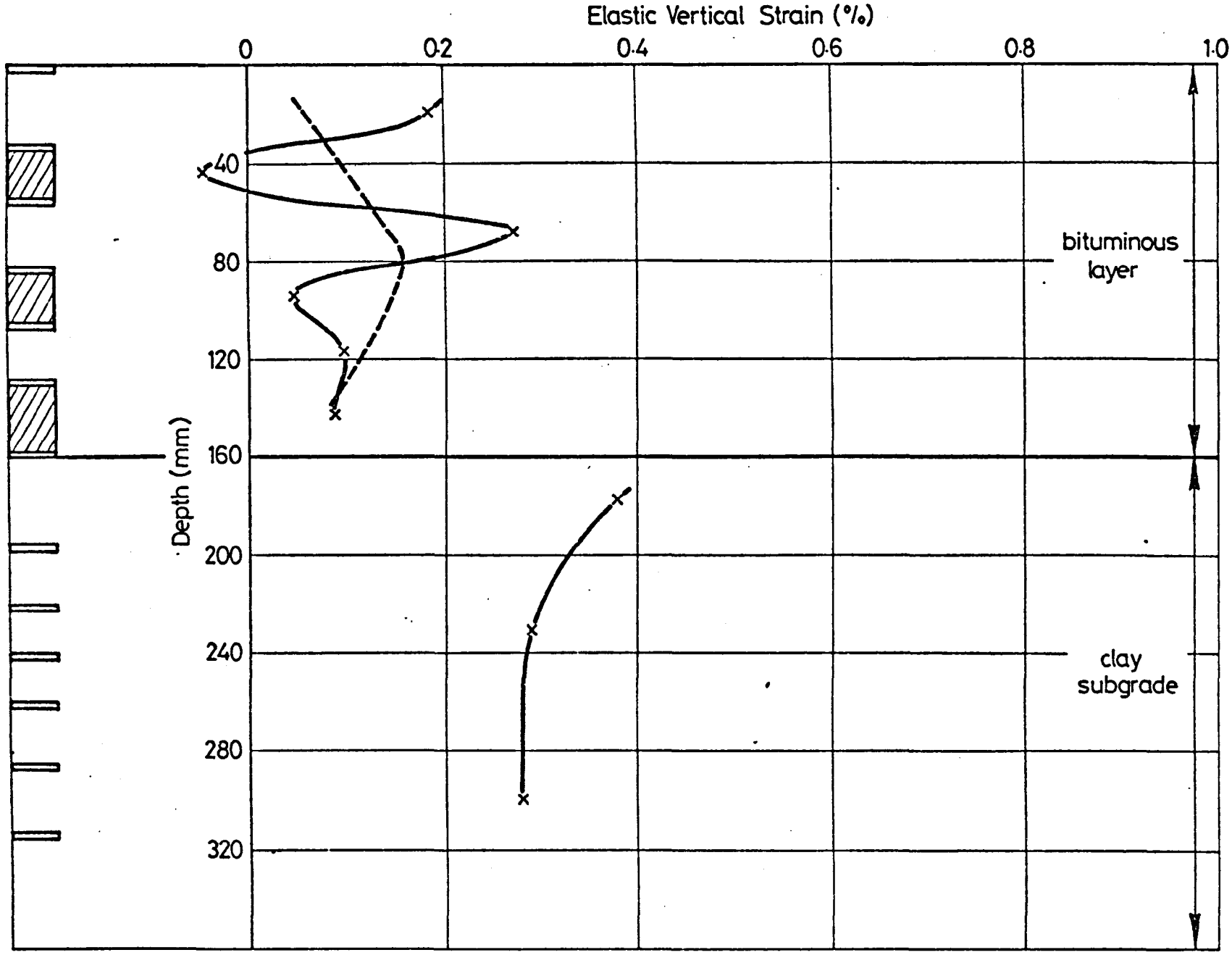

FIG. 7.5 VARIATION OF ELASTIC VERTICAL STRAIN WITH DEPTH, PAVEMENT NO. 1

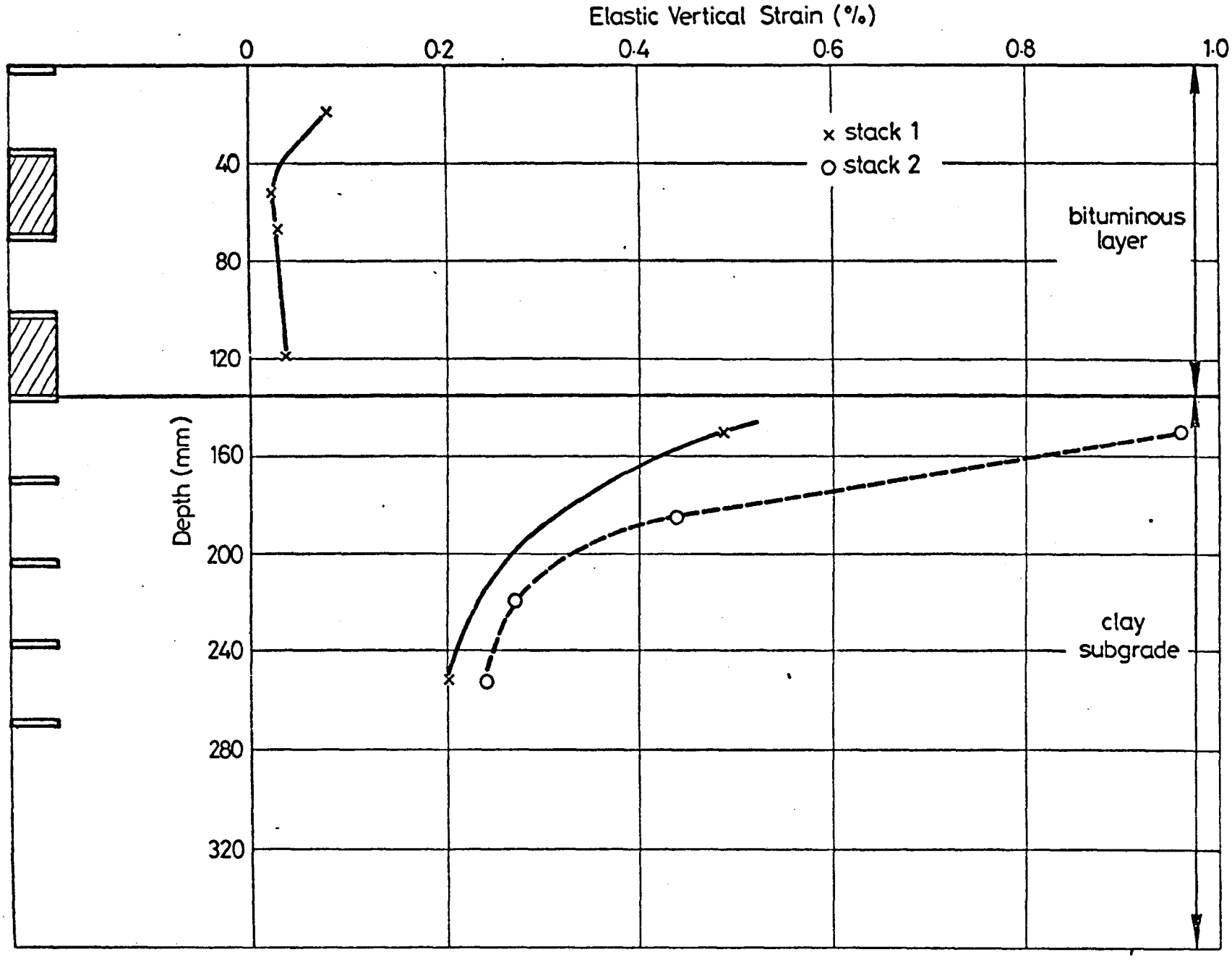

FIG. 7.6 VARIATION OF ELASTIC VERTICAL STRAIN WITH DEPTH, PAVEMENT NO. 2

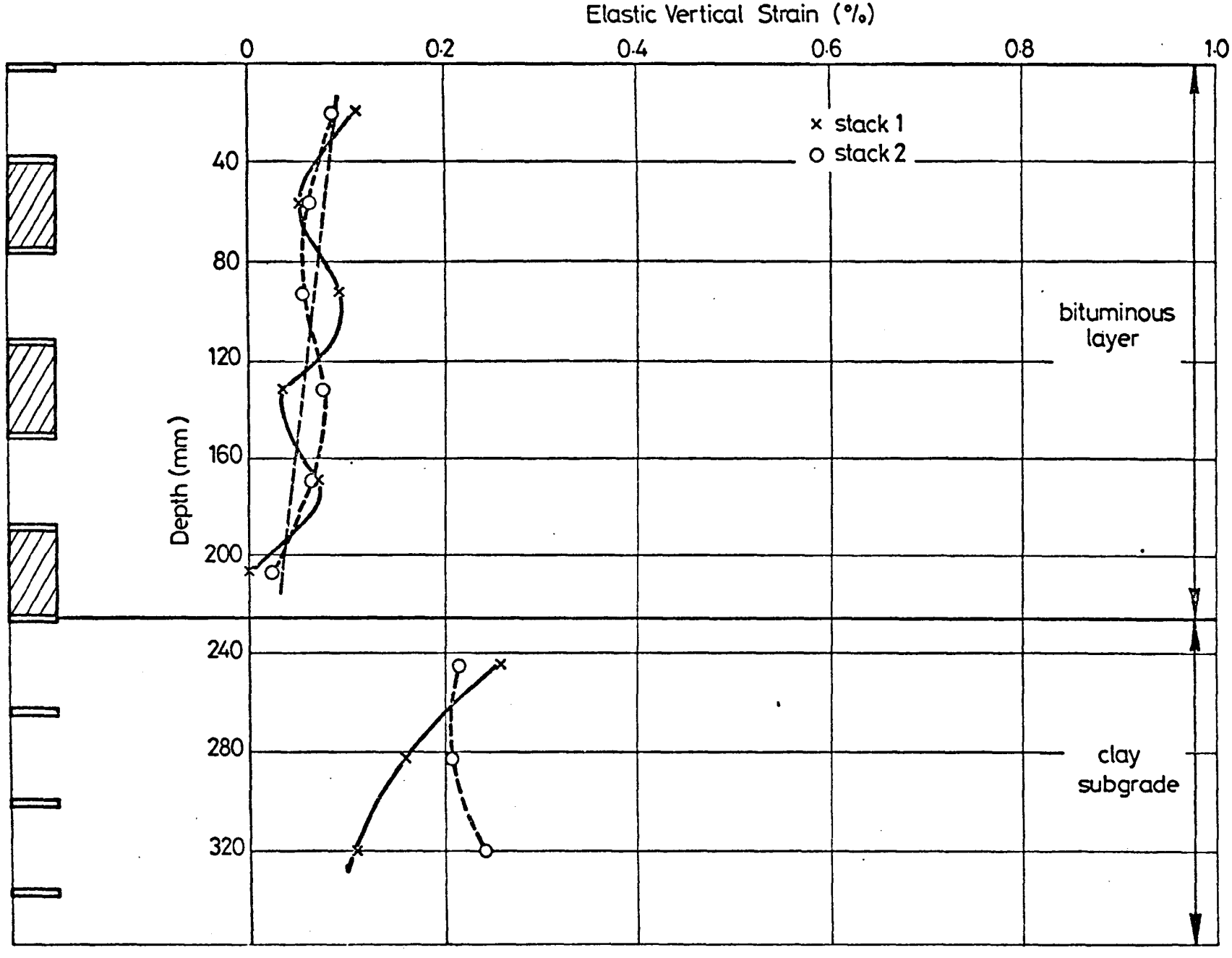

FIG. 7.7 VARIATION OF ELASTIC VERTICAL STRAIN WITH DEPTH, PAVEMENT NO. 3

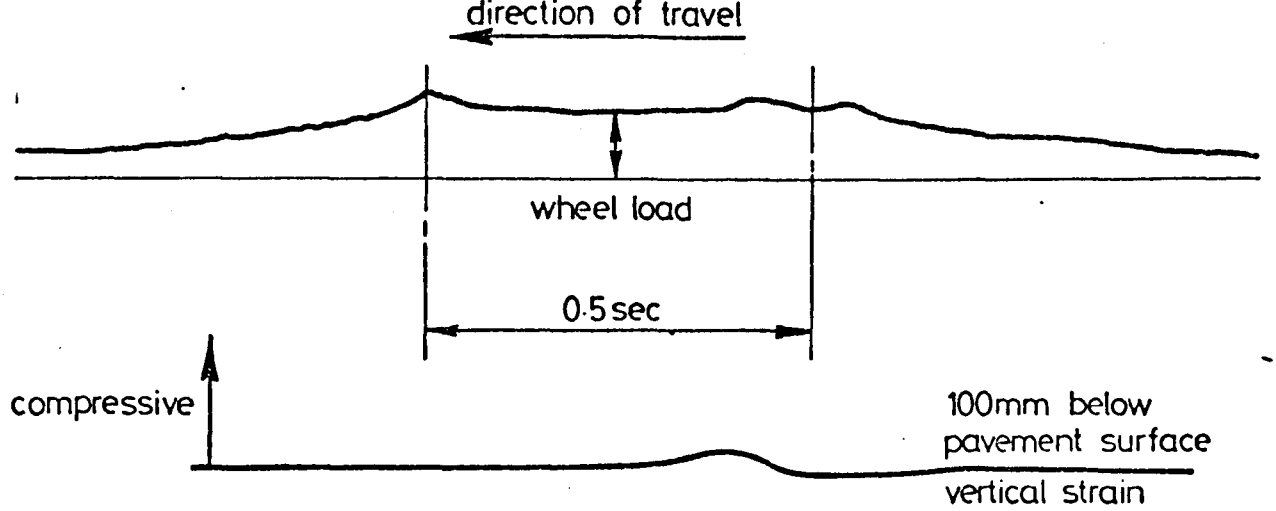

(a) Strain pulse in the bituminous layer

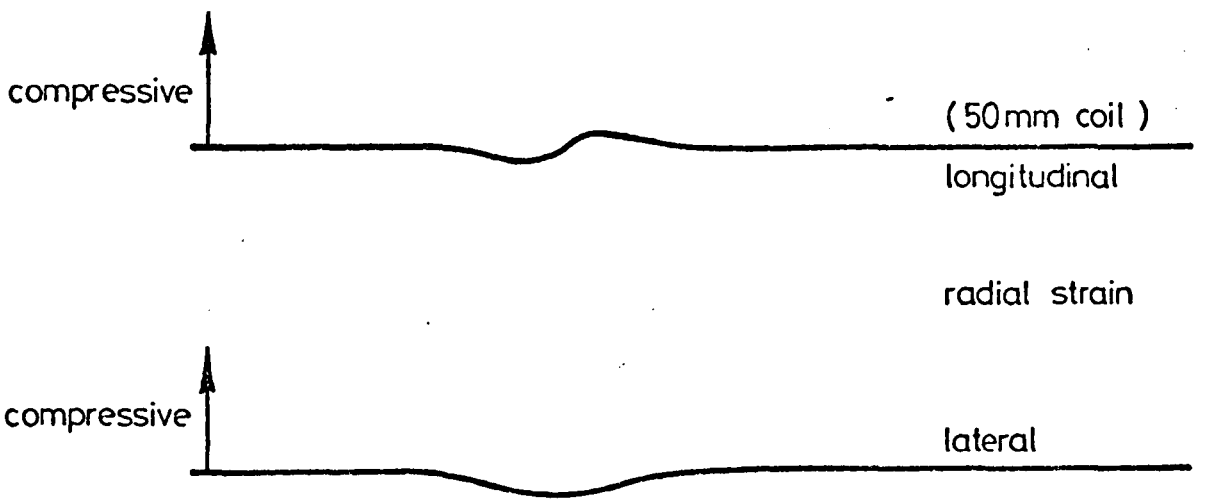

(b) Strain pulses at the interface

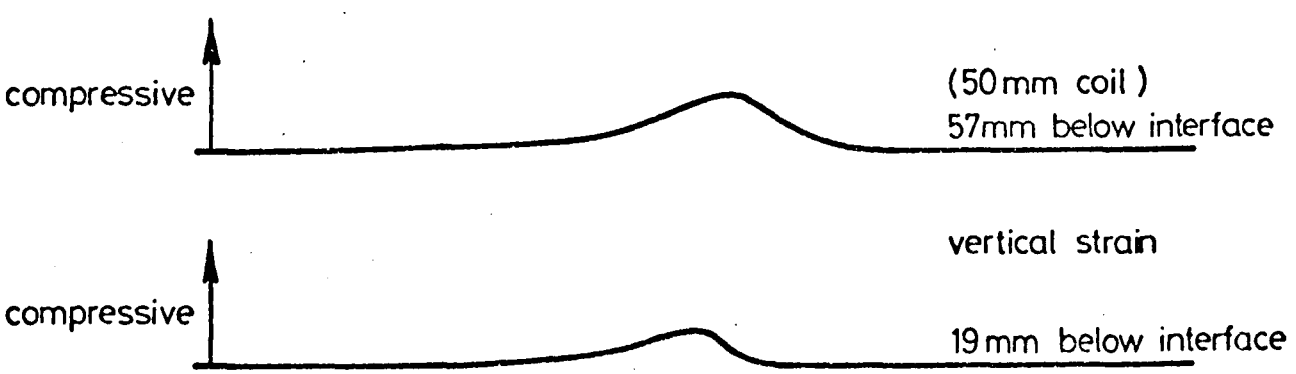

(c) Strain pulses in the subgrade

FIG. 7.8 RESPONSE OF STRAIN COILS, PAVEMENT NO. 3

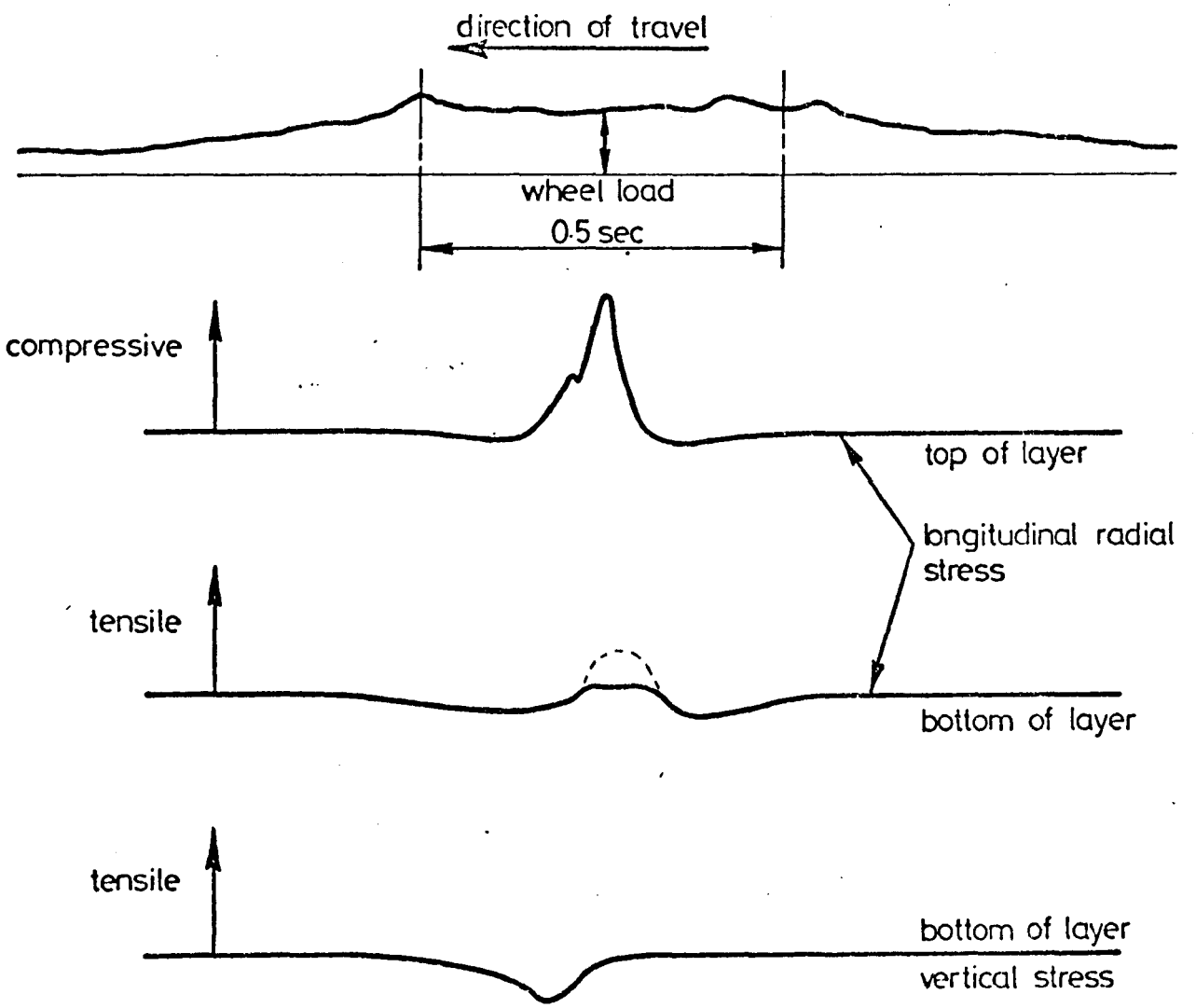

(a) Stress pulses in the bituminous layer

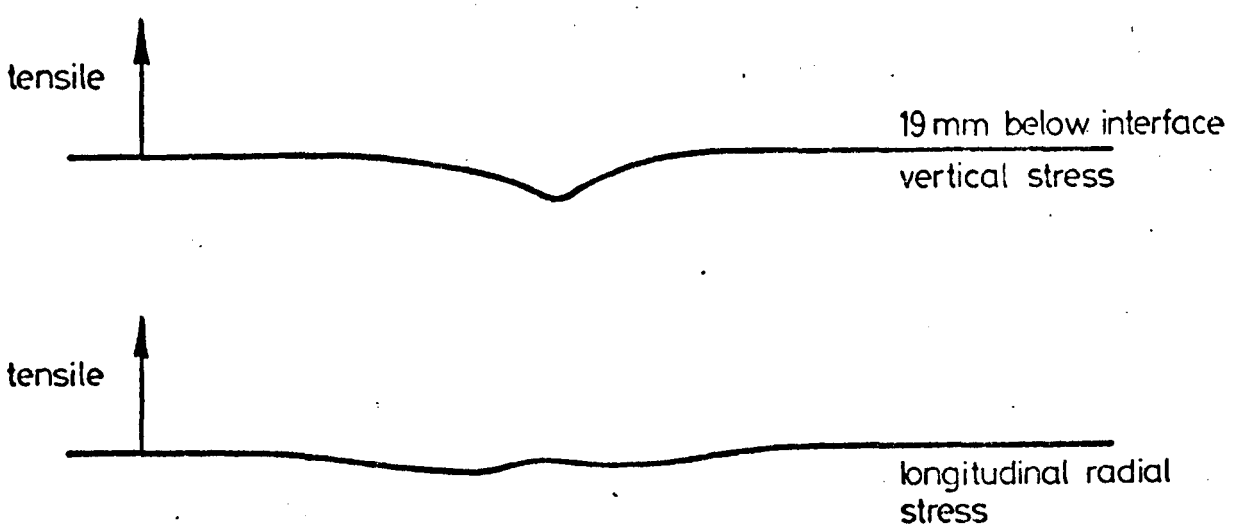

(b) Stress pulses in the subgrade

FIG. 7.9 RESPONSE OF PRESSURE CELLS, PAVEMENT NO. 3

CHAPTER EIGHT

THEORETICAL ANALYSIS OF THE EXPERIMENTAL PAVEMENTS

8.1 INTRODUCTION

The approach adopted for the prediction of permanent deformation in the pavements has already been outlined in a previous Chapter (see section 3.2). This is based on proposals by Romain (19) and Barksdale (20) involving linear or non-linear elastic analysis of the pavement to determine the stress distribution over a network of elements, and subsequent prediction of the vertical permanent strain in each element from the results of characterisation tests on the pavement materials. Subsequent integration of permanent strain with depth gives the permanent deformation at the pavement surface.

The framework adopted for determining the permanent deformation characteristics (and resilient properties) was the stress invariant approach suggested by Brown (21) based on repeated load triaxial test-:ing. The linear and non-linear elastic analyses of pavements were carried out with the computer programs BISTRO (60) and DEFPAV (24) respectively.

8.2 INITIAL CALCULATIONS

An estimate of the resilient properties of the two pavement materials was used to calculate a preliminary stress distribution for the first pavement (BISTRO), on the basis of which a provisional test programme was devised. Subsequent testing provided measured values of the resilient properties, which were then used to check whether the programme was adequate.

8.3 APPLICATION OF THE STRESS INVARIANT APPROACH

A rigorous prediction of permanent deformation depends on the ability to predict the permanent strain in all elements of the pave-:ment within a reasonable distance of the wheel load. Achievement of this would give the profile of the rut as well as the rut depth.

Figure 8.1 illustrates that the repeated load triaxial test can exactly simulate in-situ stresses on the axis of symmetry of the wheel load, except near the bottom of a bituminous layer where the two radial stresses are tensile. One approach to representing stresses in this location is also shown, in which the radial stress on the test sample is taken to be the in-situ vertical stress. Such an approach was adopted by Morris et al (25) and McLean and Monismith (26), but is only approximate since one tensile stress is applied instead of two.

Exact reproduction of the in-situ stresses at locations off the load axis is impossible, since all three stresses differ, and an approximate approach such as that mentioned above to represent the tensile stresses on axis would be unsound. Use of the stress invariant approach (21) partially overcomes these problems, since its application does not involve exact reproduction of the individual stress components. The approach is based on the assumption that permanent strain depends on the levels of two stress invariants, the normal and shear stresses (p and q) in the material, causing volume change and shear distortion respectively.

As described in Chapter 3, the invariant approach aims to reproduce the in-situ values of p and q in the triaxial tests, and, by measurement of the deformation of the specimens, to obtain corresponding permanent strain invariants (v_p and ε_p). The stress and strain invariants are defined as:

$$p = \tfrac{1}{3}(\sigma_1 + \sigma_2 + \sigma_3) \tag{8.1}$$

$$q = \frac{1}{\sqrt{2}} \sqrt{[(\sigma_1 - \sigma_2)^2 + (\sigma_2 - \sigma_3)^2 + (\sigma_3 - \sigma_1)^2]} \tag{8.2}$$

$$v_p = \varepsilon_{p1} + \varepsilon_{p2} + \varepsilon_{p3} \tag{8.3}$$

$$\varepsilon_p = \frac{\sqrt{2}}{3} \sqrt{[(\varepsilon_{p1} - \varepsilon_{p2})^2 + (\varepsilon_{p2} - \varepsilon_{p3})^2 + (\varepsilon_{p3} - \varepsilon_{p1})^2]} \tag{8.4}$$

where σ_1, σ_2, σ_3, ε_{p1}, ε_{p2} and ε_{p3} are the principal stresses and strains respectively.

Under the conditions of axial symmetry occurring in the triaxial test, two of the principal stresses are equal ($\sigma_1 = \sigma_2 = \sigma_c$ or $\sigma_2 = \sigma_3 = \sigma_c$, where σ_c is the confining stress), hence for the test:

$$p = \tfrac{1}{3}(\sigma_1 + 2\sigma_3) \text{ or } \tfrac{1}{3}(2\sigma_1 + \sigma_3) \tag{8.5}$$

$$q = (\sigma_1 - \sigma_3) \tag{8.6}$$

$$v_p = (\varepsilon_{p1} + 2\varepsilon_{p3}) \text{ or } (2\varepsilon_{p1} + \varepsilon_{p3}) \tag{8.7}$$

$$\varepsilon_p = \frac{2}{3} (\varepsilon_{p1} - \varepsilon_{p3}) \tag{8.8}$$

and, q becomes identical to the deviator stress.

The deviator stress is the major principal stress minus the minor principal stress, and, therefore, must always be positive. This differs from the usual soil mechanics definition where the deviator stress is the axial stress minus the confining stress, and could therefore be positive or negative. However, the definition used herein for deviator stress (equation (8.6)) is consistent with the general definition for q (equation (8.2)), which must always give positive values because it is the square root of a positive number.

In order to illustrate the range of stresses which can be applied in the triaxial test, a plot of q versus p is shown in Figure 8.2, where, for convenience, q is shown as negative where the confining

stress is greater than the axial stress. The plot demonstrates that only half of the theoretically possible combinations of p and q can be achieved, due to the restriction that negative values of confining stress are impossible. The boundary between the accessible and inaccessible areas is the line representing uniaxial stress conditions ($\sigma_c = 0$).

The only in-situ stress conditions for which the sign of q could be assessed in the same manner as that described above, for the triaxial test stress conditions, are those occurring on the axis of the loaded area where the principal stresses are vertical and horizontal with the two horizontal stresses equal. For any off-axis situation the three principal stresses are different and the principal planes are inclined to the vertical and horizontal. In this case q must always be positive as may be seen from equation (8.2). A method of assigning a sign to q, by considering a third stress invariant, has been suggested by Thrower (68), as discussed in Chapter 3. However, this was not considered herein, since there was no evidence to suggest that the effect of the sign is important.

The effects of considering only positive values of q may be seen in Figure 8.3, which shows the type of p versus q plot referred to from now on. The inaccessible area becomes relatively smaller, and a significant area between the uniaxial tension and compression lines may be investigated by using a tensile axial stress. The area to the right of the uniaxial compression line may be investigated with the axial stress greater than the confining stress, or, vice-versa. The following Chapter shows that the majority of stress conditions, predicted by linear or non-linear analysis for both pave-:ment materials, can be reproduced in the triaxial test.

The two permanent strain invariants, v_p and ε_p, obtained in the

triaxial test (equations (8.7) and (8.8)), for each of the values of p and q investigated, should, ideally, be solved to give the three in-situ principal permanent strains. Values of v_p and ε_p for stress conditions other than those investigated could be obtained by inter-:polation, or, extrapolation, if circumstances permit. Subsequent application of Mohr's circle would enable a value of the vertical permanent strain to be obtained, and then the permanent deformation to be calculated. However, there are three unknowns and only two equations, and therefore some simplifying assumption has to be made. The approach adopted herein was to assume that the in-situ vertical permanent strain is equal to the major principal strain measured in the repeated load test. This is likely to err on the safe side for design purposes.

8.4 LINEAR OR NON-LINEAR ANALYSIS

Initially, linear elastic analysis (60) was used to calculate stress distributions. It was thought that this would be adequate, since previous investigators (78) had found that, provided the resilient modulus and Poisson's ratio were carefully selected, agree-:ment was obtained with in-situ measurements, although this conclusion seems less certain under high temperatures (79).

Results from the characterisation tests showed that the dense bitumen macadam was remarkably non-linear, particularly when a tensile stress was applied, and the Keuper marl showed non-linearity typical of a cohesive soil. It was therefore decided to adopt a non-linear analysis, and to use the finite element computer program DEFPAV (24). This program has the added advantage of calculating permanent deform-:ations from "creep equations" selected by the user from those already existing in the program, or from the results of independent tests. In this case, the calculations were based on equations derived from

the material characterisation tests (Chapter 9). The development of these equations is described in Chapter 11.

The locations for the calculations using the linear elastic analysis, for pavement 1, are shown in Figure 8.4. Similar arrange-:ments were used for pavements 2 and 3, but the loading conditions differed. Figure 8.5 shows the network of elements used in the non-linear analysis for pavement 1. Again, similar networks were used for pavements 2 and 3, with slight differences in the loading. For both types of analysis the greatest density of calculations were carried out near the surface of the pavement and close to the loaded area. The only restriction on the number of calculations was in the non-linear analysis where the maximum number of elements allowed was 225.

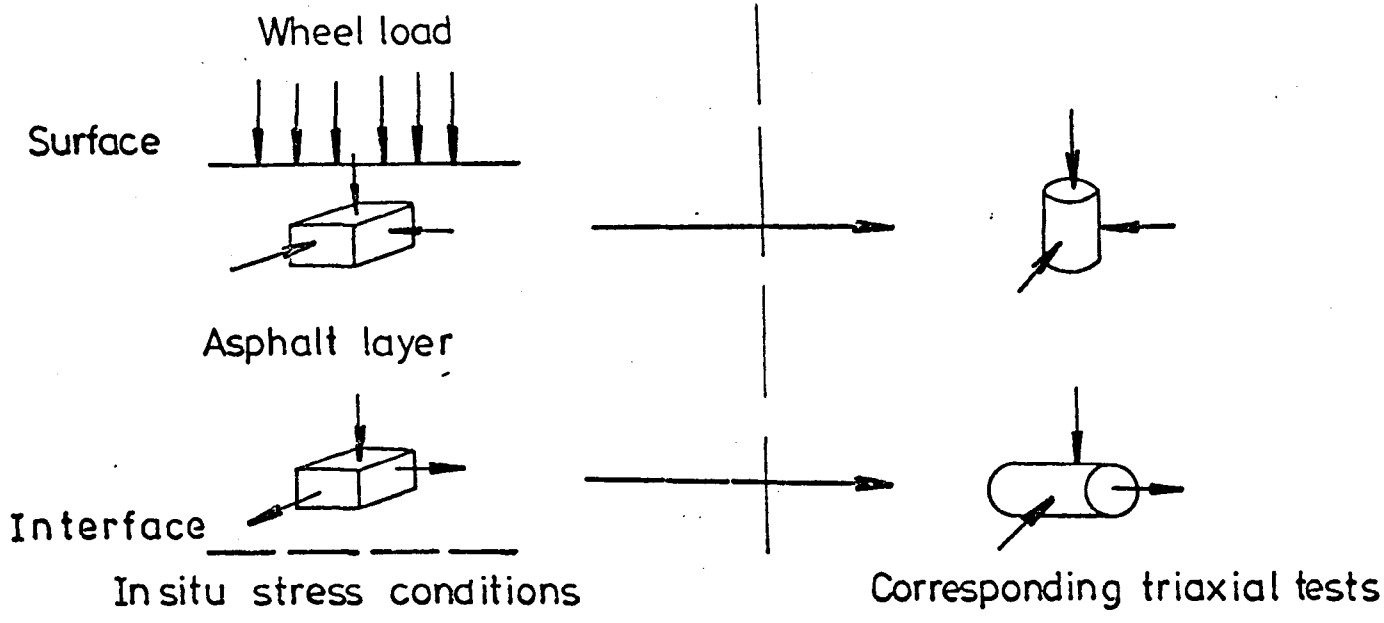

FIGURE 8.1 COMPARISON OF IN-SITU AND TRIAXIAL STRESS CONDITIONS

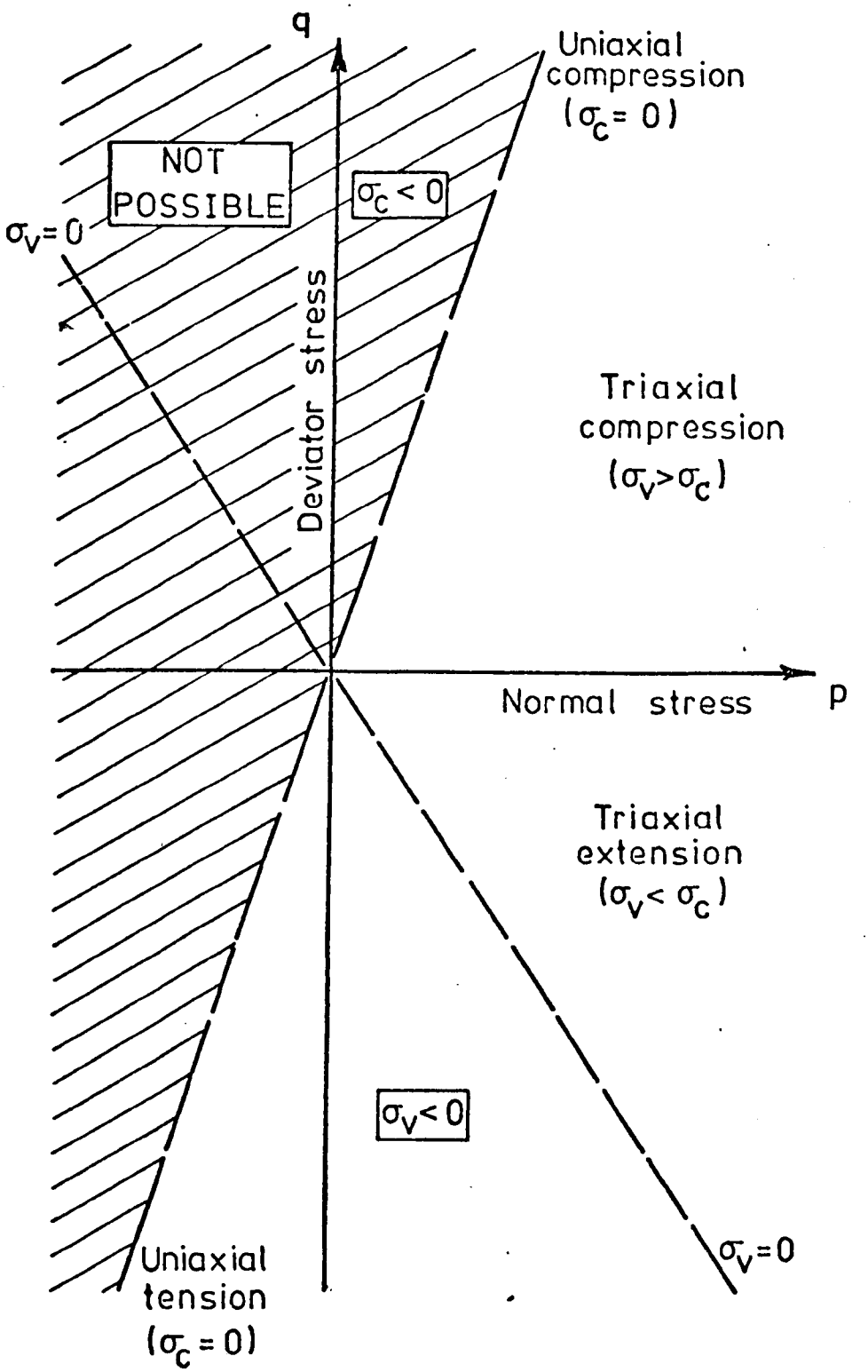

FIGURE 8.2 IDEALISED RANGE OF STRESSES WHICH CAN BE APPLIED IN THE TRIAXIAL TEST

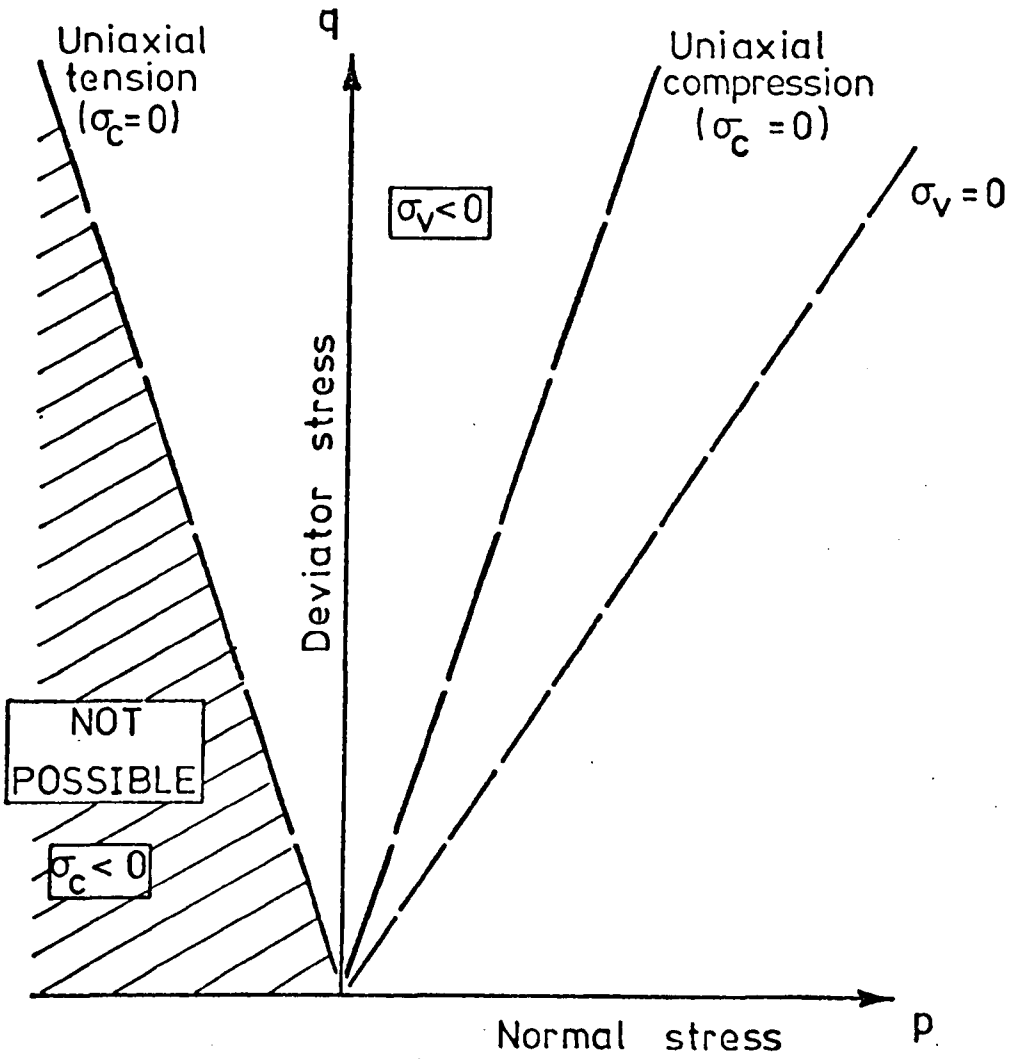

FIGURE 8.3 RANGE OF STRESSES WHICH CAN BE APPLIED IN THE TRIAXIAL TEST

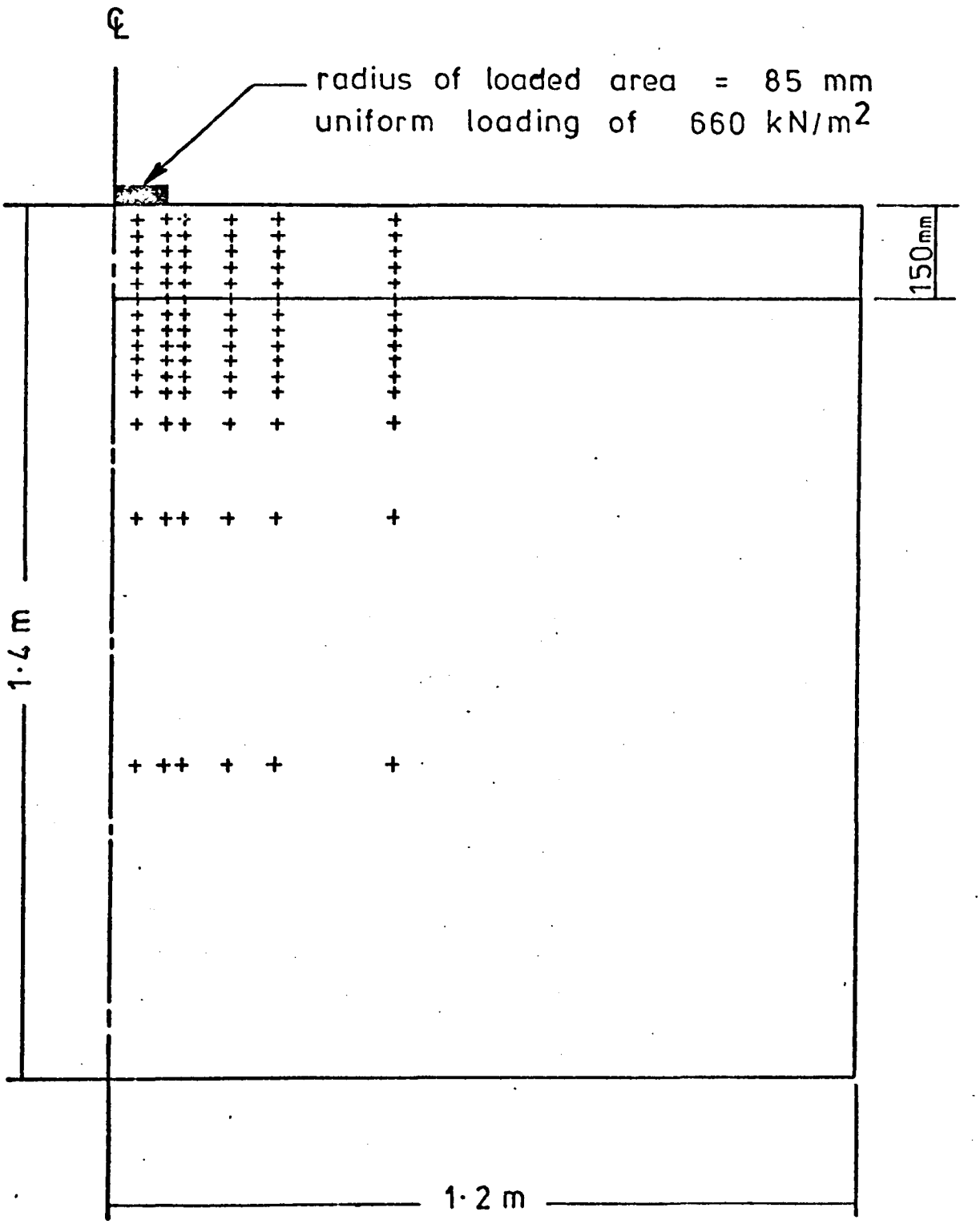

FIGURE 8.4. LOCATIONS FOR CALCULATIONS USING LINEAR ELASTIC ANALYSIS

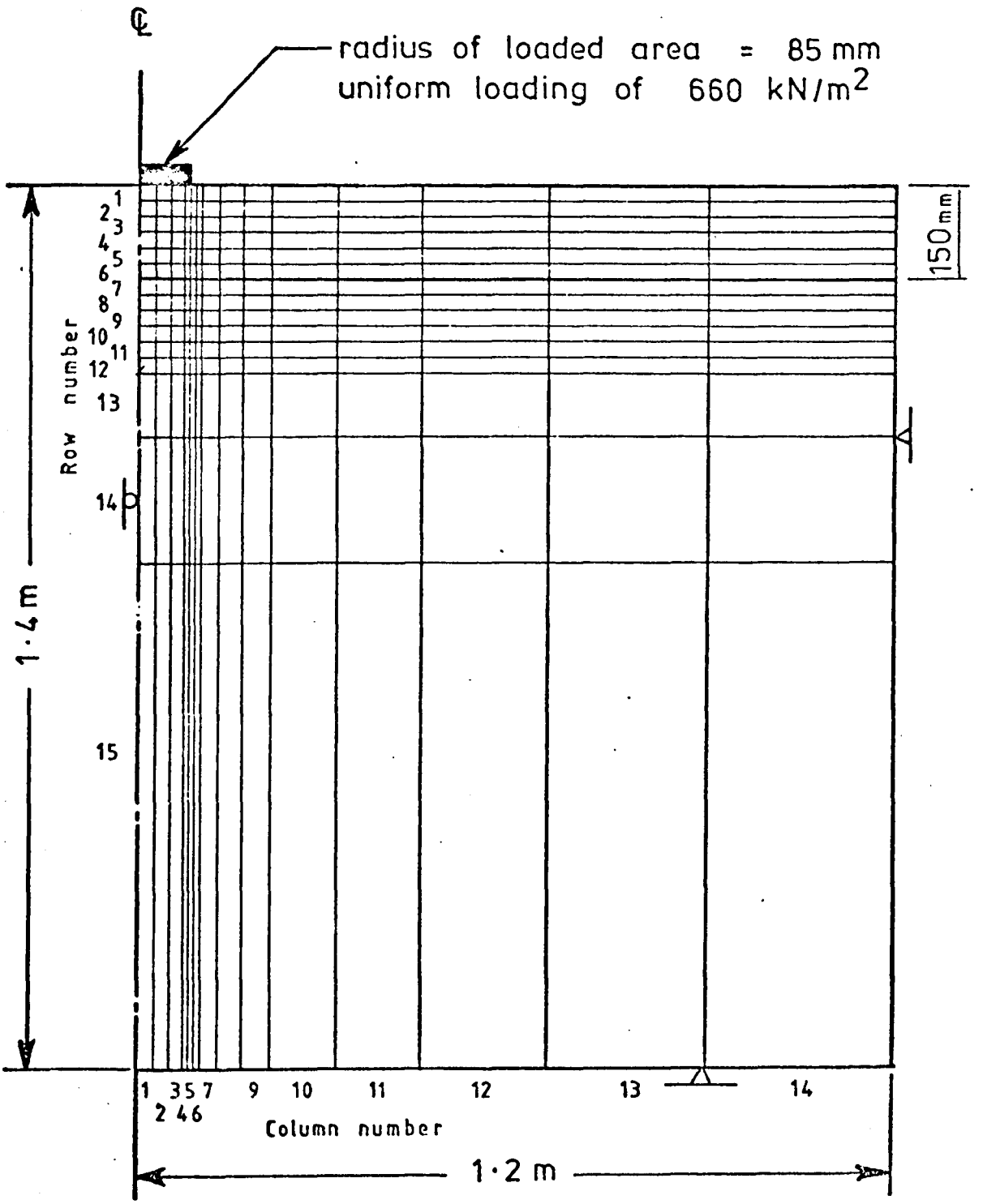

FIGURE 8.5 FINITE ELEMENT NETWORK FOR THE NON-LINEAR ELASTIC ANALYSIS

CHAPTER NINE

MATERIAL CHARACTERISATION TESTS

9.1 INTRODUCTION

Both pavement materials were characterised using electro-hydraulic servo-controlled testing machines, which had been previously developed at Nottingham (51, 80, 81). 100mm diameter cores of Keuper marl were taken prior to the laying of each DBM layer, and 100mm diameter DBM cores were taken several days after the completion of paving.

The majority of tests carried out on the DBM were on cores from pavement 1. A few DBM cores from the two subsequent pavements, which incorporated nominally the same material, were tested for comparison with that used in pavement 1. All the tests were conducted at 30°C, the temperature of the pavement experiments.

The majority of tests for the Keuper marl were carried out on cores taken in between the testing and excavation of pavement 1 and the laying of the DBM for pavement 2. A number of cores had been taken before the paving of pavement 1 and stored in latex rubber membranes, but these leaked severely, causing the cores to dry. Subsequent cores were sealed in wax before they were stored. A few cores were taken following the excavation of pavement 2 and were tested for comparison with the previous tests.

9.2 DENSE BITUMEN MACADAM

9.2.1 Introduction

The test conditions were based on the results of a linear elastic analysis (60) of pavement 1 and they are shown superimposed in the complete p, q plot for in-situ conditions in Figure 9.1. Once tests

had been completed at several of these stress conditions, it became apparent that the material exhibited considerable non-linearity. A non-linear analysis (24) was therefore carried out using the results of these tests to check that the original test conditions would cover this new stress distribution. It was found necessary to add only two more test conditions. The non-linear analysis based on the results of the complete test programme for pavement 1 is shown in Figure 9.2.

Lines representing uniaxial compression and uniaxial tension are shown in Figures 9.1 and 9.2, having slopes of +3 and -3 respectively*. Tests carried out at any point on one of these lines requires no confining pressure, only a compressive or tensile axial stress respect-:ively. Points to the right of the uniaxial compression line require axial compression plus confining stress (compression tests), and points between the uniaxial compression and tension lines require axial tension plus confining stress (tension tests). The uniaxial tension line represents the limit which can be reached in a triaxial test, i.e. consider the mean normal stress:

$$p = \tfrac{1}{3}(\sigma_v + 2\sigma_c)$$

if $\sigma_c = 0$, $p = \sigma_v/3$ and $q = \sigma_c - \sigma_v$, where σ_v the vertical stress is tensile, and σ_c, the confining stress is compressive.

$$\therefore \quad q = -\sigma_v \text{ and } p = -q/3$$

No test condition to the left of the uniaxial tension line can be represented by a triaxial test. However, particularly judging by the non-linear analysis (Figure 9.2) this represents a very small portion of the tension zone in the bituminous layer.

When testing at a particular combination of p and q, which did not

* This representation ignores the effect of the third stress invariant and follows the approach suggested by Brown (36).

lie on either the uniaxial tension or compression lines, a problem arose in selecting the suitable stress path. This was due to the fact that facilities for applying a cyclic confining stress were not available. This meant that the only fluctuation of p would be due to the vertical cyclic stress, and the stress paths would be restricted to lines parallel to either the uniaxial compression or tension lines.

Previous testing of a nominally identical mix by Snaith (22) indicated that similar permanent strains were obtained in tests with constant and cyclic confining stresses, when the constant value equalled the mean of the cyclic one.

Consequently, the combinations of constant confining stress and vertical cyclic stress were chosen on this basis, as illustrated in Figure 9.3 for p = 400 kN/m^2 and q = 400 kN/m^2.

9.2.2 Test Programme

The test conditions shown in Figures 9.1 and 9.2 were selected on the basis of analyses of pavement 1 and although it was expected that analyses of pavements 2 and 3 would produce somewhat different stress distributions, the same basic framework was used for all three pave-:ments so that comparisons would be simplified.

Loading Frequency: The majority of tests were carried out with continuous sinusoidal loading at a frequency of 1 Hz, rather than at a frequency corresponding to the loading in the pavements. This was used for convenience, since Snaith (22) found that within a frequency range which included 1 Hz, the permanent deformation was dependent on the total time of loading, rather than the frequency and number of load applications.

Some tests were carried out at a frequency of 3.3 Hz with a

2 second rest period between each stress pulse. This corresponded to a computed loading time for pavements 1 and 2, where the known elapsed time between the wheel passing a particular point was 2 seconds. The frequency was calculated by reference to Barksdale (82), which gave a principal stress pulse time (t_B) of 0.20 seconds at the centre of a 150mm thick pavement layer, and to Brown (83) who stated that the average loading time was 1.5 t_B. This gave an average stress pulse time of 0.30 seconds, corresponding to a frequency of 3.3 Hz.

Pavement 1: A total of 24 vertical cores were taken from pavement 1 and these were primarily used for compression tests. Initially, four cores were used for compression tests where the end platens were glued to the core, so that the specimen could be bolted into the testing machine. This procedure was adopted so that there would be compatib-:ility between tension and compression tests. However, the cores used in these tests were found to barrel very badly, and it was decided to adopt the more conventional lubricated ends for compression tests (Snaith (22)).

Three tension tests were carried out with vertical cores, but these proved unsuccessful, since the cores fractured along one of the interfaces which had been formed during compaction. It was, there-:fore, decided to supplement these vertical cores with laboratory manufactured specimens of the same mix, compacted, in moulds to the same void content. Following completion of testing on pavement 1, the DBM was sawn into slabs, and horizontal cores were taken from untrafficked sections.

The manufactured specimens were used for tension testing (10 spec-:imens), and also for an investigation to compare the effects of load-:ing at a frequency of 1 Hz and a frequency of 3.3 Hz with a 2 second rest period (4 specimens). The horizontal cores were also used for

tension tests (10 cores), and for an investigation to check the isotropy of the material (3 cores). Some of the horizontal cores used for tension tests were tested at 3.3 Hz with a 2 second rest period. This ensured better control of the test, which was of short duration when continuous loading at a frequency of 1 Hz was used.

Pavement 2: Thirteen vertical and eight horizontal cores were taken from pavement 2. However, because of the high void content of the mix used for this pavement, these cores were of poor quality. It was found that, after storing them at room temperature for only a few days, the majority had deformed under their own weight. Therefore, of the remainder, two cores were tested at one test condition ($p = 133$, $q = 275$ kN/m^2, Figures 9.1 and 9.2) so that a comparison could be made with results from the same test condition on samples from pavement 1. An additional core was used to carry out an investigation of the resilient properties of the mix, by testing for a few cycles at values of p and q covering most of the range for compression tests. Frequencies of 1 Hz and 3.3 Hz with a 2 second rest period were both used.

Pavement 3: The same general approach was used as for pavement 2 in order to minimise testing. Three cores were tested at $p = 133$, $q = 275$ kN/m^2 (Figures 9.1 and 9.2), and one was used to determine the resilient properties of the mix, at both 1 Hz and 3.3 Hz with a 2 second rest period. A summary of the entire test programme is presented in Table 9.1.

9.2.3 Specimen Preparation

Each core was trimmed with a diamond tipped cutting blade so that the ends were perpendicular to the longitudinal axis and the

TABLE 9.1 SUMMARY OF TEST PROGRAMME

Test Series	Description of tests carried out
C1	The main series of compression tests on vertical cores from pavement 1.
TV1	Tension tests on vertical cores from pavement 1 and laboratory manufactured specimens of the same mix and void content.
TH1	The main series of tension tests on horizontal cores from pavement 1.
CR1	A supplementary series, on laboratory manufactured specimens to investigate the effect of using the in-situ loading frequency (3.3 Hz) with a 2 second rest period.
I1	A supplementary series to investigate the isotropy of the material from pavement 1.
C2	Compression tests on vertical cores from pavement 2.
C3	Compression tests on vertical cores from pavement 3.

length was approximately 125mm. For compression tests the cut ends were polished on the side of an abrasive cutting blade. Before the cores were tested, they were weighed in air and water, for void content determination, and after testing, a portion of some cores was used for binder content analysis.

Three pairs of locating pips, for the strain measuring devices, were glued with epoxy resin to the core using a specially prepared jig for accurate positioning. The pips can be seen in position in Figure 9.4. The top and bottom pairs were used to locate the LVDT's for longitudinal measurements, over a gauge length of 75mm, and the middle pair was used to locate a lateral strain collar incorporating another LVDT. If a confining pressure was to be applied in the test, a neoprene rubber membrane was placed over the core.

For compression tests a pair of steel end platens were employed

with finely machined surfaces. The contact between the polished ends of the core and the end platens was via two thin latex rubber discs the same diameter as the end platens, which were lubricated with silicone grease. This ensured that the core would deform in the shape of a right cylinder.

For tension tests, the ends of the cores were glued to loading platens (shown in Figure 9.4) using epoxy resin. The core could then be bolted in place in the testing machine as shown in Figure 9.5.

9.2.4 Testing Equipment

Electro-hydraulic servo-controlled testing machine: The machine, shown in Figure 9.5, had been developed for fatigue testing of bitum-:inous materials (12, 80) using a similar test configuration to that adopted for the tension tests. For compression tests the specimen, complete with end platens, was placed on the bottom loading flange, and was loaded via a ball bearing below the top of the upper loading flange. This arrangement is shown in Figure 9.6.

The hydraulic ram applied a repeated load to the specimen, which could be either unconfined or have a constant confining stress applied by air pressure. The pressure was maintained within a triaxial cell (shown in position in Figure 9.5) which was raised above the specimen when not in use, as in Figure 9.6. The cell pressure was monitored by a pressure gauge situated just outside the cell.

Deformation measurement: Longitudinal deformation was measured with two diametrically opposed LVDT's, over gauge lengths of 75mm, about the mid-height of the specimen. The LVDT's were fitted across these gauge lengths by screw-fittings to the locating pips, as shown in Figure 9.7. Thus the measurements were taken away from the areas which could be subject to end effects.

Radial deformation was also measured by an LVDT mounted across the jaws of a hinged strain collar of the type described by Snaith (22) located on two diametrically opposed targets at the centre of the specimen as shown in Figure 9.7. As the specimen expanded or contracted laterally, the gap between the free ends of the collar changed and this change was measured by the LVDT.

The monitoring devices which were employed are described within the following section.

9.2.5 Testing Procedure

All tests were carried out at 30°C, the same temperature as the pavement experiments. Prior to testing, each specimen was left in the temperature controlled room, which housed the testing machine, for at least 24 hours, to ensure uniform temperature conditions.

Three monitoring devices were used to provide a visual check on the outputs from the load cell and the LVDT's. These were a Digital Voltmeter (DVM), an Ultra Violet (UV) recorder, and a Cathode Ray Oscilloscope (CRO), all of which are shown in Figure 9.8, together with the control equipment for the testing machine and the LVDT's. The load cell and the LVDT's had been calibrated using both the DVM and UV recorder, and as these were both used to record the response of a specimen under test, cross checking of measurements was possible. However, the UV recorder was favoured because of the ability to record simultaneously the outputs from the load cell and the LVDT's.

Each test was continued for either 100,000 cycles, or until excessive deformation had occurred and the core responded erratically, or, in the case of a tension test, when fracture of the specimen had occurred.

9.2.6 Results

Processing: The behaviour of a specimen during a test was recorded on the oscillograph paper, and occasionally, a reading was taken from the DVM. The outputs could, in general, be processed by hand during the course of a test, parallel with the necessary control of the test machine.

At frequent intervals of time, the vertical and radial permanent and resilient strains were computed from the measured deformations. The vertical deformation from each vertical LVDT was monitored separately, and an average value used unless one was obviously in error, a phenomenon which could occur if a locating pip became loose. The resilient modulus and Poisson's ratio were computed from the resilient strains, and were used to check and update the values used in the elastic analyses.

From this information a table of results and graphs of the material behaviour were constructed. For those test conditions where more than one specimen was tested, the results were averaged. Where a test was carried out at a frequency of 3.3 Hz with a 2 second rest period, the number of cycles was divided by 3.3 to obtain the elapsed time.

Presentation: Table 9.2 summarises the results of the seven series of tests outlined in Table 9.1. Where a binder content analysis was carried out on the test specimen, the actual value obtained is shown, otherwise an average value for the set of specimens from each pavement is shown. The void content was obtained from a knowledge of the binder content and bulk specific gravity of a specimen and the specific gravities of the binder and aggregate.

The initial resilient modulus was based on the resilient strain near the beginning of a test, once the desired amplitude of vertical

TABLE 9.2 SUMMARY OF RESULTS OF DBM CHARACTERISATION TESTS

Stress Conditions (kN/m^2)			Test Frequency	Binder Content (%)	Void Content (%)	Resilient Properties			Length of Test (secs)	No. of Tests
p	q	σ_3				Initial Modulus (MN/m^2)	Final Modulus (MN/m^2)	Initial Poisson's Ratio		
TEST SERIES C1										
133	400	0	A	4.5	5.8	700	770	.40	3,200	3
133	275	20.5	A	4.8	4.8	700	780	.40	25,000	2
133	150	41.5	A	4.9	4.8	500	330	.30	100,000	1
400	800	66.5	A	4.7	5.8	1,125	1,175	.11	18,000	2
400	400	133.0	A	4.7	5.3	900	625	.30	65,000	1
400	275	154.0	A	4.6	6.0	750	500	.50	50,000	1
400	150	175.0	A	4.7	5.8	1,000	675	.38	100,000	2
150	650	300.0	A	4.7	5.2	925	500	.30	100,000	2
800	800	267.0	A	4.7	5.8	1,540	1,650	.40	70,000	1
800	400	333.0	A	4.9	5.0	1,300	1,000	.43	100,000	2
TEST SERIES TV1										
0	50	8.3	A	4.7	6.3	100	80	-	900	1
0	150	25.0	A	4.7	5.9	250	100	-	110	2
-16.6	50	0	A	4.7	6.2	100	50	-	200	3
-50	150	0	A	4.7	5.8	100	70	.40	140	3
TEST SERIES TH1										
0	80	13.3	B**	4.9	4.6	400	400	.45	420	1
0	240	40.0	B	4.9	4.6	275	225	.35	180	2
-16.6	50	0	A*	4.9	4.1	250	180	-	1,000	3
-50	150	0	A	4.7	5.2	300	250	.40	80	3
TEST SERIES I1										
133	275	20.5	A	4.9	4.6	1,175	820	.45	10,000	3
TEST SERIES C2										
133	275	20.5	A	4.9	9.7	450	500	.70	1,500	2
Vary			A & B	4.9	9.7	-	-	-	-	1
TEST SERIES C3										
133	275	20.5	A	4.95	8.3	400	420	.50	20,000	3
Vary			A & B	4.95	8.3	-	-	-	-	1

* A = 1 Hz ** B = 3.3 Hz + 2 secs rest

cyclic stress had been correctly set. The final resilient modulus was that determined just before the end of a test. The initial resilient Poisson's ratio was the ratio of the radial to longitudinal resilient strain measured at the same time as the initial resilient modulus.

The results of the investigation of the effect of rest periods, series CR1, are not tabulated. Two tests were conducted with continuous cycling, and two with rest periods, and although not conclusive, the results did show that after equal periods of time, the vertical permanent strains were similar. This conclusion is supported by Cooper et al (84) and Snaith (22). It was henceforth assumed that the permanent deformation was time dependent, and the most convenient form of loading was used in each test. For analysis of results, the number of cycles was subsequently converted to time.

Permanent Strain Behaviour: Figures 9.9 to 9.16 show both the vertical and radial permanent strain results plotted against time on semi-logarithmic bases, which conveniently present the results for an entire test. It was found that, when the vertical strain results were plotted on a completely logarithmic basis, as will be shown in Chapter 11, they were in a more convenient form to evolve a permanent strain model.

The results of test series C1 indicated the sensitivity of the behaviour of the material to the stress parameters p and q. In general, increasing q increased the permanent strain, and increasing p decreased it, the most critical combination being when p was low and q was high, which resulted in high deformations and early failure of the material. This was particularly true for the tension tests (series TH1, Figures 9.15 and 9.16) where, with a zero or negative p value, the test specimens were able to sustain only a low value of q for a few cycles of the load.

The general results of both test series TV1 and TH1 are shown in

Table 9.2. The TH1 results were more consistent and thought to be more representative, since the repeated axial tension was applied in the same direction as in-situ.

The results from series I1 (Figure 9.13) show that the horizontal cores underwent more deformation than the vertical ones, a fact also observed in comparing the results of series TV1 and TH1. This is probably due to the noticeable orientation of the larger aggregate particles, which would result in the aggregate interlock in the two directions being different.

The results from series C1, C2 and C3 are compared in Figure 9.14, and indicate that the material from pavements 2 and 3 underwent more deformation than that from pavement 1. This could be attributed to the higher void contents of the material from pavements 2 and 3, resulting from a combination of poorer aggregate grading and compaction, compared with pavement 1.

Resilient Properties: Figures 9.17 to 9.19 show plots of resilient modulus versus p for each pavement. The plot for pavement 1 includes results from all the tests in series C1 and TH1. The plots for pave-:ment 2 and 3 are from much more limited data, the majority of points being obtained from a number of tests on one specimen.

Broadly speaking, the resilient modulus behaviour for all three pavements followed the same trend, exhibiting considerable non-linearity, as would be expected under the test conditions of high temperature and fairly long loading times. From the limited data available, there appeared to be little difference in the moduli measured at 1 Hz and 3.3 Hz with a 2 second rest period. This is probably because the material was able to recover more during the rest period, and thus the measured deformations were comparable for the two modes of loading. Had both modes utilised continuous cycling, the higher frequency would result in a higher modulus.

The values of the initial resilient Poisson's ratio were not plotted since no distinct relationship emerged. However, the values measured are shown in Table 9.2 and for series C1 and TH1 (pavement 1) have an average value of approximately 0.40. Snaith (22) found that the value of Poisson's ratio was particularly dependent on temperature, which was constant for all tests carried out in this project. He also found that Poisson's ratio decreased with increasing confining pressure, which is roughly equivalent to increasing p. No such trend could be distinguished from the results presented herein.

9.3 KEUPER MARL SUBGRADE

9.3.1 Introduction

The stress conditions for tests on the clay cores were determined from linear elastic analysis, assuming a modulus based on the empirical relationship:

$$E = 10 \times CBR \ (MN/m^2)$$

Standard CBR tests on the clay indicated a value of 5%, thus, initially, the modulus was taken as 50 MN/m^2. The results of the analysis using this modulus are shown in Figure 9.20 with the test conditions superimposed. The number of tests required was comparatively small due to the small spread of the stress distribution.

After completion of several tests, it became apparent that the non-linearity of the clay was too great to approximate with a linear analysis, and hence a non-linear analysis was adopted. The results of this are shown in Figure 9.21, compared with the linear analysis. It can be seen that the spread of the stress conditions to be covered is wider than for the linear analysis, but still thought to be sufficiently narrow to be approximated by a straight line. Therefore, the test conditions chosen from the linear analysis were retained, so as to

avoid extensive additional tests in the limited time which was available.

The limitation on the form of the test path used was similar to that which applied to the DBM characterisation tests, i.e. constant confining stress. The selection of appropriate stress paths was identical to that outlined for the DBM tests.

9.3.2 The Test Programme

The test conditions for the basic programme are shown in Figures 9.20 and 9.21. However, in order to develop a more rigorous model for the permanent deformation behaviour of the clay, one more test condition was added, $q = 70\ kN/m^2$. Hence, all tests were carried out on the line $q = 5.0 + 1.75\ p$, at one of the following values of q: 15, 30, 40, 50 and 70 kN/m^2.

Ten cores were taken following the testing and excavation of pavement 1. These cores were found to be dryer and more dense than those taken at the time of construction, as may be seen in Figure 6.2, where the dry density versus moisture content plot is shown. It was therefore decided to use these cores largely for a preliminary investigation, and to establish a testing technique. This group of tests was designated series K1.

A further ten cores were taken before the construction of pavement 2, from new material which had been used to replace that lost after the excavation of pavement 1. These cores were of a similar density and moisture content to those taken before construction of pavement 1 (Figure 6.2). The test carried out on these cores constituted the main series designated K2.

Finally, a batch of cores was taken following the testing and excavation of pavement 2, of which three were used for characterisation tests (series K3). The densities and moisture contents

of these cores, shown in Figure 6.2, were again higher and lower respectively than cores taken before construction. It was therefore clear that the subgrade dried out and became more compact during testing, causing a reduction in moisture content of about 1.5%. The air voids in the material remained almost constant in both cases.

A small dead load equivalent to the overburden pressure, was applied to the specimen throughout a test. This had been calculated using a linear elastic analysis, for a number of positions in the subgrade, covering the range of values of q from 15 to 70 kN/m^2.

Test Frequency: All the tests were carried out at a frequency of 4 Hz, and with a 2 second rest period between pulses. The frequency was obtained by reference to Barksdale (82), and corresponded to a principal stress pulse time of 0.25 seconds which was appropriate for a position just below the surface of the subgrade.

This is at variance with the DBM tests where an average stress pulse was used. The DBM tests were carried out at a later stage than the clay tests, when it was considered more realistic to use an average stress pulse. However, the use of the exact pulse loading time is not essential for permanent strain characterisation which depends on total time. For DBM the resilient modulus at a different loading time can be found by utilising van der Poel's nomograph, and for clay, Lashine (43) showed that resilient modulus was independent of frequency over the range considered here.

9.3.3 Specimen Preparation

The equipment used for the characterisation tests was normally used for testing 75mm diameter specimens. Therefore, when the cores were removed from wax they were trimmed to this diameter using a soil lathe.

Each core was then placed in a 75mm diameter split mould and the ends trimmed to a final length of approximately 113mm. The trimmings from both operations were used for moisture content determination.

Lubricated ends consisting of two latex rubber membranes and silicone grease on polished loading platens were used to minimise lateral end restraint.

9.3.4 Test Equipment

Electro-hydraulic servo-controlled test machine: A machine designed specifically for testing soils (51, 81) was used for the clay characterisation tests and is shown in Figure 9.22. In principal, this machine was identical to that used for the DBM tests. However, the triaxial cell was different, being entirely detachable from the machine. The load was transmitted to the specimen via a loading piston passing through a bearing at the top of the cell. The contact between the piston and the loading ram was through a half ball-bearing.

The load cell was located below the triaxial cell and hence any friction between the loading piston and the cell would be included in the measurement. The friction was minimised by lubricating the bearing and piston with "Vaxiella" oil before each test, and maintaining the level of oil in a small reservoir around the top of the bearing where the piston entered the cell.

The testing equipment was capable of cycling the cell pressure, but to simplify the test procedure, and maintain compatibility with the DBM tests, a constant cell pressure was used. The confining medium was de-aired water, and the cell pressure was measured by a transducer located at the top of the cell.

Drainage connections on the cell were blocked off, as were tappings for a pore-pressure measuring device, since drainage could not occur in the test pavement, and pore-pressure measurements could not be made in

this partially saturated material.

Deformation Measurement: Longitudinal deformation was measured by an LVDT, mounted rigidly to the loading frame as shown in Figure 9.22. The cyclic output from the LVDT thus included the deformation of the whole vertical loading system. This effect could be calibrated out by measuring the cyclic deformation of the system with a rigid specimen in place of the soil. The error was largely due to the cyclic deform-:ation of the lubricated latex rubber discs used to create "free" end conditions between the test specimen and the end platens. Thus, the calibration operation was carried out before each test using the same lubricated latex discs which were to be used in the test.

The radial deformation was measured at the centre of the test specimen by two pairs of 25mm diameter strain coils whose response was monitored by a Bison instrument, each pair mounted on diametrically opposite sides of the specimen as shown in Figure 9.23. The inner coil of each pair was attached to the specimen, and the outer one mounted onto a carrier whose movement was controlled by a micrometer. Calibration of the coils was carried out before each test, using the micrometers to alter the separation of each pair by a known amount, and recording the change in signal on a UV recorder.

The coils were identical to those used in the test pavement, and reference should be made to Chapter 5 for a description of the principles of operation.

9.3.5 Testing Procedure

Following the preparation of the test specimen, the triaxial cell top was clamped to the base, the loading piston inserted and the cell filled with de-aired water. The cell was then placed on the loading pedestal, the cell pressure line connected, and all electrical connect-:ions made. The cell pressure transducer was de-aired, and zeroed,

and the output from the load cell zeroed. Finally, the LVDT for measuring vertical strain was placed in position, so that it was at one end of its range.

Three devices (DVM, UV recorder and CRO) were again used to monitor outputs from the load cell, strain coils, and the LVDT, and are shown in Figure 9.24 with the control equipment for the testing machine. The load cell and the LVDT had been calibrated using both the DVM and the recorder and the strain coils using the recorder only. The UV recorder was used to register the behaviour of a speci-:men under test with intermediate checks from the DVM.

A test was continued for either 100,000 cycles or until excessive deformation had occurred. In some cases, premature failure of the specimen occurred due to a 'spike' of electrical noise being picked up by the control equipment and causing a sudden surge of load. As a result of this phenomenon, several tests did not fulfil their potential.

9.3.6 Results

Processing: The results were processed from the UV recorder paper by hand during the course of the test. The vertical and radial permanent and resilient strains were computed at frequent intervals, and the resilient modulus and Poisson's ratio computed from the resilient strains. A table and graphs of the material behaviour were constructed. Where more than one test was carried out at any test condition, the results were averaged, any obviously erratic results being discarded.

Presentation: A summary of all the successful tests is provided in Table 9.3. The initial resilient modulus was that measured at the start of a test, once the desired amplitude of vertical stress had been achieved. The final resilient modulus was that measured just before the end of a test. The initial resilient Poisson's ratio was the

TABLE 9.3 SUMMARY OF RESULTS OF KEUPER MARL CHARACTERISATION TESTS

Stress Conditions (kN/m^2)			Moisture Content (%)	Dry Density (lb/ft^3)	Resilient Properties			Cycles in Test	No. of Tests
p	q	σ_3			Initial Modulus (MN/m^2)	Final Modulus (MN/m^2)	Initial Poisson's Ratio		
TEST SERIES K1									
14.3	30	1.8	15.4	114.6	70	65	.28	14,000	2
25.7	50	2.0	15.5	116.1	38	33	.44	60,000	3
TEST SERIES K2									
5.7	15	1.8	17.4	109.8	30	30	.33	100,000	3
14.3	30	2.0	17.5	110.6	15	15	.27	20,000	4
25.7	50	3.9	17.0	110.9	10	10	.48	34,000	2
37.1	70	6.9	17.7	110.0	15	15	.35	14,000	2
TEST SERIES K3									
20.0	40	2.8	16.0	114.2	42	42	.30	100,000	1
37.1	70	6.9	16.0	113.0	40	31	.45	90,000	1

ratio of the radial to longitudinal resilient strain measured at the same time as the initial resilient modulus.

Permanent Strain Behaviour: Figures 9.25 to 9.27 show both the vertical and radial permanent strains plotted against the number of cycles, on a semi-logarithmic basis, for the three test series. In most cases, the lines were straight, which was convenient in develop-:ing the permanent strain model. The results are such that, in all tests, the volumetric strain was compressive, thus compaction always occurred.

Resilient Properties: Figure 9.28 shows the plot of resilient modulus versus q for the test series K2. The modulus for q = 70 kN/m^2 was higher than expected, which was probably due to the fact that the two tests carried out, at this condition, were on cores which had already been tested at a lower value of q. The material showed the usual stress softening non-linearity associated with cohesive materials.

The results for resilient Poisson's ratio are not plotted, but, as can be seen from Table 9.3, there appears to be a trend of increas-:ing Poisson's ratio with increasing q. Again, the result shown for series K2 where q = 70 kN/m^2 is at variance with the general trend.

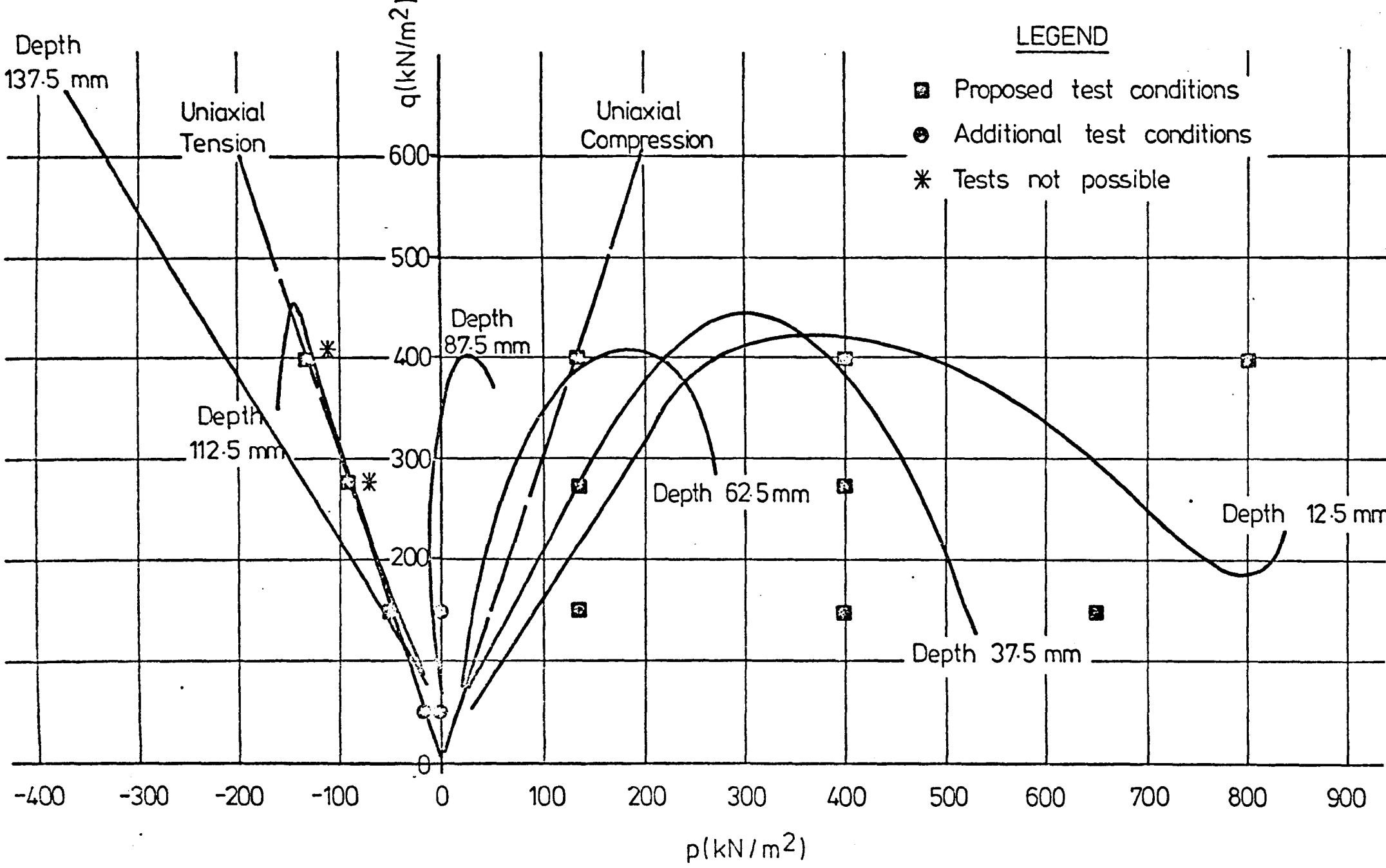

FIG. 9.1 STRESSES IN THE DBM (PAVEMENT NO. 1) BY LINEAR ELASTIC THEORY, WITH LABORATORY TEST CONDITIONS

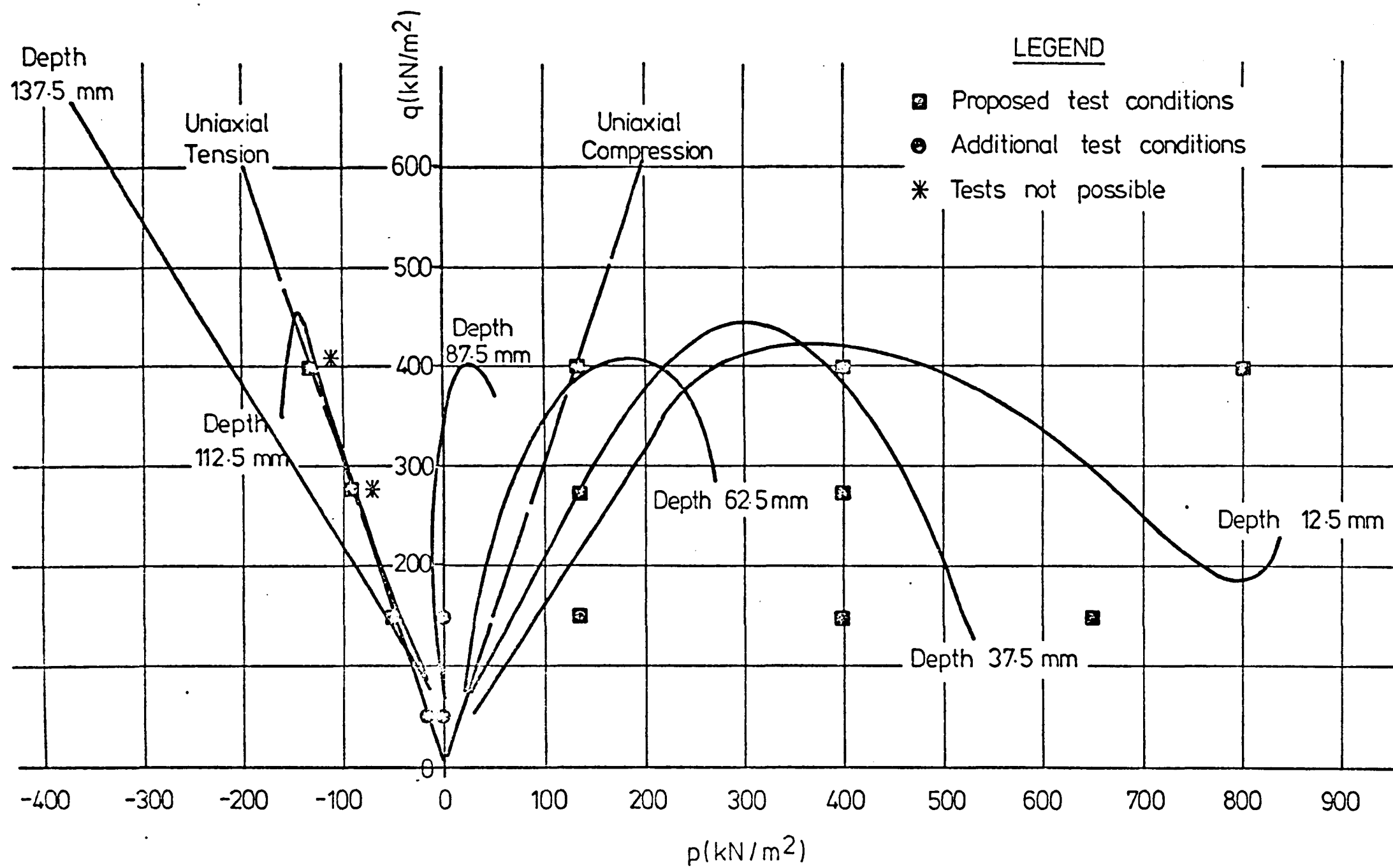

FIG. 9.1 STRESSES IN THE DBM (PAVEMENT NO. 1) BY LINEAR ELASTIC THEORY, WITH LABORATORY TEST CONDITIONS

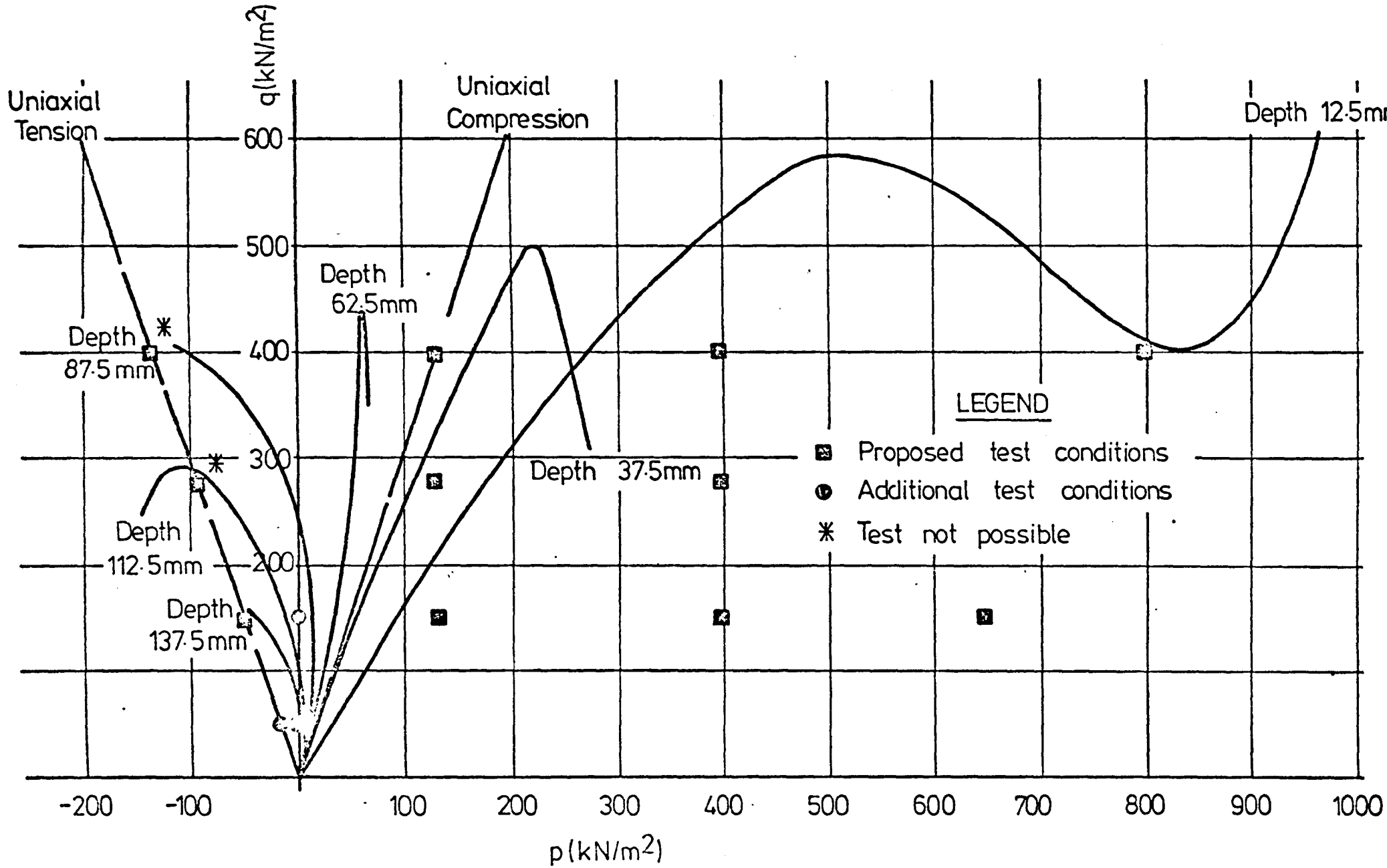

FIG. 9.2 STRESSES IN THE DBM (PAVEMENT NO. 1) BY NON-LINEAR ELASTIC THEORY, WITH LABORATORY TEST CONDITIONS

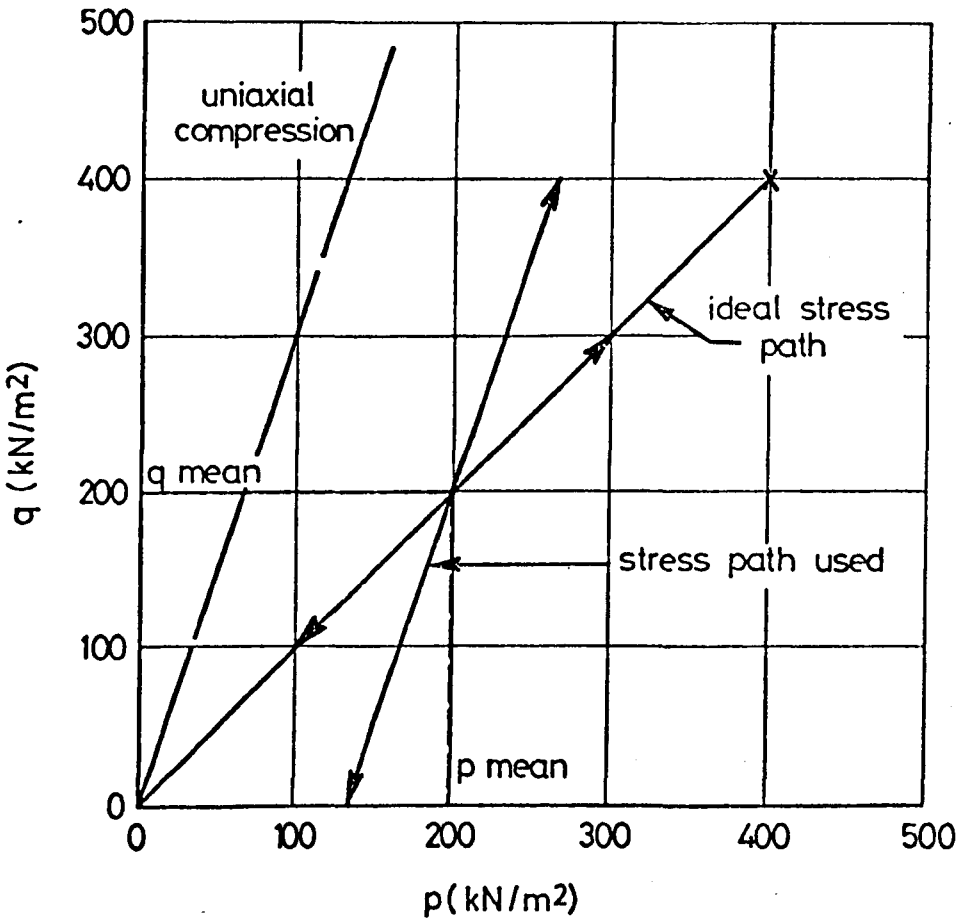

FIG. 9.3 TYPICAL STRESS PATH FOR THE DBM TESTS

FIGURE 9.4 SPECIMEN WITH LVDT LOCATING PIPS, AND END PLATENS ATTACHED

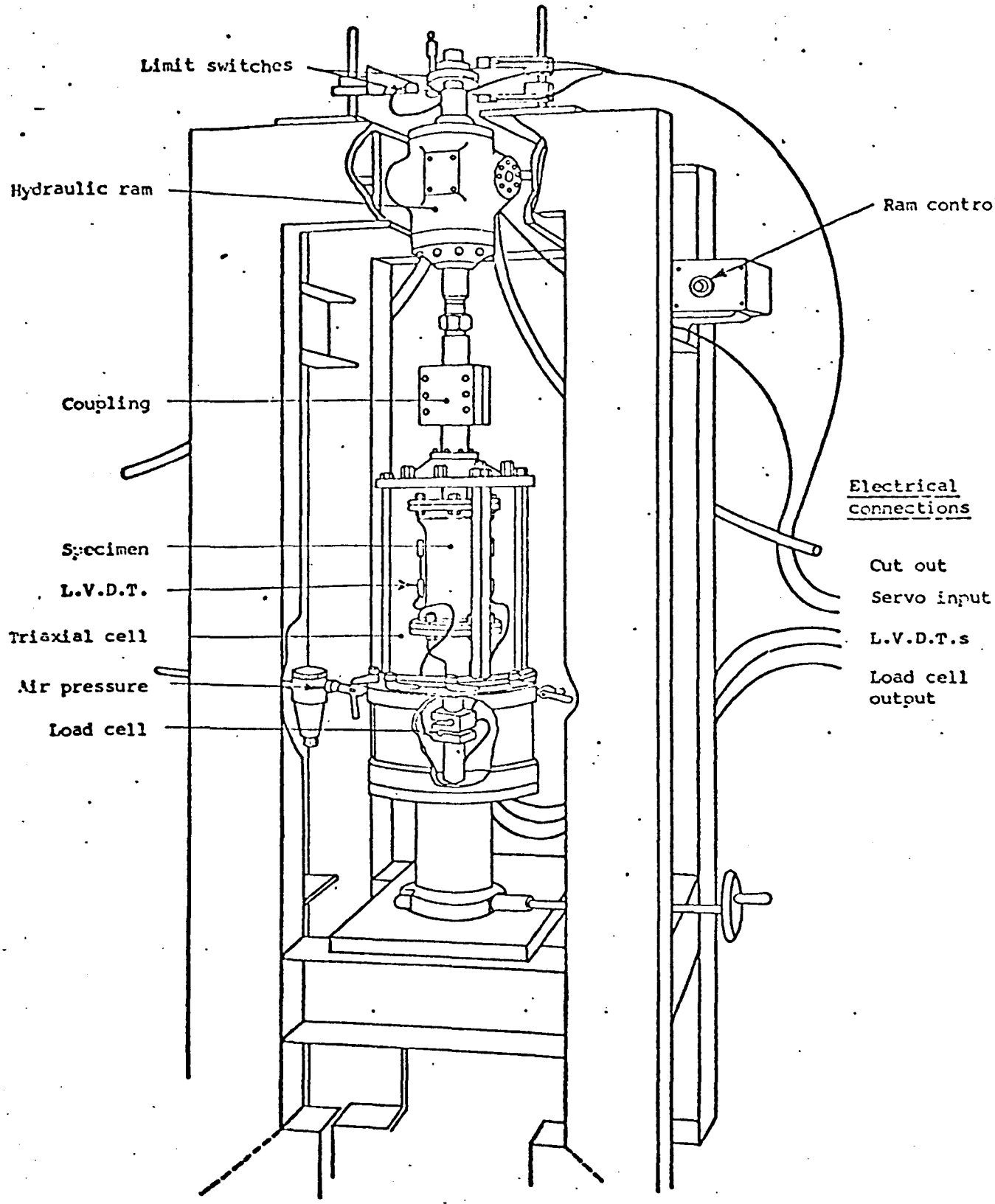

FIG. 9.5 ELECTRO-HYDRAULIC SERVO-CONTROLLED TEST MACHINE FOR TESTING ASPHALTIC MATERIALS

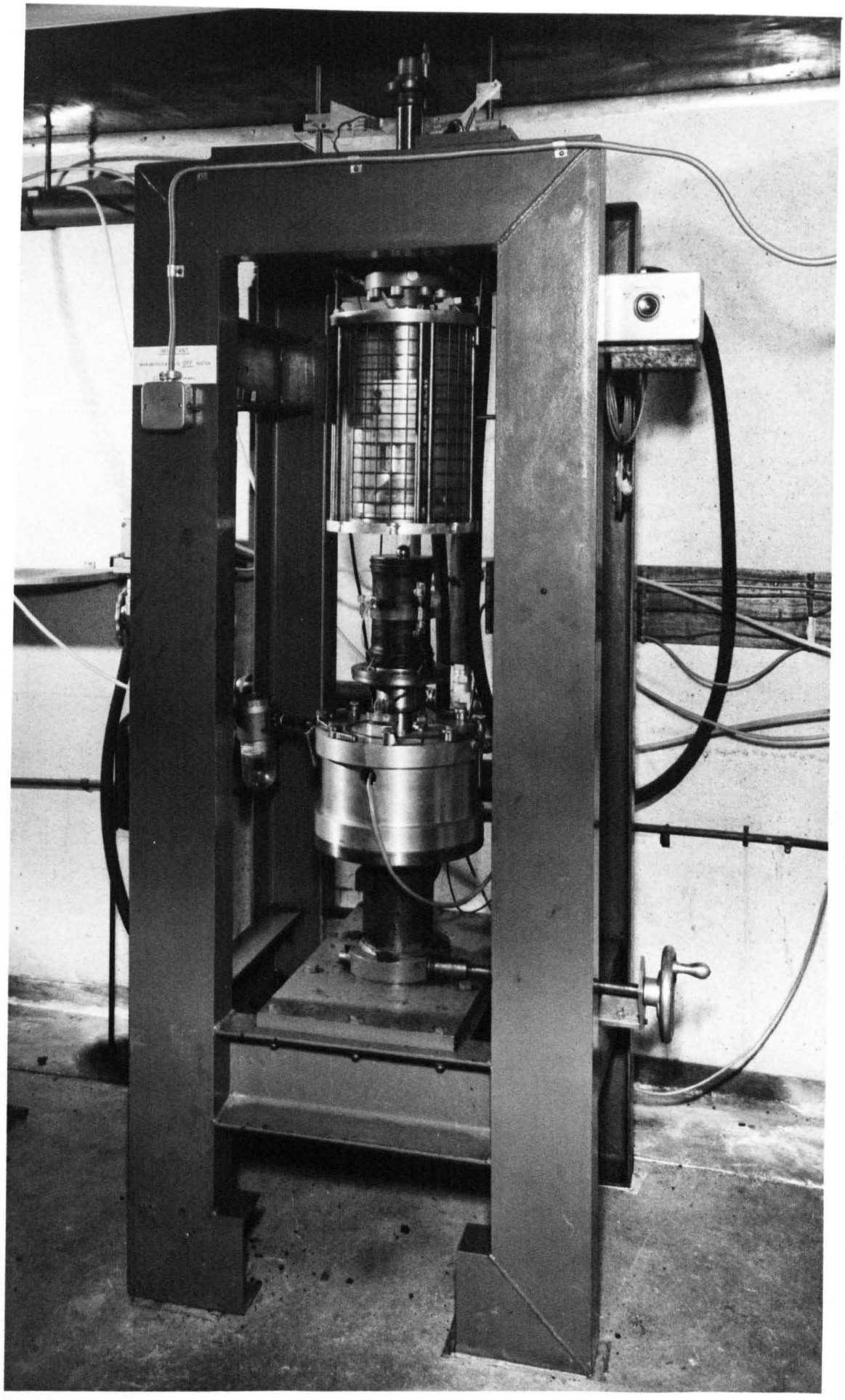

FIGURE 9.6 A DBM SPECIMEN SHOWN IN POSITION IN THE TESTING MACHINE

FIGURE 9.7 A DBM SPECIMEN WITH LVDT's ATTACHED

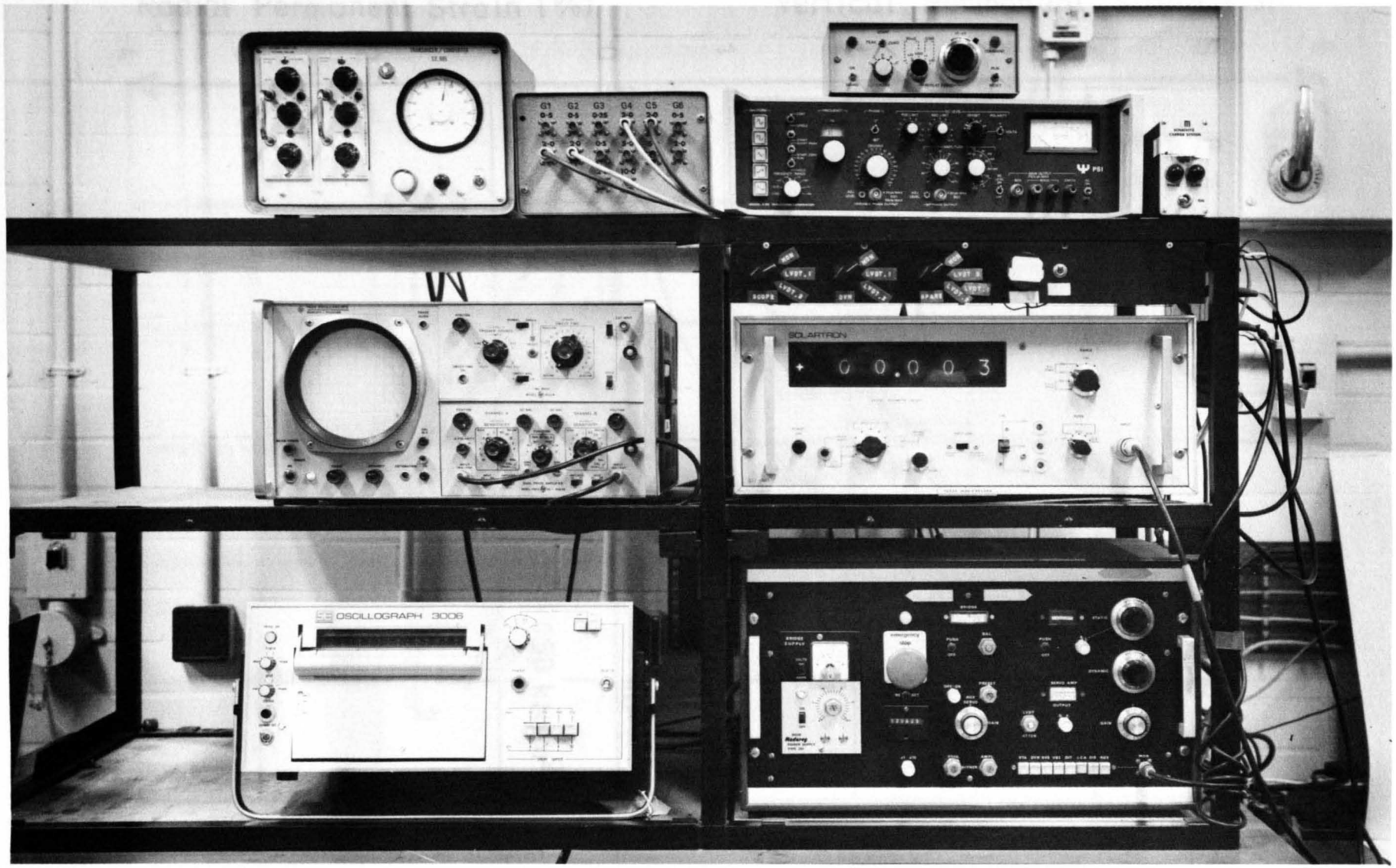

FIGURE 9.8 MONITORING AND CONTROL EQUIPMENT FOR DBM TESTS

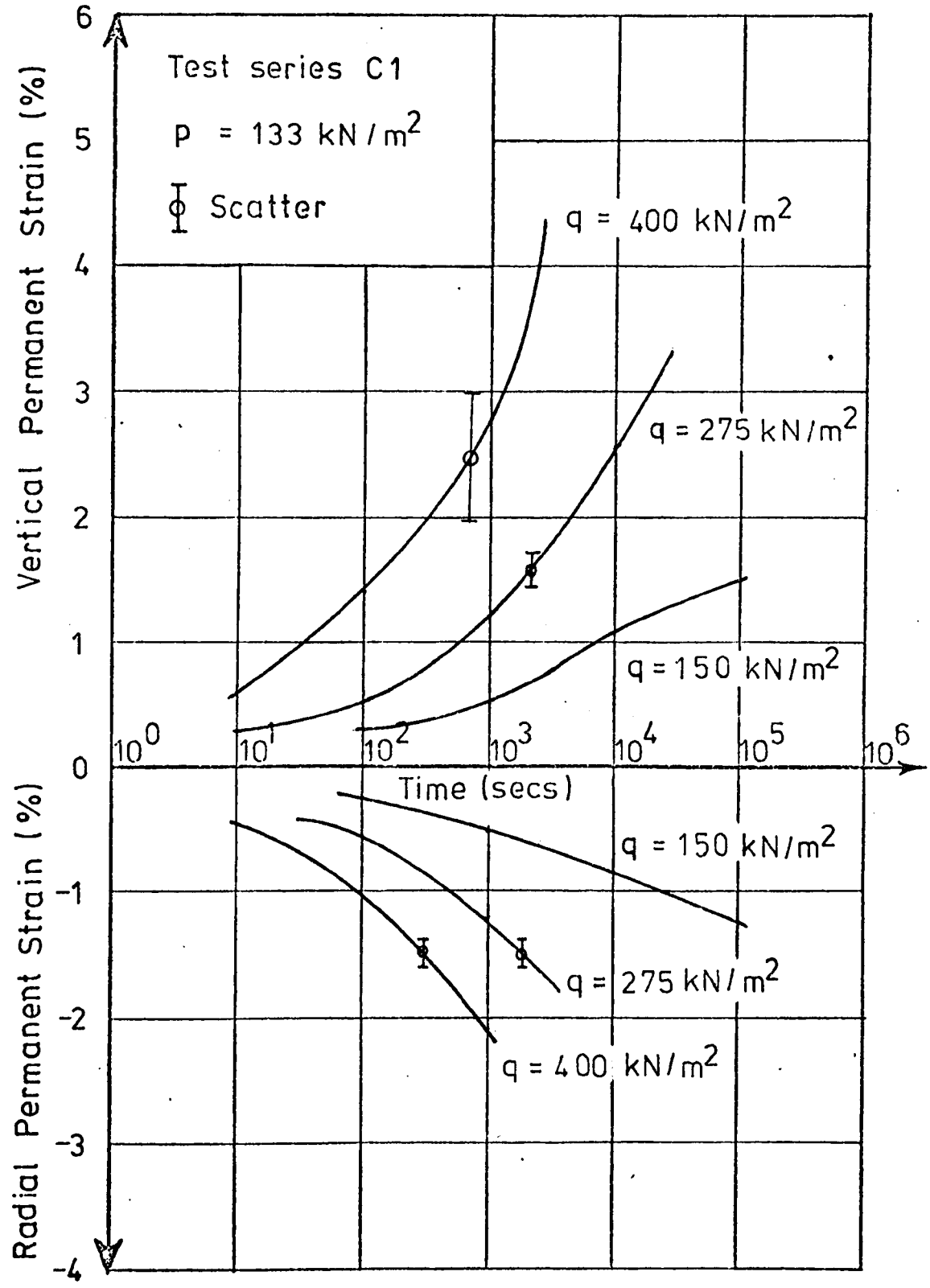

FIGURE 9.9 THE INFLUENCE OF q ON THE PERMANENT STRAIN RESPONSE OF DBM, p = 133 kN/m²

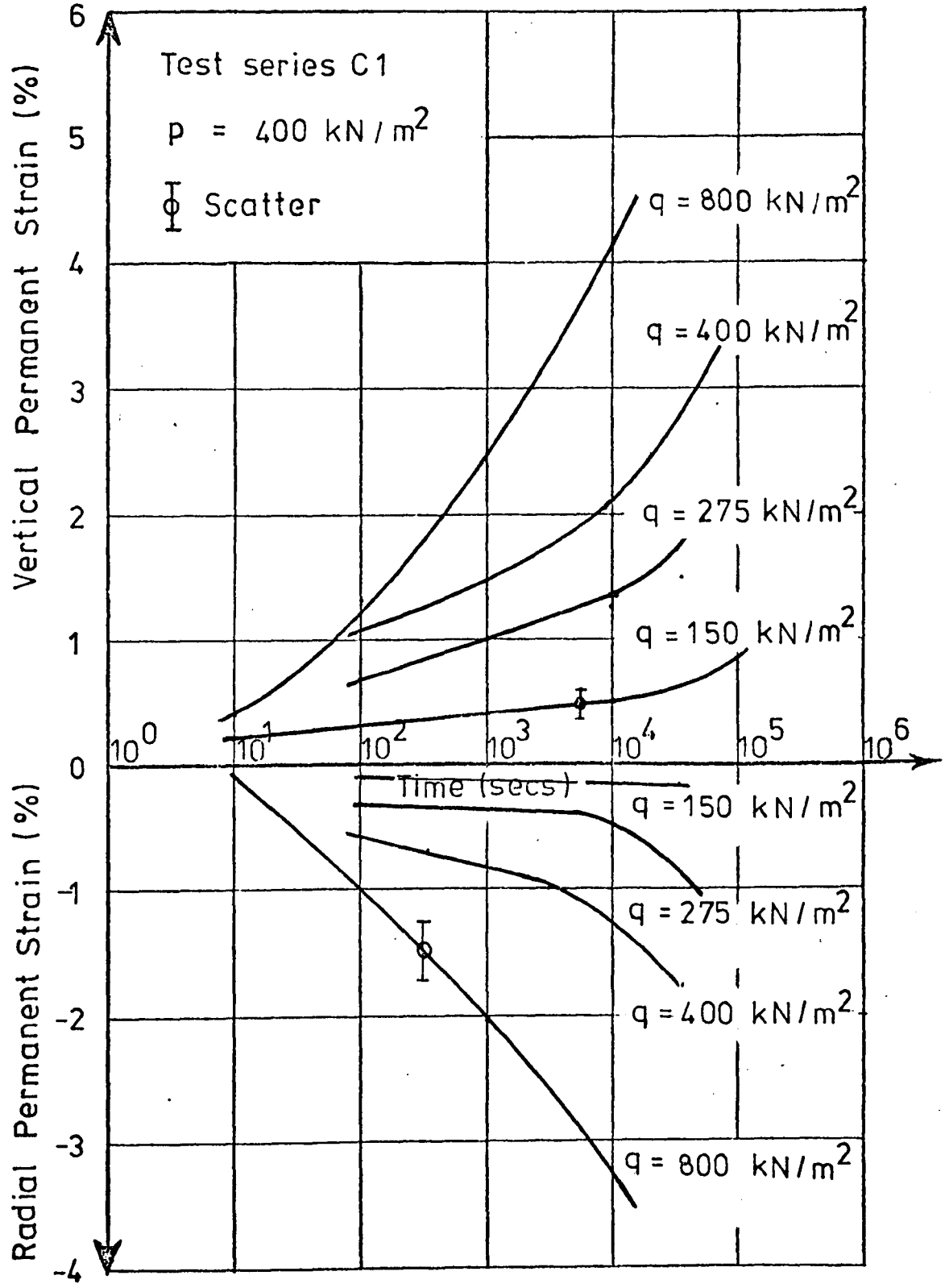

FIGURE 9.10 THE INFLUENCE OF q ON THE PERMANENT STRAIN RESPONSE OF DBM, p = 400 kN/m²

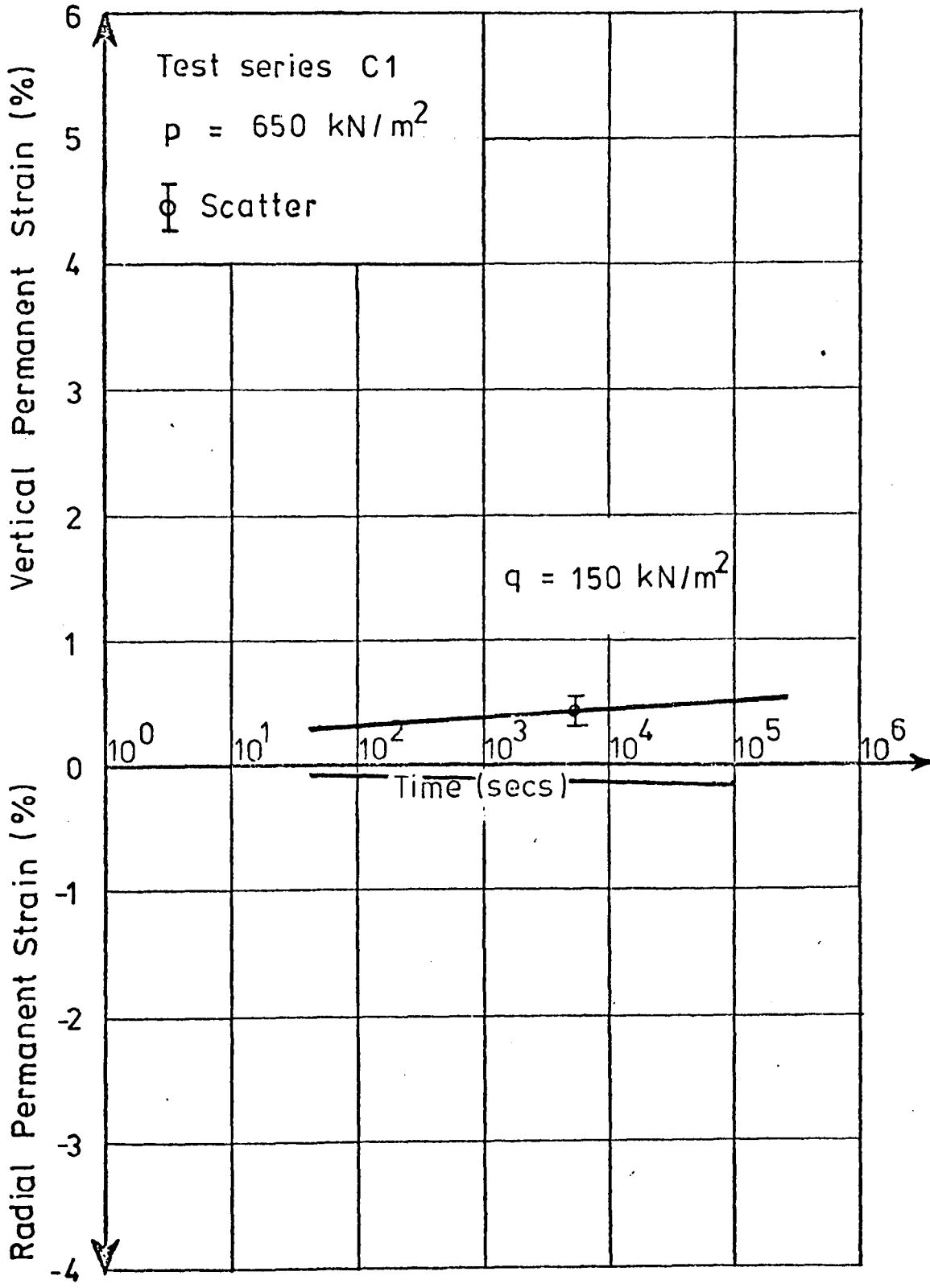

FIGURE 9.11 THE INFLUENCE OF q ON THE PERMANENT STRAIN RESPONSE OF DBM, p = 650 kN/M²

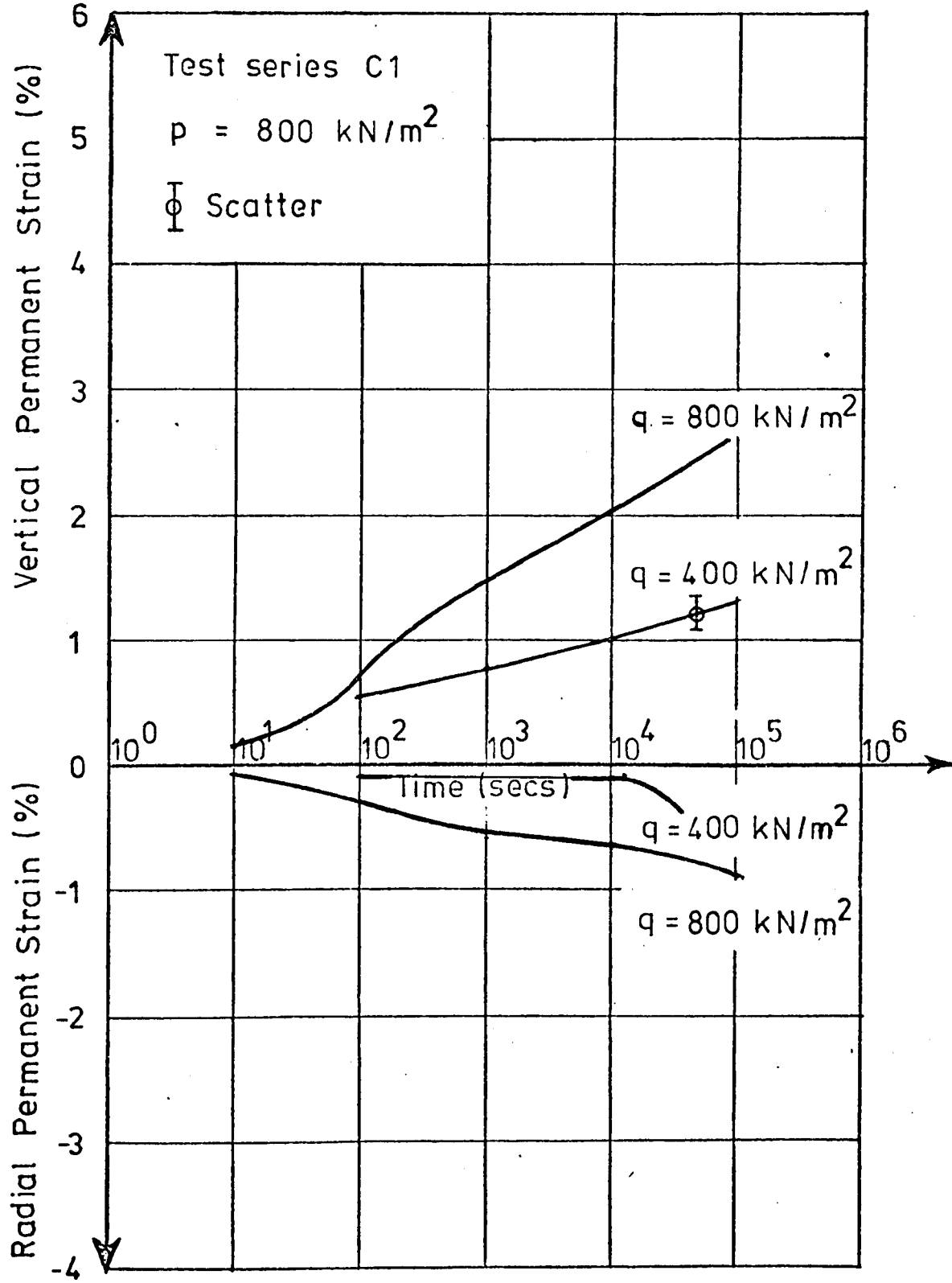

FIGURE 9.12 THE INFLUENCE OF q ON THE PERMANENT STRAIN RESPONSE OF DBM, p = 800 kN/m²

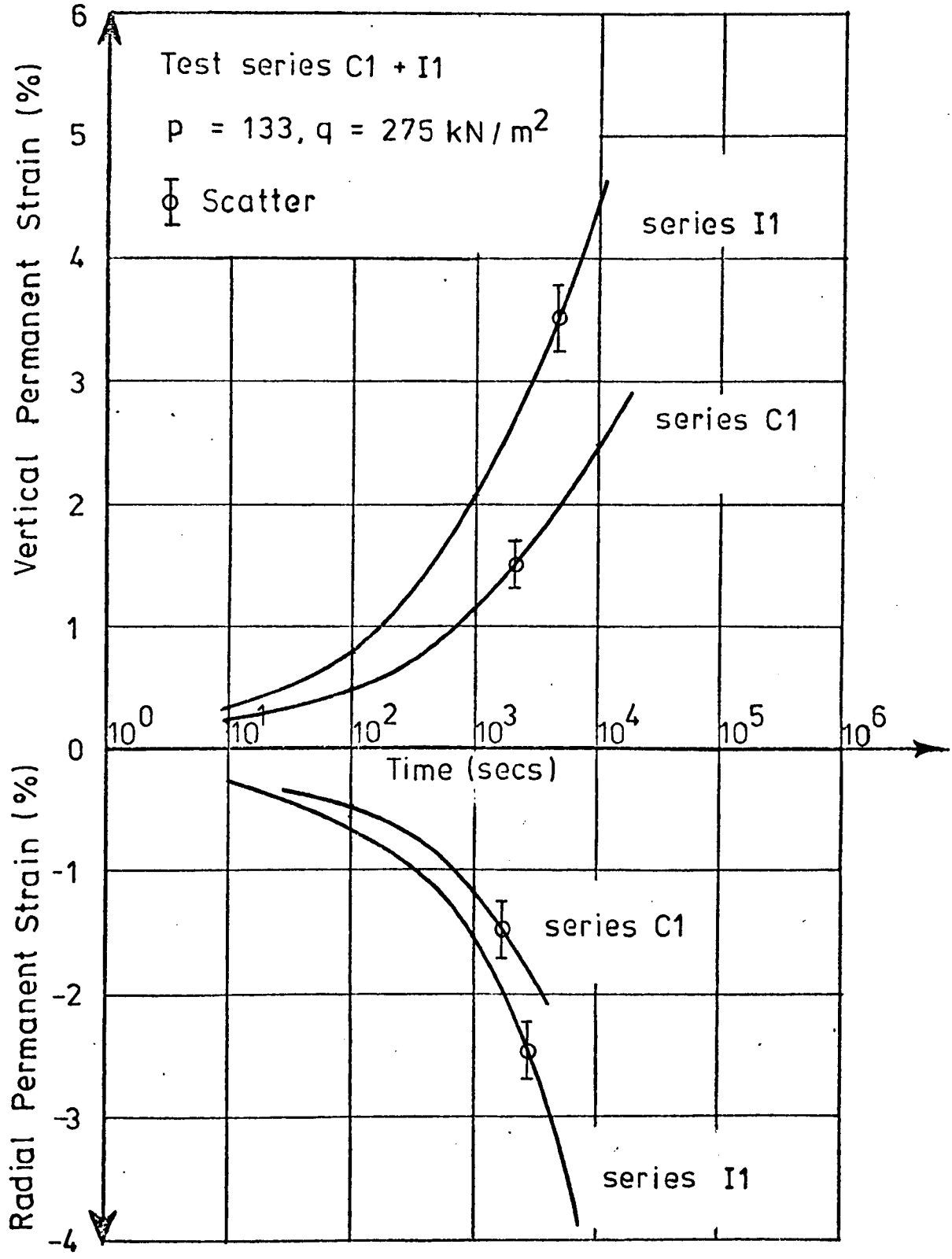

FIGURE 9.13 COMPARISON OF PERMANENT STRAIN BEHAVIOUR OF DBM CORES TAKEN VERTICALLY AND HORIZONTALLY

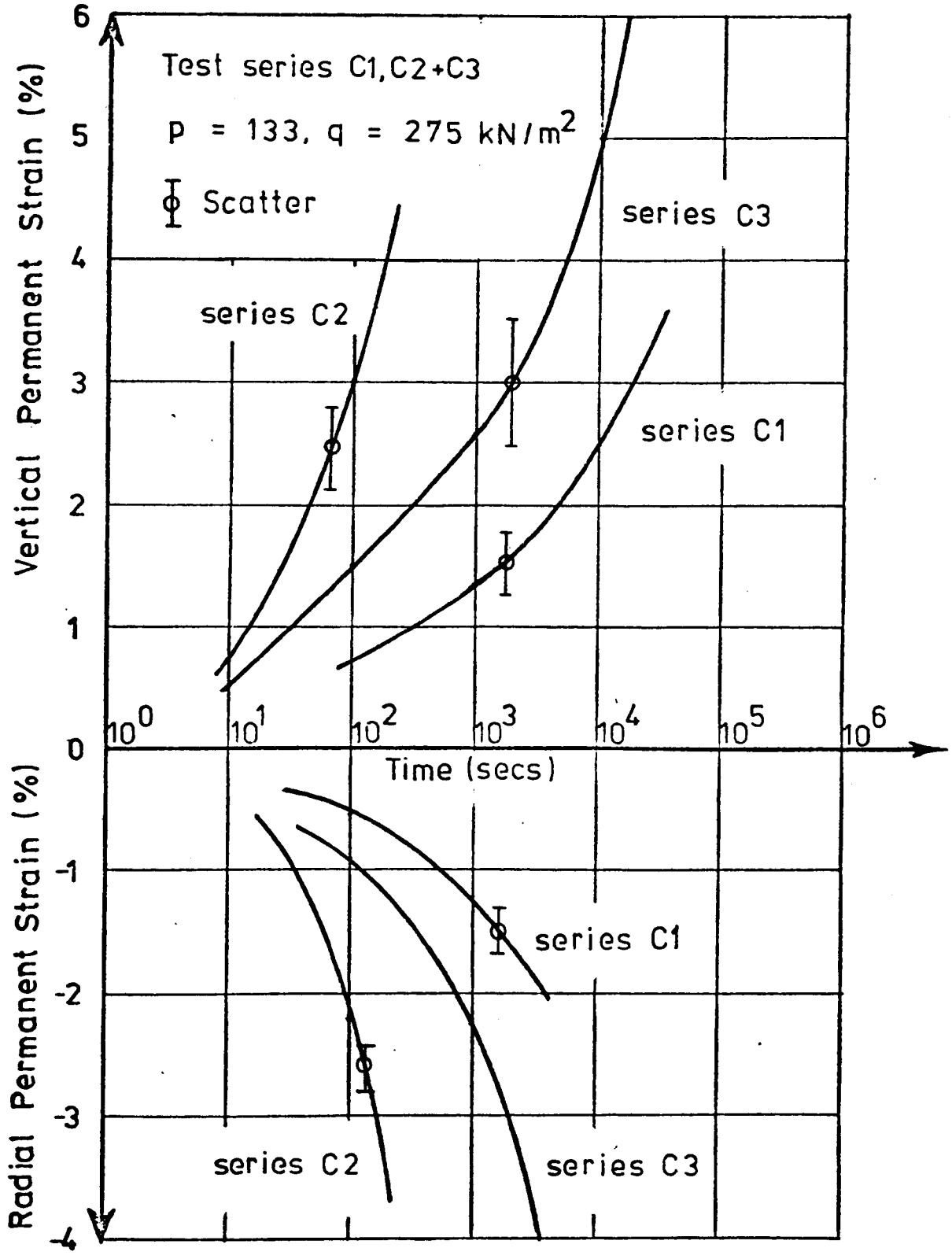

FIGURE 9.14 COMPARISON OF PERMANENT STRAIN BEHAVIOUR OF DBM CORES FROM EACH PAVEMENT

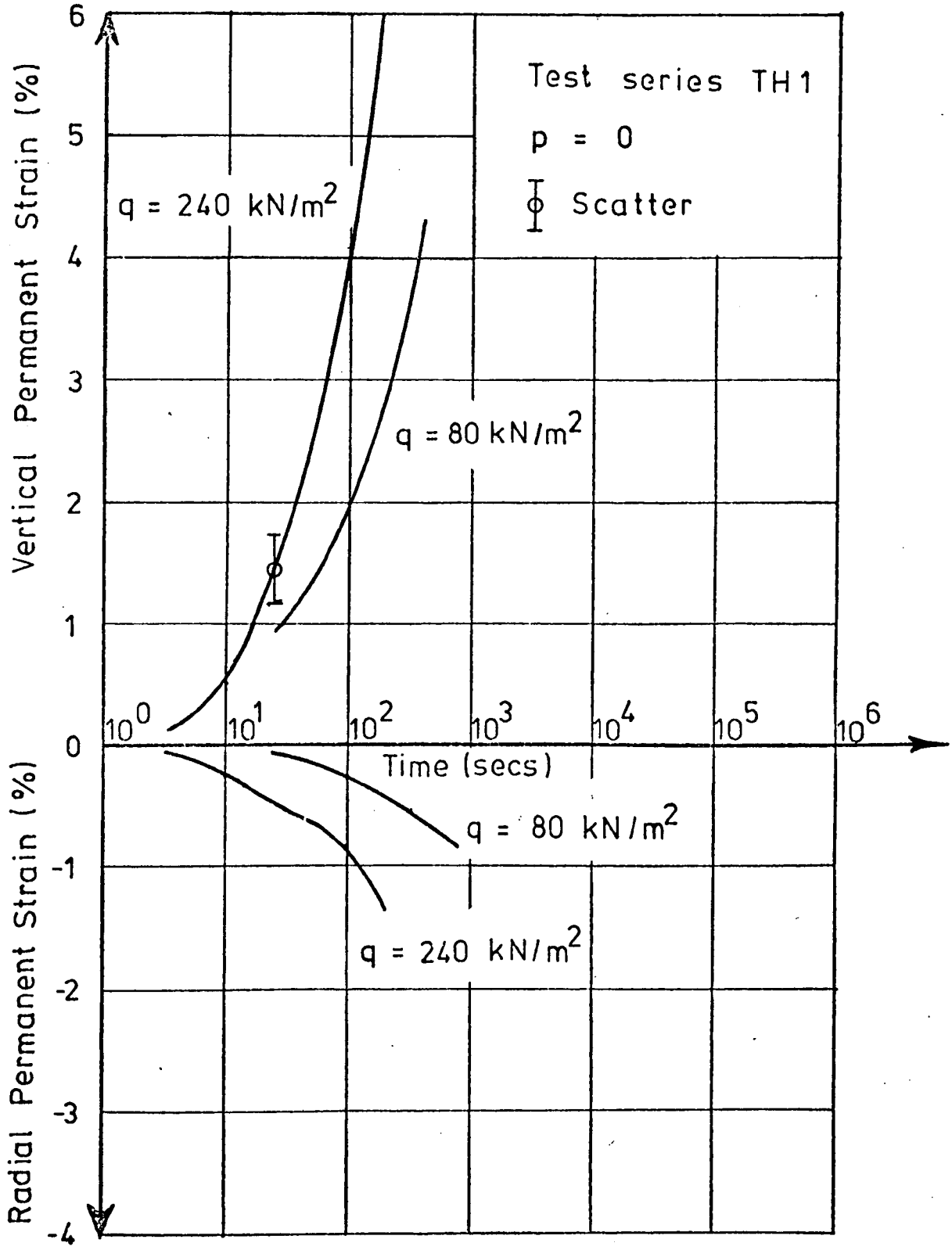

FIGURE 9.15 THE INFLUENCE OF q ON THE PERMANENT STRAIN RESPONSE OF DBM, p = 0

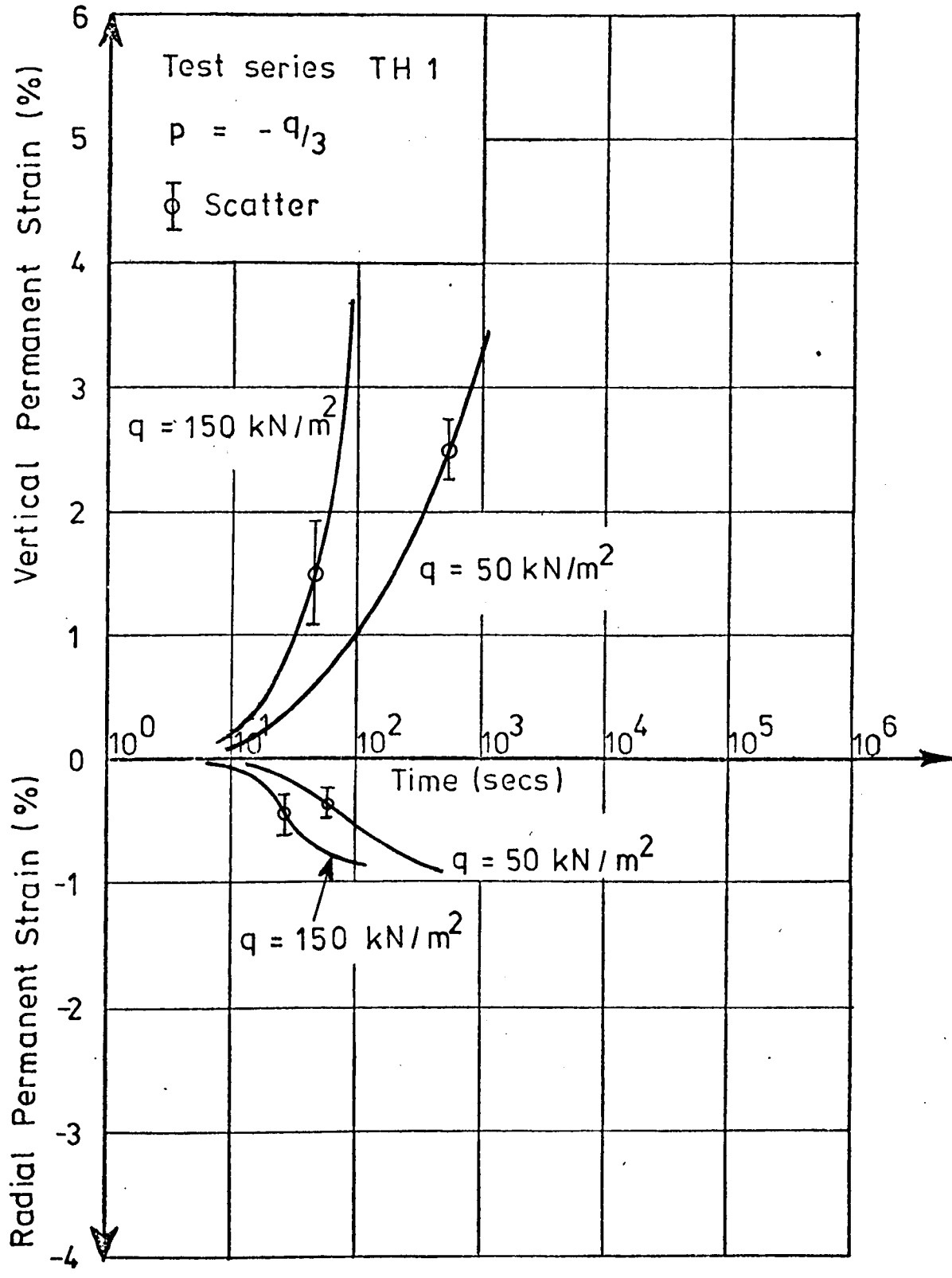

FIGURE 9.16 THE INFLUENCE OF q ON THE PERMANENT STRAIN RESPONSE OF DBM, p = q/3

Pavement 1

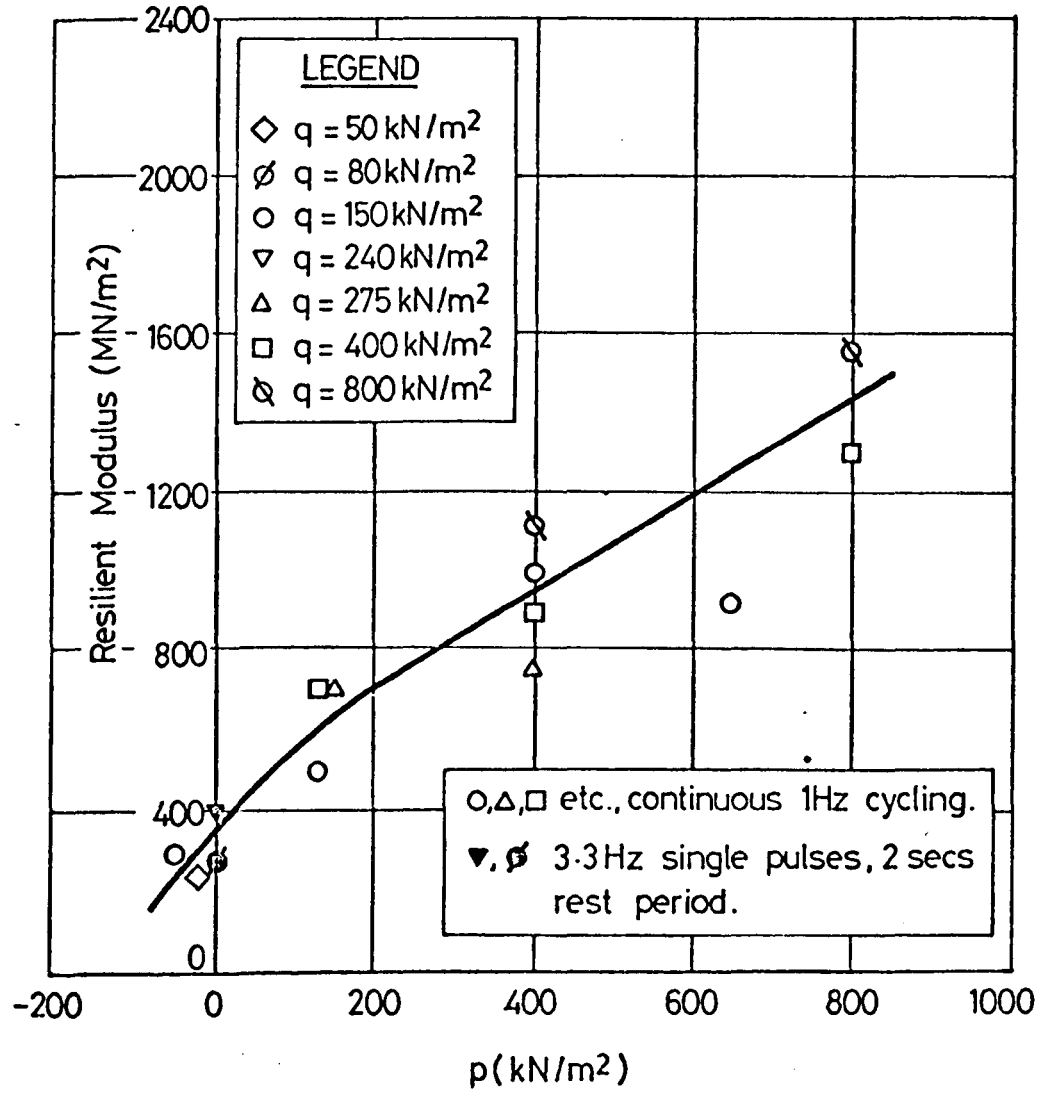

FIG. 9.17 THE EFFECT OF p AND q ON THE RESILIENT MODULUS OF DBM CORES FROM PAVEMENT NO. 1

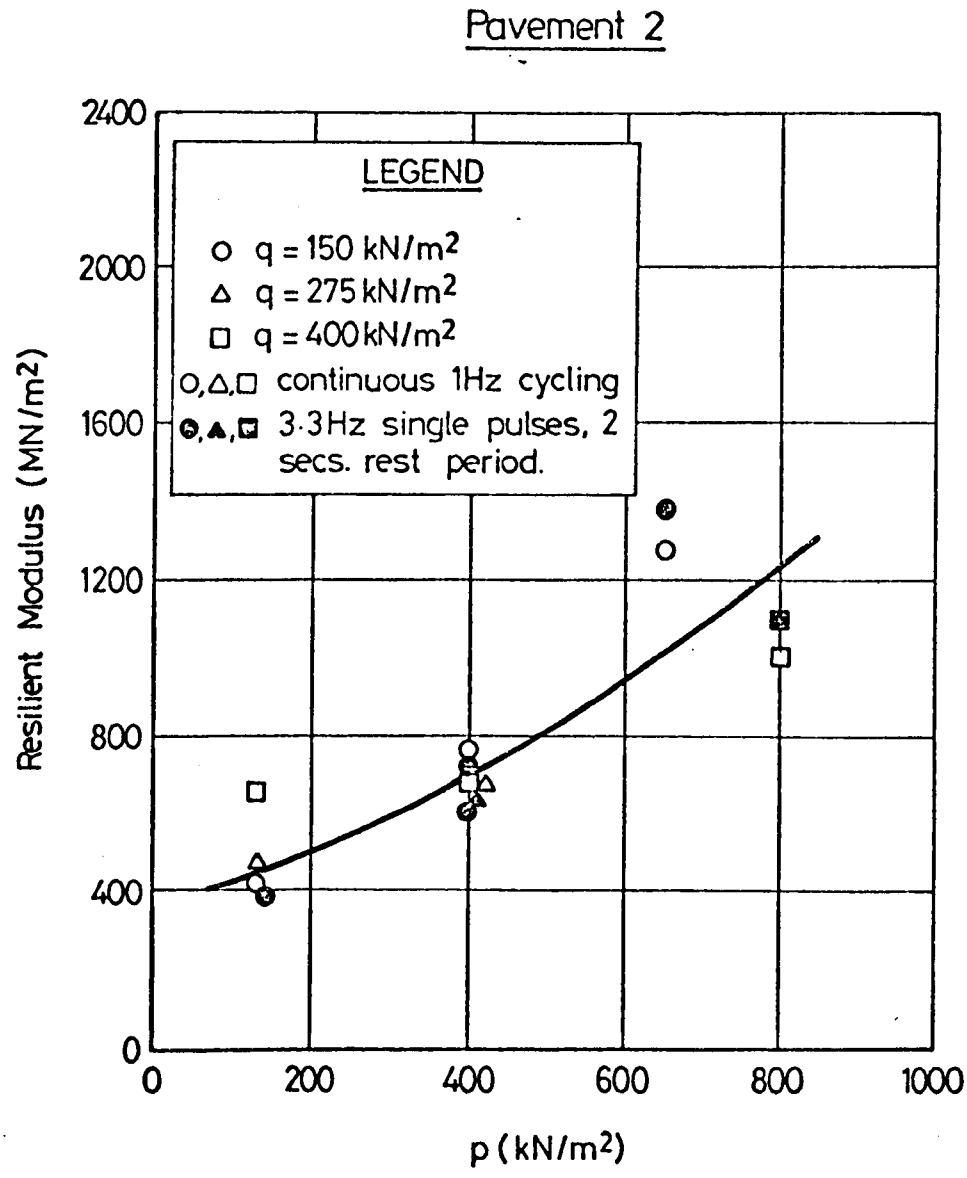

FIG. 9.18 THE EFFECT OF p AND q ON THE RESILIENT MODULUS OF DBM CORES FROM PAVEMENT NO. 2

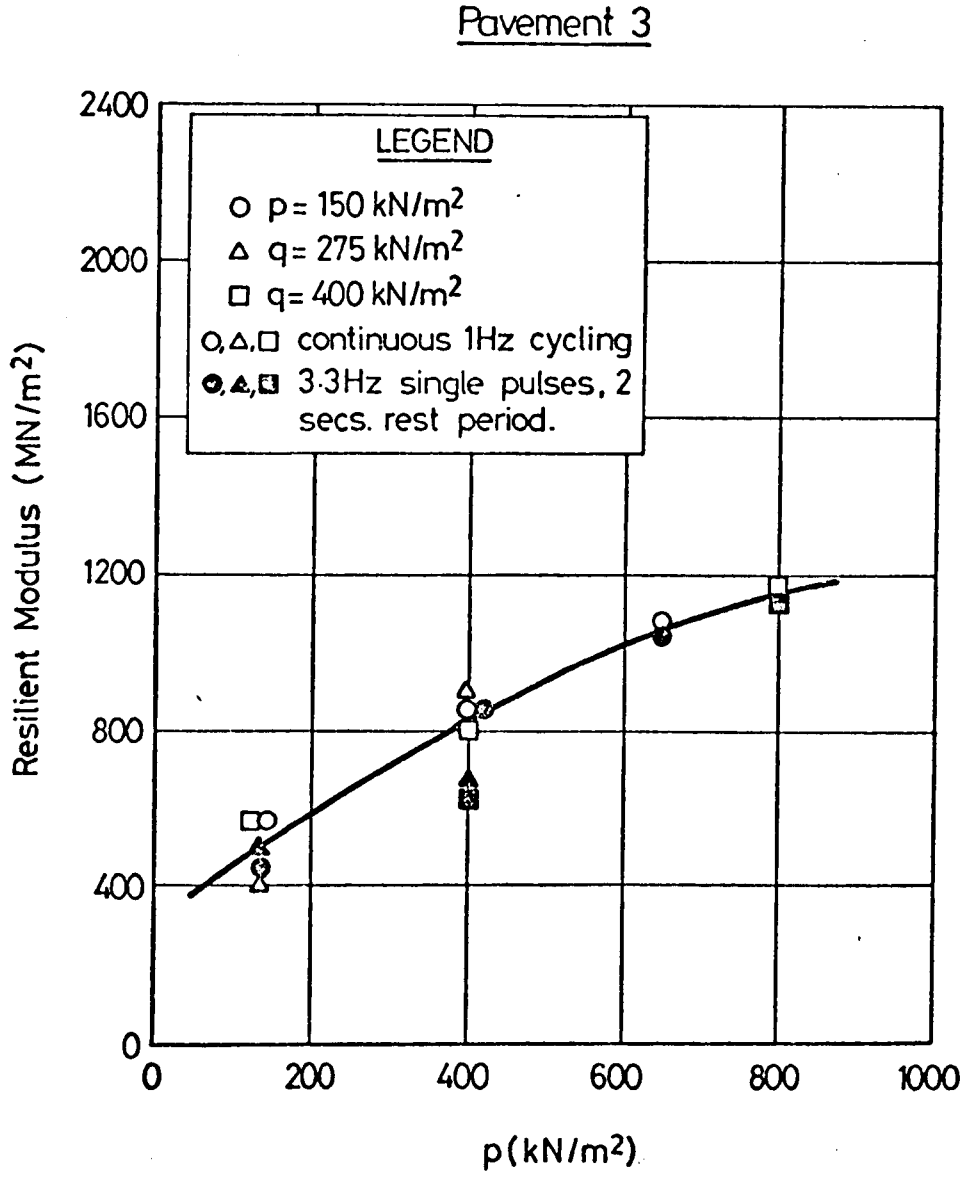

FIG. 9.19 THE EFFECT OF p AND q ON THE RESILIENT MODULUS OF DBM CORES FROM PAVEMENT NO. 3

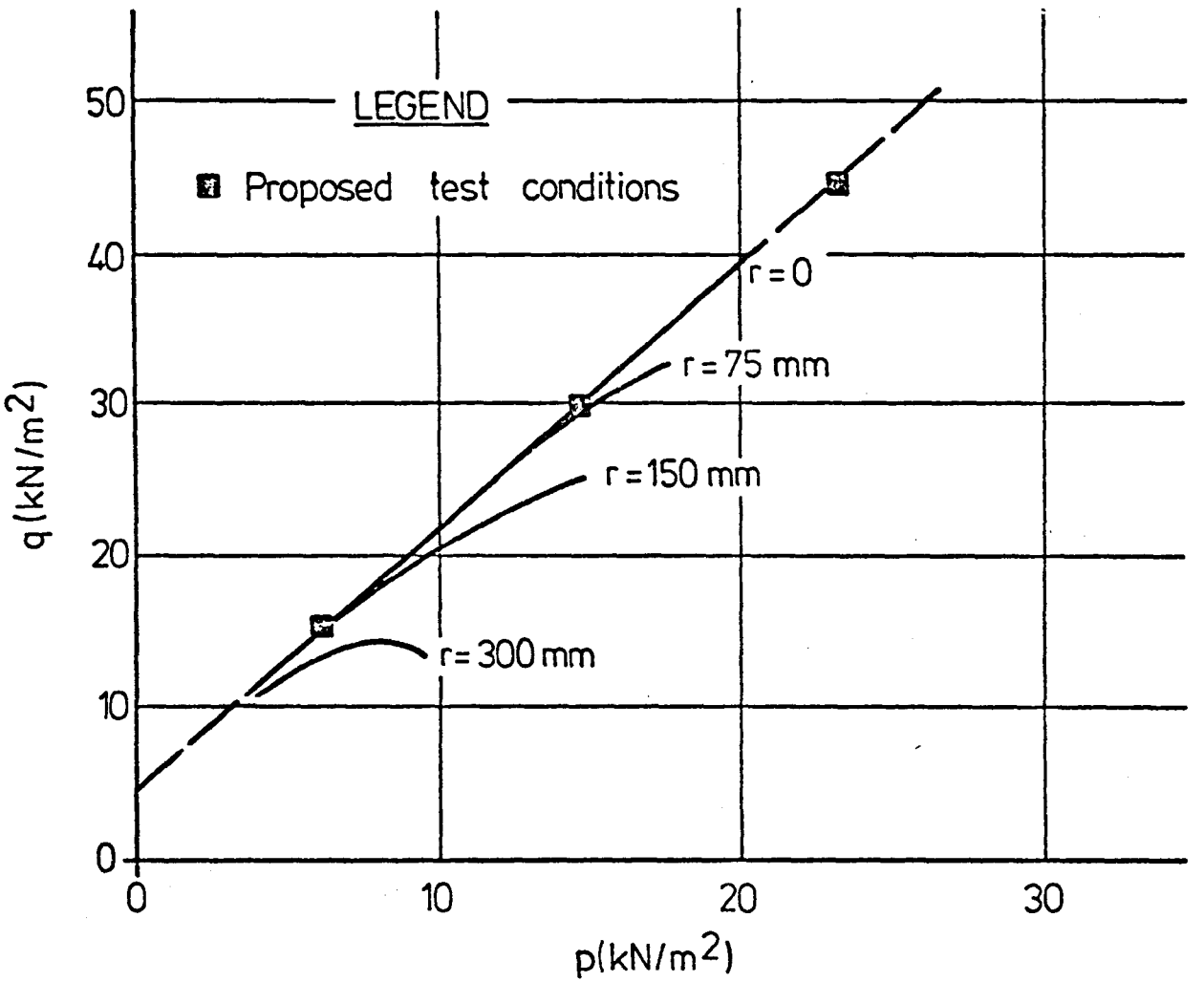

FIG. 9.20 STRESSES IN THE SUBGRADE (PAVEMENT NO. 1) BY LINEAR ELASTIC THEORY, WITH LABORATORY TEST CONDITIONS

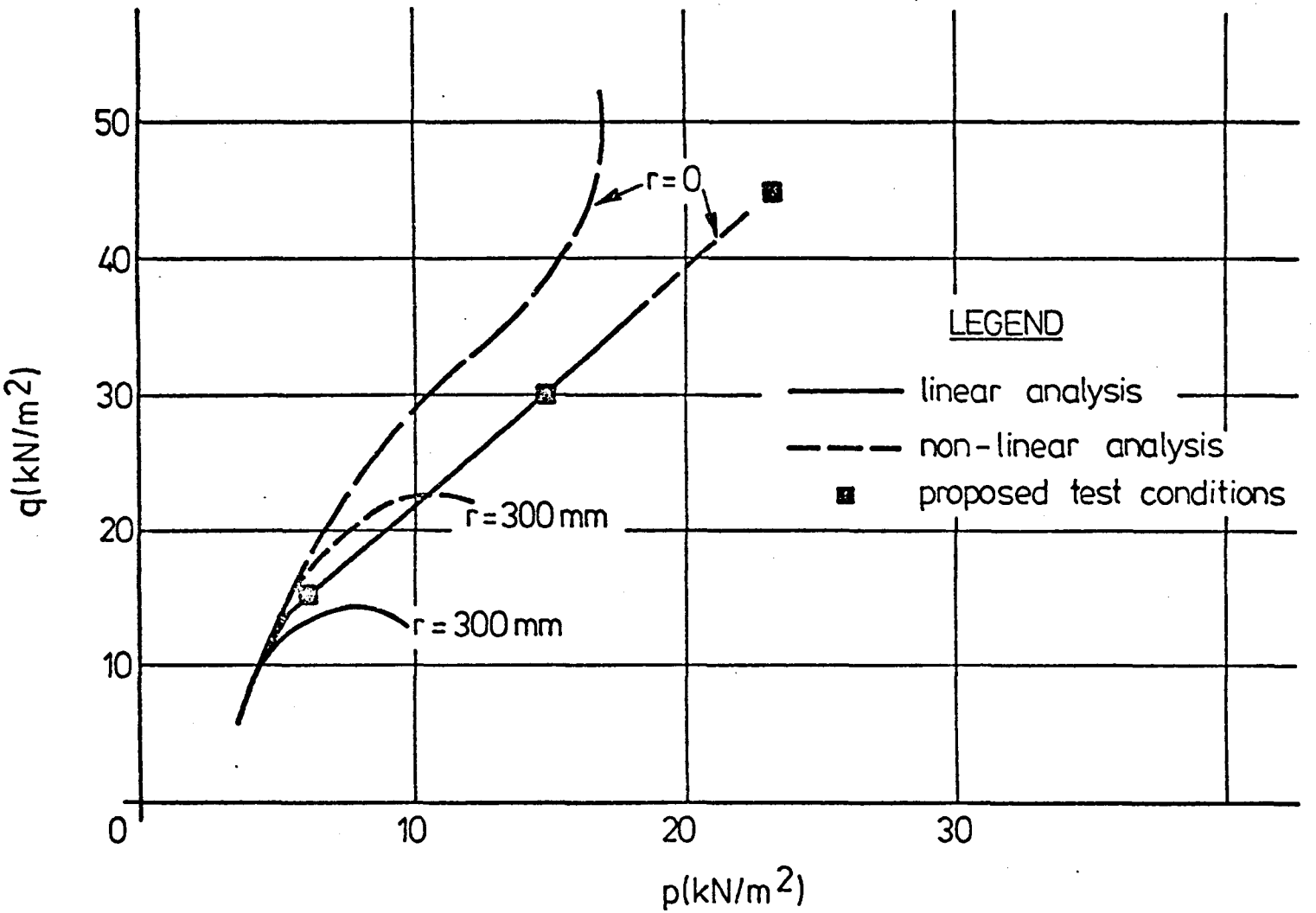

FIG. 9.21 COMPARISON OF STRESSES IN THE SUBGRADE (PAVEMENT NO. 1) BY LINEAR AND NON-LINEAR ELASTIC THEORY

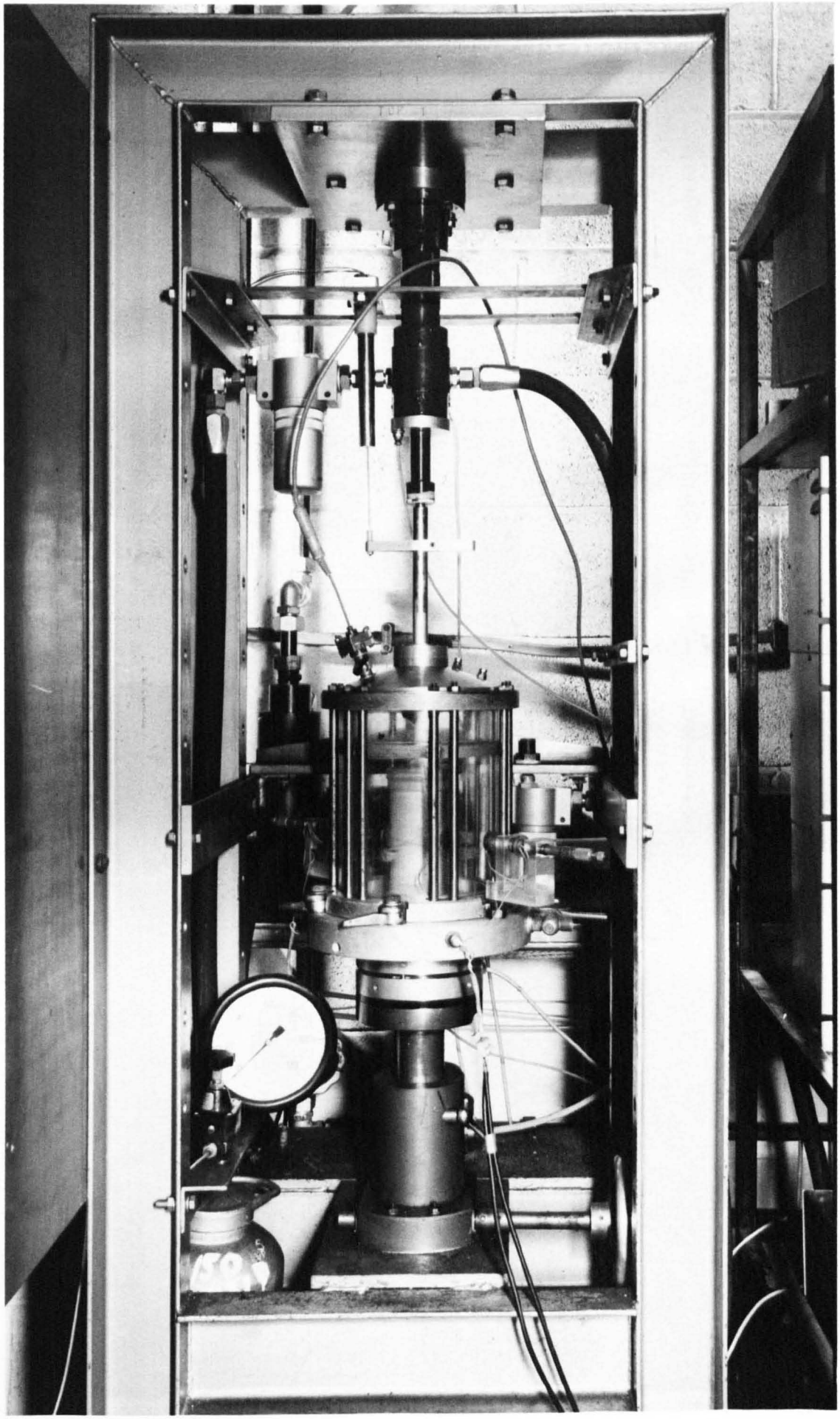

FIGURE 9.22 A KEUPER MARL SPECIMEN SHOWN IN POSITION IN THE TEST MACHINE

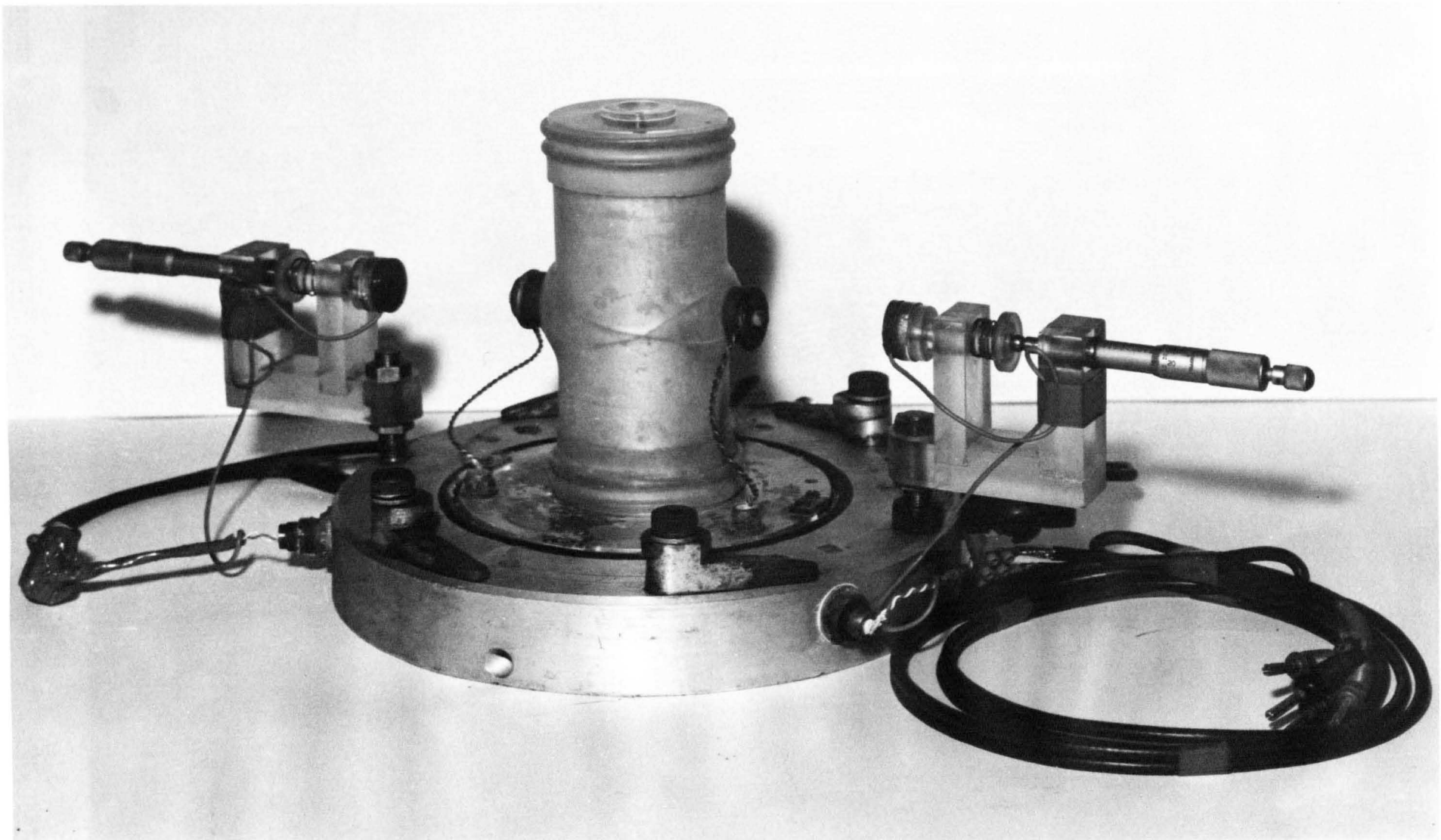

FIGURE 9.23 A KEUPER MARL SPECIMEN SET UP ON THE CELL-BASE WITH THE STRAIN COILS IN POSITION

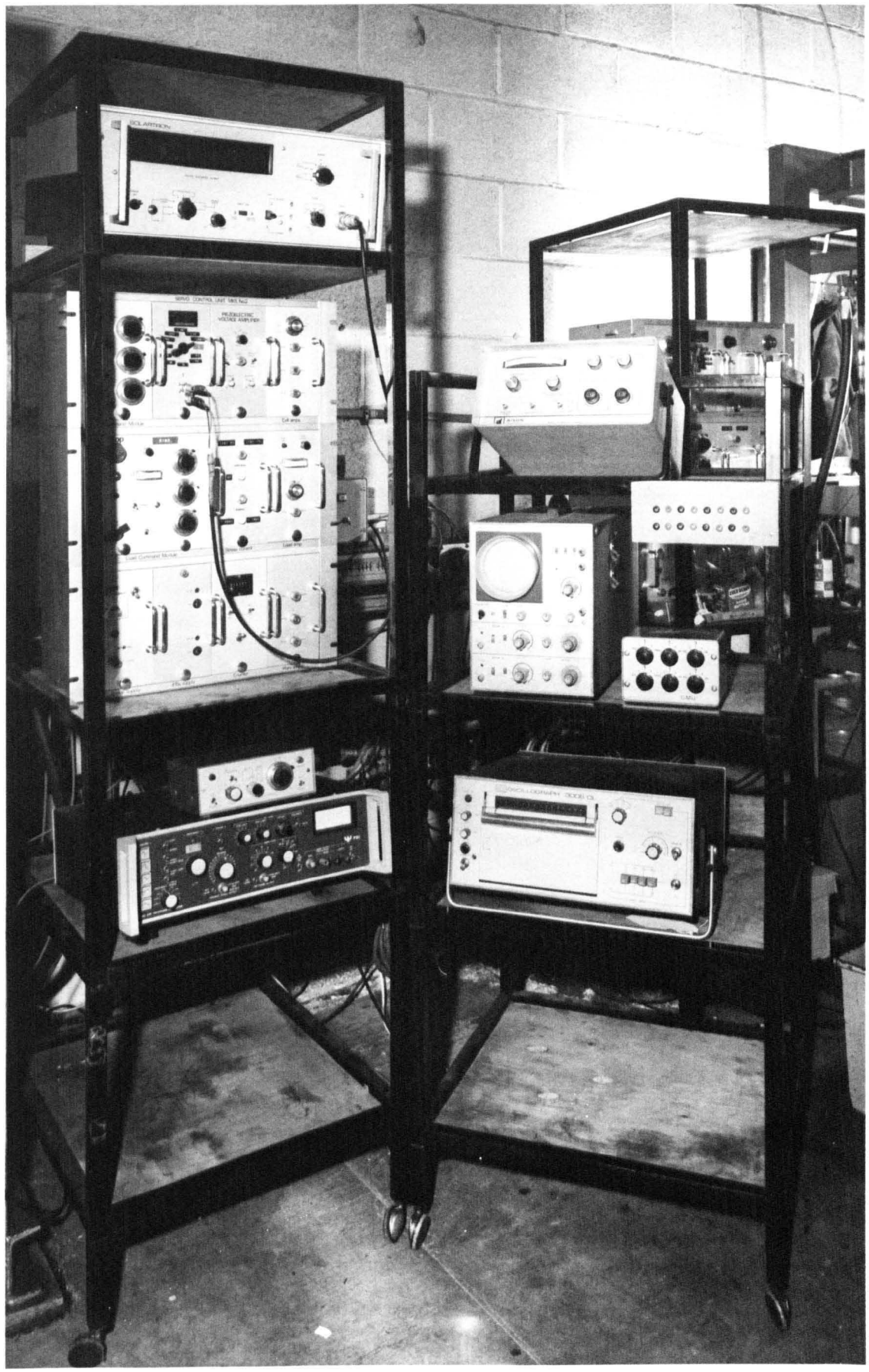

FIGURE 9.24 MONITORING AND CONTROL EQUIPMENT FOR THE KEUPER MARL TESTS

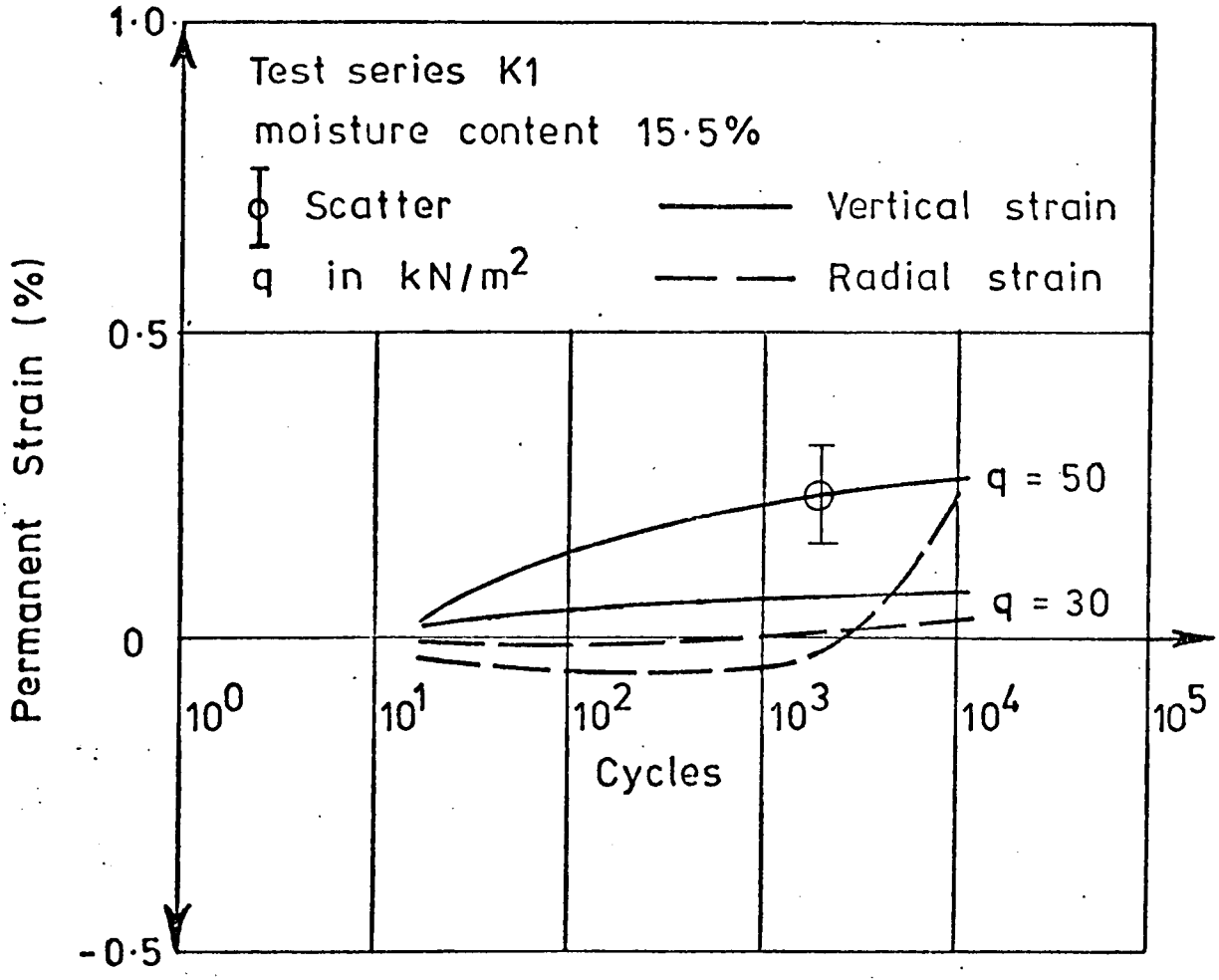

FIGURE 9.25 THE EFFECT OF q ON PERMANENT STRAIN RESPONSE OF KEUPER MARL, TEST SERIES K1

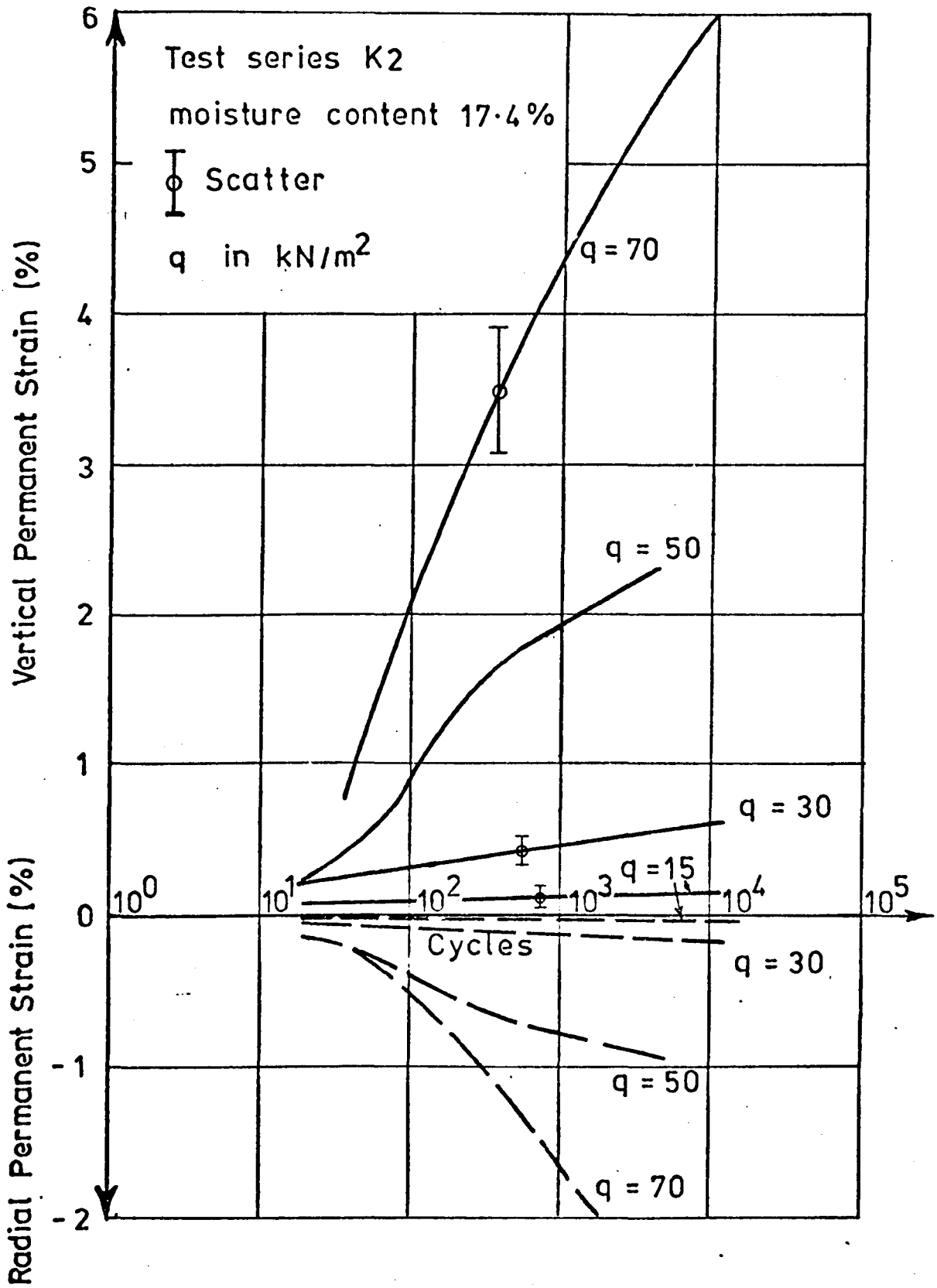

FIGURE 9.26 THE EFFECT OF q on PERMANENT STRAIN RESPONSE OF KEUPER MARL, TEST SERIES K2

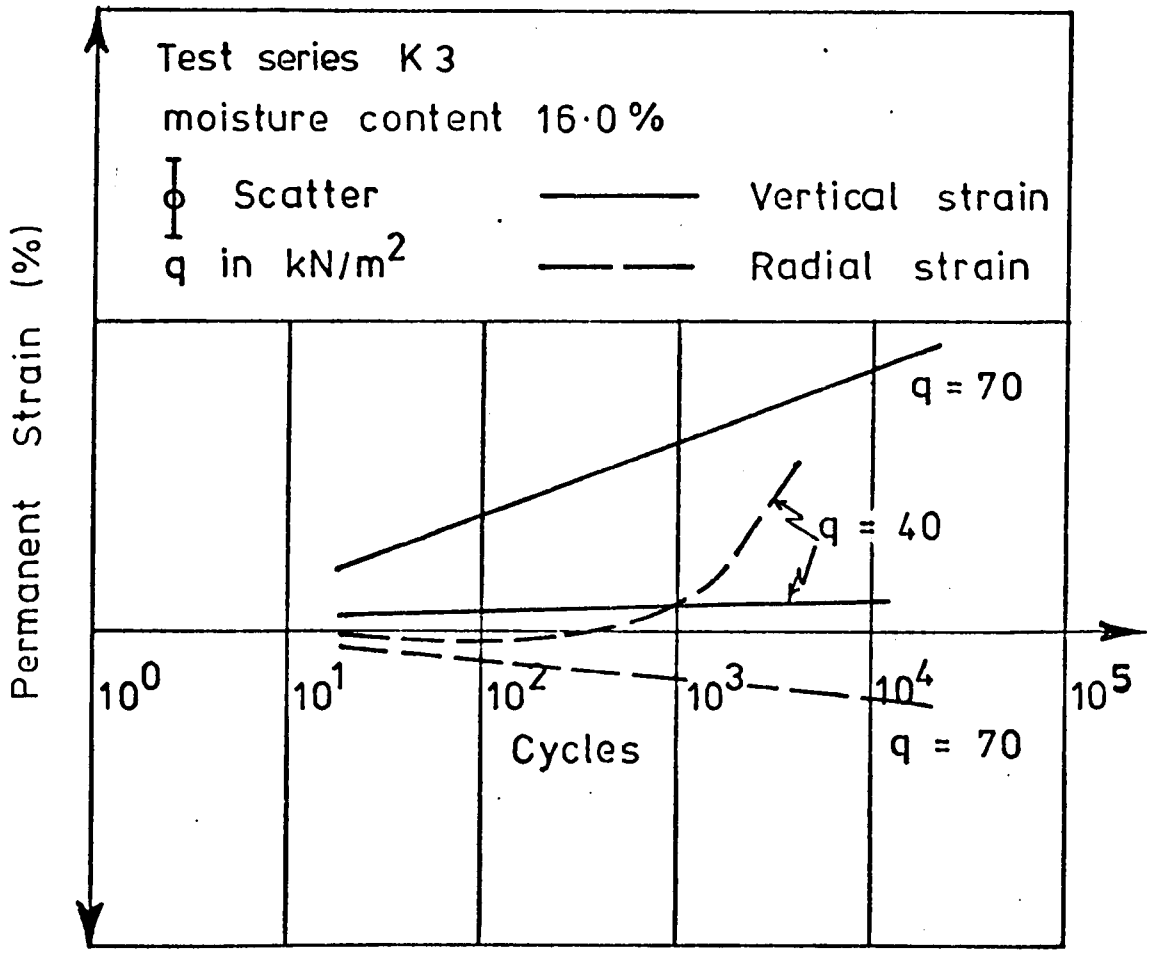

FIGURE 9.27 THE EFFECT OF q ON PERMANENT STRAIN RESPONSE OF KEUPER MARL, TEST SERIES K3

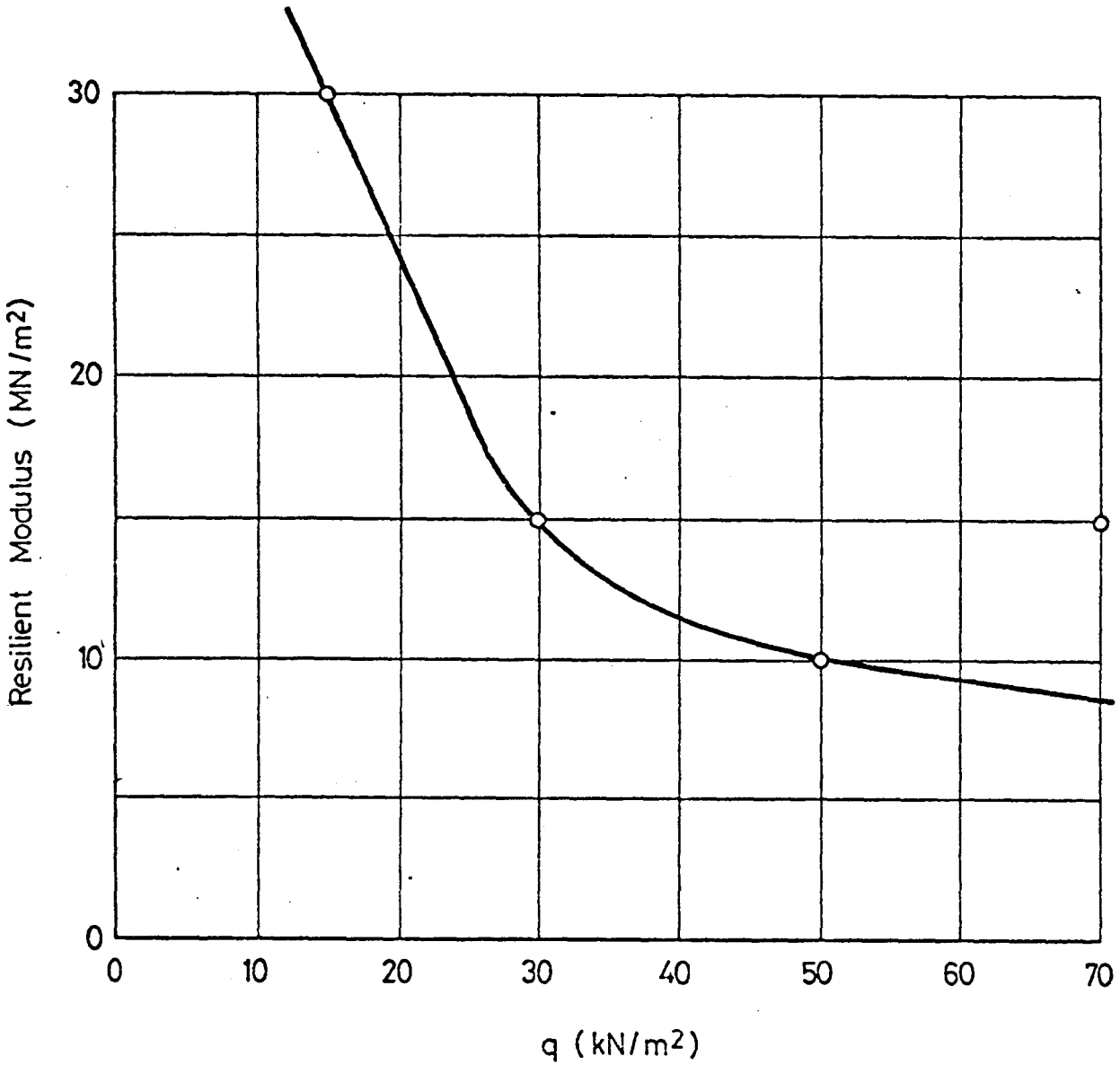

FIG. 9.28 THE EFFECT OF q ON THE RESILIENT MODULUS OF KEUPER MARL, TEST SERIES K2

CHAPTER TEN

PREDICTIONS OF RESILIENT BEHAVIOUR

10.1 INTRODUCTION

As described in Chapter 7, measurements of resilient stresses and strains were taken in each pavement at various positions. Comparison of these measurements with those predicted by elastic analysis (linear or non-linear) provided an indication of the accuracy of the analysis.

The most comprehensive set of results from each pavement was provided by the strain coils, which supplied strain distributions with depth in each pavement, and radial strains at the interface in pavements 2 and 3. Strain gauges used in all three pavements in the DBM provided additional information, as did two strain cells in the subgrade, although instrument failure was common with both these types.

Pressure cells provided measurements of stress in each pavement. Radial stresses and strains were measured at the surface of the subgrade in pavements 1 and 2; not very successfully in the first case. Addit-:ional cells were installed in the DBM for pavement 3, to measure radial stresses in the top and bottom of the layer. Emphasis was placed on the measurement of the compressive radial stress at the top of the layer since this parameter was likely to be more difficult to determine theoretically than vertical stress.

The following sections present comparisons of measurements with predictions from both linear and non-linear analyses, using resilient constants obtained from the materials characterisation tests described in Chapter 9. The linear elastic analysis, utilised layer theory (BISTRO) (60), whereas the non-linear analysis used finite elements (DEFPAV) (24) (See Chapter 8).

10.2 SELECTION OF ELASTIC CONSTANTS

Discussion in Chapters 8 and 9 showed that both pavement materials had markedly non-linear elastic properties. For this reason a computer program capable of carrying out a non-linear analysis was favoured (DEFPAV), and the relationships plotted in Figures 9.17 to 9.19 and 9.28 were used as input data for the resilient moduli of the DBM and Keuper marl. A constant Poisson's ratio was used for each material, since the characterisation tests had not highlighted any particular trend in relation to the stress conditions. However, Snaith (22) showed that such trends do exist although usually overshadowed by temperature effects, and work has been carried out at Nottingham (56) so that a variable Poisson's ratio can be used with DEFPAV.

Although a non-linear analysis was favoured, a linear analysis was not discounted, since development of the permanent deformation prediction techniques could show an approximate approach using linear analysis to be adequate. Non-linear analysis is generally much more expensive, in terms of computing time, than the linear approach, and therefore an approximate approach may be necessary in order to make the prediction procedure viable for design purposes.

Linear analyses were carried out using the computer program BISTRO, compensating partly for the effects of non-linearity by dividing the two-layer pavement system into a number of sub-layers and selecting appropriate moduli and Poisson's ratios. Normally, this procedure involves a certain amount of manual iteration in order to ensure that the moduli correspond to the expected stresses, as determined by Figures 9.17 to 9.19 and 9.28. It should be noted that even if such a procedure results in adequate analysis, the need for manual calculations and possible alteration of modulus values negates the advantage gained by saving computing time. The values of moduli actually used in the linear analyses, for which results are presented in this Chapter, were

in fact chosen from the results of the DEFPAV non-linear calculations and hence manual iteration was not necessary.

10.3 COMPARISONS OF MEASURED AND PREDICTED STRESSES

In the case of pavement 1, only four pressure cells were installed in the subgrade, two to measure vertical stress and two to measure radial stress. Only one of the vertical cells survived construction of the pavement, and this gave extremely variable measurements of stress during testing. Although both radial cells gave measurements of stress throughout the tests, the results were again variable. Thus, comparisons between measured and predicted values were virtually impossible, although it could be concluded that they were of the same order.

Measurements of stresses were much more successful with pavements 2 and 3. Two more cells were installed in the clay for pavement 2, resulting in three measurements of vertical stress and three of radial stress, since all six cells survived construction. The results of these measurements were reported in Chapter 7, and are shown in Figure 10.1 with the predicted values superimposed for comparison. The measured vertical stresses are higher than both the linear and non-linear predictions, particularly near the axis of the load. The measured radial stresses are also higher and at all radial distances.

For pavement 3, four cells were included in the subgrade, with an additional five cells in the DBM, three near the top of the layer to measure radial stress, and one of each to measure vertical and radial stresses near the bottom of the layer. The results from all cells, except those measuring radial stress at the bottom of the DBM, were reasonable, and are shown compared with predicted values in Figures 10.2 and 10.3. Because of the development of tensile stress at the bottom of the DBM, quantitatively correct results could not be obtained at this location (see Section 7.3).

Figure 10.2 is for the stresses in the DBM and shows reasonable comparison between the measured radial stress at the top of the layer, near the axis, and the predicted values. However, the measured vertical stress at the bottom of the layer was higher than the predicted value. Figure 10.3 is for the stresses in the clay and shows the same trends as Figure 10.1 for pavement 2. Both the measured vertical and radial stresses are greater than the predicted values, with the measurement for the radial stress considerably larger than the predicted value. Earlier research also showed that measured radial stresses were higher than predicted values (49).

10.4 COMPARISON OF MEASURED AND PREDICTED STRAIN

Figures 10.4 to 10.6 show the results of strain measurements for each pavement, with the maximum vertical strain plotted against depth and compared with the corresponding predicted strains. The results from pavements 2 and 3 (Figures 10.5 and 10.6) are the average of read-:ings from two stacks of strain coils, whereas those for pavement 1 (Figure 10.4) are for only one stack, which showed much more variability, and included the results from the strain gauges, which were found to operate better in this pavement than the subsequent ones.

The measurement of vertical strain at the top of the DBM layer was higher, in all cases, than the predictions; otherwise no trend occurred in the DBM, with the comparison for pavement 3 being very good. The predictions of strain in the subgrade were lower than the measured strains for all three pavements.

Figures 10.7 to 10.9 showed how the strains varied with radial distance for pavements 2 and 3, for those positions where sufficient information was available. For pavement 2, measurements were available for the vertical strain at 275mm depth in the subgrade, where the

measured values were again much higher than the predictions, and for the radial longitudinal strain at the interface where agreement was very good. For pavement 3, more measurements were available, with two sets of vertical measurements compared for the subgrade, and both the lateral and longitudinal radial strains at the interface. In all cases, the predicted values are much less than the measured ones.

10.5 RESILIENT CONSTANTS DERIVED FROM IN-SITU MEASUREMENTS

For a three-dimensional stress field with principal stresses σ_1, σ_2 and σ_3, the generalised Hooke's law can be applied, so that the principal strains are given by equations of the form:

$$\varepsilon_1 = \frac{1}{E}\left[\sigma_1 - \nu(\sigma_2 + \sigma_3)\right] \qquad (10.1)$$

This is an approximation where the materials are non-linear.

Thus, if the stresses and strains at a point are known, simultaneous equations may be obtained, and solved for E and ν.

For the three pavement experiments, measurement of stresses had been very limited, and it was only possible to compute the resilient constants for one position in the subgrade, 32mm below the interface. This was for a position on the axis of the load, thus the two horizontal stresses and strains should be equal, and only two simultaneous equations were obtained.

An alternative method of computation, which is more appropriate for non-linear behaviour, is to calculate G and K, from:

$$K = \frac{p}{v} \quad \text{and} \quad G = \frac{\tau_{oct}}{\gamma_{oct}} \qquad (10.2)$$

where p is the mean normal stress, v is the volumetric strain, τ_{oct} is octahedral shear stress and γ_{oct} the octahedral shear strain, and:

$$p = \tfrac{1}{3}(\sigma_1 + \sigma_2 + \sigma_3)$$

$$v = \varepsilon_1 + \varepsilon_2 + \varepsilon_3$$

$$\tau_{oct} = \tfrac{1}{3}\sqrt{[(\sigma_1 - \sigma_2)^2 + (\sigma_2 - \sigma_3)^2 + (\sigma_3 - \sigma_1)^2]} \qquad (10.3)$$

$$\gamma_{oct} = \tfrac{2}{3}\sqrt{[(\varepsilon_1 - \varepsilon_2)^2 + (\varepsilon_2 - \varepsilon_3)^2 + (\varepsilon_3 - \varepsilon_1)^2]}$$

For an axisymmetric situation, $\sigma_2 = \sigma_3$, and:

$$\tau_{oct} = \frac{\sqrt{2}}{3}(\sigma_1 - \sigma_2)$$

$$\gamma_{oct} = \frac{2\sqrt{2}}{3}(\varepsilon_1 - \varepsilon_2) \qquad (10.4)$$

The resilient constants E and ν can be found by solving simultaneous equations obtained from the following expressions, though these assume linear elastic behaviour in their derivation:

$$K = \frac{E}{3(1 - 2\nu)} \quad \text{and} \quad G = \frac{E}{2(1 + \nu)} \qquad (10.5)$$

The resilient moduli and Poisson's ratios obtained by these two approximate methods are shown in Table 10.1 and show good agreement. The value of Poisson's ratio obtained from the generalised Hooke's law indicate that the clay may be very nearly incompressible.

For pavement 1, two distinct measurements of vertical and radial stress were obtained and therefore two values of the constants were computed which are substantially different.

When the computed resilient moduli for the softer clay from pave-:ments 1 and 2 (see Section 9.3) are plotted with those obtained from the characterisation tests (Figure 10.10), a stress stiffening effect is indicated. Since the computation of the moduli depends on the measurement of three parameters in each case, and only three moduli are available, this effect could be a result of erratic measurements. How-:ever, such an effect has been reported by previous researchers at high deviator stresses (36).

TABLE 10.1 RESILIENT CONSTANTS DERIVED FROM IN-SITU MEASUREMENTS IN SUBGRADE

Pavement No.		Method of Calculation	
		Generalised Hooke's Law	From G & K
1	E MN/m^2	16.9 & 4.8	16.9 & 8.7
	ν	0.37 & 0.48	0.37 & 0.40
2	E MN/m^2	6.8	8.0
	ν	0.5	0.39
3	E MN/m^2	22.1	21.1
	ν	0.53	0.47

A non-linear analysis was carried out for pavement 2, using this stress-stiffening relationship for the clay. It resulted in similar stresses and strains in the DBM to those obtained with the original stress-softening relationship, but the strains in the subgrade showed better agreement with measured values, with the stresses even lower than before.

10.6 SUMMARY

This Chapter has compared the measurements of the resilient behaviour of the test pavements with corresponding predictions from linear and non-linear analyses based on resilient constants obtained from the repeated load triaxial tests on the materials described in Chapter 9. Generally, the predicted stresses, particularly radial ones, were lower than measured values, and the predicted strains in the subgrade were much lower than measured values. The prediction

of vertical strain at the top of the DBM was always lower than the measurement, and tended towards a tensile value, whereas the measure-:ment was always a high compressive strain.

Comparison of the two elastic analyses shows good agreement, particularly for positions on the axis of the load. This may be attributed to the facts that selection of the constants for the linear analysis was based on the results of the non-linear analysis, and that the pavement structure was divided into five or six sublayers in order to deal with non-linearity. Thus, the more economical linear analysis may be used providing the constants are selected carefully. However, the particular analysis used (BISTRO) does not incorporate the permanent strain calculations, required for rut depth predictions, at the present time. For research purposes, the non-linear analysis using finite elements (DEFPAV) was found to be much more convenient since, apart from the computing time used, the associated work was far quicker.

The resilient constants determined from the in-situ measurements in the subgrade implied a stress-stiffening relationship for that material. This was thought to be due to an accumulation of errors and could not be taken as conclusive since only three measurements were available.

Several attempts were made to produce better agreement between the measured and predicted stresses and strains in each pavement, by adjust-:ing the resilient constants, but proved largely unsuccessful. Generally, the vertical strain at the top of the DBM and throughout the subgrade was under-predicted, as were stresses at the top of the sub-:grade. Theoretically, reduction of the modular ratio and adjustment of Poisson's ratio should compensate for these differences, but the non-linearity of the materials makes such adjustments very difficult.

An additional problem which arises when analysing pavements is that of anisotropy, which may be introduced into the layers due to

rolling during construction. In this case, cores taken from the DBM in each pavement indicated that the aggregate, which was very flakey, was orientated with the longer axis of each aggregate particle in a horizontal direction. An investigation of the anisotropy of the material from pavement 1 with respect to permanent deformation (Figure 9.13), indicated a greater tendency to deformation with cores taken horizontally than with cores taken vertically, although their stiffnesses were comparable. However, the anisotropy encountered with permanent strains could equally well apply with resilient strains, which, combined with non-linearity of the materials, makes analysis very difficult.

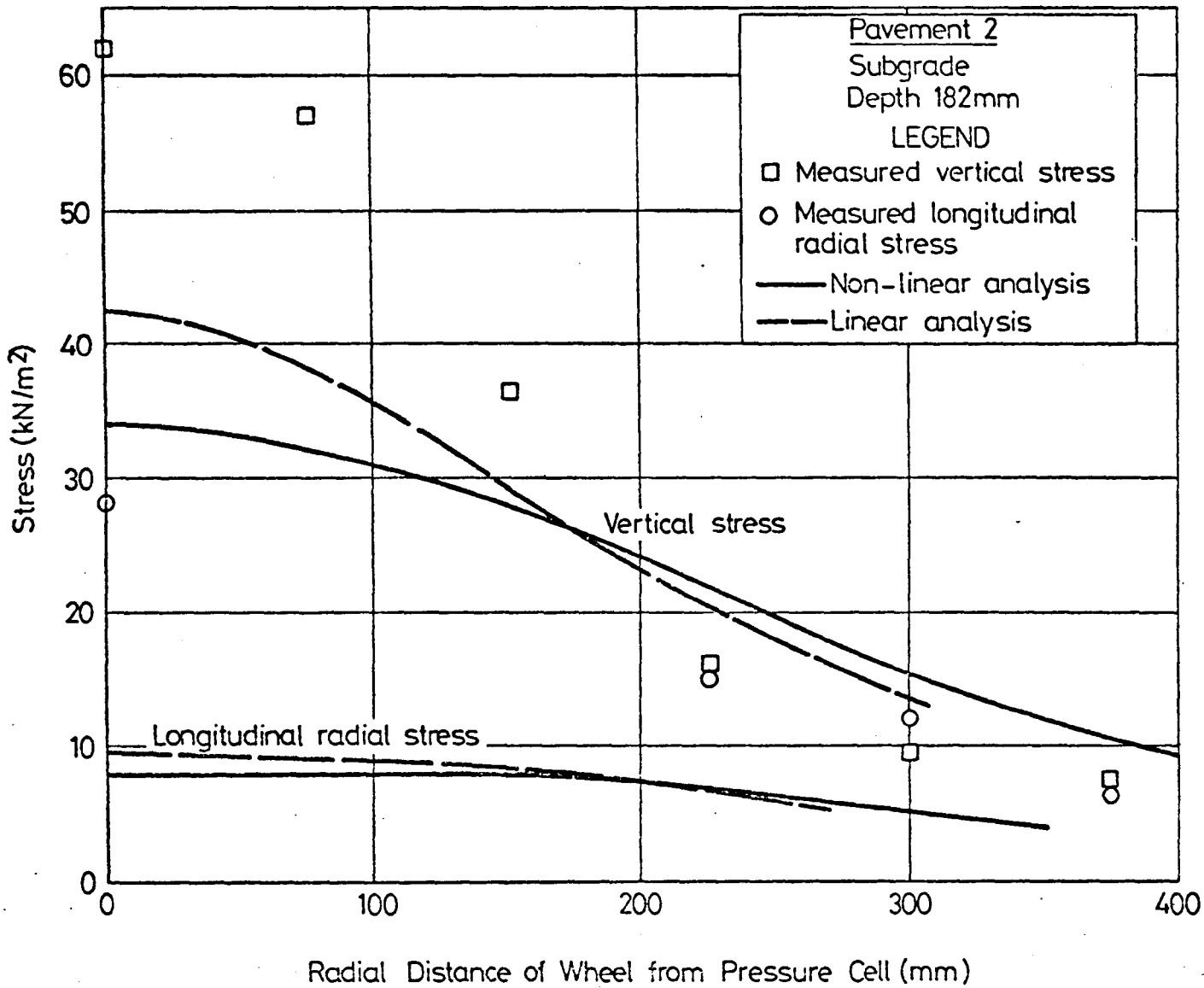

FIG. 10.1 COMPARISON OF MEASURED AND PREDICTED STRESSES (PAVEMENT NO. 2)

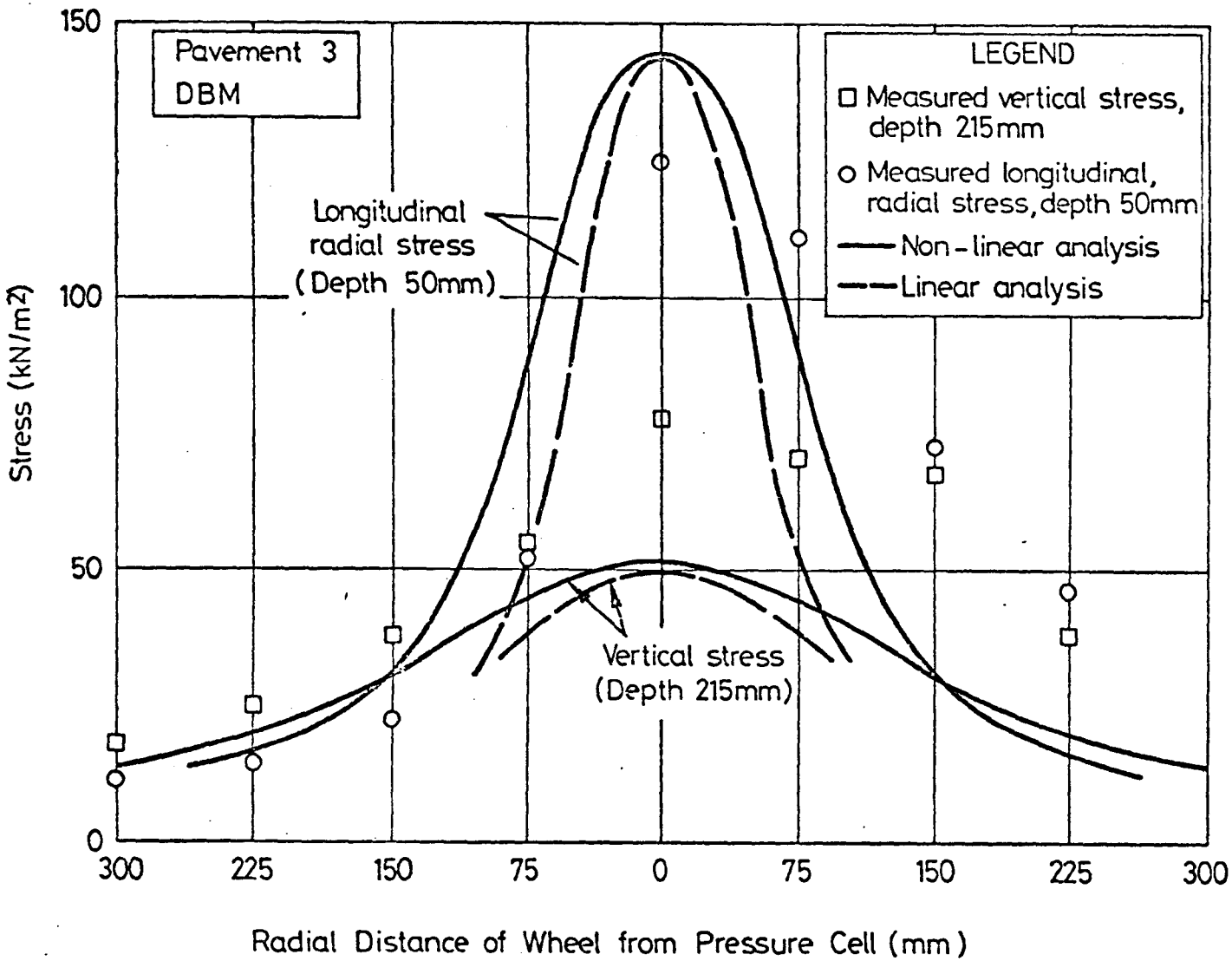

FIG. 10.2 COMPARISON OF MEASURED AND PREDICTED STRESSES IN DBM (PAVEMENT NO. 3)

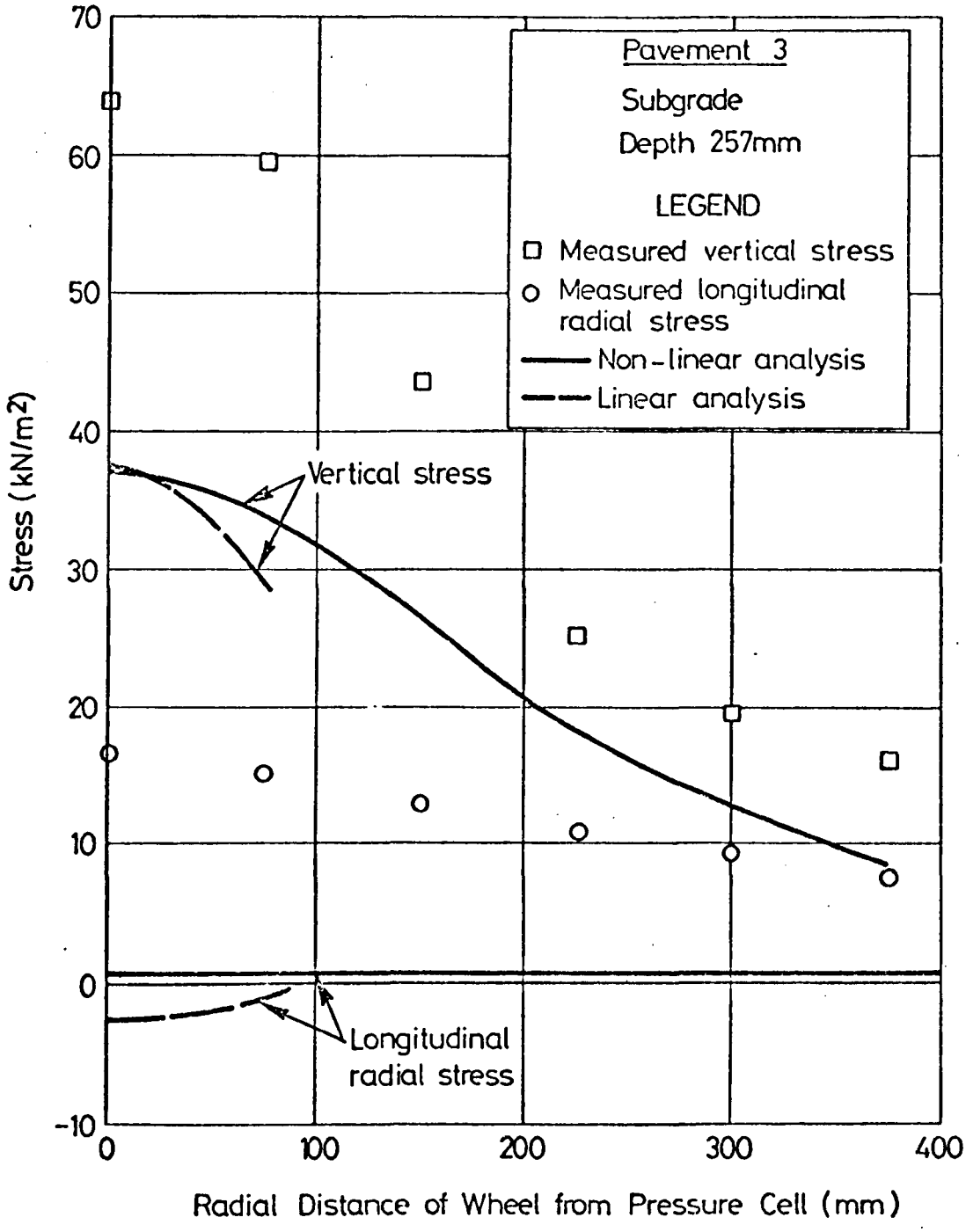

FIG. 10.3 COMPARISON OF MEASURED AND PREDICTED STRESSES IN SUBGRADE (PAVEMENT NO. 3)

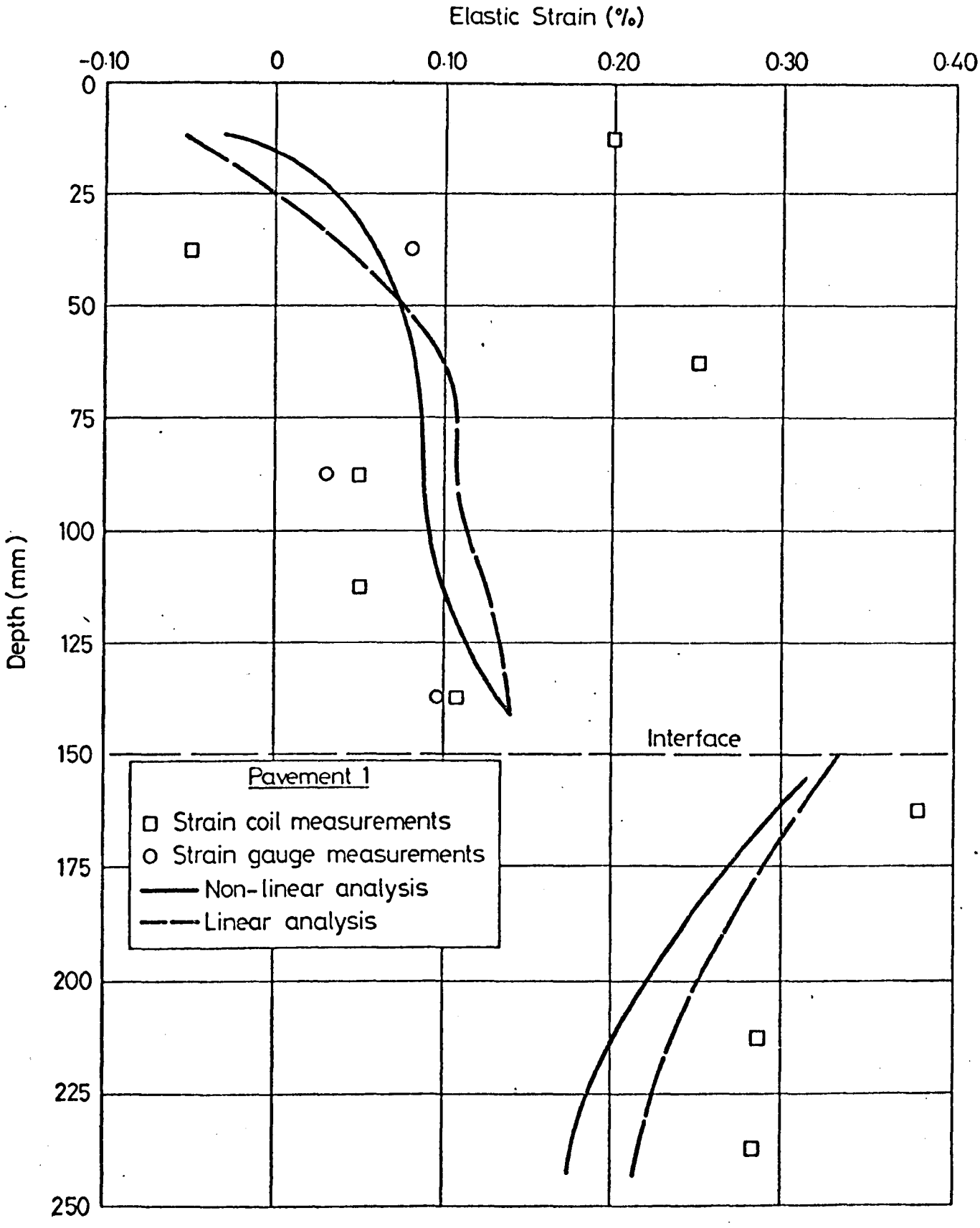

FIG. 10.4 COMPARISON OF MEASURED AND PREDICTED VERTICAL STRAINS

(PAVEMENT NO. 1)

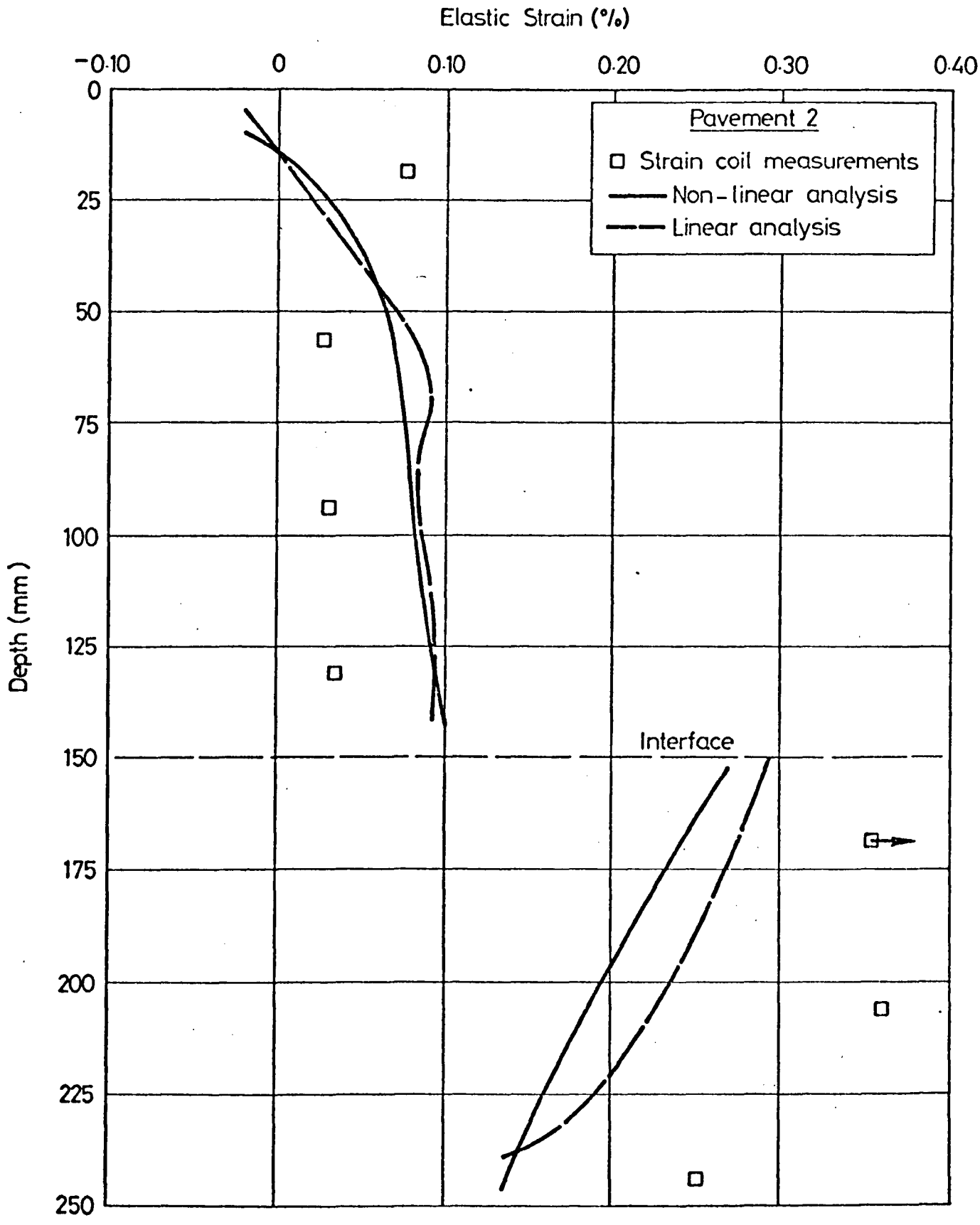

FIG. 10.5 COMPARISON OF MEASURED AND PREDICTED VERTICAL STRAINS

(PAVEMENT NO. 2)

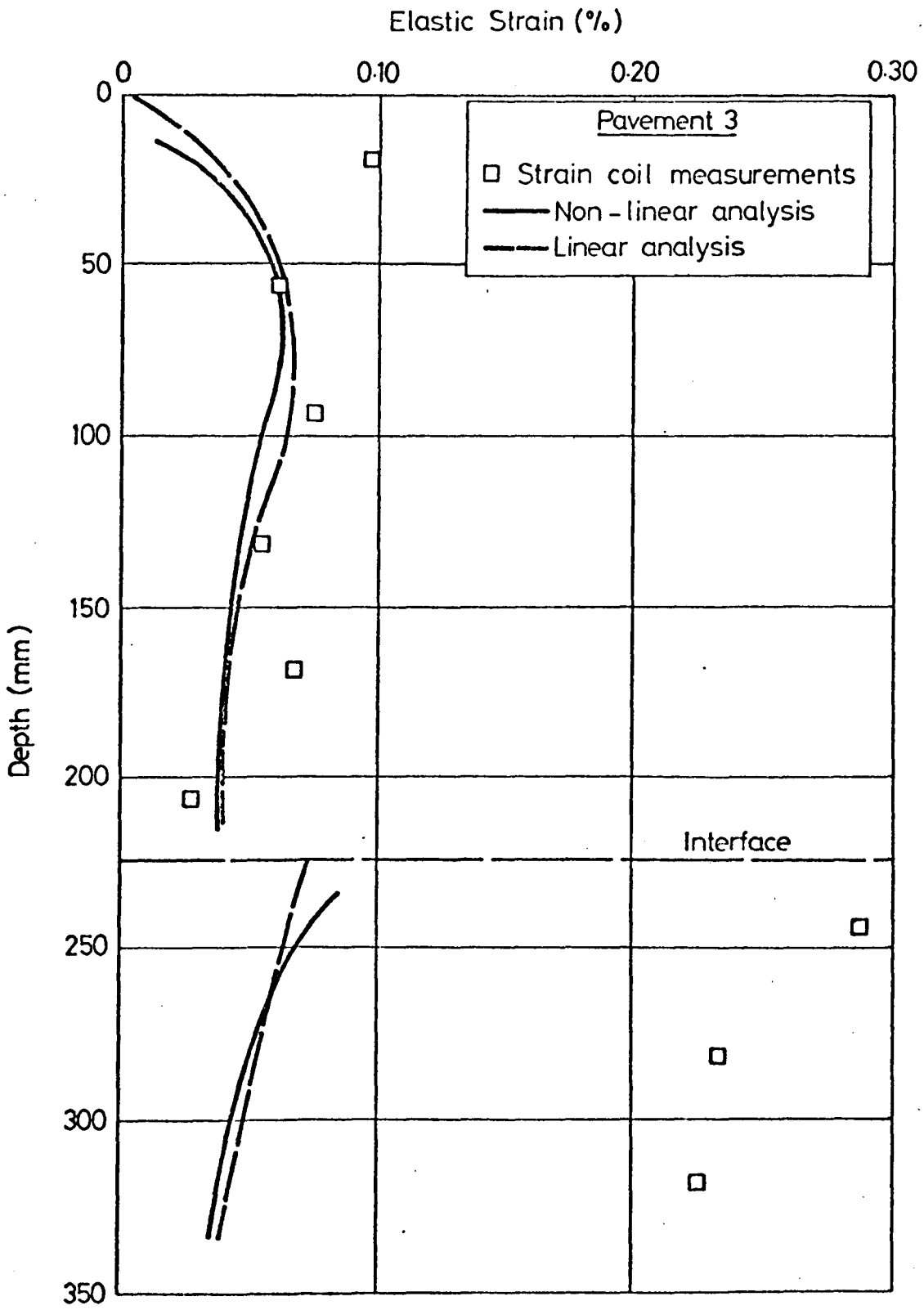

FIG. 10.6 COMPARISON OF MEASURED AND PREDICTED VERTICAL STRAINS

(PAVEMENT NO. 3)

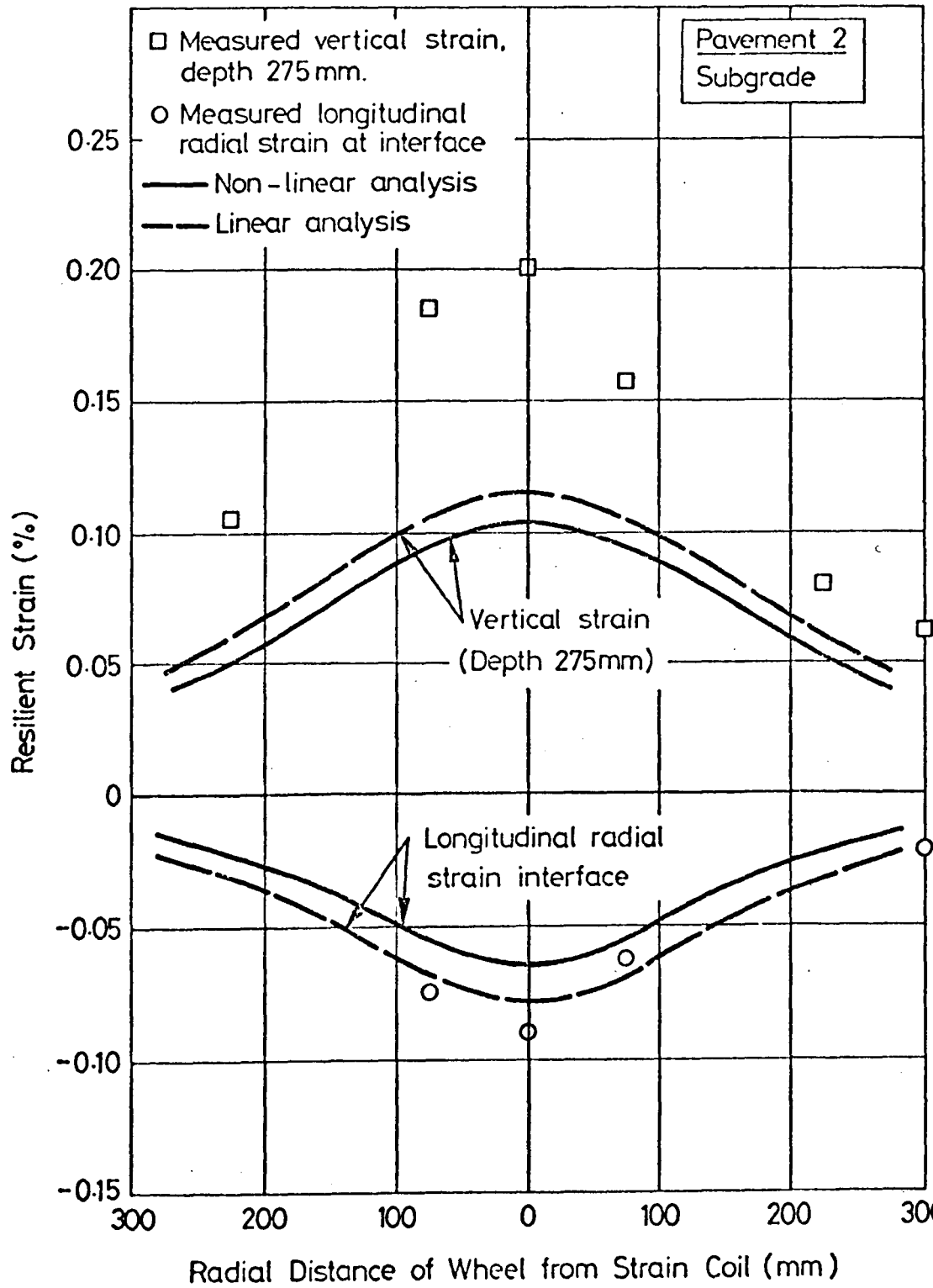

FIG. 10.7 COMPARISON OF MEASURED AND PREDICTED STRAIN VARIATION WITH RADIUS (PAVEMENT NO. 2)

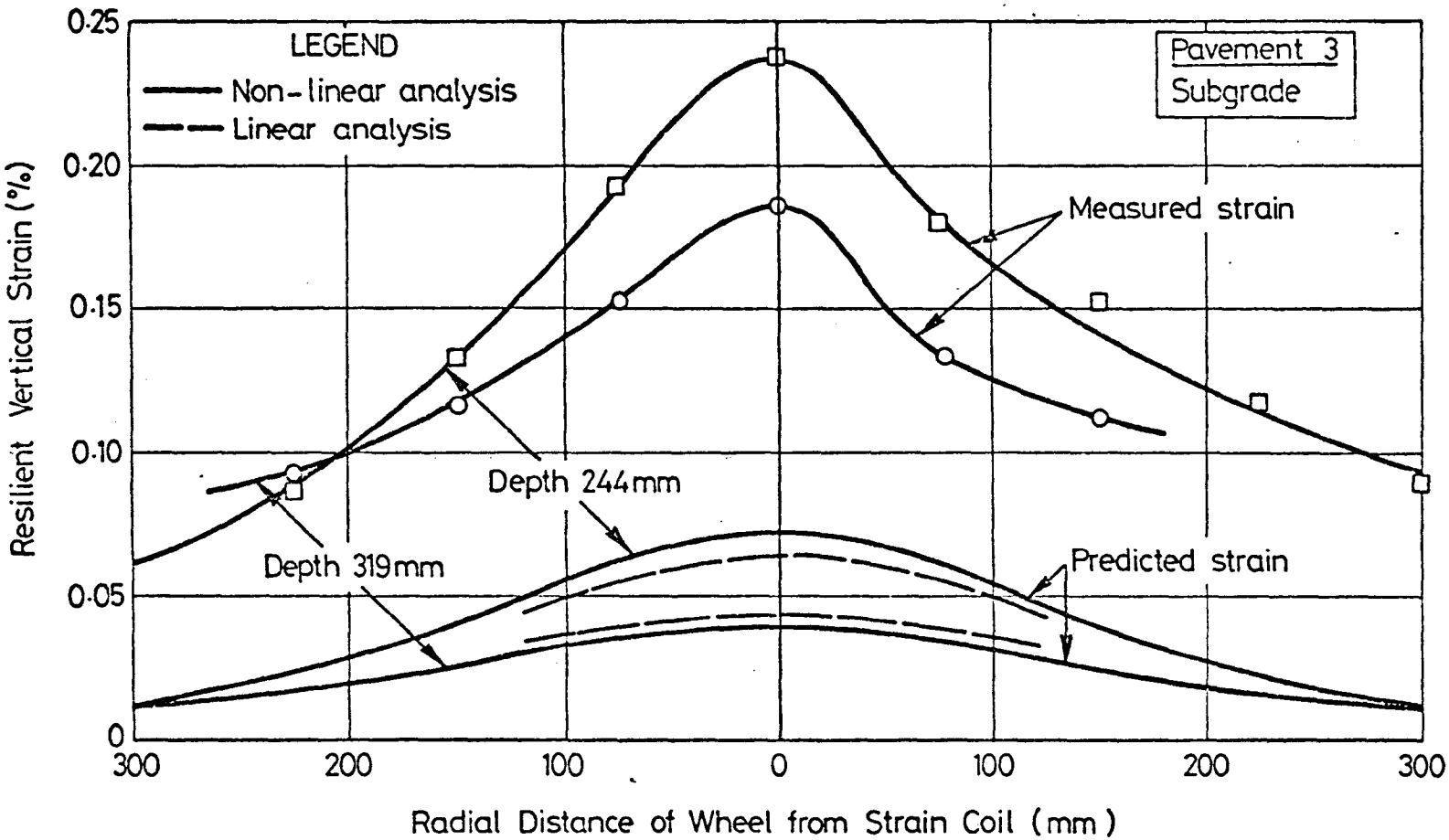

FIG. 10.8 COMPARISON OF MEASURED AND PREDICTED VERTICAL STRAIN VARIATION WITH RADIUS (PAVEMENT NO. 2)

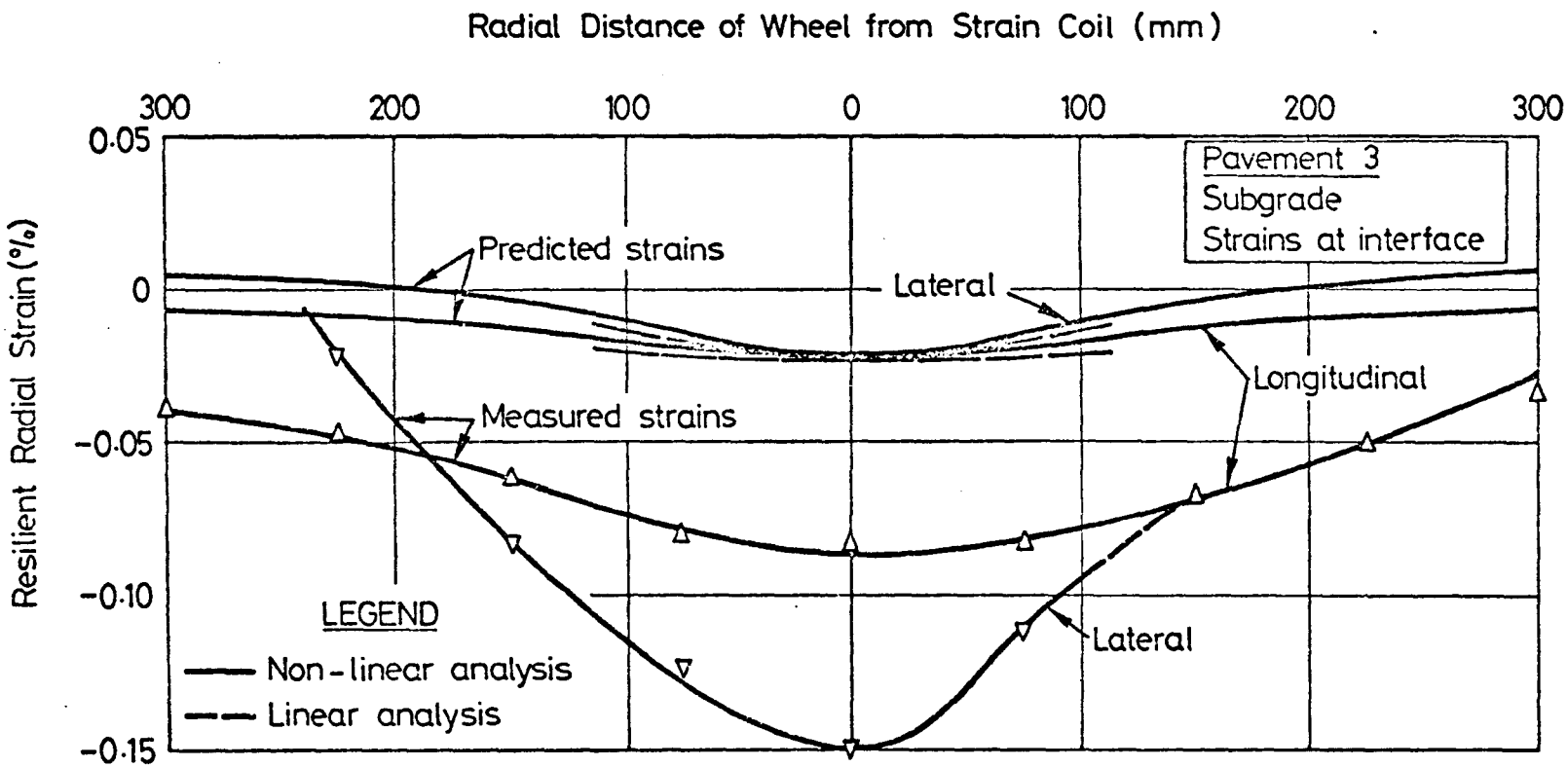

FIG. 10.9 COMPARISON OF MEASURED AND PREDICTED HORIZONTAL STRAIN VARIATION WITH RADIUS AT THE INTERFACE (PAVEMENT NO. 3)

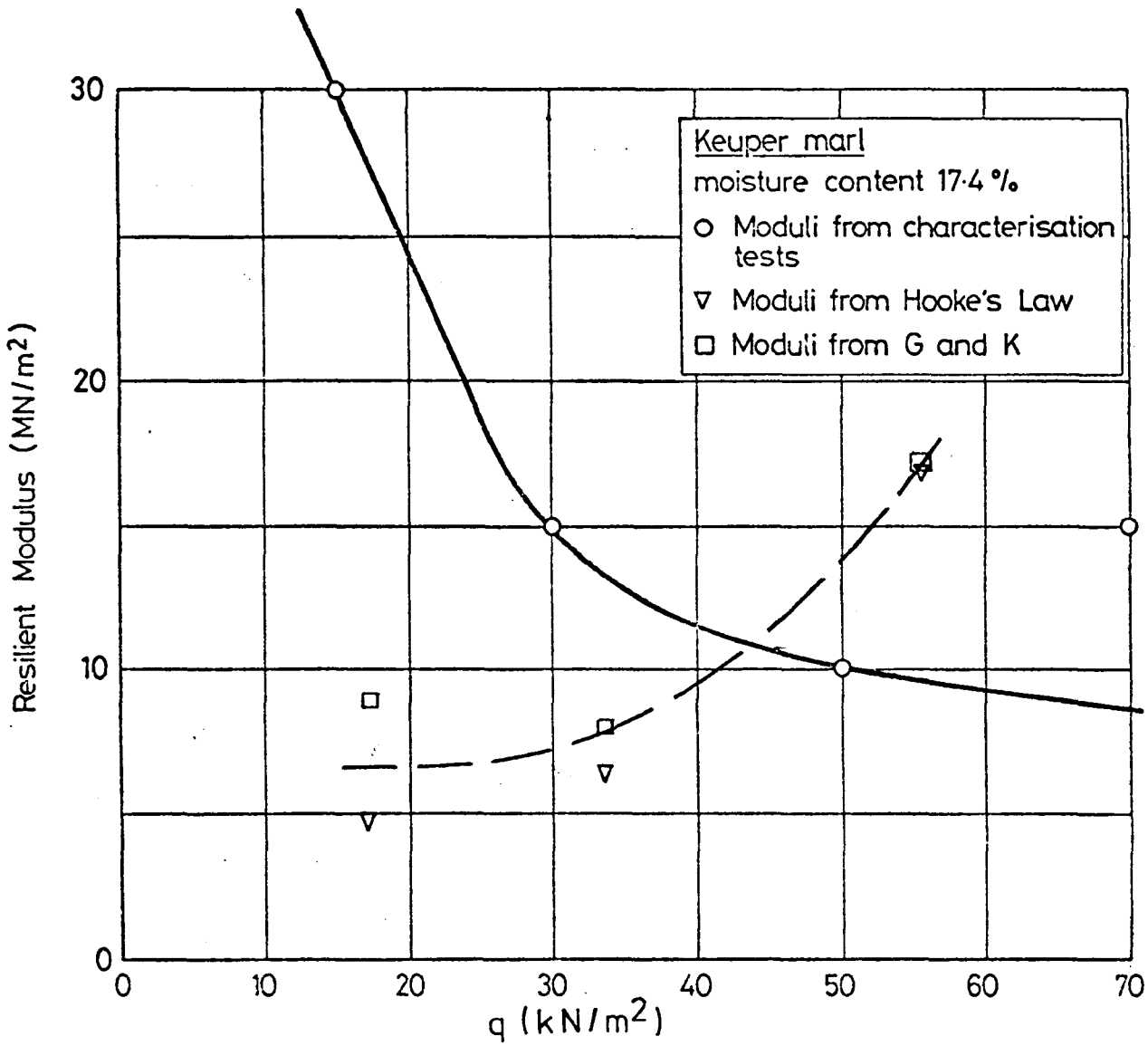

FIG. 10.10 COMPARISON OF RESILIENT MODULUS OF SUBGRADE DETERMINED FROM IN SITU MEASUREMENTS AND FROM CHARACTERISATION TESTS

CHAPTER ELEVEN

PREDICTIONS OF PERMANENT DEFORMATION

11.1 INTRODUCTION

The materials testing results reported in Chapter 9 have been used in this Chapter to develop models relating vertical permanent strain to the applied stresses both for the DBM mixes and the Keuper marl used in each of the three pavements. These models are incorp-:orated in the computer program DEFPAV (24) as "creep equations". Following the calculation of stresses in DEFPAV, the vertical permanent strains are calculated for each element in the chosen network, and these strains are then used in the final calculation of permanent deformation. The final calculation procedure is not incorporated in DEFPAV as yet, but is relatively easy to carry out.

11.2 DEVELOPMENT OF THE DBM PERMANENT DEFORMATION MODELS

11.2.1 Introduction

The vertical permanent strain results which were plotted in Figures 9.9 to 9.12 and Figure 9.14 have been replotted in Figures 11.1 to 11.4 using a logarithmic scale for the permanent strain. A model was developed for the DBM used in each pavement, from these Figures, using the results from pavement 1 (test series C1 and TH1) as guidelines to the behaviour of pavements 2 and 3 for which only a few results were available.

11.2.2 Model for pavement 1

Figures 11.1 to 11.3 show that, for a particular value of p, a series of parallel lines represented the response of the material to

q and to time. Snaith (22) found that the permanent strain behaviour of a DBM could be represented by a series of straight lines, although not parallel since his tests were at different values of p. He developed a model for his material by determining an intercept and a slope value and related these to the test conditions. The same general approach has been followed in analysing the results presented herein.

The intercepts with the vertical axis in Figures 11.1 to 11.3 were moved such that they coincided for all values of p, at a particular value of q. This adjustment did not affect the accuracy of the representation significantly. The plot for p = 650 kN/m^2 and q = 150 kN/m^2 (Figure 11.3) did not comply with the trend established at the other test conditions, which was probably due to the difficulty of measuring the deformations, which were very small under these conditions. Thus, this plot was weighted lightly when choosing the adjusted intercepts, which were approximately the average values from the other test conditions. The adjusted intercepts are shown as closed symbols in Figures 11.1 to 11.3.

It was very difficult to interpret the results of the tension tests since they had been of short duration, and accurate measurements of strain had been difficult. In order to reproduce the in-situ stress conditions, at positions where two of the principal stresses are tensile (biaxial tension), it was necessary to apply an axial tension (uniaxial tension) in the triaxial test. This necessitated a much higher tensile stress in the test than exists in-situ and therefore resulted in higher permanent strains. This fact was corroborated by the results which, when plotted on a logarithmic basis, did not fall within the pattern established for the compression tests; the intercepts and slopes of the lines being higher. Therefore, in the development of the model, the intercepts were assumed to have the same values as those for the compression tests, and the slope values were assumed to fall on a smooth

curve developed from the compression tests (Figure 11.7).

A representation of the straight line logarithmic plots is given in Figure 11.5. The equation of this general line is:

$$\log \varepsilon_{vp} = A + B\ (\log t - 1) \qquad (11.1)$$

Thus, to obtain a value for the vertical permanent strain (ε_{vp}), all that is required are values of the intercept (A), and slope (B) of the line, and the total time (t)*. The intercept depends on q, and the slope on p. Plots of A versus q, and B versus p are shown in Figures 11.6 and 11.7 respectively. For conveneience, the actual value of A was used, rather than the logarithm, thus equation (11.1) becomes:

$$\log \varepsilon_{vp} = \log A + B\ (\log t - 1) \qquad (11.2)$$

A computerised curve fitting procedure (85) was used to fit a Chebyshev polynomial to the plots in Figures 11.6 and 11.7, obtaining equations of the form:

$$w = \tfrac{1}{2} a_{i0}T_0(X) + a_{i1}T_1(X) + a_{i2}T_2(X)..... \\ ..... a_{ii}T_i(X) \qquad (11.3)$$

where $T_0(X) = 1$, $T_1(X) = X$, $T_2(X) = 2X^2 - 1$

$T_3(X) = 4X^3 - 3X$

$T_4(X) = 8X^4 - 8X^2 + 1$

$T_5(X) = 16X^5 - 20X^3 + 5X$ etc.

and X is the independent variable after a change of origin and scale, i.e. in this case X is given by:

$$X = (2x - x_{max} - x_{min})/(x_{max} - x_{min}) \qquad (11.4)$$

---

* The total time was obtained by multiplying the number of load applications by an average stress pulse time.

Thus, for Figure 11.6, $x = q$, $q_{max} = 800$, $q_{min} = 0$, and:

$$X = (2q - 800)/800 \qquad (11.5)$$

The resulting equations for A and B were as follows:

$$A = .5164 + .5321T_1(X) - .0500T_2(X) - .0538T_3(X) + .0238T_4(X) \qquad (11.6)$$

$$B = .2575 - .2199T_1(Y) + .0546T_2(Y) - .0156T_3(Y) \qquad (11.7)$$

where $$Y = (2(p + 150) - 1000/1000 \qquad (11.8)$$

Thus, a value for ε_{vp} may be obtained, providing the values of p, q and t are known.

11.2.3 Model for pavements 2 and 3

Figure 11.4 shows the logarithmic plot comparing behaviour of the mixes in the three pavement experiments, at the same stress conditions ($p = 133$ kN/m^2, $q = 275$ kN/m^2). The lines were parallel, with that for pavement 2 showing the greatest susceptibility to deformation. It was therefore assumed that for all other values of p, the slope values for each pavement would be the same as for pavement 1. The intercept values were found by assuming that differences between the intercepts for pavements 2 or 3 and those for pavement 1 at all values of q would be the same as at $q = 275$ kN/m^2.

Hence: $$\log A_2 = \log A_1 + .731 \qquad (11.9)$$

$$\log A_3 = \log A_1 + .301 \qquad (11.10)$$

where A_1, A_2 and A_3 are the intercepts for pavements 1, 2 and 3 respectively, as shown in Figure 11.4.

Therefore, providing p, q and t are known, the vertical permanent strain may be found from equations 11.2, 11.6 and 11.7, as for pavement 1, by substituting the appropriate value of A_2 or A_3, obtained from equations 11.9 or 11.10, into 11.2.

11.3 DEVELOPMENT OF KEUPER MARL PERMANENT DEFORMATION MODELS

Discussion in Chapter 9 indicated that the results for vertical permanent strain of Keuper marl when plotted semi-logarithmically, were in a convenient form for the development of models. The plots in Figures 9.25 to 9.27 were adjusted slightly so that all lines passed through the origin, as in Figure 11.8, which shows Figure 9.26 replotted. The general form of the equation for any line is thus:

$$\varepsilon_{vp} = b \log N \qquad (11.11)$$

where ε_{vp} is the vertical permanent strain, b is the slope of the line, and N is the number of load cycles. Thus, to obtain a value of ε_{vp} after a particular number of cycles (N), all that is required is a value of b, which is simply a function of q.* Since the test programme for the Keuper marl was based on a unique line, theoretically the value of b could depend on p or q. However, as discussed in Chapter 9, a constant confining pressure was employed in the testing, and only the mean values of p and q were reproduced. The magnitudes of q used in the testing were equivalent to those in-situ and hence this parameter was chosen to define b.

The main series of tests for this material was series K2 (Figure 11.8) which used cores taken from new material installed for pavement 2, that was similar to the material in pavement 1. Figure 11.9 shows the plot of b_2 (slope value for test series K2) versus q for this series, and again, a Chebyshev polynomial was fitted to the plot to give the following equation for b_2:

$$b_2 = .59159 + 88784T_1Z + .37704T_2(Z) + .10584T_3Z + .03058T_4Z + .00198T_5(Z) \qquad (11.12)$$

where $$Z = (q - 70)/70 \qquad (11.13)$$

*Due to the use of the principal stress pulse time rather than the average stress pulse time (see p.93), the value of N was multiplied by 1.5, so that permanent strain corresponding to the average pulse time was calculated.

A simpler equation represents the curve, for $q \leq 40$ kN/m^2:

$$\varepsilon_{vp} = (q/70)^2 \log N \qquad (11.14)$$

where $b_2 = (q/70)^2$.

This equation was found to be more satisfactory than the Chebyshev polynomial for $q \leq 40$ kN/m^2, and was therefore adopted because of its simple form. In fact, it was found that using the non-linear analyses for all three pavements, the value of q was never greater than 40 kN/m^2.

A similar model was developed for the dryer materials tested in series K1 and K3, which were combined because of their similar moisture contents, and together, the results provided sufficient information to construct a $b_{1,3}$ (slope factor for test series K1 and K3) versus a q plot (shown in Figure 11.10). An equation of similar form to (11.14) was found to provide a best fit line through the points, over the entire range tested, giving:

$$\varepsilon_{vp} = (q/130)^2 \log N$$

where $b_{1,3} = (q/130)^2$.

The model developed from test series K2 was used for predictions on pavement 1 and for the layer of new material added during the construction of pavement 2. The model developed from series K1 and K3 was used for predictions on pavement 3 and for the old material in pave-:ment 2.

11.4 PREDICTION PROCEDURE

11.4.1 Multi-track tests

The permanent strain models were incorporated in DEFPAV which computed vertical permanent strain for a network of elements after any number of load repetitions in a single wheel track.

However, the main experiment for each test pavement was a multi-track test, consisting of a pseudo-normal distribution of load repetitions in nine equally spaced wheel tracks over a 600mm width of pavement. Therefore, in order to obtain values of rut depth and rut profile, it was necessary to obtain the vertical permanent strain in each element due to the wheel travelling in each of the nine tracks. This was achieved by adopting a "time hardening" cumulative loading procedure (40). This procedure is illustrated in Figure 11.11 with an alternative "strain hardening" procedure. The former was favoured, because it is simpler to apply and had been validated by tests on nominally the same DBM (84). A cumulative loading procedure is thus used to predict the strain accruing in an element subjected to differ-:ing stresses, which may be caused by loads of differing magnitude passing directly over the element, or by loads of the same magnitude at different radii from the element, which is the case here.

Cumulative loading procedure: Figure 11.12 shows the distribution of wheel passes used in the multi-track tests, for a total number of passes of 10^5. Rather than calculate the permanent deformation at the points on the centre line of each wheel track, points midway between adjacent wheel tracks were chosen, since all elements below such a point were affected equally by each adjacent track. There is no great advantage in either method, however, although the second is easily combined with a finite element analysis. The permanent strains accruing in the columns of elements below points A_R to F_R (Figure 11.12) were found, and those in the columns below A_L to F_L were exactly the same. The reasons for using points E_R and F_R, E_L and F_L are explained later in the text.

The cumulative loading construction used to determine the permanent strain accruing in an element 62.5mm below point A_R in Figure 11.12, is shown in Figure 11.13. This was for pavement 1 assuming a DBM layer

thickness of 150mm, the nominal thickness of the surfacing for this structure (the actual depth of DBM, found from measurement of cores and slabs taken after testing, was 145 ± 5mm.). As may be seen in Figure 11.12, the point A_R is affected by wheel loads at radii of 37.5mm (22,000 plus 18,000), 112.5mm (18,000 plus 12,000), 187.5mm (12,000 plus 6,000), 262.5mm (6,000 plus 3,000), and 337.5mm (3,000). In order to obtain the total permanent strain due to the wheel acting at these five radii, the stress conditions in the element were calculated, and a strain line obtained for each radius. This was achieved by using DEFPAV, and obtaining permanent strain outputs for a suitable range of load repetitions. The strain lines are shown in Figure 11.13. In order to obtain these it was necessary to choose the network of elements for use in DEFPAV such that a column of elements fell below each of the radii, although there could be intermediate columns. Primarily, DEFPAV calculates stresses and strains at the centre of each element in the network, i.e. at various radii and depths from a stationary point of loading. However, the results may also be used to give the stresses and strains in a particular element as the load position varies, which was the procedure adopted to obtain the strain lines for any element.

The construction assumed that the wheel moved from right to left in Figure 11.12, when changing tracks, and that 3,000 passes occurred at a radius of 262.5mm continuously, then 6,000 at a radius of 187.5mm and so on, until, finally, 3,000 passes again occurred at a radius of 337.5mm. This was at variance with the actual loading pattern where small numbers of passes occurred at each position, and, in the case of pavements 2 and 3, in random order, until the total number of passes (100,000) was achieved. However, the final computed result would be the same in each case.

The path followed along the strain lines in the cumulative loading construction is indicated by arrows in Figure 11.13. Initially 3,000

passes at a radius of 262.5mm resulted in a vertical permanent strain of ε_{vp1}. This was approximately equivalent to 200 passes at r = 187.5mm. A further 6,000 passes at r = 187.5mm resulted in an additional permanent strain ε_{vp2}, and a total of ε_{vp1} plus ε_{vp2}, and so on. The fourth and fifth stages of loading occur at the same radius, r = 37.5mm, and therefore 40,000 passes result at that radius. The seventh stage of loading was for 12,000 passes at a radius of 187.5mm. However, it may be seen from Figure 11.13 that horizontal projection from point α on the r = 112.5mm strain line, to the r = 187.5mm strain line, would pass through more than one decade, and the resulting additional permanent strain achieved would be negligible. The same would apply to the remaining two stages. Thus, the total vertical permanent strain accruing in this element, after 10^5 wheel passes, was the value at α; 7.8%.

The equivalent number of passes: Figure 11.13 shows that the total vertical permanent strain achieved after 10^5 total passes would have been achieved by 57,000 passes had they all been applied at a radius of 37.5mm. This number of passes was termed the "equivalent number of passes". A similar construction procedure to that outlined above was carried out for all the other elements vertically below point A_R (radius 37.5mm), resulting in the equivalent passes, permanent strains and element deformations shown in Table 11.1. The total surface deformation shown (at this radius of 37.5mm) was assumed to be the rut depth, since it was not possible with finite elements to obtain the deformations at the exact centre of the spectrum of wheel passes. The stress distribution occurring there would be only slightly different from that at r = 37.5mm, resulting in a very similar deformation.

The mean number of equivalent passes: It was found possible to select a number of passes approximately equal to the average of the number of equivalent passes for all elements at a radius of 37.5mm, that would give the same surface deformation. This number was termed the mean number of

TABLE 11.1 PAVEMENT 1

RESULTS OF TIME HARDENING CUMULATIVE LOADING CONSTRUCTION

r = 37.5mm (Point A_R)

Depth (mm)	Equivalent Passes (N)	ε_{vp}(%)	Deformation (mm)	ε_{vp}(%)	Deformation (mm)
		After N passes		After 50,000 passes (MEP)	
12.5	70,000	3.26	.815	3.17	.793
37.5	63,000	5.23	1.308	5.09	1.273
62.5	57,000	7.80	1.895	7.39	1.848
87.5	46,000	10.00	2.500	10.35	2.588
112.5	43,000	12.75	3.188	13.37	3.343
137.5	50,000	8.25	2.063	7.99	1.999
162.5	40,300	1.330	.333	1.373	.343
187.5	41,000	.875	.219	.909	.227
212.5	42,000	.625	.156	.641	.160
237.5	50,000	.465	.116	.469	.117
262.5	58,000	.385	.096	.388	.097
287.5	59,000	.338	.085	.329	.082
350	54,000	.226	.226	.228	.228
500	50,000	.086	.172	.860	.172
900	65,000	.021	.126	.020	.120
Total (Surface Deformation) = 13.49				Total = 13.49	

equivalent passes (MEP). Table 11.1 shows the permanent strains and deformations resulting in all elements below A_R after 50,000 passes at a radius of 37.5mm, with a surface deformation very similar to that obtained by the detailed procedure of Figure 11.13. This information was obtained directly from an output of DEFPAV, and involved no graphical construction. The individual permanent strains and deformations are very similar to those obtained by the cumulative loading construction since the strain lines are not particularly sensitive to the number of passes over the range 4×10^4 to 7×10^4.

Determination of MEP's for other radial positions: The surface deformation accruing at a radius of 37.5mm (below point A_R, Figure 11.12), was assumed to be the rut depth. However, to obtain a rut profile, similar deformations at points B_R to F_R were required. These deformations could be obtained by a cumulative loading construct-:ion, but this would be extremely time consuming, and an approximate method was developed based on the selection of an MEP for each position.

The constructions for point A_R in pavement 1 indicated that only the wheel passes at radii of 37.5 and 112.5mm contributed significantly to the deformation at any point, hence the need to calculate deform-:ations at points E_R, F_R, E_L and F_L for the outermost wheel positions. For point A_R the number of significant passes (i.e. those at radii of 37.5 or 112.5mm) contributing to an MEP of 50,000 was 70,000. There-:fore, to obtain an MEP for other points, the total number of passes at radii of 37.5 and 112.5mm was multiplied by 5/7 (the MEP factor). Hence, for point B, 22,000 plus 6,000 passes were applied at a radius of 112.5mm, and 18,000 plus 12,000 passes at a radius of 37.5mm, giving a total of 58,000 significant passes. Thus, the mean number of equivalent passes is given by:

$$\text{MEP} = 5/7 \times 58{,}000$$

$$= 41{,}000$$

Similar calculations for points C to F resulted in the MEP's shown in Figure 11.12.

Positions of maximum permanent strain: Table 11.2 shows a section of output from DEFPAV for permanent strain calculations over a network of elements after 50,000 total passes on pavement 1. This particular section of output was used to obtain the deformation for an MEP of 50,000, i.e. below the point A_R (Figure 11.12), at a radius of 37.5mm. The strains shown have not been converted to percentages.

The Table shows that in the upper half of the DBM layer (the top three rows of elements), the maximum permanent strain at a particular depth (shown enclosed) does not occur at the position nearest to the point of loading, i.e. when the wheel is 37.5mm from A_R (the second column in this case). Figure 11.14 shows a plan view of the pavement surface with the wheel travelling along the path MN. Table 11.2 indicates that the maximum permanent strain 12.5mm below A_R occurs when the centre of the wheel is 95mm from A_R (at point O in Figure 11.14). Similarly, the maximum permanent strains 37.5 and 62.5mm below A_R are when the wheel is 95mm and 75mm from A_R respectively. At larger depths the maximum strain does occur when the wheel passes closest to the point (at point P).

Thus, the deformation accruing below point A_R, 35.7mm from the line of travel of the wheel, is determined by choosing the maximum strain at each depth, and carrying out the usual summation procedure (Table 11.1). The deformations below all the other points, A to F, may be found by obtaining outputs from DEFPAV for the particular values of MEP at each point, or by constructing a plot of deformation versus MEP, from a set of outputs covering a suitable range of MEP, and reading off the relevant deformations.

The plot of deformation versus MEP for pavement 1 is shown in Figure 11.15. Thus a knowledge of the deformation accruing below each

Table 11.2 Permanent strain output after 50,000 passes

RADIUS OF CENTRE OF ELEMENT (mm)

	12.5	37.5	60.0	75.0	85.0	95.0	112.5	145.0	187.5	262.5	382.5	550.0
	ELEMENT COLUMN NUMBER											
Depth (mm)	1	2	3	4	5	6	7	8	9	10	11	12
12.5	0.01540	0.01420	0.01431	0.01839	0.02579	0.03168	0.03148	0.02510	0.01131	0.00374	0.00208	0.00146
37.5	0.02538	0.03026	0.03916	0.04776	0.04983	0.05087	0.04658	0.03069	0.01451	0.00791	0.00158	0.00162
62.5	0.06018	0.06588	0.07213	0.07392	0.07179	0.06825	0.05935	0.03915	0.02064	0.00598	0.00156	0.00197
87.5	0.11359	0.10354	0.09297	0.08373	0.07676	0.06975	0.05859	0.03966	0.02297	0.00777	0.00184	0.00158
112.5	0.16011	0.13365	0.10686	0.08906	0.07744	0.06739	0.05352	0.03611	0.02145	0.00844	0.00260	0.00147
137.5	0.08190	0.07988	0.07611	0.07153	0.06749	0.06210	0.05251	0.03969	0.02091	0.00921	0.00415	0.00182
162.5	0.01473	0.01373	0.01281	0.01213	0.01155	0.01087	0.00958	0.00742	0.00469	0.00320	0.00123	0.00039
187.5	0.00947	0.00909	0.00864	0.00829	0.00803	0.00775	0.00698	0.00564	0.00403	0.00293	0.00126	0.00040
212.5	0.00663	0.00641	0.00614	0.00593	0.00579	0.00564	0.00531	0.00427	0.00386	0.00270	0.00122	0.00042
237.5	0.00482	0.00469	0.00455	0.00440	0.00430	0.00443	0.00428	0.00393	0.00349	0.00249	0.00115	0.00043
262.5	0.00393	0.00388	0.00389	0.00349	0.00386	0.00385	0.00375	0.00346	0.00302	0.00225	0.00107	0.00043
287.5	0.00333	0.00329	0.00328	0.00326	0.00324	0.00322	0.00316	0.00293	0.00265	0.00200	0.00099	0.00042
350.0	0.00232	0.00228	0.00225	0.00222	0.00220	0.00217	0.00211	0.00198	0.00181	0.00136	0.00082	0.00038
500.0	0.00086	0.00086	0.00085	0.00084	0.00083	0.00082	0.00080	0.00077	0.00076	0.00066	0.00049	0.00026
900.0	0.00020	0.00020	0.00020	0.00020	0.00020	0.00020	0.00020	0.00019	0.00019	0.00018	0.00016	0.00012

RUT DEPTH (mm)

- 13.390

point enables a rut profile to be constructed.

Summary: The following steps were required to predict the rut-depth and rut profile for a particular pavement:

(a) Determine the deformation at point A (r = 37.5mm) by a series of culumative loading constructions for a column of elements. This is assumed to be the rut depth.

(b) Determine the "equivalent number of passes" for each element at this radius and compute the average.

(c) Determine the "mean number of equivalent passes" (MEP) by comparing the deformation from (a) with those from a number of DEFPAV outputs for a range of passes including the average equivalent number of passes.

(d) Divide the MEP from (c) by the total number of passes at radii of 37.5 and 112.5mm from A (significant passes) to determine an MEP factor.

(e) Determine the MEP's at points B to F by multiplying the number of "significant passes" by the MEP factor.

(f) Construct a plot of deformation versus MEP from a suitable range of DEFPAV outputs and read off the deformations corresponding to the MEP's for points B to F, to construct the rut profile.

11.4.2 Single track tests

In this case, the predictions were much more straightforward. For the three single track tests carried out, 22,000 wheel passes were applied in one track, the same number as were applied in the central track of the multi-track tests. One run with DEFPAV, giving the permanent strains after 22,000 passes, provided all the information required to predict the rut depth and rut profile.

The output for pavement 1 is shown in Table 11.3, with the positions where maximum permanent strain occur shown enclosed. With reference to Figure 11.14, in this case the permanent strains accruing below the point P are required. The maximum strains at depths of 12.5, 37.5 and 62.5mm occur at radii of 95, 95 and 75mm. For greater depths than these the maximum strains occur at a radius of 12.5mm, the closest point to the line of travel of the wheel. The rut depth was found by carrying out the usual integration process, multiplying the maximum strain at each depth by the thickness of the element and summing.

The surface profile was found by summing the maximum deformations at each radius. The procedure for a radius of 12.5mm has been described, and is similar to that followed for the other radii, but, as the radius increases, only the strains occurring below positions of greater radius were considered when determining the maximum strain in a particular element. For instance, for the column of elements at a radius of 85mm, the maximum strain at a depth of 12.5mm occurs in column 6. Thereafter, the maximum strains are all in column 5. For radii of 95mm and above, the maximum strains occur within the column of elements at that radius.

11.5 PREDICTIONS

11.5.1 Presentation

Figures 11.16 to 11.21 show the predictions of rut depths and profiles for the single and multi-track tests for each pavement, after 22,000 and 100,000 passes respectively. An exception for the single-track tests was pavement 1, where 44,000 passes were applied. The predictions for pavements 2 and 3 were carried out in the manner out-:lined for pavement 1 in Section 11.4, resulting in an MEP factor of

Table 11.3 Permanent strain output after 22,000 passes

RADIUS OF CENTRE OF ELEMENT (mm)

	12.5	37.5	60.0	75.0	85.0	95.0	112.5	145.0	187.5	262.5	382.5	550.0
Depth (mm)	ELEMENT COLUMN NUMBER											
	1	2	3	4	5	6	7	8	9	10	11	12
12.5	0.01444	0.01332	0.01336	0.01674	0.02280	0.02709	0.02592	0.01815	0.00956	0.00375	0.00149	0.00119
37.5	0.02057	0.02469	0.03181	0.03836	0.03999	0.04069	0.03657	0.02545	0.01036	0.00286	0.00113	0.00117
62.5	0.04481	0.04919	0.05372	0.05489	0.05330	0.05076	0.04431	0.02910	0.01524	0.00436	0.00113	0.00142
87.5	0.07855	0.07215	0.06527	0.05902	0.05434	0.04957	0.04200	0.02869	0.01669	0.00565	0.00134	0.00114
112.5	0.10486	0.08877	0.07192	0.06043	0.05288	0.04629	0.03720	0.02550	0.01532	0.00610	0.00189	0.00107
137.5	0.05470	0.05349	0.05110	0.04811	0.04547	0.04191	0.03568	0.02535	0.01473	0.00664	0.00303	0.00132
162.5	0.01365	0.01273	0.01188	0.01124	0.01070	0.01007	0.00883	0.00688	0.00435	0.00296	0.00114	0.00036
187.5	0.00877	0.00843	0.00801	0.00768	0.00744	0.00713	0.00647	0.00523	0.00374	0.00272	0.00117	0.00038
212.5	0.00614	0.00594	0.00569	0.00549	0.00537	0.00522	0.00492	0.00391	0.00358	0.00250	0.00113	0.00039
237.5	0.00447	0.00435	0.00421	0.00409	0.00398	0.00403	0.00397	0.00364	0.00315	0.00231	0.00106	0.00040
262.5	0.00364	0.00359	0.00361	0.00361	0.00358	0.00357	0.00348	0.00321	0.00280	0.00208	0.00099	0.00040
287.5	0.00309	0.00305	0.00304	0.00302	0.00300	0.00298	0.00293	0.00276	0.00245	0.00185	0.00092	0.00039
350.0	0.00215	0.00212	0.00208	0.00206	0.00204	0.00201	0.00196	0.00184	0.00167	0.00126	0.00076	0.00035
500.0	0.00080	0.00079	0.00078	0.00077	0.00077	0.00076	0.00074	0.00072	0.00071	0.00061	0.00045	0.00024
900.0	0.00019	0.00019	0.00019	0.00019	0.00018	0.00018	0.00018	0.00018	0.00018	0.00016	0.00014	0.00011

SURFACE DEFORMATION (mm)

10.500	9.861	9.162	8.606	8.164	7.699	6.762	4.832	2.950	1.418	0.663	0.391

9/14 in each case, i.e. the MEP at a distance of 37.5mm from the central wheel track was 45,000 in each case with the significant number of passes 70,000 as before. Figures 11.16 to 11.21 also showed the measured profiles of the rut for comparison with those predicted. A summary of the rut depth predictions and measure-:ments is presented in Table 11.4.

Figures 11.22 to 11.24 show the predictions of the vertical permanent strain versus depth, for the multi-track tests after 100,000 passes, compared with the corresponding measured values. Figures 11.25 to 11.27 show plots of rut depth against MEP at r = 37.5mm for the multi-track tests, and against the number of passes for the single track tests. For the single track tests the MEP is equal to the total number of passes, since all passes are applied in the same track.

11.5.2 Comparison with measurements

Table 11.4 shows that the predictions of rut depth are adequate, since, with the exception of the multi-track test for pavement 2, all are within 33 per cent of measured values. For pavements 1 and 2 the predictions were higher than the measured values, and for pavement 3 they were lower. The separate predictions of the deformation in each material show that there was a tendency to overpredict the deform-:ation in the DBM and to under-predict in the Keuper marl. Hence, compensating errors tended to produce a more accurate total deformation (rut depth).

It is very difficult to assess quantitatively the accuracy of the predictions, because of the many stages in the development of the models. The non-linear analysis did not predict the in-situ stresses very accurately (see Section 10.3), the method of triaxial testing was approximate, the deformation measuring devices were subject to errors,

TABLE 11.4 COMPARISON OF MEASURED AND PREDICTED RUT DEPTHS

Test	Source of result	Deformation (mm)		Rut Depth (mm)
		DBM	Subgrade	
Pavement 1 Multi-track 10^5 passes	Measurement	7.4	5.0 (Assumed)	12.4
	Prediction	12.0	1.5	13.5
Pavement 1 Single track 22,000 passes	Measurement	-	-	8.4
	Prediction	9.0	1.5	10.5
Pavement 2 Multi-track 10^5 passes	Measurement	11.4	9.9	23.4
	Prediction	38.5	1.0	39.3
Pavement 2 Single track 22,000 passes	Measurement	-	-	24.7
	Prediction	29.5	0.9	30.4
Pavement 3 Multi-track 10^5 passes	Measurement			
	Stack 1	13.3	2.2	14.6
	Stack 2	11.0	0.9	-
	Prediction	9.8	0.8	10.5
Pavement 3 Single track 22,000 passes	Measurement	-	-	12.3
	Prediction	7.7	0.5	8.2

and the samples of material varied, sometimes considerably, hence the scatter of results (Chapter 9). The development of the permanent deformation models introduces more errors, which are particularly difficult to assess in the DBM where tensile stresses occur. It is also very important to remember that errors exist in the measurement of deformations in the pavements, particularly those giving the distribution of permanent strain with depth from which the permanent deformations in each material are computed. For instance, Table 11.5

shows the results of the three methods of measuring the component deformation in each material for pavement 1. In this case, the DBM deformation was measured together with the total rut depth, the Keuper marl deformation being assumed to be the difference. The difference between the deformation determined by measurements on slabs and from the strain coil stack was 33 per cent of the latter. However, the measurements of rut depth were made with a surveying level for pave-:ments 1 and 2 and with a profilometer for pavements 2 and 3, and both methods were considered to be accurate to within 0.5mm. Hence, comparison of total predicted deformations with total measured deform-:ations are considered to be more reliable.

Comparison of the predicted and measured permanent strain versus depth plots (Figures 11.22 to 11.24) show that, with the exception of pavement 3, the predictions are much higher than the measured values in the lower half of the DBM. This is caused largely by the problems of representing tensile stresses in the DBM by use of the triaxial test. Comparison also shows that the predictions at the very top of the DBM for pavements 1 and 3 are approximately 50 per cent lower than the measured values. This could be caused by variations in the contact pressure between the tyre and the pavement. (86). These variations between the predicted and measured permanent strain distributions partly explain the inaccuracies in predicted total deformation in the DBM.

The under-prediction of deformation in the Keuper marl is more difficult to explain. Figure 11.23 shows that in pavement 2, the measured permanent strain at the surface of the subgrade, after 10^5 passes, was approximately 20 per cent, whereas the predicted value was 0.83 per cent. This discrepancy is partly due to the difference between the measured in-situ stresses and those predicted, which are lower. The predicted stresses at the surface of the subgrade in pave-:ment 1 give a value of q of approximately 33 kN/m^2 which gives a value of permanent strain of 1.37 per cent after 10^5 passes. The measured

TABLE 11.5 MEASUREMENTS OF DEFORMATION IN EACH MATERIAL FOR PAVEMENT 1.

Method of Measurement	Deformation of DBM (mm)	Deformation of subgrade (mm)	Total rut depth (mm)
Strain coil stack (25mm)	6.3	6.1 (Assumed)	12.4
Large coils (50mm)	7.4	5.0 (Assumed)	12.4
Measurements on slabs	8.4	4.0 (Assumed)	12.4
Average	7.4	5.0	12.4

stresses could give a value of q as high as 55 kN/m^2 which would correspond to a permanent strain of approximately 4.0 per cent. Measurements tended to show that the stresses could be even higher at the beginning of a test, a fact corroborated by the form of the permanent strain accumulation at the surface of the clay in pavement 2 (Figure 7.3) where the majority of the strain was achieved after 10^4 passes. The predictions for the rut profiles (Figs 11.16 to 11.21) are variable, that for the multi-track test in pavement 1 being very close indeed, and for the same test in pavement 2 being 60 per cent too large. However, the general shape of the predicted profiles is good for the multi-track tests and fair for the single-track tests.

The rut formed in the multi-track test for pavement 3 shows a distinct heaving at the edges (Figure 11.20), a condition impossible to predict by the model used here, which assumes that the in-situ vertical strain is equal to the major principal strain in the triaxial test, which is always compressive. However, it is often the case that for positions near the surface of the pavement which are outside the loaded area, the principal planes rotate sufficiently to cause a tensile minor principal strain to be closest to the vertical, which may cause heaving.

To develop a model which could predict this phenomenon would be far more complicated than that developed herein, and would still require approximations to be made for the values of vertical and radial strains if characterisation was to be based on the triaxial test (see Chapter 8).

Comparison of the plots of rut depth versus MEP (Figures 11.25 to 11.27) with those of rut depth versus the total number of wheel passes shows that a multi-track test could be approximated by a single track test, provided that the MEP is used. When plotted in this way, the rut depths in each test were always within 25 per cent.

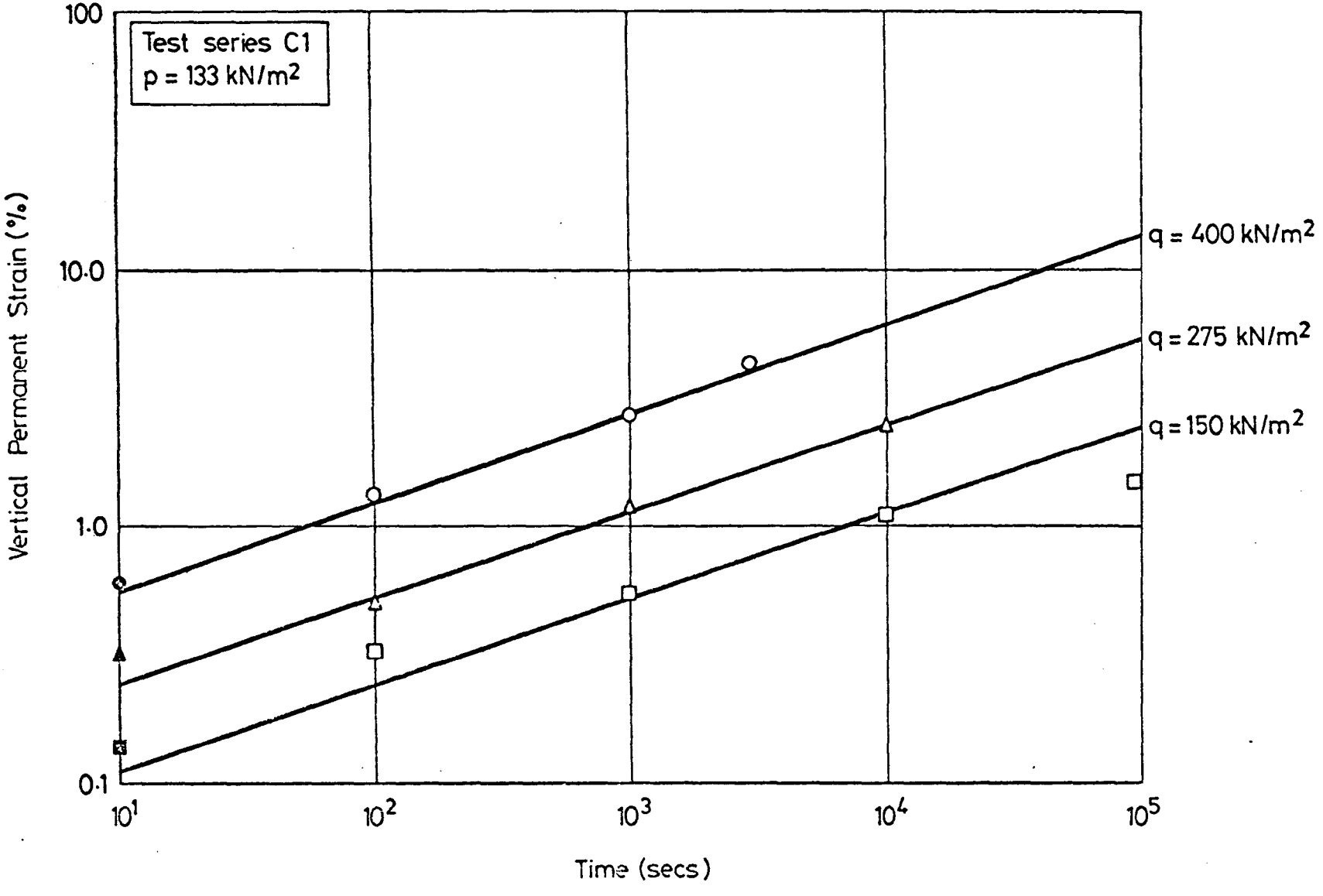

FIG. 11.1 THE INFLUENCE OF q ON VERTICAL PERMANENT STRAIN OF DBM, p = 133 kN/m^2

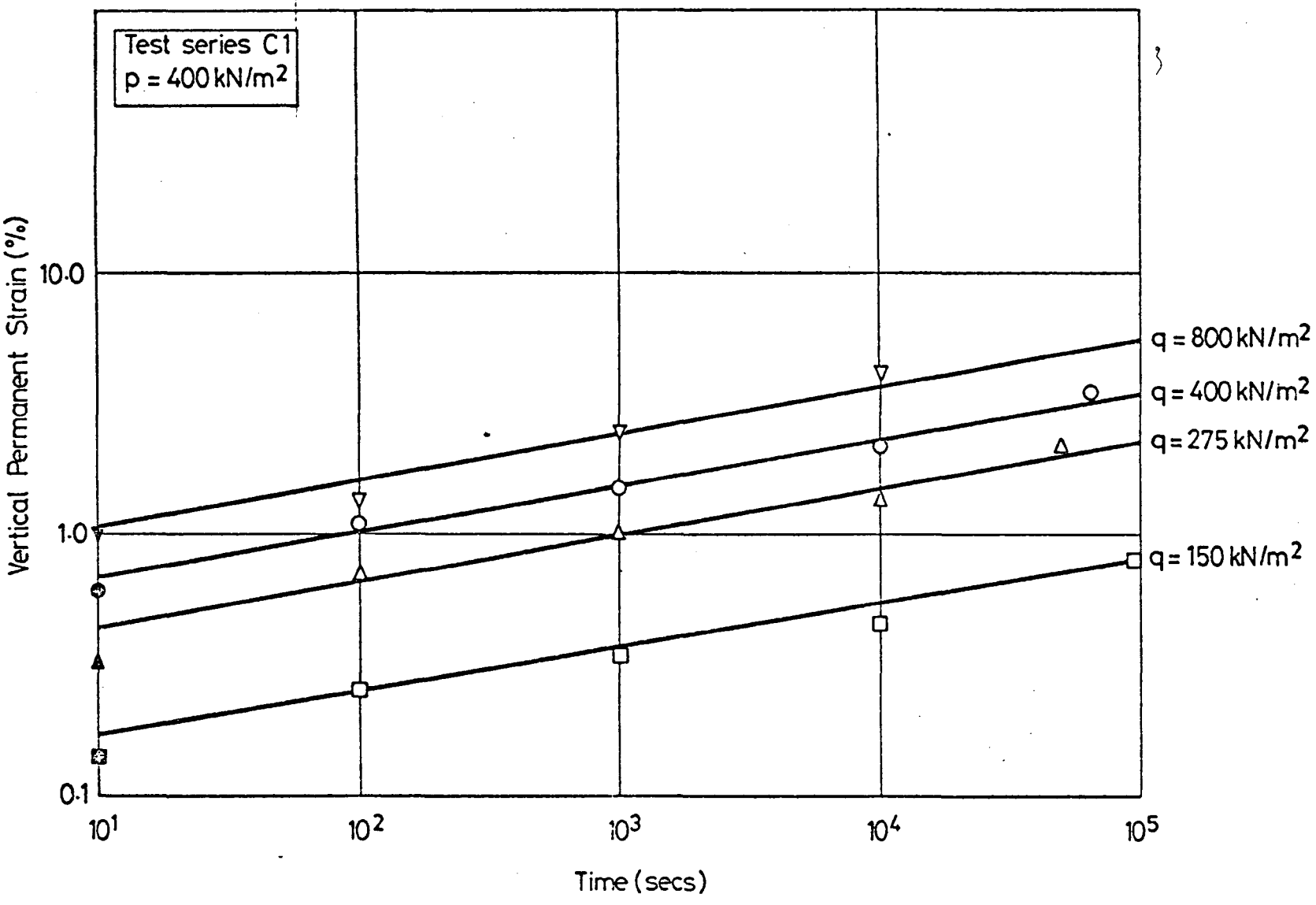

FIG. 11.2 THE INFLUENCE OF q ON VERTICAL PERMANENT STRAIN OF DBM, p = 400 kN/m^2

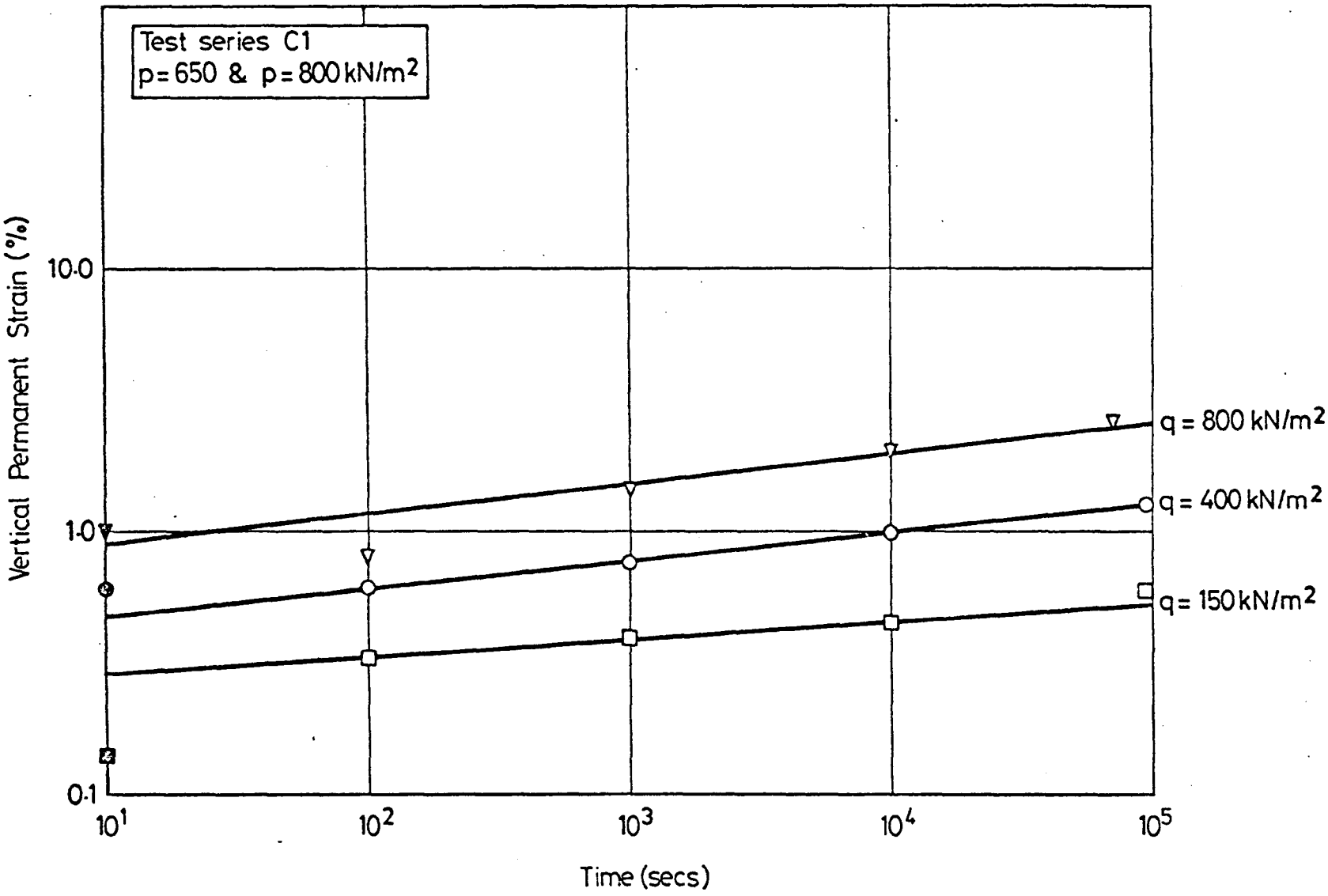

FIG. 11.3 THE INFLUENCE OF q ON VERTICAL PERMANENT STRAIN OF DBM, p = 650 and 800 kN/m^2

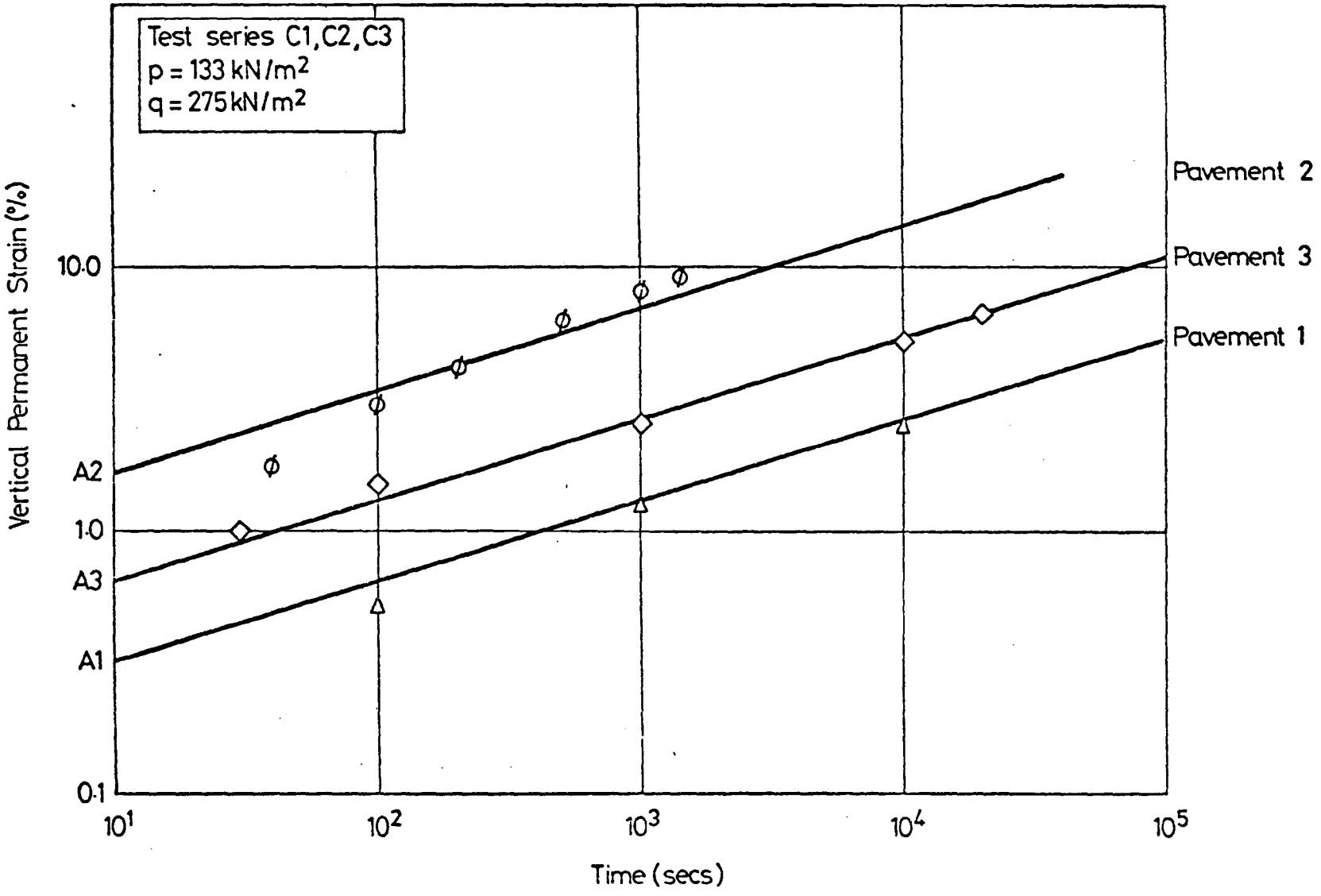

FIG.11.4 COMPARISON OF VERTICAL PERMANENT STRAINS ACHIEVED WITH DBM CORES FROM EACH PAVEMENT

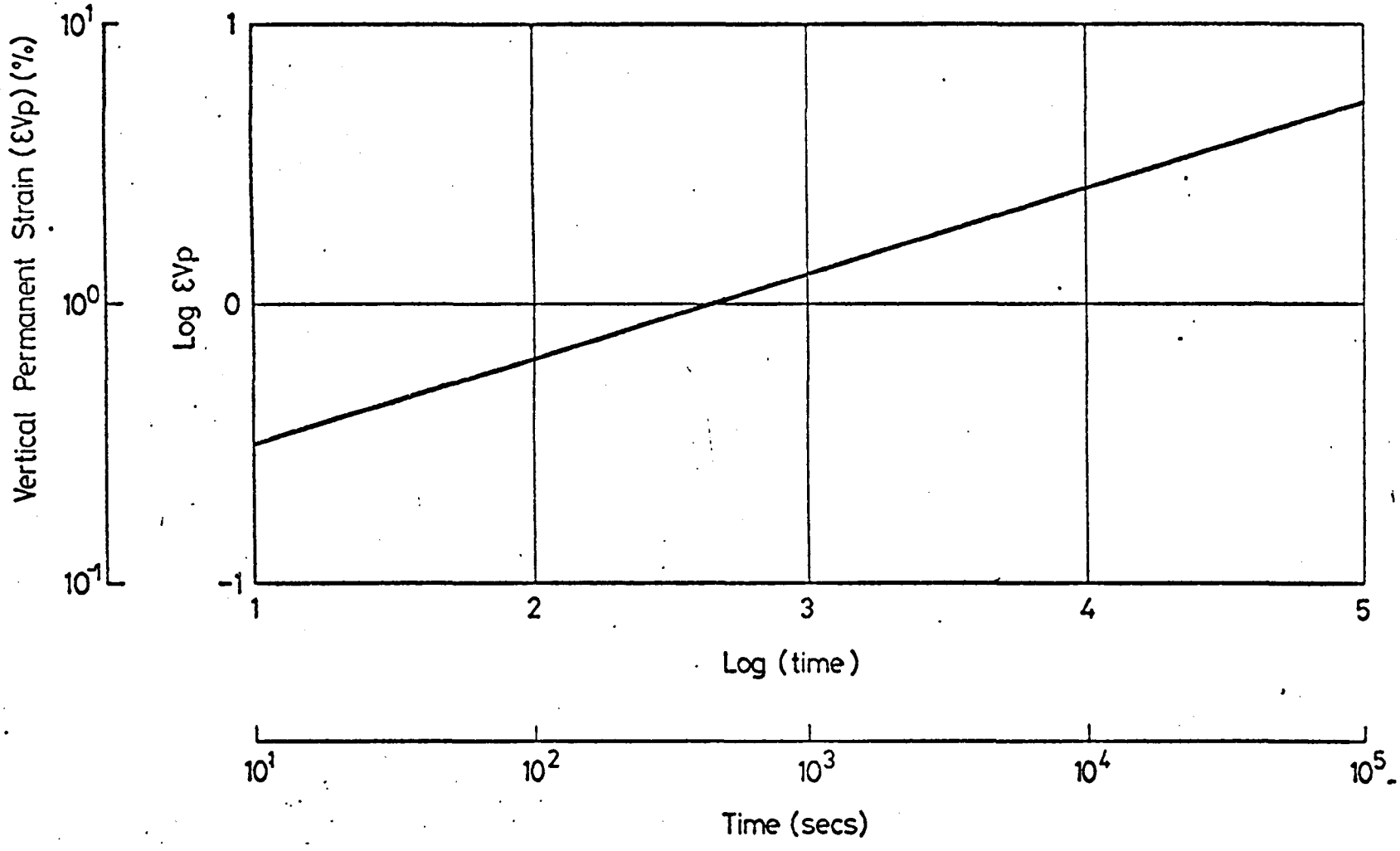

FIG. 11.5 IDEALISED LOGARITHMIC PLOT OF VERTICAL PERMANENT STRAIN VERSUS TIME

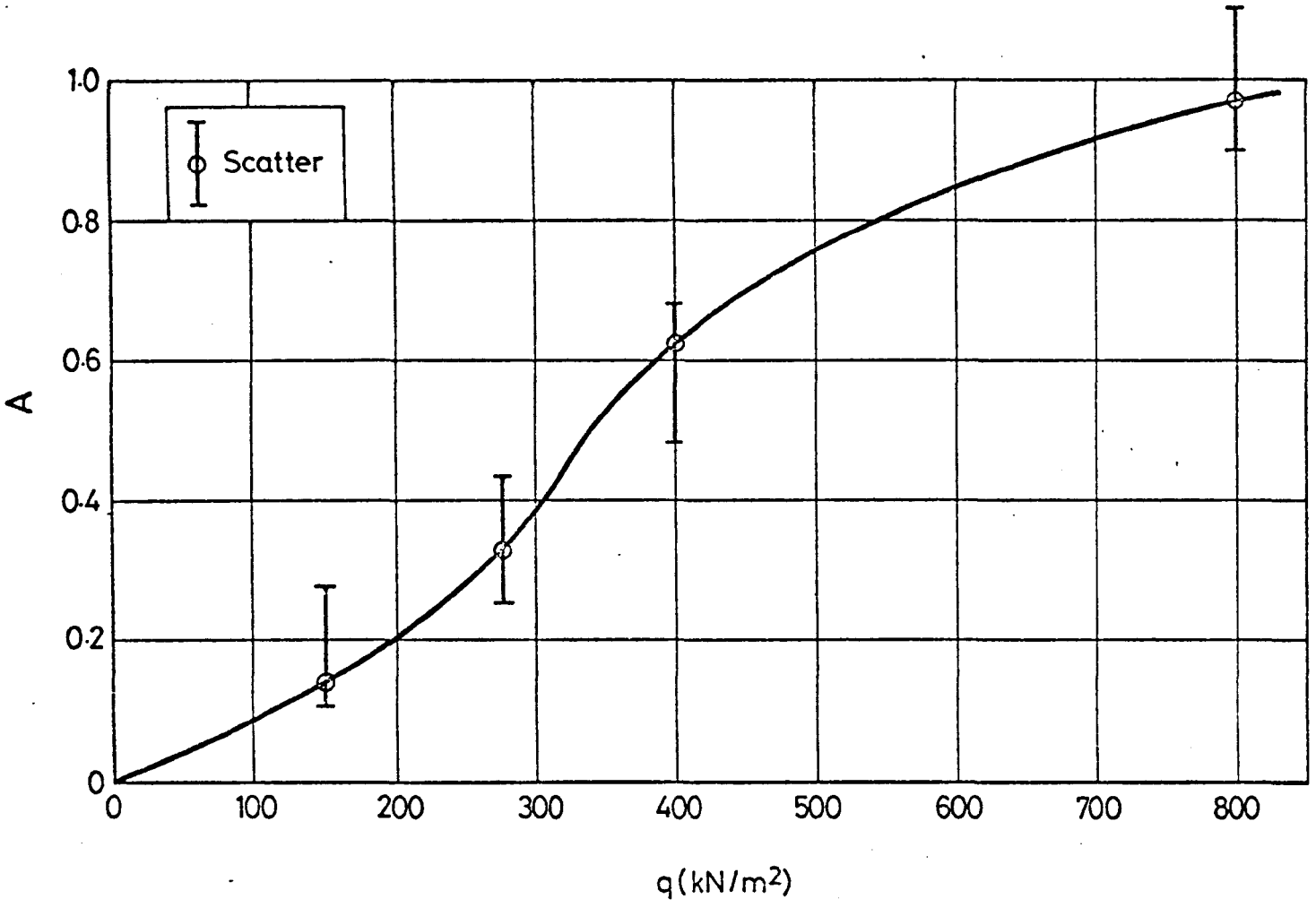

FIG. 11.6 INTERCEPT VALUE VERSUS OCTAHEDRAL SHEAR STRESS (PAVEMENT NO. 1)

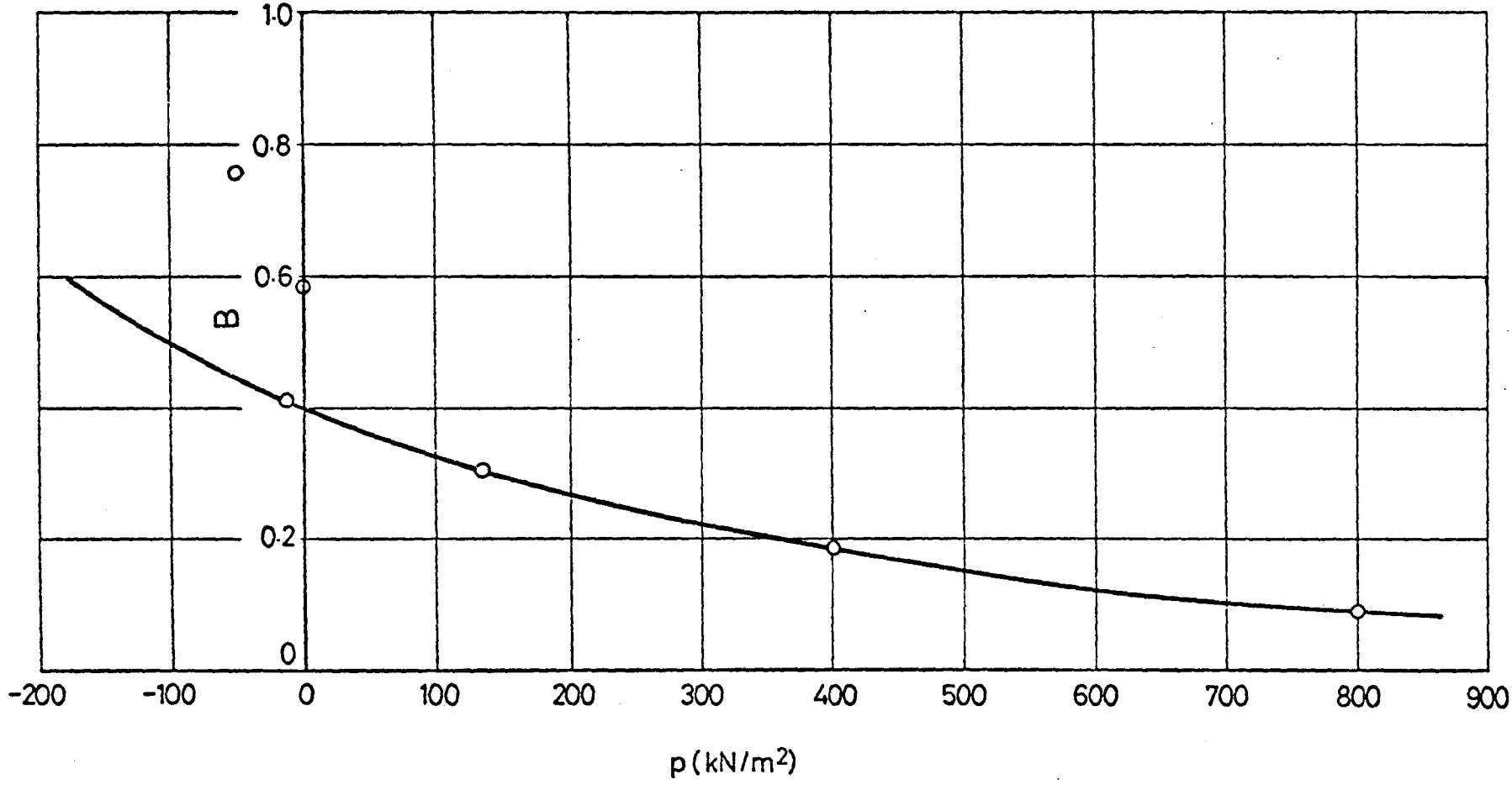

FIG. 11.7 SLOPE FACTOR VERSUS MEAN NORMAL STRESS DBM, PAVEMENT NO. 1

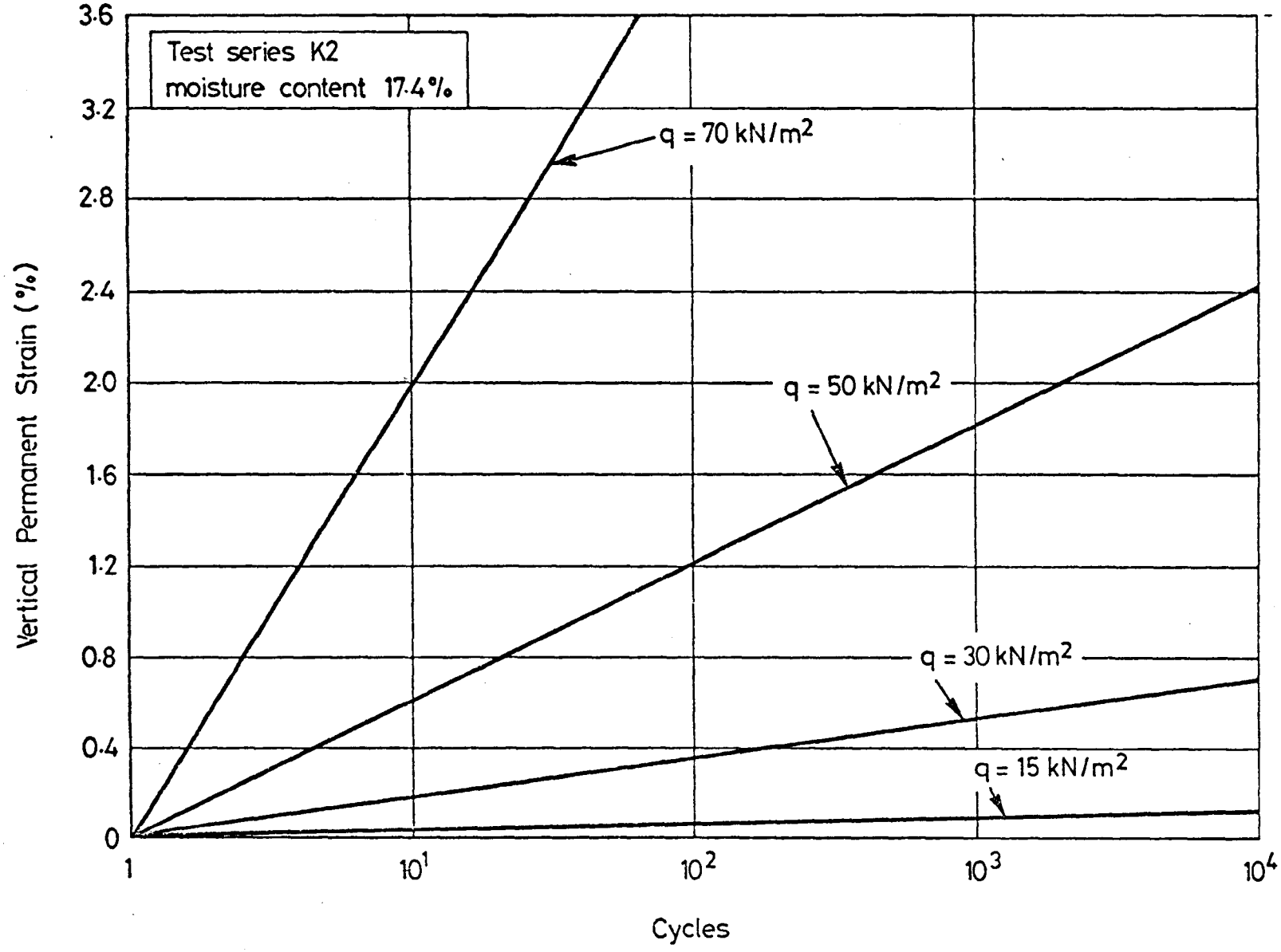

FIG. 11.8 ADJUSTED PLOT SHOWING EFFECT OF q ON VERTICAL PERMANENT STRAIN OF KEUPER MARL

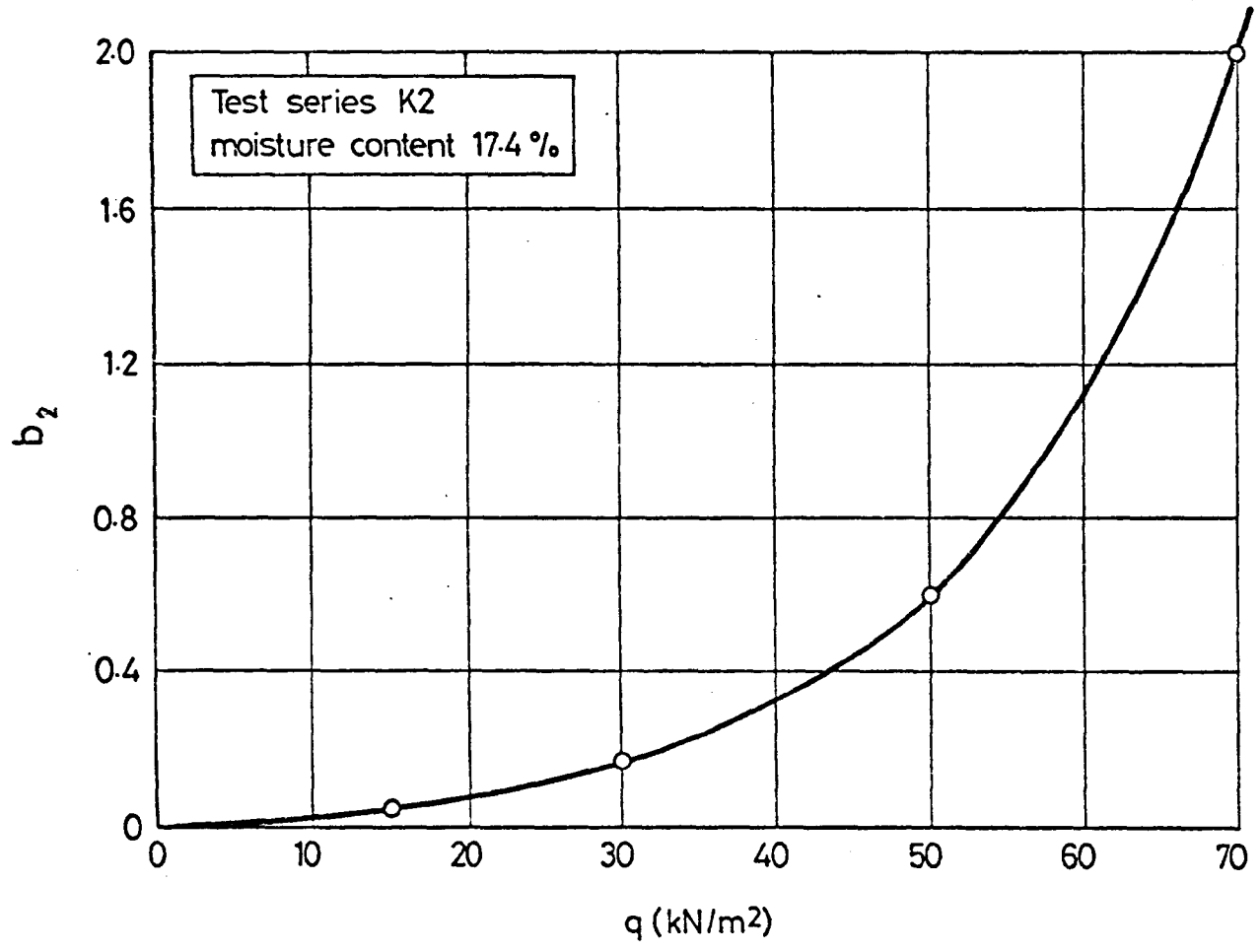

FIG. 11.9 SLOPE FACTOR VERSUS OCTAHEDRAL SHEAR STRESS (KEUPER MARL, TEST SERIES K2)

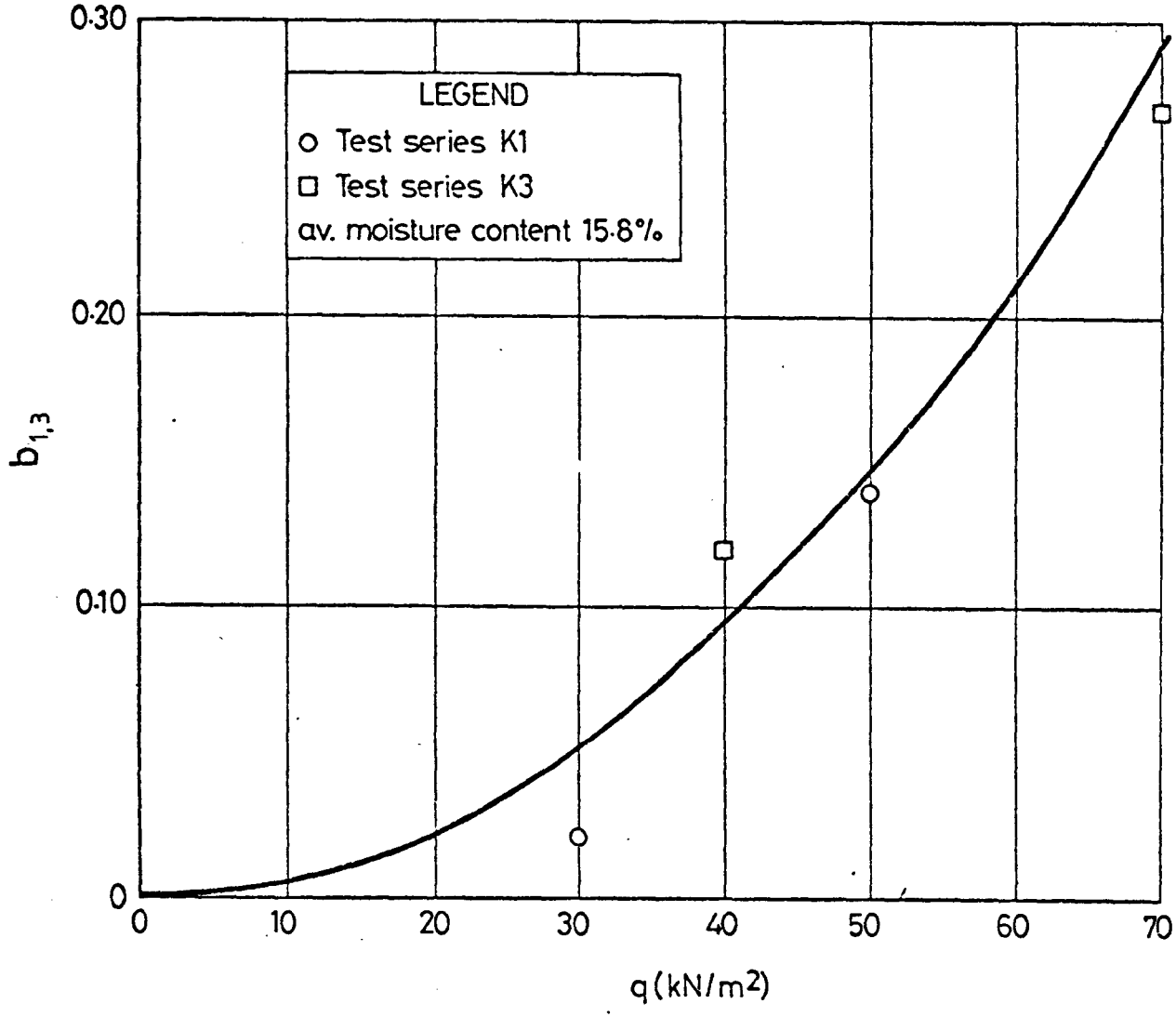

FIG. 11.10 SLOPE FACTOR VERSUS OCTAHEDRAL SHEAR STRESS (KEUPER MARL, TEST SERIES K1 AND K3)

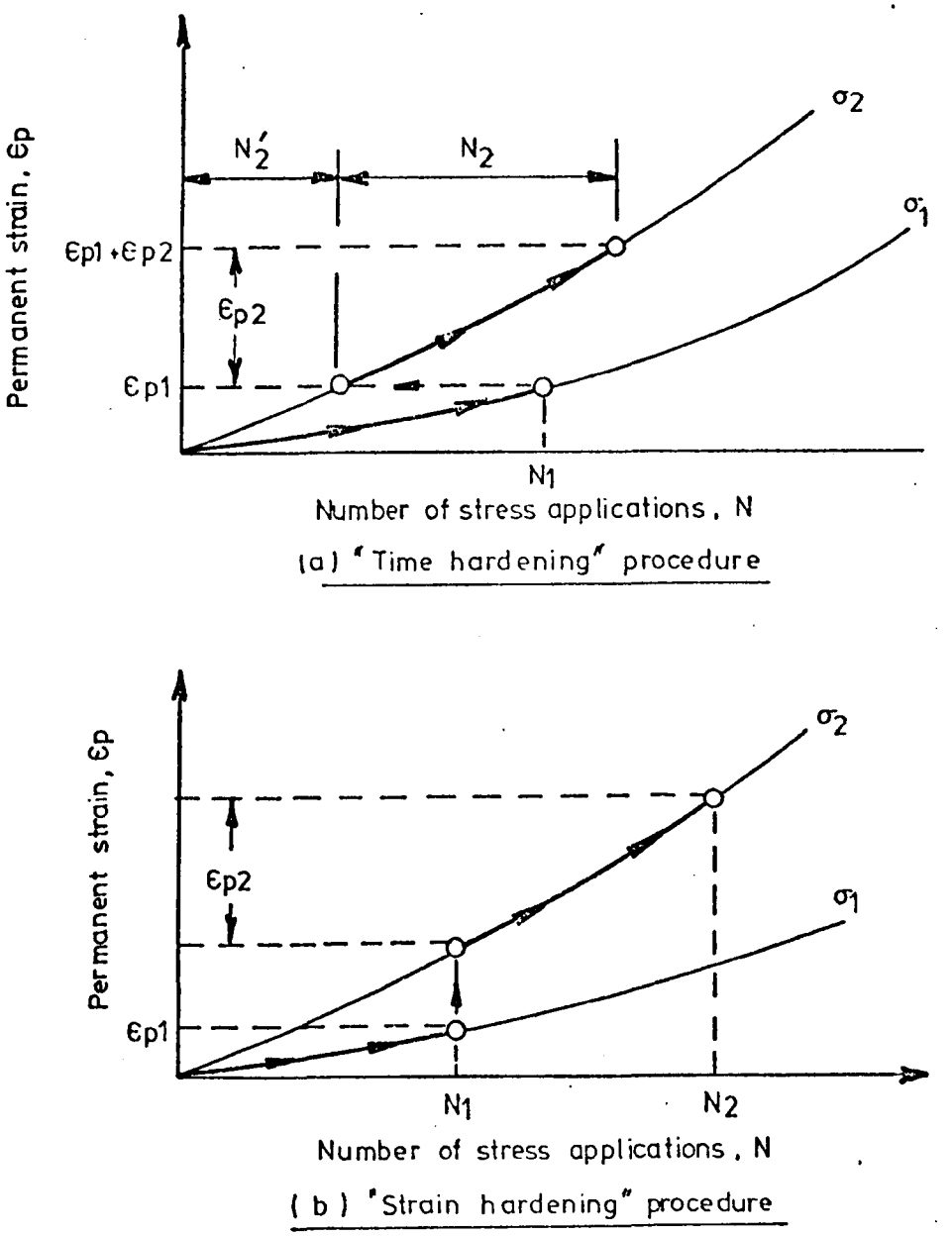

FIG. 11.11 PROCEDURES TO PREDICT THE CUMULATIVE PERMANENT STRAIN FROM THE RESULTS OF SIMPLE LOADING TESTS (AFTER MONISMITH ET AL (40))

Pavement 1

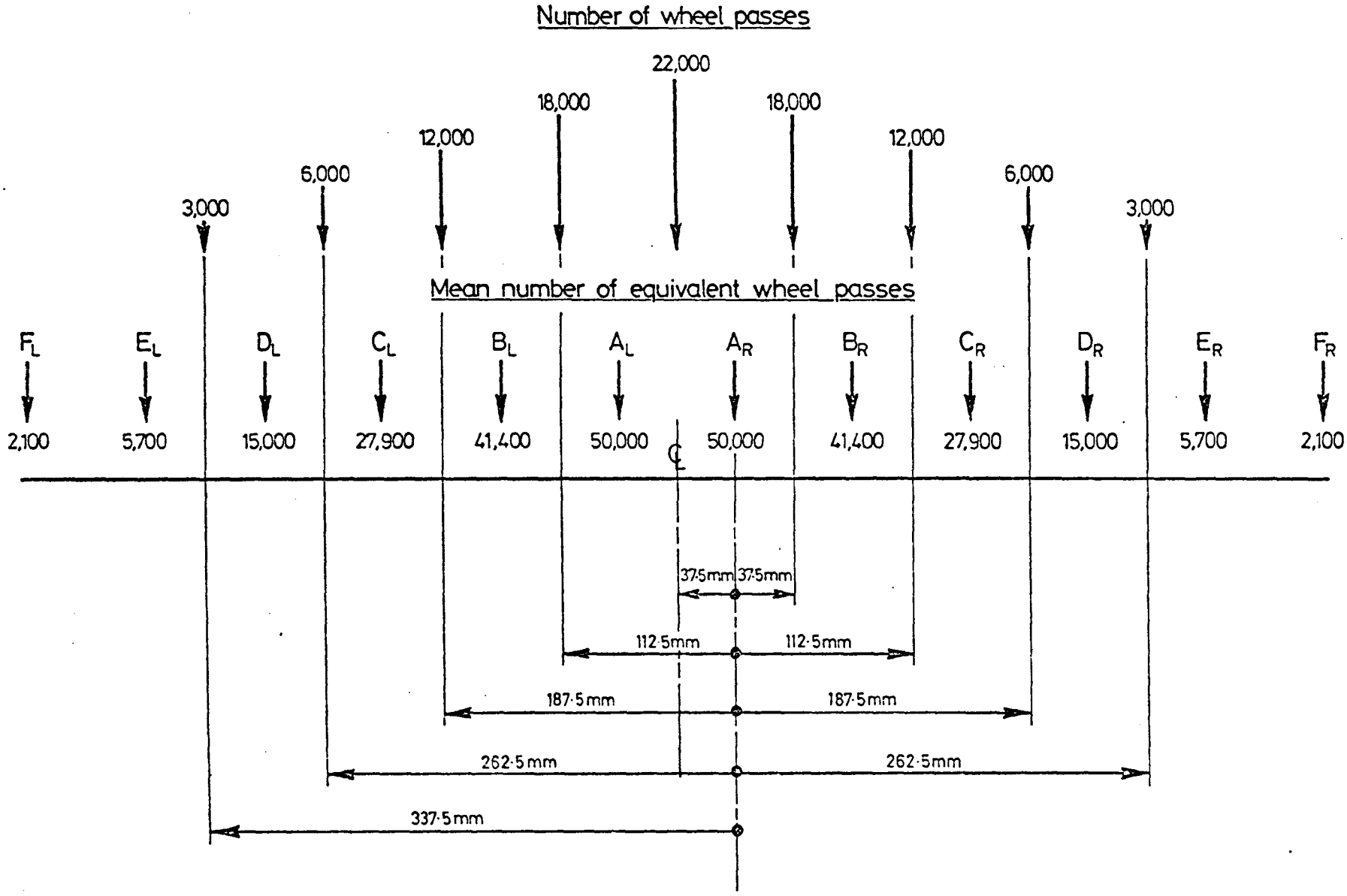

FIG. 11.12 DISTRIBUTION OF WHEEL PASSES USED IN THE MULTI-TRACK TESTS, WITH MEP VALUES FOR PAVEMENT NO. 1

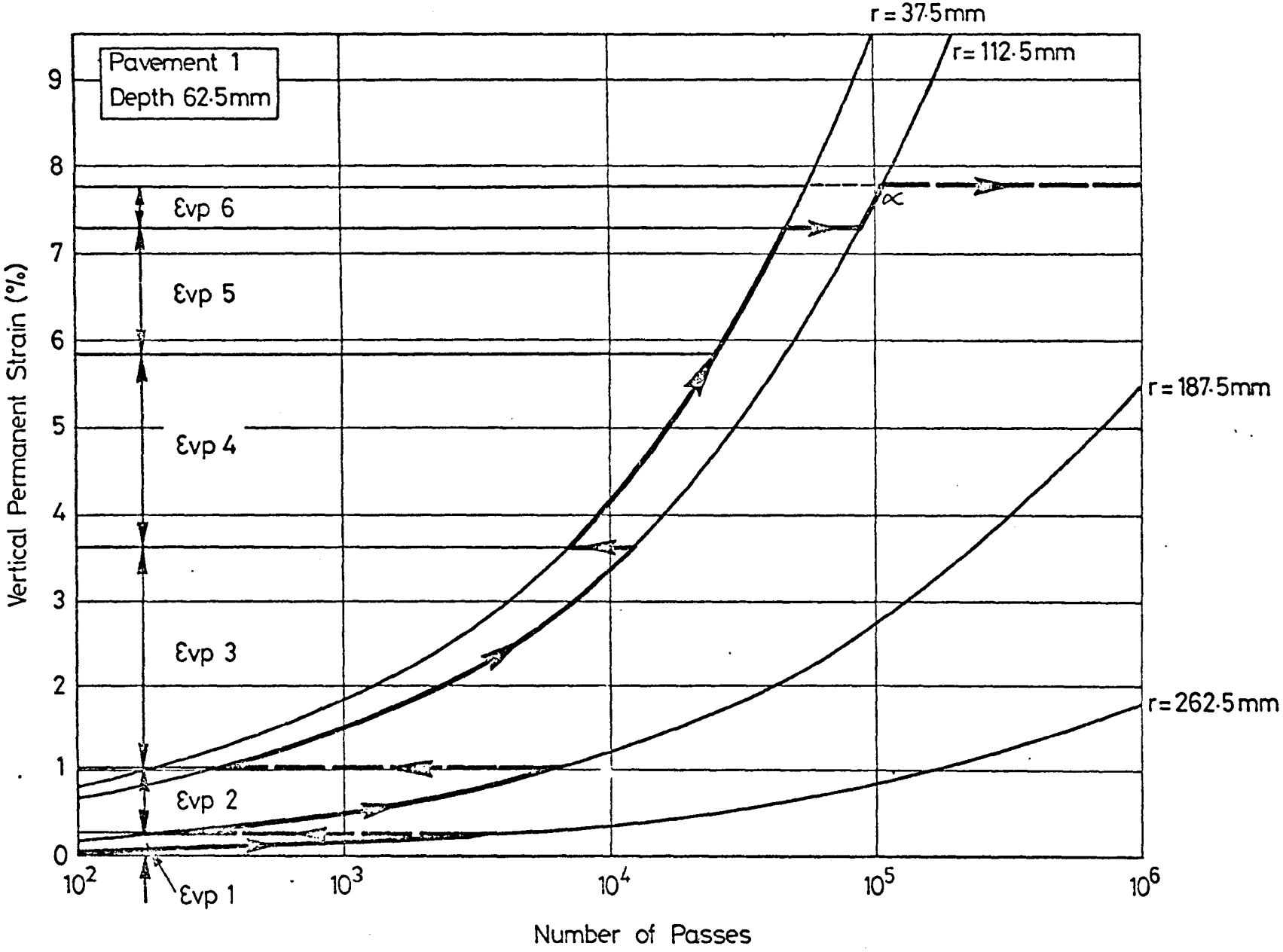

FIG. 11.13 TIME HARDENING CUMULATIVE LOADING PROCEDURE FOR A POSITION IN PAVEMENT NO. 1

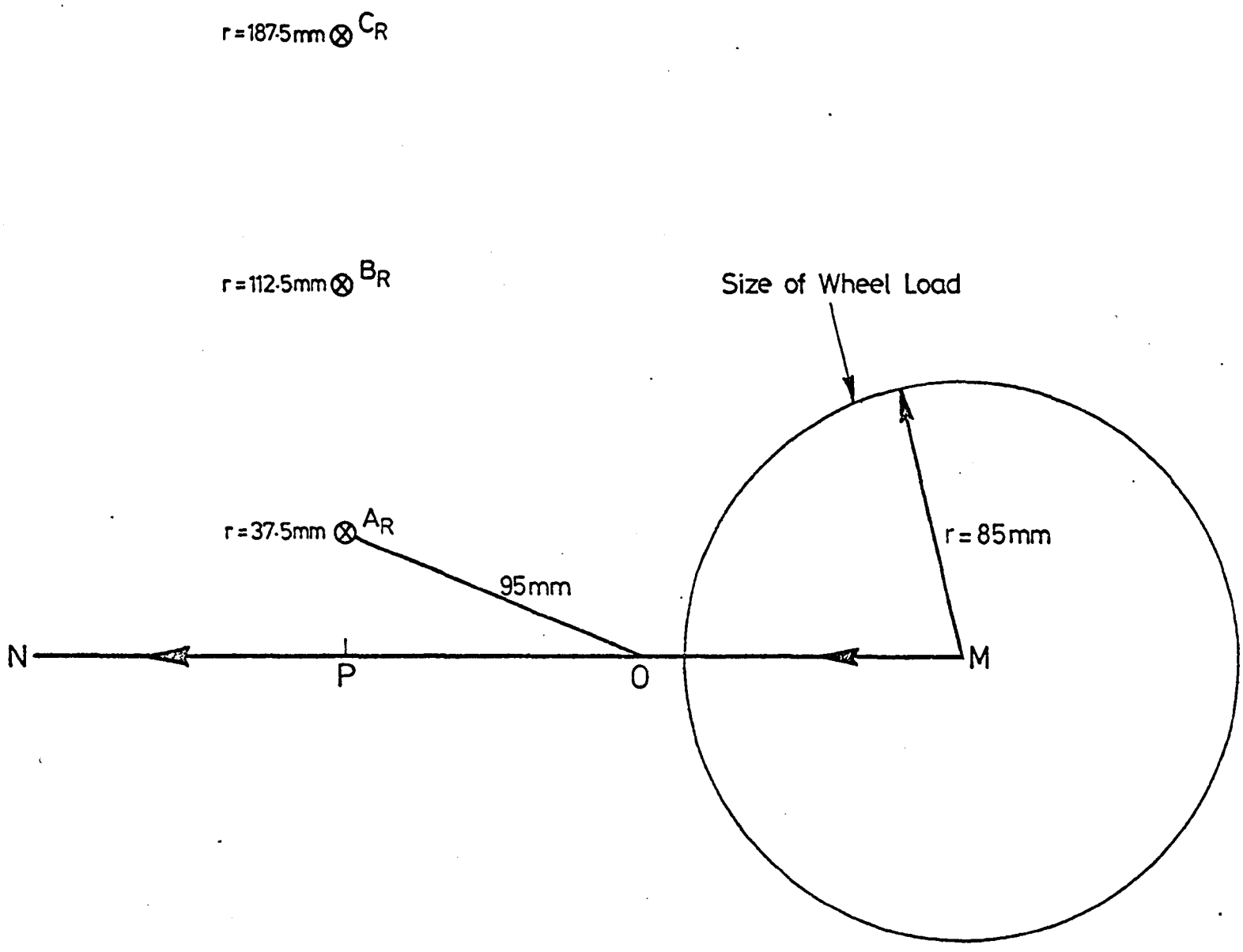

FIG. 11.14 PLAN VIEW OF PAVEMENT SURFACE

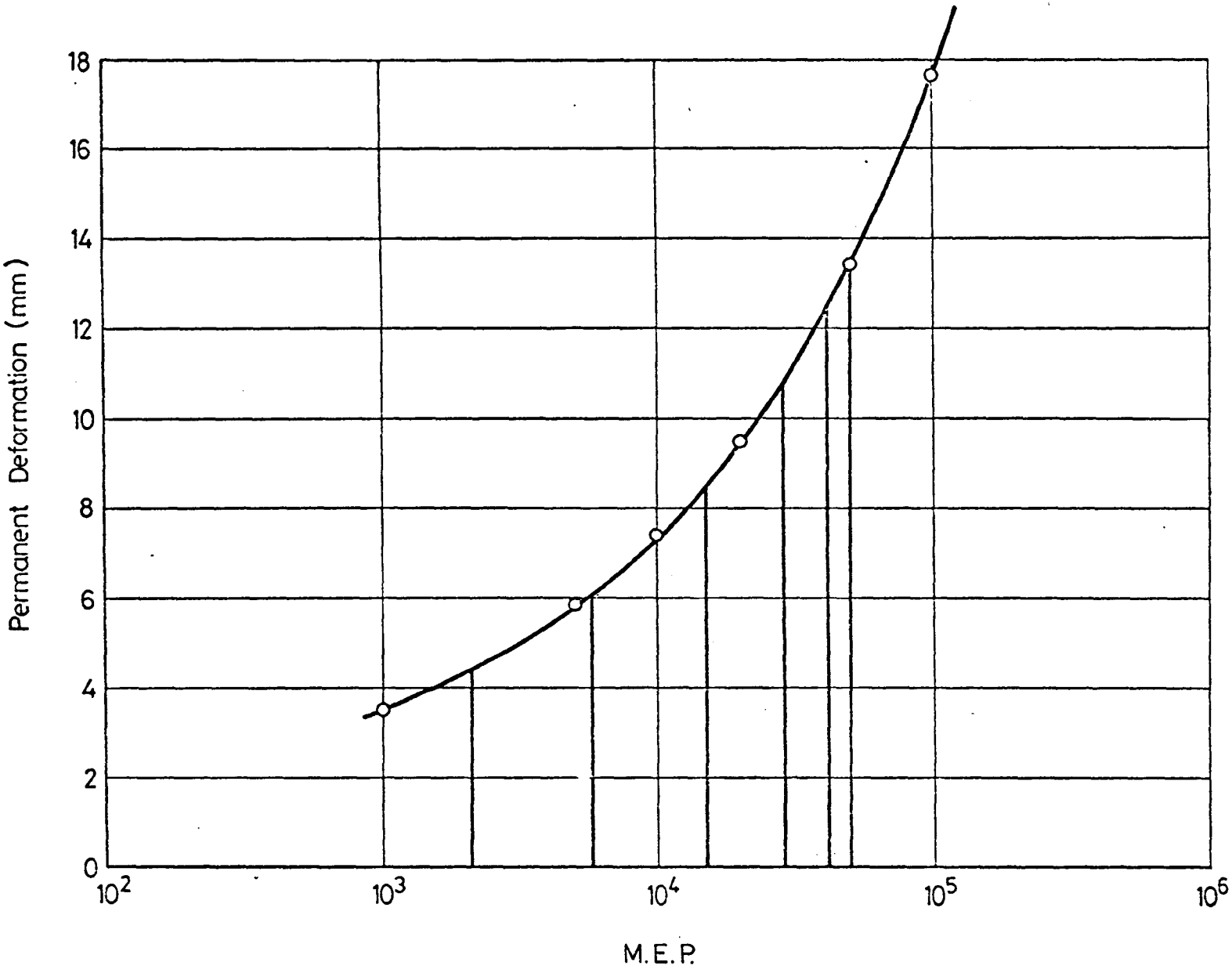

FIG. 11.15 PERMANENT DEFORMATION VERSUS MEAN NUMBER OF EQUIVALENT PASSES

Pavement 1

Multi-track Test

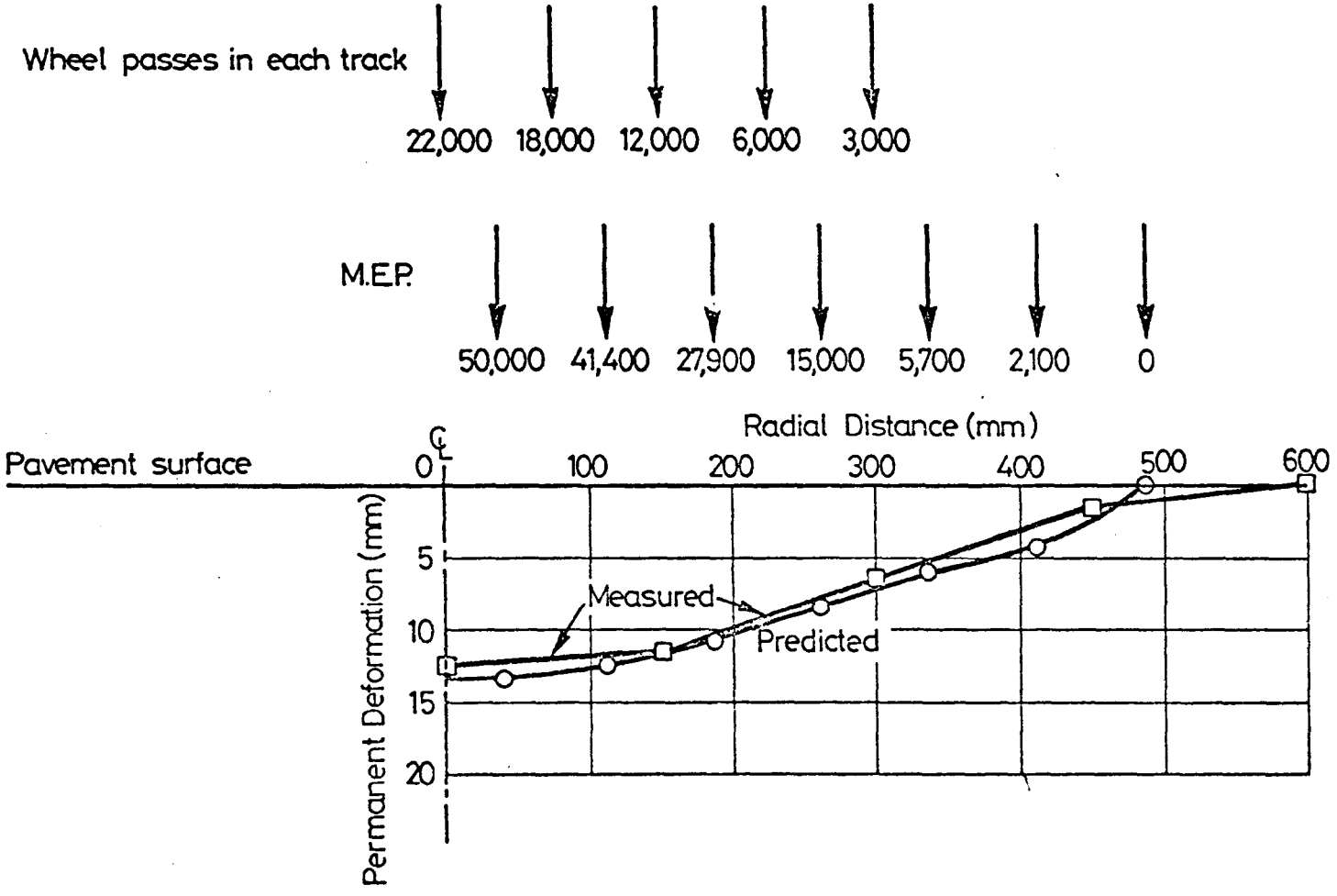

FIG. 11.16 MEASURED AND PREDICTED RUT PROFILES FOR THE MULTI-TRACK TEST (PAVEMENT NO. 1)

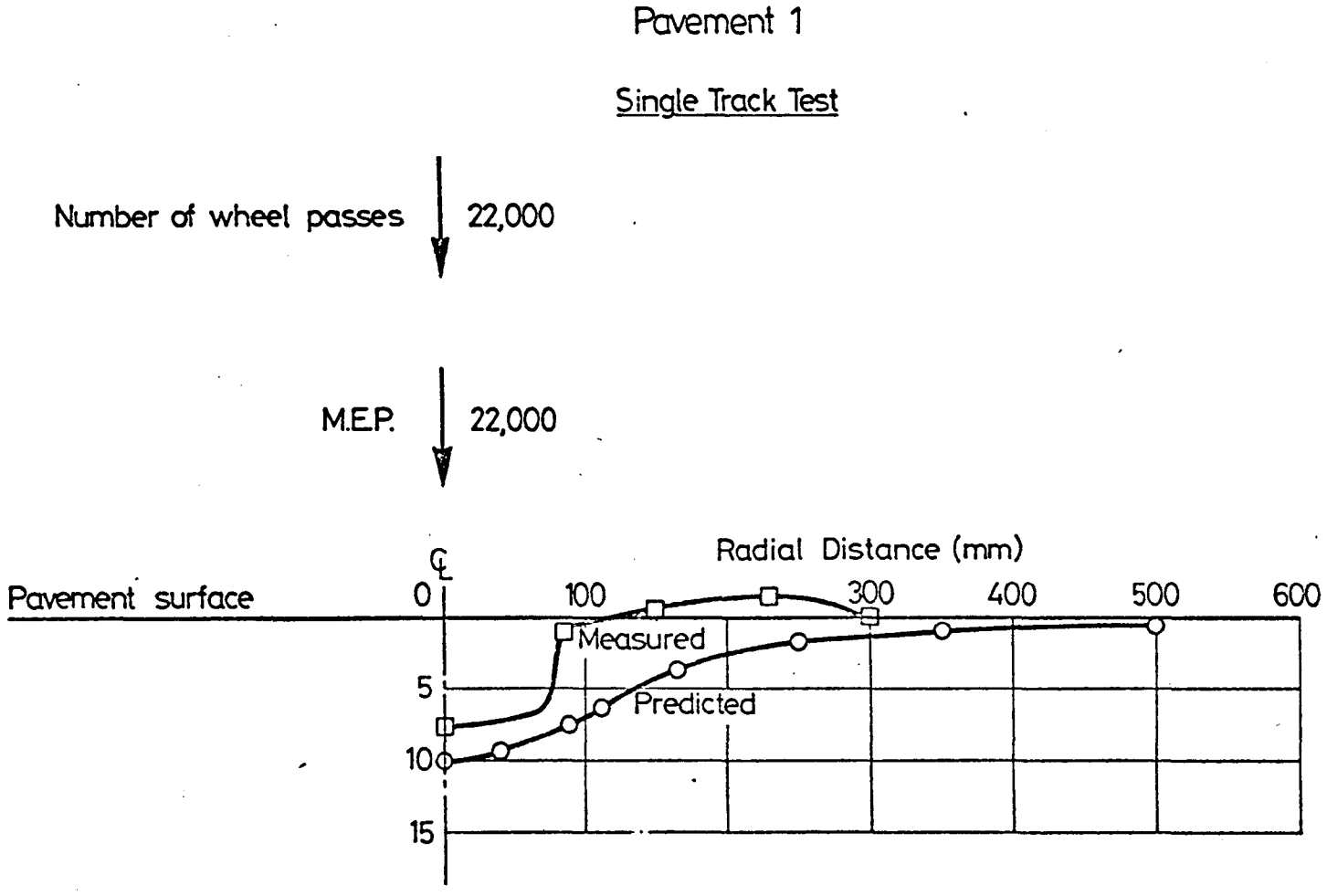

FIG. 11.17 MEASURED AND PREDICTED RUT PROFILES FOR THE SINGLE TRACK TEST (PAVEMENT NO. 1)

Pavement 2

Multi-track Test

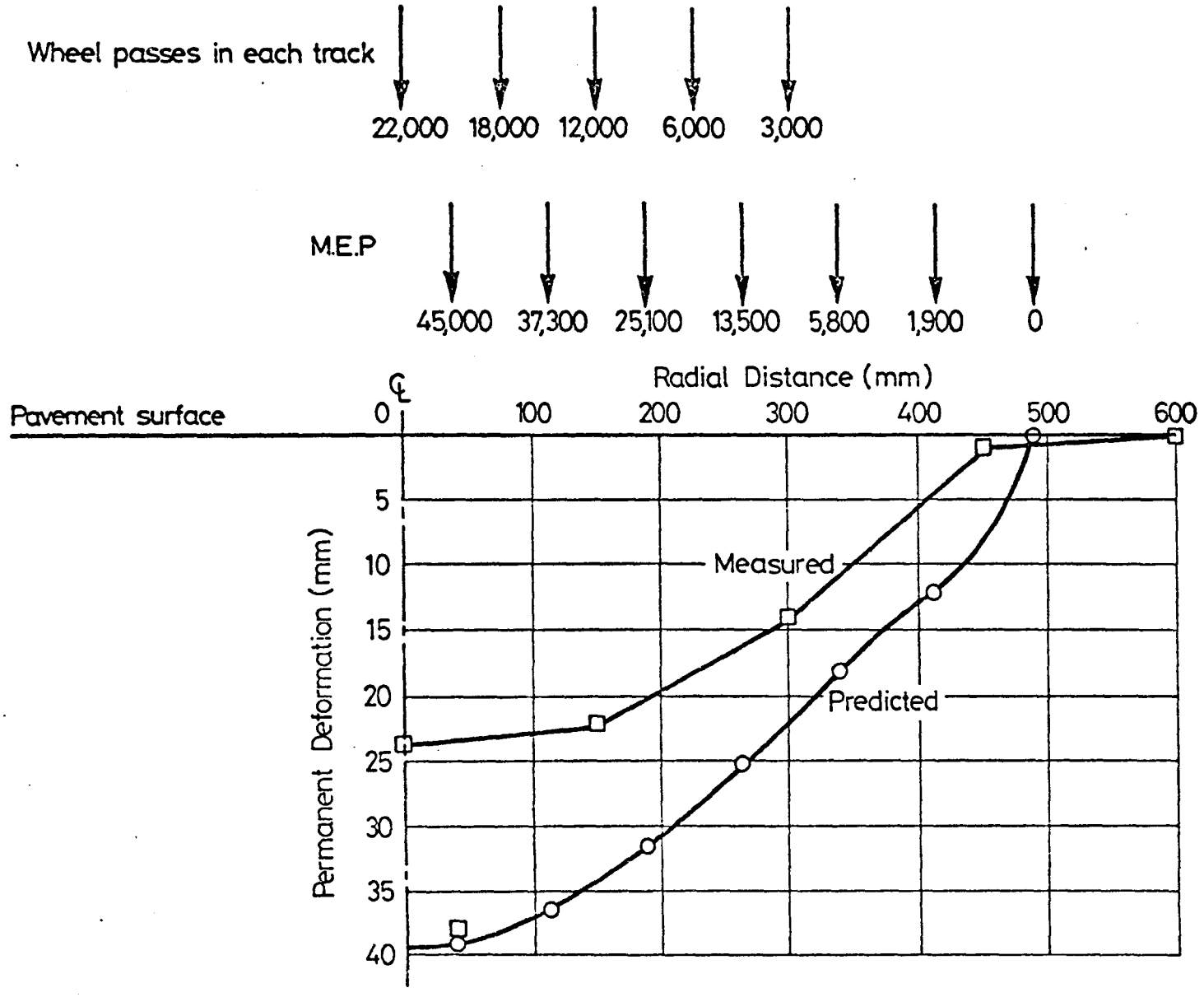

FIG. 11.18 MEASURED AND PREDICTED RUT PROFILES FOR THE MULTI-TRACK TEST (PAVEMENT NO. 2)

Pavement 2

Single Track Test

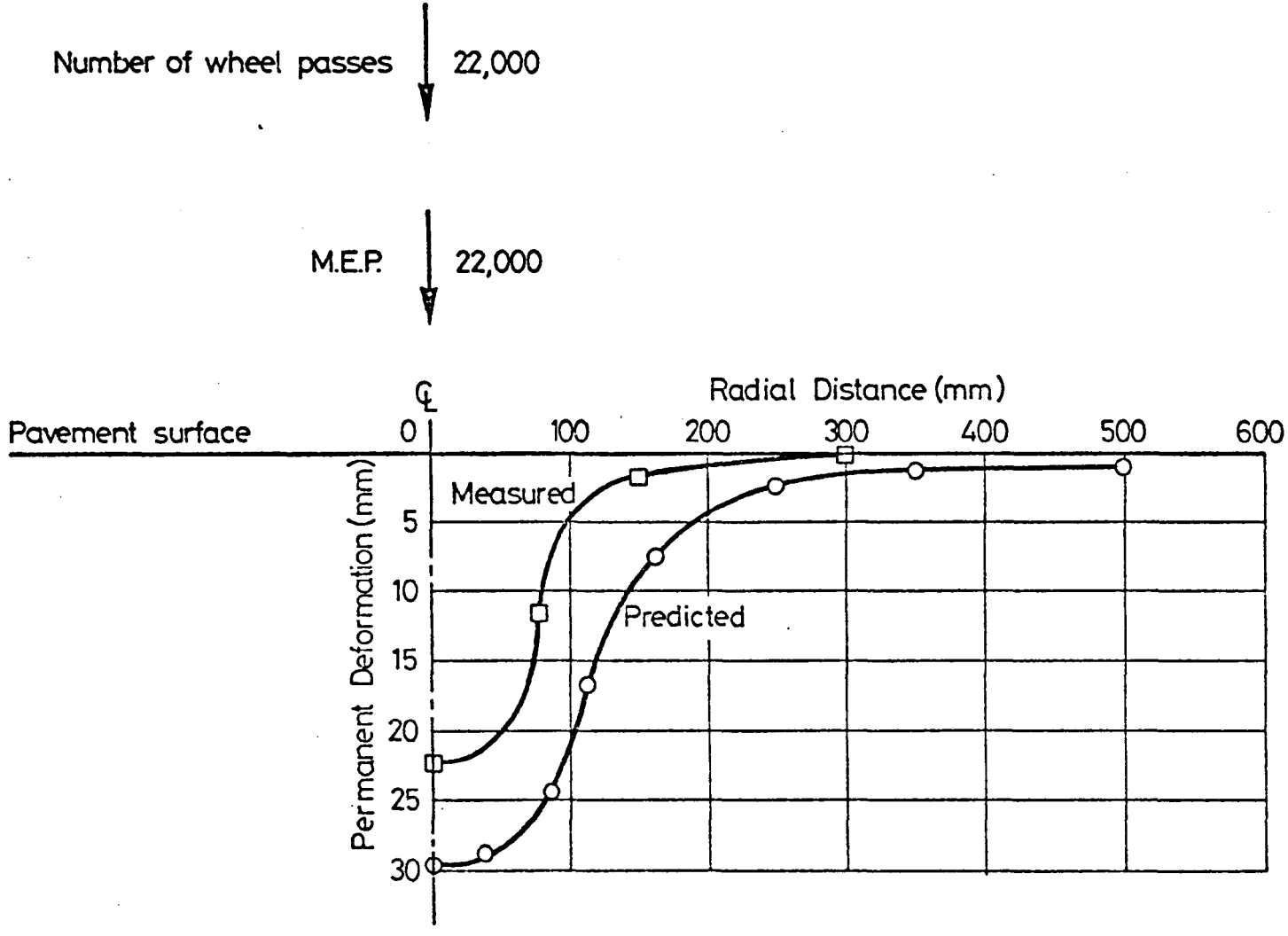

FIG. 11.19 MEASURED AND PREDICTED RUT PROFILES FOR THE SINGLE TRACK TEST (PAVEMENT NO. 2)

Pavement 3

Multi-track Test

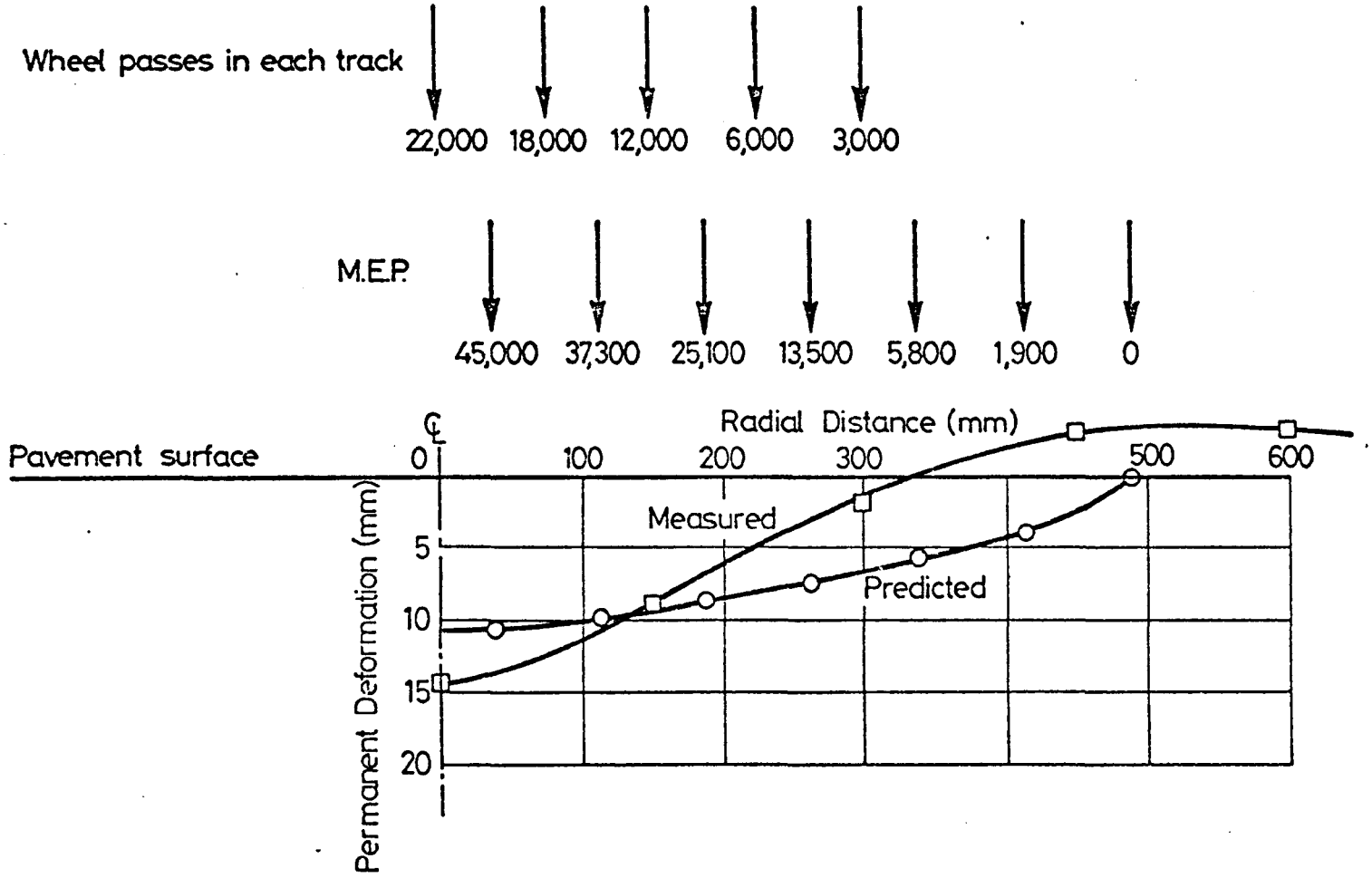

FIG. 11.20 MEASURED AND PREDICTED RUT PROFILES FOR THE MULTI-TRACK TEST (PAVEMENT NO. 3)

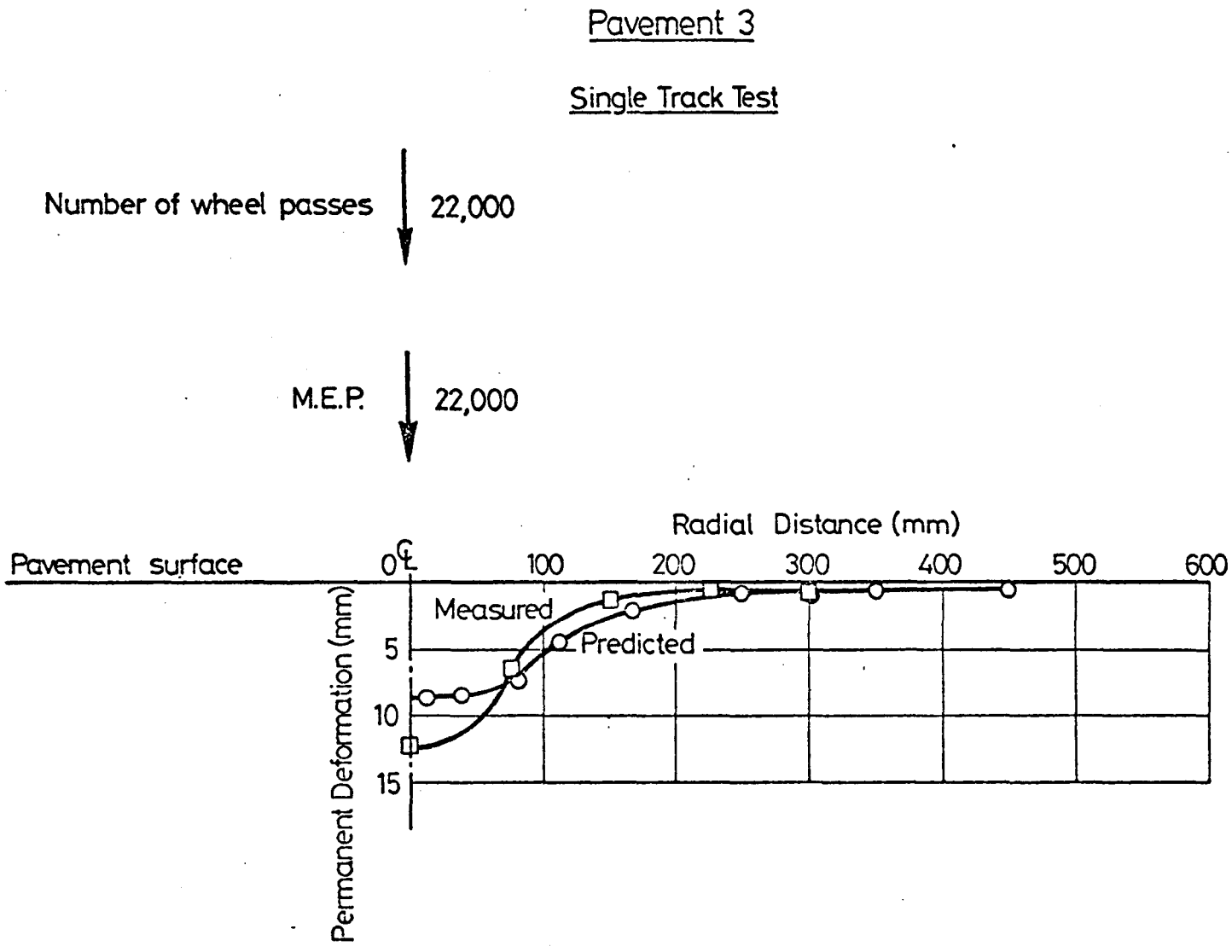

FIG. 11.21 MEASURED AND PREDICTED RUT PROFILES FOR THE SINGLE TRACK TEST (PAVEMENT NO. 3)

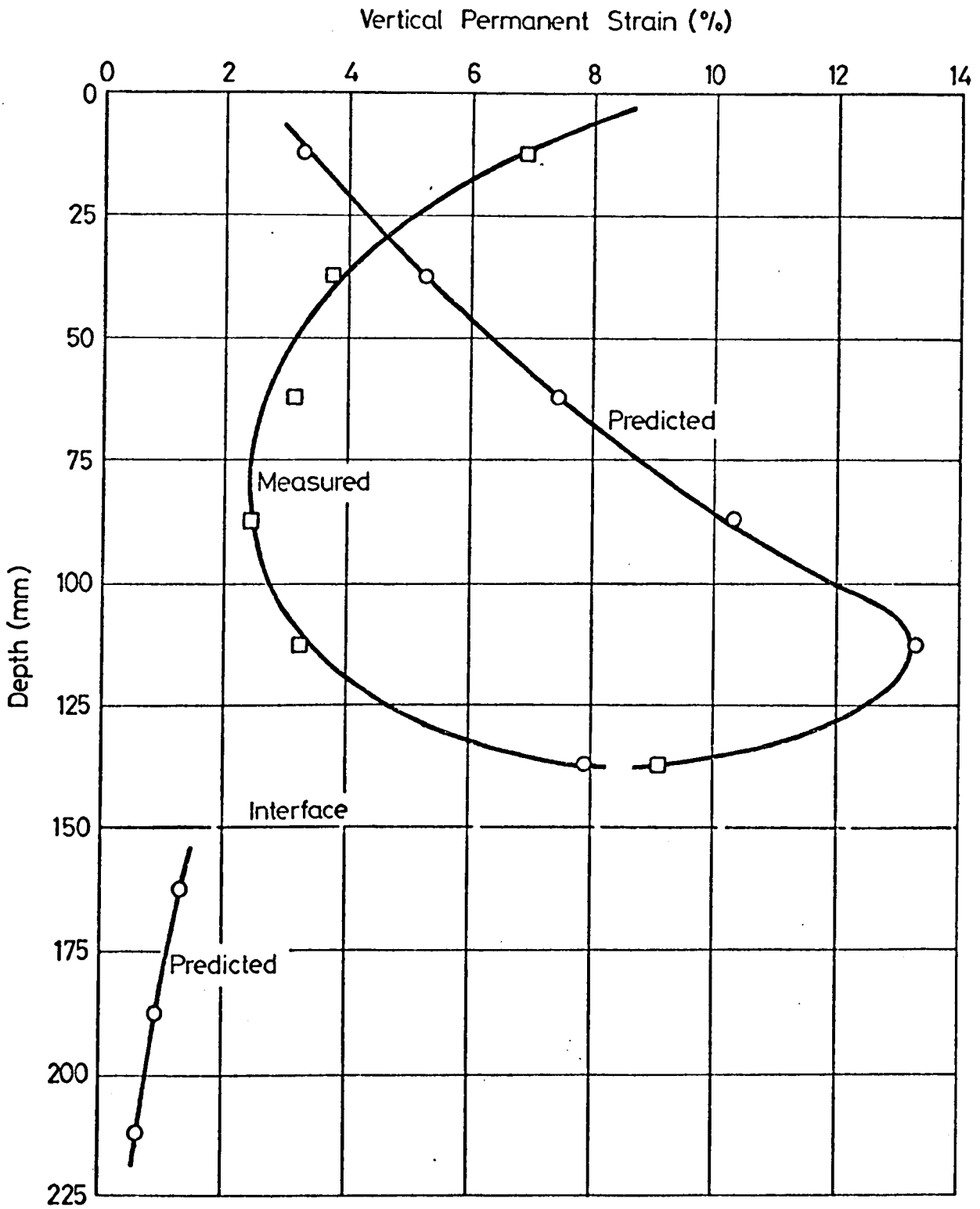

FIG. 11.22 COMPARISON OF MEASURED AND PREDICTED VERTICAL PERMANENT STRAIN (PAVEMENT NO. 1)

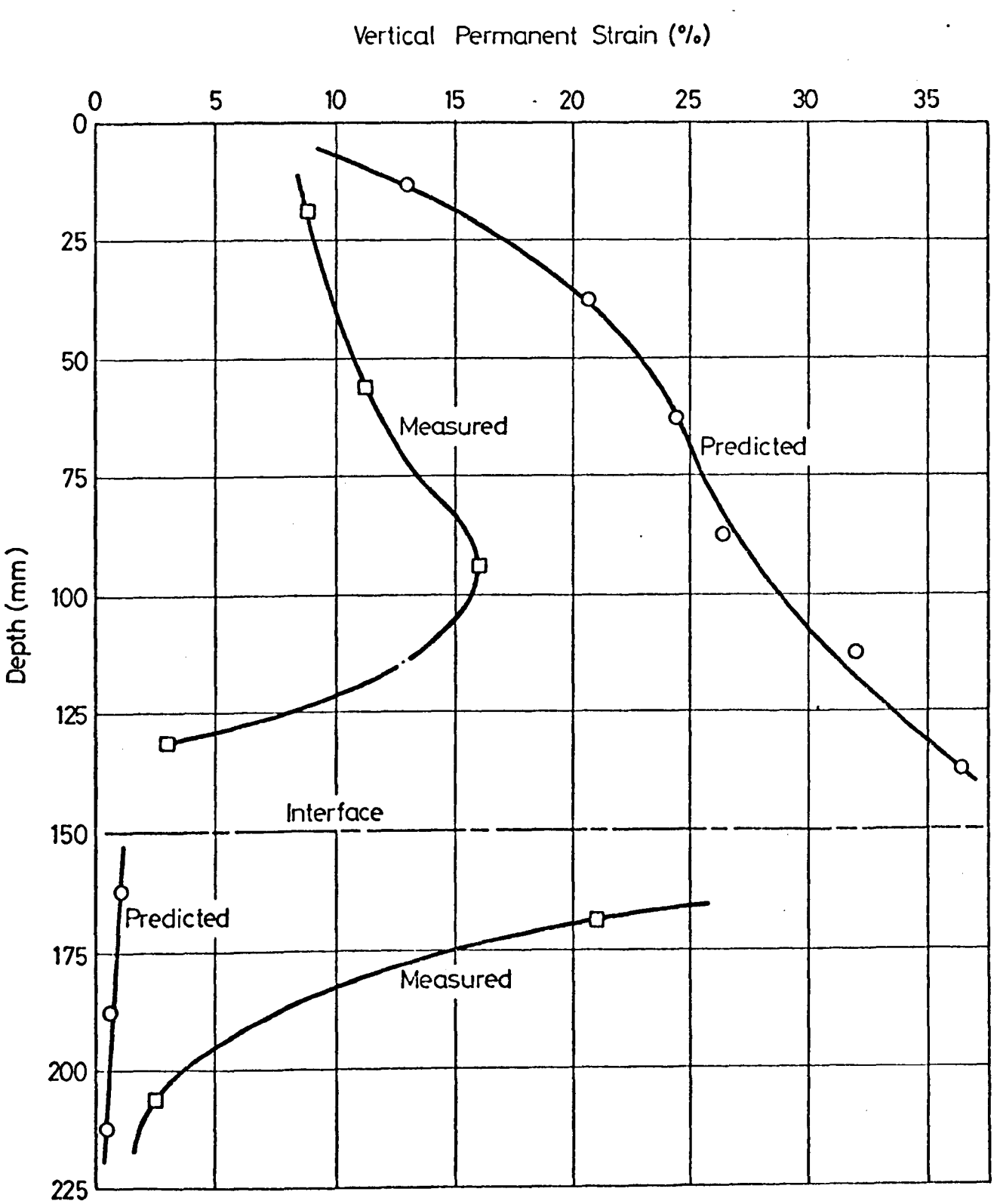

FIG. 11.23 COMPARISON OF MEASURED AND PREDICTED VERTICAL PERMANENT STRAIN (PAVEMENT NO. 2)

Pavement 3

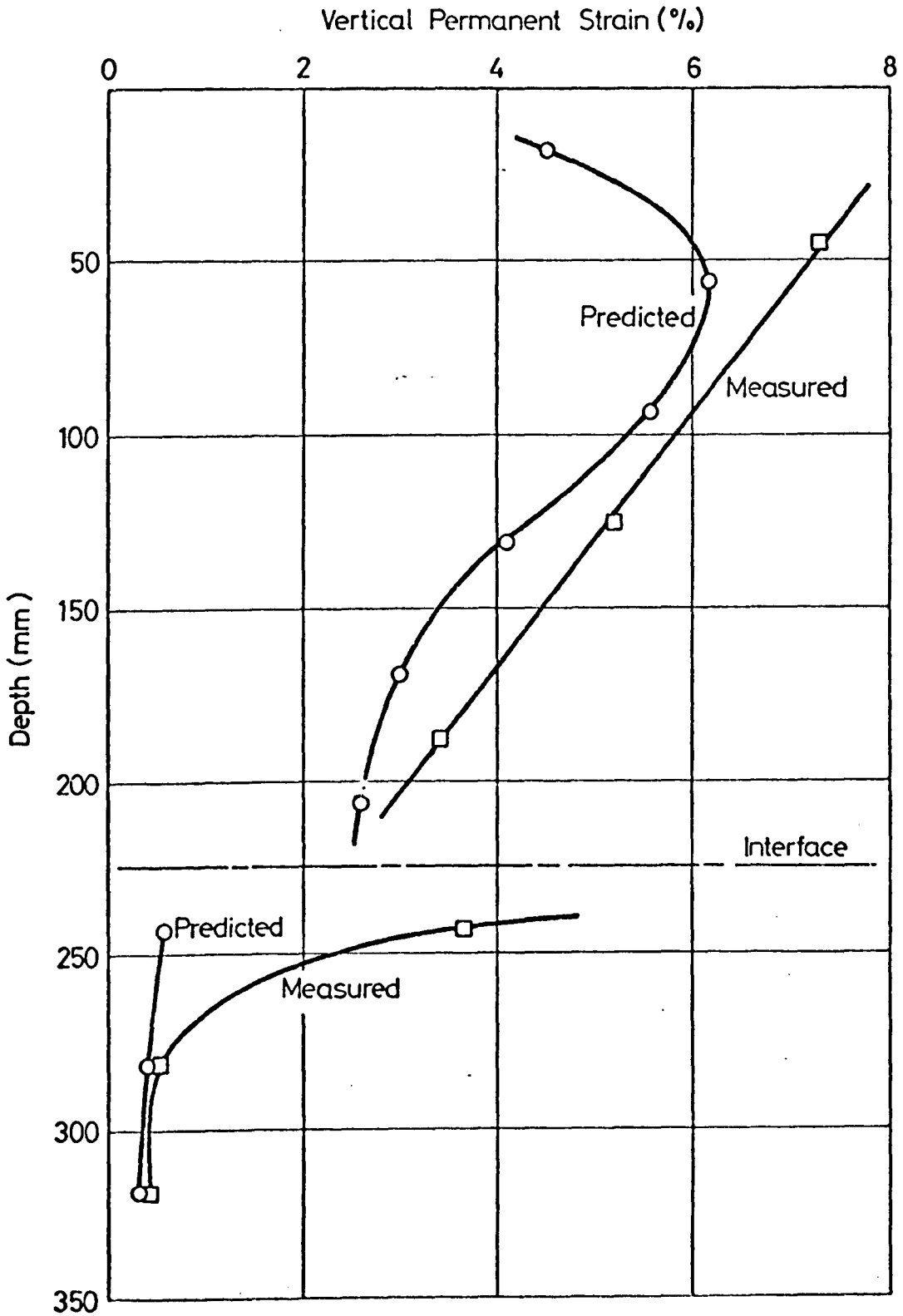

FIG. 11.24 COMPARISON OF MEASURED AND PREDICTED VERTICAL PERMANENT STRAIN (PAVEMENT NO. 3)

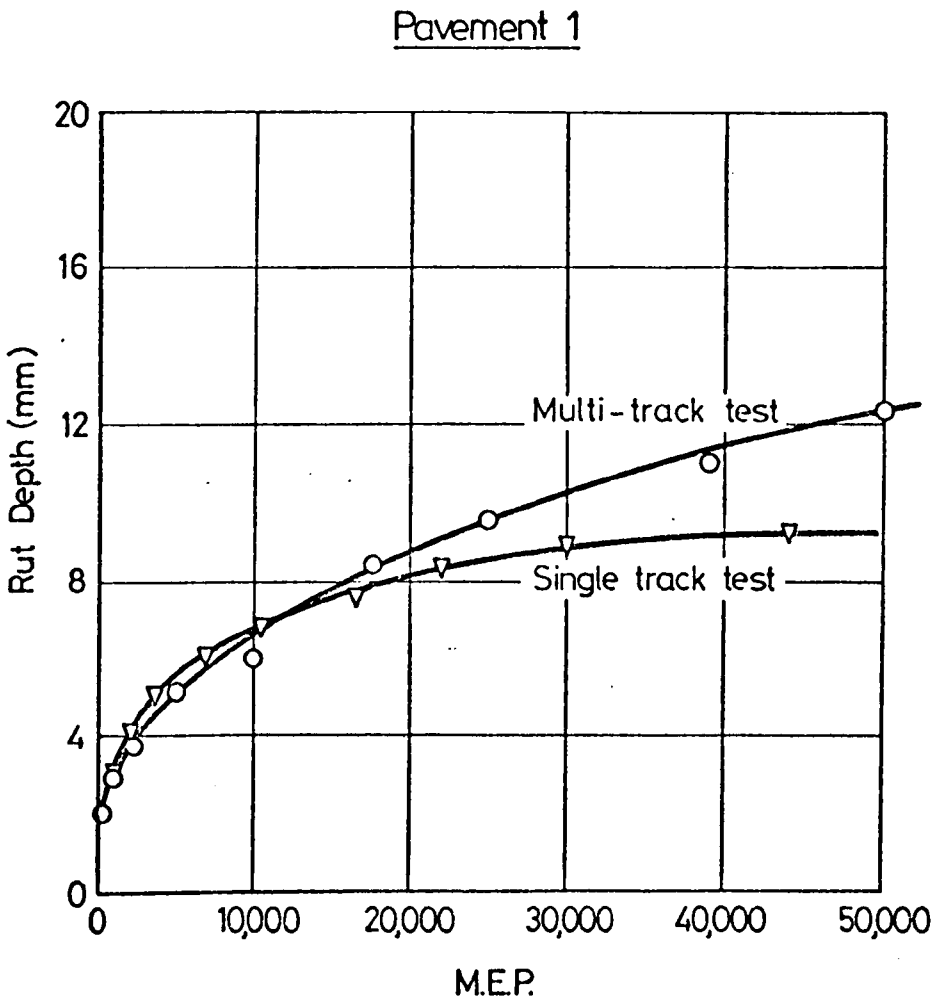

FIG. 11.25 RUT DEPTH VERSUS MEAN NUMBER OF EQUIVALENT PASSES

(PAVEMENT NO. 1)

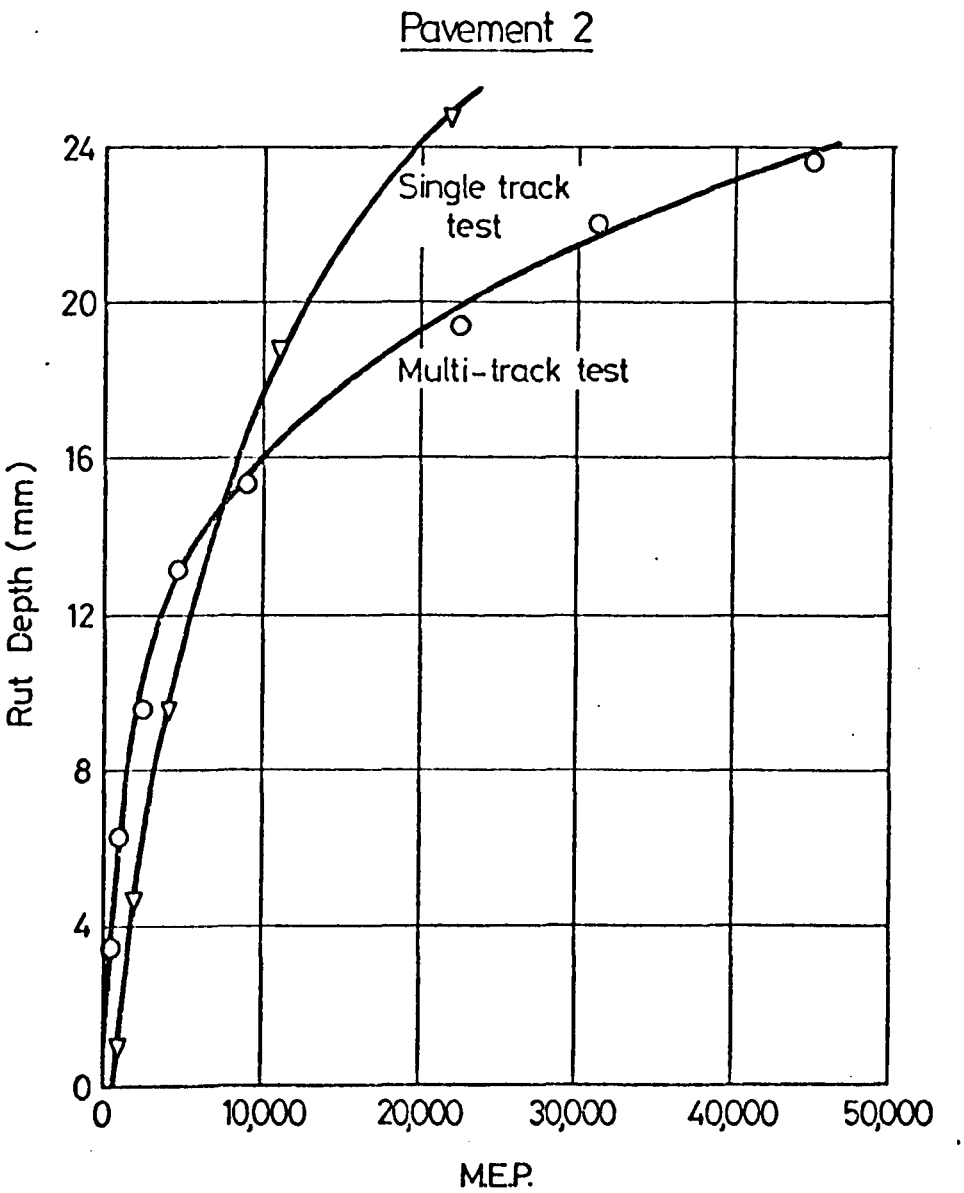

FIG. 11.26 RUT DEPTH VERSUS MEAN NUMBER OF EQUIVALENT PASSES

(PAVEMENT NO. 2)

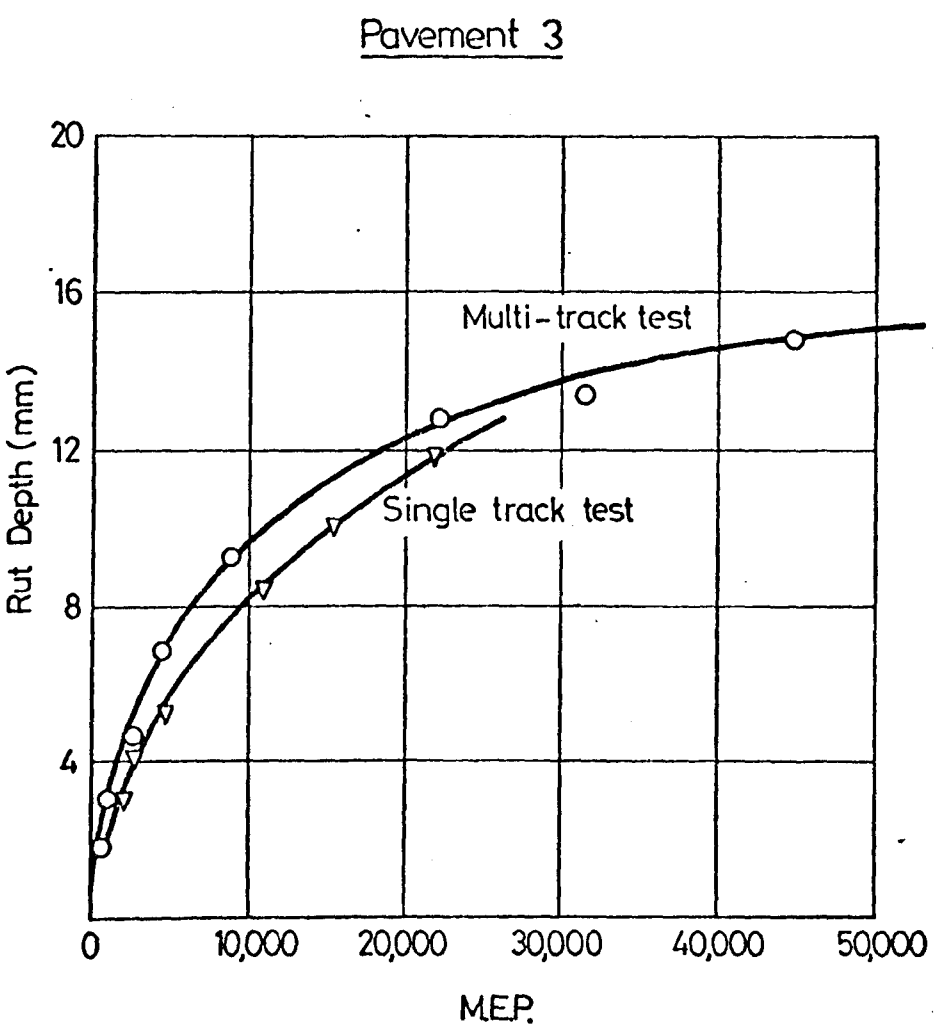

FIG. 11.27 RUT DEPTH VERSUS MEAN NUMBER OF EQUIVALENT PASSES (PAVEMENT NO. 3)

CHAPTER TWELVE

DISCUSSION OF RESULTS

12.1 INTRODUCTION

The aims of the work described in this thesis were to improve knowledge of the permanent deformation behaviour of flexible pave-:ments, and to develop a prediction technique which can be incorp-:orated in a sub-system within a pavement design procedure. The achievement of these aims depends heavily on the successful develop-:ment of the pavement test facility and accurate measurements from the instrumentation, since the validity of the approaches used for prediction rely on an accurate knowledge of the loading conditions and good comparison of predictions of in-situ performance with that measured.

Only three pavements were tested, which were all two layer structures using nominally similar materials, and all were tested at 30°C. Hence, information was limited to the response and analysis of pavements with thick bituminous layers at high temperatures.

A major part of the work was devoted to materials character-:isation tests to provide essential input data for the theoretical calculations. Some of the problems of carrying out such tests, which by necessity were on a comprehensive scale, were highlighted.

12.2 THE PAVEMENT TEST FACILITY AND INSTRUMENTATION

One criticism of the pavement tests carried out is that the loaded wheel travelled in both directions, whereas in practice, pavements are only loaded in one direction (71). It was thought that the effect of shear stress reversal produced by the two-way loading

may produce a different permanent deformation behaviour from that produced with one-way loading. Figures 12.1 and 12.2 illustrate the variation in shear stress and the rotation of the principal planes for a typical element in a pavement subject to one-way and two-way trafficking. Figure 12.1 shows that there is a difference in the shear stress variations, and Figure 12.2 shows that the rotation of the principal planes differs, being in the same sense, anti-clockwise, for one-way loading, but alternatively anti-clockwise and clockwise for two-way loading. It, therefore, seems that the direction of loading may be a critical factor.

Generally, the loading facility performed well, producing constant speed and constant load over the area required, and producing a normal distribution of wheel passes automatically.

The performance of the instrumentation was discussed in Chapter 7. Briefly, measurement of permanent and resilient strains with strain coils, and of stress with Nottingham pressure cells, was successful. The need for more care in the installation of strain gauges was highlighted, and also the careful selection of carrier blocks for both strain coils and gauges.

The most difficult variable to quantify in the use of in-situ instrumentation is the error due to installation technique. The effects of this can be minimised by carrying out careful calibration tests in which the particular instrument is installed in a representative specimen of the site material using the same placement techniques.

12.3 MATERIAL CHARACTERISATION TESTS

The use of stress invariants proved to be a good basis for planning the materials tests, leading to the development of permanent strain models for both materials which were expressed in terms of the two stress invariants, mean normal stress (p) and deviator stress (q). The models were capable of predicting in-situ performance for a wider range of

stress conditions than those developed hitherto, although some approximations had to be introduced to overcome the inherent limit-:ations of the triaxial testing system.

The resilient properties determined by the characterisation tests indicated that both the dense bitumen macadam, at 30°C, and the Keuper marl were very non-linear in their response. This necessitated a non-linear or pseudo non-linear analysis to evaluate stresses and elastic strains in the pavements.

The tensile tests carried out on the DBM demonstrated the difficulty in obtaining results at low or tensile mean normal stress levels. This is because tension can only be applied in the axial direction in the triaxial test, resulting in large tensile strains and, generally, early failure.

Comparison of the results from identical tests on vertical and horizontal cores from pavement 1 indicated a degree of anisotropy in permanent strain response. This was attributed to the flakiness of the aggregate, which aligned horizontally during compaction of the mix, and resulted in higher strains for horizontal cores, probably because the aggregate interlock would be less in that direction.

The models for the permanent strain behaviour of both pavement materials were based on the straight line relationships observed when vertical permanent strain was plotted logarithmically against time for the DBM and semi-logarithmically for the Keuper marl. Snaith (22) observed a similar relationship for his test results on DBM, but his results did not indicate that at constant p the lines for a range of q were parallel. Previous tests on compacted clay (40) and normally consolidated Keuper marl (43) at sub-failure conditions, showed approximately linear relationships between permanent strain and log time, as observed for the compacted Keuper marl tested in this work. However, as reported in Chapter 2, when the results of these tests

and those reported by Brown et al (42) on an overconsolidated Keuper marl are plotted completely logarithmically, straight line relationships are obtained.

It is interesting to note that if Figure 2.7, which shows the results of Brown et al replotted logarithmically with best fit straight lines, is rearranged slightly (Figure 12.3) a series of parallel lines can be obtained for the various values of q at each value of p without significant error. This behaviour is similar to that observed for the DBM test results reported herein, but differs in that the lines are also parallel for any value of p. It may also be observed that the set of lines obtained when Lashine's (43) results are plotted logarithmically are approximately parallel. For both sets of results, these observations apply after an initial settling down period of up to 1,000 cycles. Similarly, when the vertical permanent strain results of the Keuper marl tests reported herein, are plotted logarithmically (see Figure 12.4 for test series K2) a set of parallel lines is obtained after the settling down period of approximately 500 cycles. However, the tests were of a shorter duration than those of Brown et al (42) and Lashine (43) and hence the lines are not so well defined.

12.4 VALIDITY OF PREDICTIONS

12.4.1 Introduction

The main aim of this work was to develop a satisfactory procedure for the prediction of permanent deformation in flexible pavements. The approach adopted was to calculate the stresses in a pavement by means of a suitable elastic analysis and then, in a separate procedure, calculate the corresponding vertical permanent strains. Integration of this strain with depth gave the permanent deformation of the surface.

12.4.2 Elastic Analyses

Clearly, if the predictions of permanent strains are to have the greatest possible accuracy, the preceding elastic analysis should also be as accurate as possible. The materials characterisation tests showed that both materials were substantially non-linear under the test conditions, which were typical of those producing permanent deformation in in-situ pavements, necessitating a non-linear analysis. The finite element computer program DEFPAV was adopted for the non-linear analysis, and this also had the advantage that the permanent strain calculations could be calculated within the program. However, even when using the non-linear stress-elastic-strain relationships derived from the materials testing, the predicted values of stress and elastic strain were generally much lower than the measured values. Particularly, the elastic strain near the surface of the DBM, and that throughout the subgrade were substantially underpredicted. Providing that the measurements are accurate, the former case is understandable, since, at this location, errors, due to the assumption that the wheel load is circular and uniformly distributed, will be greatest. The subsequent use of the calculated stresses to predict permanent strains was therefore unlikely to produce very accurate results.

A series of calculations using adjusted moduli was carried out in an attempt to produce better correlation. This could only be achieved if much lower moduli were assigned to the top of the DBM and all the subgrade. The physical reasons for these changes are not immediately apparent.

There are three possible explanations for the poor correlation of measured and predicted stresses and elastic strains. Firstly, the measurements themselves could have a sizeable error, and since replication of results was limited this is feasible particularly with regard to stress. However, the overall permanent deformation measurement with

strain coils was shown to be accurate and it seems likely that individual measurements of both permanent and elastic strains were accurate. Secondly, at the high temperature (30°C) used for the experiments, the assumption of elastic behaviour is suspect and the usual engineering expedient of using a stiffness corresponding to the temperature and loading time conditions for the bituminous layer may be inappropriate. However, no feasible alternative exists. Alternatively, the actual values of modulus for both materials obtained from the repeated load tests may not be repres-:entative of in-situ conditions. Clearly, it would be preferable to use values obtained from in-situ measurements, which requires substantial instrumentation. In-situ measurements for the subgrade material indicated that a stress-stiffening effect may occur, in contrast to the stress-softening relationship indicated by the characterisation tests. An elastic analysis carried out with the calculated in-situ values of subgrade modulus did not result in a better correlation of stresses and strains. However, this approach should be investigated further and could perhaps be supplemented with measurements obtained with a falling weight deflectometer or wave propagation techniques.

12.4.3 Permanent Deformation Predictions

In view of the difficulties experienced in calculating stresses, only tentative comments can be made with regard to prediction of permanent deformation.

If the procedures used were to be judged solely on the accuracy of rut depth prediction, then reasonable success could be claimed. However, this is a mistake which has been made in the past (25, 87) and this work was intended to provide more detailed information on the contribution of all parts of the pavement to the overall deform-

:ation. This was achieved, but the measured distributions of permanent strain differed substantially from the predictions. Particularly, the predicted deformations in the sub-grade were very small, which could be attributed in part to the predicted stresses being too small. If permanent strains corresponding to in-situ measurements of stress were obtained, they agreed closely with in-situ values. Conversely, the prediction of permanent strain in the tensile zone of the DBM for both pave-:ments 1 and 2 was considerably greater than that measured. This seems to be attributable to the problem of reproducing the stress conditions in this zone in the triaxial test which could result in unrepresentative moduli for the elastic analysis, and also erratic values of permanent strain. Additional errors could accumulate due to approximations in the modelling of permanent strain behaviour and in the prediction procedure based on a cumulative loading procedure, although all such approximations could be justified or were unavoidable.

The major approximation was that the in-situ vertical permanent strain was equivalent to the major principal strain measured in the repeated load triaxial test, and consequently will always be compressive. Since certain stress conditions can result in an increase in volume, this assumption should tend to overpredict rut depth. However, if heaving occurs at the edge of the rut, thus increasing the effective depth of the rut, underprediction of rut depth may result even though the volume change due to the predicted rut is greater than that due to the actual one, as may be seen in Figure 11.21 for pavement 3.

The detailed procedure for obtaining a rut depth and rut profile due to a lateral distribution of wheel loads was based on the concept of a "mean number of equivalent passes" (MEP). It was shown that a

correlation could be obtained between such "multi-track" loading and "single-track" loading, when the former was considered as single track loading with the number of passes at any particular time equal to the MEP. Since the prediction of rut depth for single track loading does not necessitate a cumulative loading procedure the MEP concept could have considerable potential for simplifying design procedures. However, a detailed understanding must be obtained before rational simplifications can be introduced, particularly if the resulting design method is to be applicable to a range of situations.

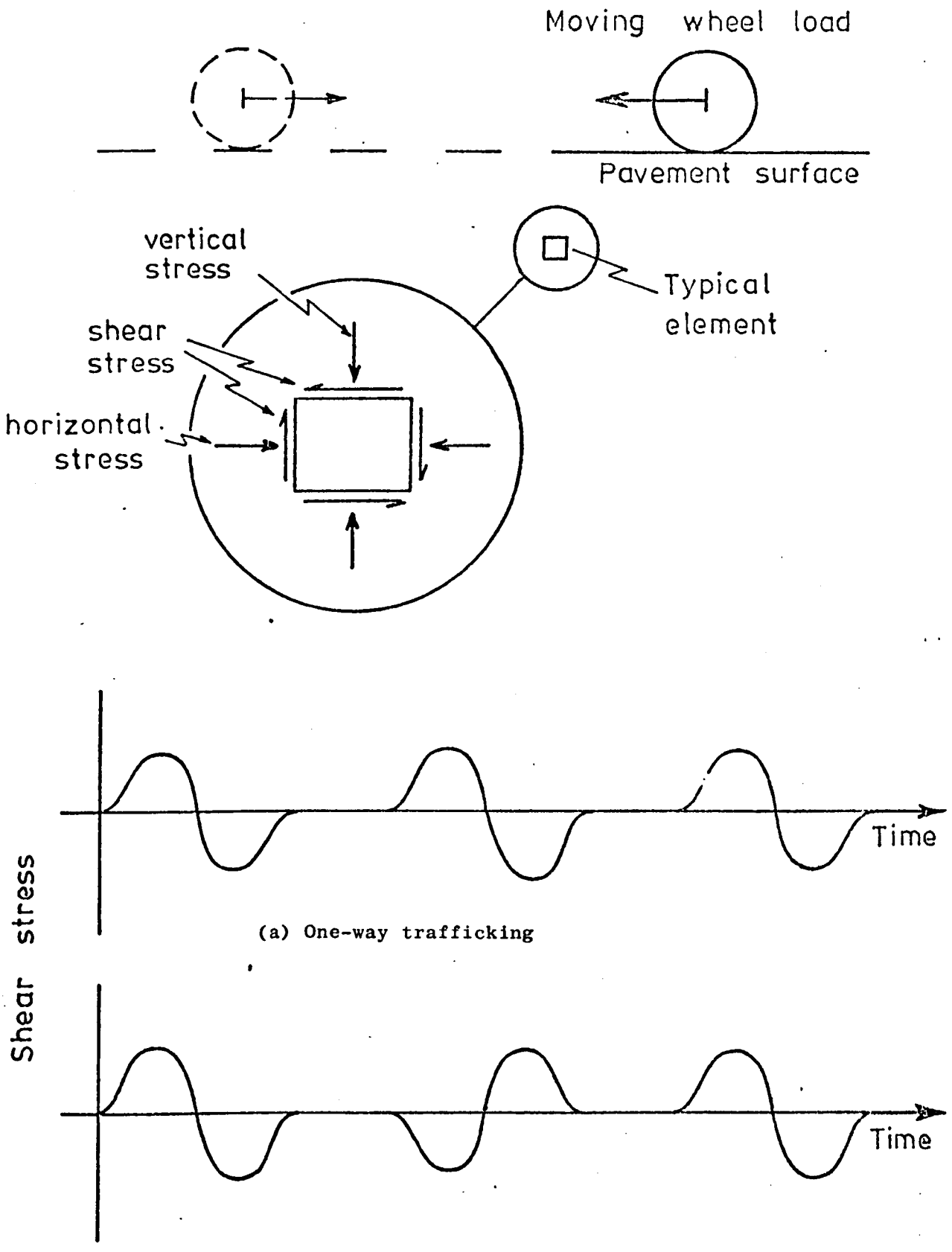

FIG. 12.1 SHEAR STRESS VARIATION IN A TYPICAL PAVEMENT ELEMENT AS A WHEEL PASSES OVERHEAD

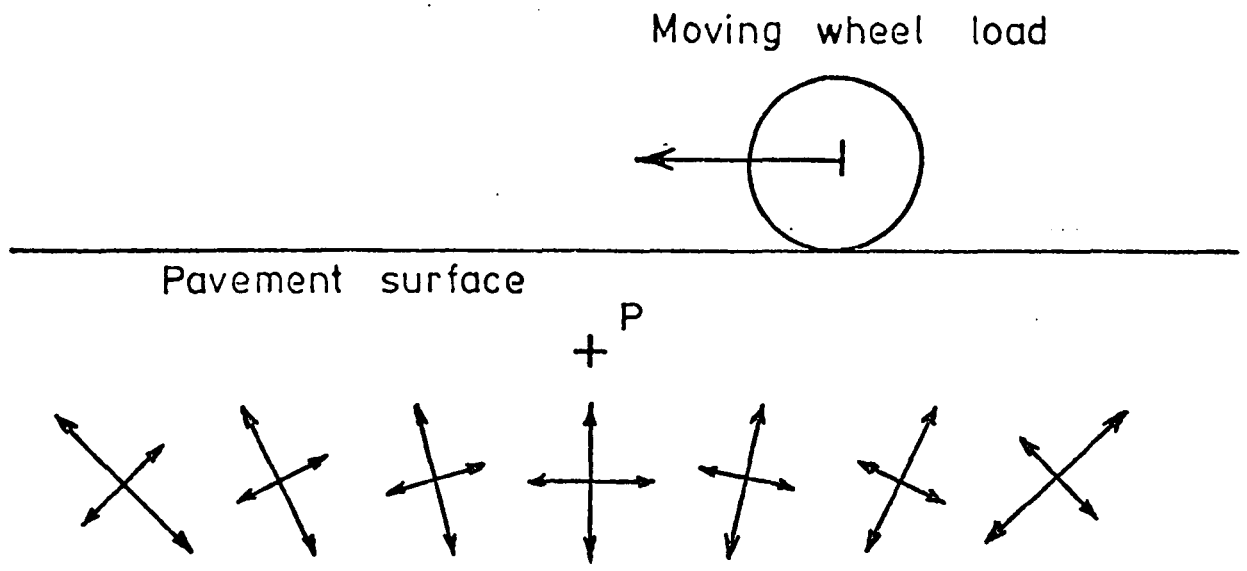

(a) Wheel travels right to left

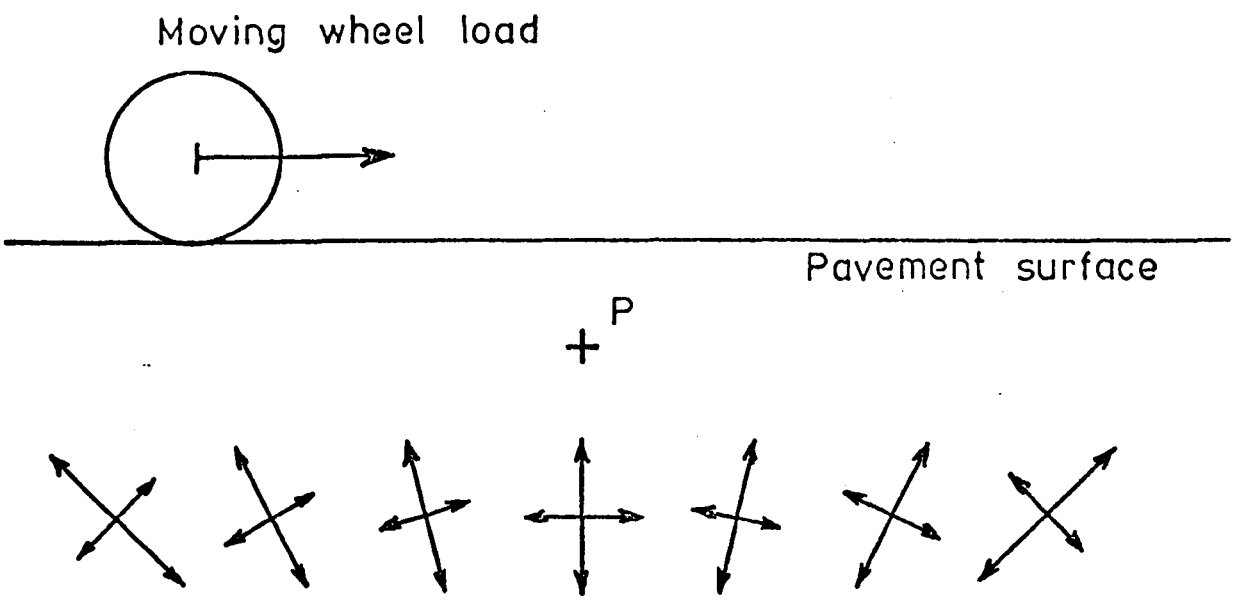

(b) Wheel travels left to right

FIG. 12.2 ROTATION OF PRINCIPAL PLANES AT A TYPICAL LOCATION (P) AS A WHEEL PASSES OVERHEAD

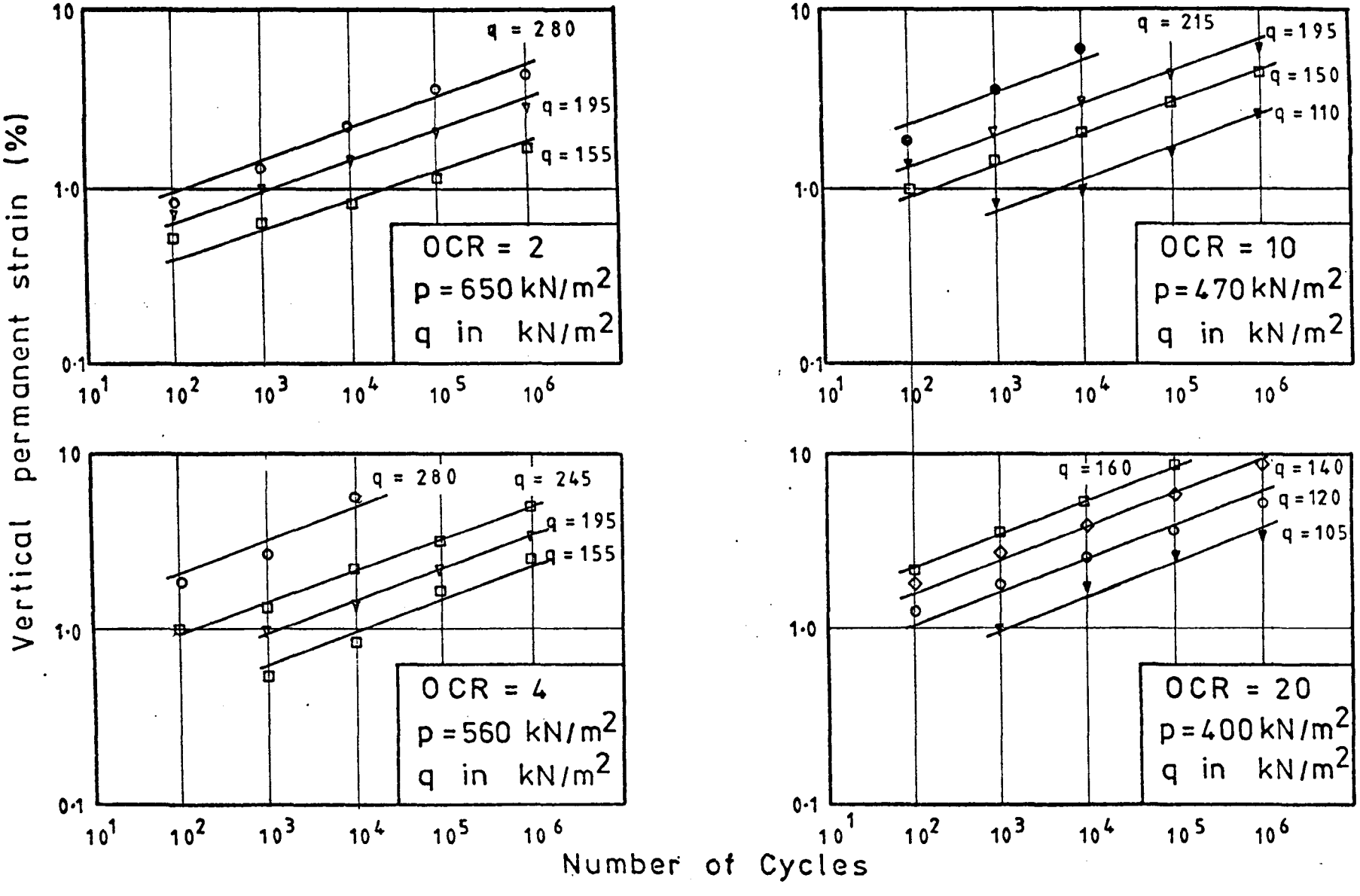

FIG. 12.3 LOGARITHMIC PLOT FOR PERMANENT STRAIN BEHAVIOUR OF KEUPER MARL (AFTER BROWN ET AL (42))

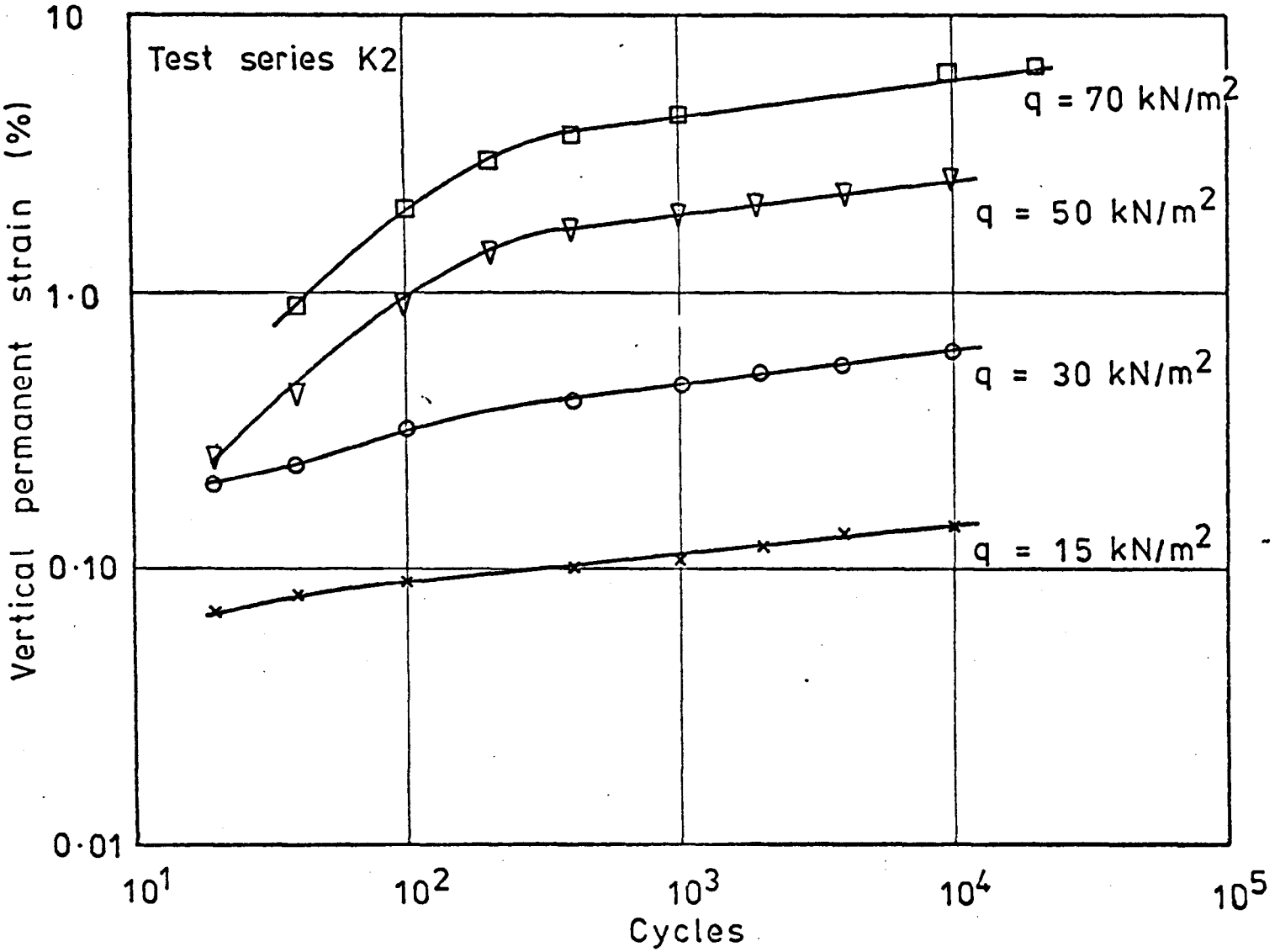

FIG. 12.4 THE EFFECT OF q ON THE VERTICAL PERMANENT STRAIN RESPONSE OF KEUPER MARL, TEST SERIES K2

CHAPTER THIRTEEN

CONCLUSIONS

Three semi-full scale pavements were tested at constant temperature (30°C) using a rolling wheel facility applying realistic loads and speeds. Measurements of resilient and permanent deform-:ation response obtained with in-situ instrumentation were compared with predictions resulting from elastic analysis combined with permanent deformation models developed from repeated load triaxial testing. The following conclusions may be drawn from this work:

13.1 IN-SITU INSTRUMENTATION

(1) Strain coils can successfully be used to obtain detailed information on both permanent and elastic strains in bituminous and subgrade materials.

(2) Pressure cells may be used with success in the subgrade and show potential for use in bituminous materials.

(3) Carrier blocks for strain measuring devices in bituminous materials should only be used if it is unavoidable, and the material used should not be stiffer than the surround-:ing material.

(4) The need for as many replicate measurements as possible of a particular in-situ stress or strain has been confirmed.

13.2 MATERIALS CHARACTERISATION TESTS

(1) The use of stress invariants to specify in-situ stress conditions proved useful in planning material character-:isation tests and in developing stress-strain models.

(2) The limitations of the triaxial test configuration for reproducing in-situ conditions in a bituminous layer were demonstrated, particularly with regard to the tensile stress zone at the bottom of such a layer.

(3) The resilient response of both pavement materials was found to be non-linear and dependant on the level of mean normal stress.

(4) The relationship between the measured vertical permanent strain (ε_{vp}) and the elapsed time (t) for the DBM was found to be of the form:

$$\log \varepsilon_{vp} = A + B \log t \quad .$$

and for a particular value of mean normal stress (p) the value of B was constant.

(5) The relationship between the measured vertical permanent strain (ε_{vp}) and the number of cycles (N) for Keuper marl was found to be of the form:

$$\varepsilon_{vp} = b \log N$$

13.3 PREDICTIONS OF RESILIENT RESPONSE

(1) Under the relatively high temperature conditions (30^{o}) and for the particular materials used (dense bitumen macadam and a silty clay) non-linear elastic theory was required to predict resilient response.

(2) Stress and elastic strains were generally underpredicted.

(3) Accurate prediction of stresses is required if the permanent deformation calculations are to be accurate.

13.4 PREDICTIONS OF PERMANENT DEFORMATION

(1) A detailed procedure for calculating the rut profile resulting from a given lateral distribution of wheel passes was developed, utilising the computer program DEFPAV.

(2) The rut depth for a lateral distribution of wheel loads could be calculated by considering the "mean number of equivalent passes" (MEP) acting at the centre of the distribution.

(3) The overall predictions of rut depth were reasonably good, but the method tended to overestimate the contribution from the bituminous layer and underestimate that from the subgrade. These discrepancies could be directly related to those between the predicted and measured stresses.

13. 5 GENERAL CONCLUSIONS

(1) There is a need for much more research of this nature, particularly with regard to the in-situ behaviour of pavement materials, and modelling of the resilient response, before a complete understanding of the permanent deformation problem can be approached.

CHAPTER FOURTEEN

RECOMMENDATIONS FOR FURTHER WORK

14.1 INTRODUCTION

In the first Chapter it was emphasised that relatively little research had been carried out into the permanent deformation behav-:iour of flexible pavements and their component materials. That which has, including the work reported herein, has provided valuable information, but also emphasised the fact that much more research is required to achieve a level of understanding necessary to produce a comprehensive design sub-system. The proposals of Romain (19) and Barksdale (20) are a sound basis for an analytical procedure, such as the one developed herein. But, as has been shown, many areas need to be explored further.

An interim solution between the present empirical design procedures and future fundamentally based ones is to utilise the wealth of in-situ measurements available to predict permanent deform-:ations, viz, relate the future deformation of a road to that already measured in a road of similar construction and subject to similar loading and temperature variations. Such an approach is similar to that used in the development of the Road Note No. 29 design charts, although it could be used as a separate design sub-system in conjunc-:tion with one to prevent fatigue. Also, data could be stored and updated, using modern computer facilities, and readily accessed. However, the drawbacks would be similar to those of other empirically based design methods, particularly in extension of the method to new situations, such as use of new materials, freak weather conditions, and different loading conditions.

The following recommendations are made with the achievement of a fundamentally based permanent deformation design sub-system in mind, but many of them also apply to furthering knowledge of the overall repeated load behaviour of flexible pavements and their materials.

14.2 FURTHER IN-SITU TESTING

The semi full-scale pavement experiments described herein provided the most convenient form of acquiring in-situ measurements. Further tests, on a three layer pavement structure, have continued at Nottingham University (88), but a widespread research effort is required if a significant amount of data is to be collected within a reasonable period of time (say a decade), since even such accele-:rated tests are very time consuming. The tests should be aimed at establishing firmly the distributions of stress, elastic strain, and permanent strain in different types of pavement, and should consequently contain comprehensive instrumentation. As many replicate measurements as possible should be obtained, and where possible all parameters should be measured at identical locations, for ease of comparison and so that values of resilient moduli can be obtained. All tests should be accompanied by adequate materials characterisation tests so that the validity of predictions of both resilient and permanent deform-:ation behaviour can be checked.

The strain coils and pressure cells, used in the pavement tests described herein, performed adequately. However, installation is difficult and time consuming, particularly if a high density of instrumentation is used. Cables are a particular problem, and there-:fore use of instruments emitting radio signals or other cableless types should be seriously considered.

Finance for a research effort such as that prescribed above is

very difficult to obtain. A possible and desirable alternative is to monitor performance of existing roads, which has the advantage of avoiding construction costs, but the disadvantage that the transient loading and environmental conditions are especially difficult to monitor. Ideally, once techniques for prediction of permanent deformation have been thoroughly validated by semi full-scale tests they should be extended to the real road situation for complete validation.

14.3 MATERIALS CHARACTERISATION

Repeated load triaxial tests provide the most convenient means of obtaining both the resilient and permanent deformation characteristics of pavement materials. However, creep testing is much simpler to implement and should become widely used to obtain permanent deformation characteristics. The levels of creep stress equivalent to given repeated stresses, for all materials and forms of loading, need to be established before such tests can be fully implemented (see section 3.1).

One problem with repeated load tests is the high cost of the equipment. However, it seems likely that simplified equipment could be used; viz, pneumatically operated instead of servo-hydraulically, continuous loading with no choice of frequency, and only constant confining pressure. Tests carried out with such equipment could be used in conjunction with creep tests to provide the essential resilient and permanent deformation characteristics of pavement materials.

At present, few materials have been thoroughly investigated over a realistic range of stress conditions. The invariant approach provides a means of assessing the in-situ stress conditions, and has flexibility when applied to the triaxial stress situation. It is recommended that this approach is applied generally to pavement

materials. In order to do this with complete confidence it will be necessary to establish whether a third invariant is necessary to completely describe a given stress situation (i.e. if the p - q approach is used, whether the sign of q is important).

With regard to the deformation measurement instrumentation, this should be mounted on the specimen wherever possible and in both the vertical and radial directions. The radial deformation requires particular attention, since, in the past, poor measurements in this direction have resulted in poor definition of the Poisson's ratio, or the bulk and shear moduli.

Finally, there is a need for a unified method of testing, and collaboration between various research centres. A significant amount of research is duplicated but often incompatible due to the idiosyncrasies of individual laboratories. A particular area of concern is the treatment of the initial part of a repeated load test, with particular regard to the permanent strain. Some testing machines are capable of applying the full stress immediately, whereas others need to approach the full stress gradually and therefore the behaviour at this very important stage of the loading differs considerably. Clearly, a standard method of interpreting and correcting results for this initial stage should be established.

14.4 PREDICTION OF RESILIENT BEHAVIOUR

The prediction of stresses for the purpose of assessing permanent strains presents the greatest problem, as highlighted herein. This is largely because pavement materials are non-linear under the conditions which produce permanent deformation and possibly behave inelastically, and because the areas where high permanent strains occur (viz, the top and bottom of the bituminous layer) are particularly difficult to model. It is therefore essential to use non-linear elastic analyses and also to

specify the non-linearity accurately. The recommendations of the previous section should help to fulfil the latter point. Also, much more information from in-situ tests is required before the accuracy of predictions can be completely assessed.

As demonstrated with the predictions of resilient behaviour described in Chapter 10, a pseudo non-linear analysis can produce predictions of similar accuracy to a full non-linear analysis. Unless a significant advantage can be gained from the use of the latter, the former should be used, and it may even be possible to achieve similar accuracy with a linear analysis. If this was the case, then the use of desk-top computer facilities would be feasible, and such programs that exist (89) for use with these facilities should be investigated for the purpose of predicting stresses and for the ultimate calculation of permanent strains.

14.5 PREDICTION OF PERMANENT DEFORMATION

The successful prediction of permanent deformation depends largely on comprehensive materials characterisation and accurate prediction of resilient behaviour, therefore concentration of effort on these two points is of primary importance. The continued use of an invariant approach is recommended as a basis for both characterisation tests and the prediction procedures.

The major error in the interpretation of results from the characterisation tests was due to the approximation required to obtain a value for the in-situ vertical permanent strain. An alternative to this procedure, based on the calculation of volumetric permanent strains is outlined in the Appendix, and investigation of this more fundamentally sound procedure is recommended.

No matter what method is used to obtain the permanent strain due to a particular loading, a cumulative loading procedure is still

required to determine the effect of a distribution of loads. In extending prediction techniques to a real road situation, where the transient temperatures conditions need to be considered, an approach similar to that used herein for calculating rut depth and rut profile could be used.

REFERENCES

1. BRITISH ROAD FEDERATION, *"Analysis No. 17"*, March 1977.

2. BRITISH ROAD FEDERATION, *"Basic road statistics 1976"*.

3. ROAD RESEARCH LABORATORY, *"A guide to the structural design of pavements for new roads"*, Department of the Environment, Road Note No. 29, 3rd Edit., HMSO, 1970.

4. DEPARTMENT OF TRANSPORT, *"Specification for road and bridge works"*, 5th Edit., HMSO, 1976.

5. CRONEY D. and LOE J.A., *"Full scale pavement design experiment on A1 at Alconbury Hill, Huntingdonshire"*, Proc. Instn. Civil Engineers, 1965, Vol. 30, pp 225 - 70.

6. PROCEEDINGS of the 1st International Conference on the Structural Design of Asphalt Pavements, Vol. 1, Ann Arbor, Michigan, 1962.

7. PROCEEDINGS of the 2nd International Conference on the Structural Design of Asphalt Pavements, Vol. 1, Ann Arbor, Michigan, 1967.

8. PROCEEDINGS of the 3rd International Conference on the Structural Design of Asphalt Pavements, Vol. 1, London, 1972.

9. PROCEEDINGS of the 4th International Conference on the Structural Design of Asphalt Pavements, Vol. 1, Ann Arbor, Michigan, 1977.

10. SHELL INTERNATIONAL PETROLEUM CO. LTD., *"Shell 1963 design charts for flexible pavements"*, London, 1963.

11. BROWN S.F. and PEATTIE K.R., *"The structural design of bituminous pavements for heavy traffic"*, Proc. Instn. Civil Engineers, 1973, Vol. 57, pp 83 - 97.

12. PELL P.S. and COOPER K.E., *"The effect of testing and mix variables on the fatigue performance of bituminous materials"*, Proc. Assn. Asphalt Paving Technologists, Vol. 44, pp 1-37, 1975.

13. LISTER N.W., *"The transient and long term performance of pavements in relation to temperature"*, Proc. 3rd Int. Conf. on the Struct. Design of Asphalt Pavements, London, 1972, pp 94-100.

14. LISTER N.W. and POWELL W.D., *"Research into the compaction of bituminous materials"*, Asphalt and Coated Macadam Assn. Seminar 74, London, 1974.

15. CRONEY D., *"Failure criteria for flexible pavements"*, Proc. 3rd Int. Conf. on the Struct. Design of Asphalt Pavements, London, 1972, pp 608-612.

16. BRITISH ROAD FEDERATION, *"Road maintenance - Survey of the problems involved in expenditure cuts"*, 1977.

17. BRODRICK B.V., *"The development and performance of a wheel loading facility and in-situ instrumentation for pavement experiments"*, M.Phil. thesis, Univ. of Nottingham, 1977.

18. BROWN S.F., BELL C.A., and BRODERICK B.V., *"Permanent deformation of flexible pavements"*, Research Report to ERO, US Army, Univ. of Nottingham, 1974.

19. ROMAIN J.E., *"Rut depth prediction in asphalt pavements"*, Proc. 3rd Int. Conf. on the Struct. Design of Asphalt Pavements, London, 1972, Vol. 1, pp 705-710.

20. Ibid BARKSDALE R.D., *"Laboratory evaluation of rutting in base course materials"*, pp 161-174

21. BROWN S.F., *"An improved framework for predicting permanent deformation in asphalt layers"*, Transportation Research Record 537, 1975, pp 18-30.

22. SNAITH M.S., *"Deformation characteristics of dense bitumen macadam subjected to dynamic loading"*, Ph.D. thesis, Univ. of Nottingham, 1973.

23. BROWN S.F. and SNAITH M.S., *"The permanent deformation characteristics of a dense bitumen macadam subjected to repeated loading"*, Proc. Assn. Asphalt Paving Technologists, 1974, Vol. 43, pp 224-252.

24. KIRWAN R.S. and SNAITH M.S., *"Further investigations towards a rational method of design for flexible pavements"*, Final Tech. Report to US Army, Trinity College, Dublin, April, 1975.

25. MORRIS J., HAAS R., REILLY P. and HIGNELL E., *"Permanent deformation in asphalt pavements can be predicted"*, Proc. 49th Annual Meeting of Assn. Asphalt Paving Technologists, Feb., 1974.

26. McLEAN D.B. and MONISMITH C.L., *"Estimations of permanent deformation in asphalt concrete layers due to repeated traffic loading"*, Proc. Annual Meeting of Highway Research Board, Jan. 1974.

27. HAAS R.C.G., KAMEL N.I. and MORRIS J., *"Brampton test road: analysis of performance by elastic layer theory and its application to pavement design and management in Ontario"*, Final Report on Project W-24, Ontario Joint Transp. and Comm. Res. Program, 1972.

28. HOFSTRA A. and KLOMP A.J.G., *"Permanent deformation of flexible pavements under simulated road traffic conditions"*, Proc. 3rd Int. Conf. on the Struct. Design of Asphalt Pavements, London, 1972, Vol. 1, pp 613-621.

29. HEUKELOM W. and KLOMP A.J.G., *"Consideration of calculated strains at various depths in connection with the stability of asphalt pavements"*, Proc. 2nd Int. Conf. on the Struct. Design of Asphalt Pavements, Ann Arbor, Michigan, 1967, pp 155-168.

30. BROWN S.F., *"Discussion on permanent deformation"*, Proc. 3rd Int. Conf. on the Struct. Design of Asphalt Pavements, 1972, Vol. 2, pp 186-187.

31. BROWN S.F. and BELL C.A., *"The validity of design procedures for the permanent deformation of asphalt pavements"*, Proc. 4th Int. Conf. on the Struct. Design of Asphalt Pavements, Ann Arbor, Michigan, 1977, Vol. 1, pp 467-482.

32. AUSSEDAT G. and AZIBERT C.L., *"The mechanism of rutting of base layers"(in French)*, Rev. Gen. des Routes et des Aerodromes, No. 498, May 1974.

33. KLOMP A.J.G. and DORMAN G.M., *"Stress distribution and dynamic testing in relation to road design"*, Proc. ARRB, 1964.

34. SEED H.B., CHAN C.K. and MONISMITH C.L., *"Effect of repeated loading on the strength and deformation of compacted clay"*, Proc. Highway Research Board, Vol. 34, pp 541-558, 1955.

35. SEED H.B. and CHAN C.K., *"Effect of stress history and frequency of stress application on deformation of clay subgrades subjected to repeated loading"*, Proc. Highway Research Board, Vol. 37, pp 555-575, 1958.

36. SEED H.B., CHAN C.K. and LEE K.L., *"Resilience characteristics of subgrade soils and their relation to fatigue failure in asphalt pavements"*, Proc. 1st Int. Conf. on the Struct. Design of Asphalt Pavements, Ann Arbor, Michigan, 1962, pp 611-636.

37. SEED H.B., MITRY F.G., MONISMITH C.L. and CHAN C.K., *"Prediction of pavement deflections from laboratory repeated load tests"*, Report TE 65-6, Dept. of Civil Eng., Inst. of Transp. and Traffic Eng., Univ. of California, 1965.

38. SEED H.B. and McNEILL R.L., *"Soil deformations under repeated stress applications"*, ASTM, STP, No. 232, pp 177-196, 1957.

39. SEED H.B. and FEAD J.W.N., *"Apparatus for repeated load tests on soils"*, ASTM, STP, No. 254, 1959.

40. MONISMITH C.L., OGAWA N. and FREEME C.R., *"Permanent deformation characteristics of subgrade soils due to repeated loading"*, Transportation Research Record 537, 1975, pp 1-17.

41. NOT USED

42. BROWN S.F., LASHINE A.K.F. and HYDE A.F.L., *"Repeated load triaxial testing of a silty clay"*, Geotechnique, Vol. 25, No. 1, 1975, pp 95-114.

43. LASHINE A.K.F., *"Some aspects of the characteristics of Keuper marl under repeated loading"*, Ph.D. thesis, Nottingham Univ. 1971.

44. GLYNN T.E. and KIRWAN R.W., *"A stress-strain relationship for clays subjected to repeated loading"*, Proc. 7th Int. Cong. on Soil Mechs. and Found. Eng., Vol. 1, Mexico, 1969, pp 159-163.

45. HYDE A.F.L., *"Repeated load triaxial testing of soils"*, Ph.D. thesis, Nottingham Univ., 1974.

46. SCHOFIELD A.N. and WROTH C.P., *"Critical state soil mechanics"*, London, 1968, McGraw-Hill.

47. LASHINE A.K.F., *"Deformation characteristics of a silty clay under repeated loading"*, Proc. 8th Int. Cong. on Soil Mechs. and Found. Eng., Moscow, 1973, pp 237-244.

48. WILLIAMS G.T., *"Stress/Strain relationships of granular soils"*, Thornton Report R1297, 1963, 'Shell' Research Ltd.

49. BROWN S.F. and PELL P.S., *"An experimental investigation of the stresses, strains and deflections in a layered pavement structure subjected to dynamic loads"*, Proc. 2nd Int. Conf. on the Struct. Design of Asphalt Pavements, Ann Arbor, Michigan, 1967, pp 487-503.

50. HICKS R.G., *"Factors influencing the resilient response of granular materials"*, Ph.D. thesis, Univ. of California, 1970.

51. LASHINE A.K., BROWN S.F. and PELL P.S., *"Dynamic properties of soils"*, Report No. 2, submitted to Koninklijke-Shell-Laboratorium, Amsterdam, 1971.

52. BROWN S.F., *"Repeated load testing of a granular material"*, Journal of the Geot. Eng. Div., Proc. ASCE, Vol. 100, No. GT7, July, 1974.

53. BROWN S.F. and HYDE A.F.L., *"Significance of cyclic confining stress in repeated load triaxial testing of granular material"*, Transportation Research Record 537, 1975, pp 49-58.

54. ALLEN J.J. and THOMSON M.R., *"Resilient response of granular materials subjected to time-dependant lateral stresses"*, Transportation Research Record 510, 1974, pp 1-13.

55. BOYCE J.R., *"The behaviour of a granular material under repeated loading"*, Ph.D. thesis, Univ. of Nottingham, 1976.

56. PAPPIN J.W., Private Communication, Univ. of Nottingham.

57. HILLS J.F., *"The creep of asphalt mixes"*, Journal of the Institute of Petroleum, Nov. 1973.

58. HILLS J.F., BRIEN D. and VAN DE LOO P.J., *"The correlation of rutting and creep tests on asphalt mixes"*, Journal of the Inst. of Petroleum, Paper IP 74-001, January, 1974.

59. VAN DE LOO P.J., *"A practical approach to the prediction of rutting in asphalt pavements - THE SHELL METHOD"*, Proc. Annual Meeting of Transportation Research Board, Washington, Jan. 1976.

60. PEUTZ M.G.F., VAN KEMPEN H.P.M. and JONES A., *"Layered systems under normal surface loads"*, Highway Research Record No. 228, 1968, pp 34-45.

61. VAN DE POEL C., *"Time and temperature effects on the deformation of bitumen and bitumen-mineral mixtures"*, Journ. Soc. Plastics Engineers, Vol. 11, 1955, pp 47-64.

62. DE HILSTER E. and VAN DE LOO P.J., *"Prediction of the permanent deformation on the Nottingham test pavement"*, Memo BR/471/76, Koninklijke-Shell Laboratorium, Amsterdam, 1976.

63. KIRWAN R.W., SNAITH M.S. and GLYNN T.E., *"A computer based subsystem for the prediction of pavement deformation"*, Proc. 4th Int. Conf. on the Struct. Design of Asphalt Pavements, Ann Arbor, Michigan, 1977, Vol. 1, pp 509-518.

64. BROWN S.F. and COOPER K.E., *"Permanent deformation of dense bitumen macadam under creep and repeated loading"*, Colloquium 77 - Plastic Deformability of Bituminous Mixes, Zurich, Sept., 1977.

65. HUSCHEK S., *"Evaluation of rutting due to viscous flow in asphalt pavements"*, Proc. 4th Int. Conf. on the Struct. Design of Asphalt Pavements, Ann Arbor, Michigan, 1977.

66. Ibid THROWER E.N., *"Methods of predicting deformation in road pavements"*.

67. TIMOSHENKO S.P. and GOODIER J.N., *"Theory of Elasticity"*, 3rd Ed., McGraw-Hill Book Co. Inc., New York, 1970, pp 219-234.

68. THROWER E.N., *"Stress invariants and mechanical testing of pavement materials"*, Transport and Road Research Lab. Report LR 810, DOE, 1978.

69. ANSELL P., *"Cyclic simple shear testing of granular material"*, Ph.D. thesis, Univ. of Nottingham, 1977.

70. BROWN S.F., *"State-of-the-art on field instrumentation for pavement experiments"*, Proc. TRB Technical Committee A2K01, 1976.

71. BROWN S.F., BELL C.A. and BRODRICK B.V., *"Permanent deformation of flexible pavements"*, Research Report to ERO, US Army, Univ. of Nottingham, 1974.

72. BROWN S.F. and BRODRICK B.V., *"Stress and strain measurements in flexible pavements"*, Proc. Conf. on Measurements in Civil Engineering, Newcastle, England, 1977.

73. BRATTON J., *"Pressure cells in bituminous materials"*, B.Sc. thesis, Univ. of Nottingham, 1977.

74. MINISTRY OF TRANSPORT, *"Specification for road and bridge works"*, HMSO, 1969.

75. BRITISH STANDARDS INSTITUTION, *"Coated macadam for roads and other paved surfaces"*, BS4987, 1973.

76. BRITISH STANDARDS INSTITUTION, *"Methods of testing soils for civil engineering purposes"*, BS1377, 1975.

77. BISON INSTRUMENTS INC., *"Instruction manual, Bison instruments soil strain gauge model 4101A"*.

78. KLOMP A.J.G. and NIESMAN Th.W., *"Observed and calculated strains at various depths in asphalt pavements"*, Proc. 2nd Int. Conf. on the Struct. Design of Asphalt Pavements, Ann Arbor, Michigan, 1967, pp 671-688.

79. THROWER E.N., LISTER N.W. and POTTER J.F., *"Experimental and theoretical studies of pavement behaviour under vehicular loading in relation to elastic theory"*, Proc. 3rd Int. Conf. on the Struct. Design of Asphalt Pavements, London, 1972, pp 521-535.

80. McELVANEY J., *"Fatigue of bituminous mixture under compound-loading"*, Ph.D. thesis, Univ. of Nottingham, 1972.

81. CULLINGFORD G., LASHINE A.K.F. and PARR G.B., *"Servo controlled equipment for dynamic triaxial testing of soils"*, Geotechnique, Vol. 22, No. 3, Technical Note, 1972, pp 526-529.

82. BARKSDALE R.D., *"Compressive stress pulse times in flexible pavements for use in dynamic testing"*, Highway Research Record No. 345, 1971, pp 32-44.

83. BROWN S.F., *"Determination of Young's modulus for bituminous materials in pavement design"*, Highway Research Record No. 431, 1973, pp 38-49.

84. COOPER K.E., BROWN S.F., McELVANEY J. and PELL P.S., *"Permanent deformation of bituminous materials"*, Research Report submitted to TRRL, Univ. of Nottingham, 1975.

85. COX M.G. and HAYES J.G., *"Curve fitting: a guide and suite of algorithms for the non-specialist user"*, National Phys. Lab. Report NAC26, 1973.

86. LISTER N.W. and JONES R., *"The behaviour of flexible pavements under moving wheel loads"*, Proc. 2nd Int. Conf. on the Struct. Design of Asphalt Pavements, Ann Arbor, Michigan, 1967, pp 1021-1035.

87. BROWN S.F., Discussion of *"Permanent deformation in asphalt pavements can be predicted"*, by Morris et al, Proc. Assn. Asphalt Paving Technologists, Vol. 43, 1974, pp 67-70.

88. BRODRICK B.V. and BROWN S.F., *"Performance of flexible pavements incorporating fabrics"*, Report No. BVB/1, submitted to ICI Fibres, Ltd., August, 1978.

89. ULLIDTZ P., Presentation at the Annual Meeting of the Pavement Study Group, Rouen, September, 1978.

APPENDIX

PERMANENT STRAIN MODEL BASED ON VOLUMETRIC STRAIN

A.1 INTRODUCTION

It has already been stated in Chapter 8 that direct determination of the three in-situ principal permanent strains is impossible because the two strain invariant equations for volumetric and shear strain (v_p and ε_p), obtained from the characterisation tests, cannot be solved for three unknowns. The approximation which was used for the predict-:ions described in previous Chapters was to assume that the vertical permanent strain in-situ was equal to the major principal permanent strain measured in the triaxial test. This probably results in predicted vertical permanent strains which are greater than if they could be obtained from applying Mohr's circle to the principal permanent strains. Also, the predicted vertical strain is always compressive, which is not always the case in-situ since heaving often occurs at the sides of a rut. Hence, if an approximate method of obtaining the in-situ principal permanent strains could be developed, realistic vertical permanent strains could be obtained. An initial attempt at the development of such a method is outlined below. The method depends on the assumption that the principal resilient and permanent strains are closely related.

A.2 PREDICTION BASED ON DETERMINATION OF IN-SITU PRINCIPAL PERMANENT STRAINS

Intuitively it seems likely that at a particular location in a pavement the principal permanent strains will be proportional to the

principal resilient strains, since it is assumed that they occur in the same directions. The following equations would result:

$$\begin{aligned} \varepsilon_{p_1} &= k\,\varepsilon_{r_1} \\ \varepsilon_{p_2} &= k\,\varepsilon_{r_2} \\ \varepsilon_{p_3} &= k\,\varepsilon_{r_3} \end{aligned} \qquad \text{(A.1)}$$

and hence,

$$\varepsilon_{p_1} + \varepsilon_{p_2} + \varepsilon_{p_3} = k(\varepsilon_{r_1} + \varepsilon_{r_2} + \varepsilon_{r_3}) \qquad \text{(A.2)}$$

where, ε_{r_1}, ε_{r_2} and ε_{r_3} are the principal resilient strains, and, ε_{p_1}, ε_{p_2} and ε_{p_3} are the principal permanent strains. Equation (A.2) relates the resilient volumetric strain (v_r) and the permanent volumetric strain (v_p), viz:

$$v_p = k\,v_r \qquad \text{(A.3)}$$

and, since v_p can be obtained directly from a model of the results of the triaxial characterisation tests and the corresponding value of v_r can be obtained from an elastic analysis, the constant k may be readily determined. Consequently, the values of principal permanent strains can be predicted from the predicted resilient strains, and application of Mohr's circle would result in a value for the vertical permanent strain.

The accuracy of the predicted principal permanent strains can be checked in each case by comparing the value of permanent shear strain calculated from these three strains, from:

$$\varepsilon_p = \frac{\sqrt{2}}{3}\sqrt{[(\varepsilon_{p_1} - \varepsilon_{p_2})^2 + (\varepsilon_{p_2} - \varepsilon_{p_3})^2 + (\varepsilon_{p_3} - \varepsilon_{p_1})^2]} \qquad \text{(A.4)}$$

with that obtained from a model of the results from the characterisation tests.

The validity of the approach outlined above was checked in a preliminary way by considering the prediction of permanent strains in the DBM layer of pavement 1. The following steps summarise the approach:

1) Carry out an elastic analysis to give predicted values of the in-situ resilient principal strains, the resilient volumetric strain, and the two stress invariants p and q.
2) Determine the permanent volumetric and shear strains (v_p and ε_p) from models developed from the results of the characterisation tests. The models are described below.
3) Determine the constant k, and hence calculate values for the in-situ principal permanent strains.
4) Check the values of shear strain obtained from the model (step (2)) with those calculated from the principal permanent strains, and if reasonable agreement is obtained proceed with the calculation of vertical permanent strains.

The results of these preliminary calculations are presented below, following a description of the permanent strain models.

Models for the permanent volumetric and shear strain behaviour

The permanent volumetric and shear strains for pavement 1 were calculated from the results presented in Chapter 9. Figures A.1 to A.5 show the semi-logarithmic plots of permanent strain versus time for all the stress conditions except p = 650, q = 150 kN/m^2, where both v_p and ε_p were very small. The results for volumetric strain indicate that at low values of p the strain was tensile but became compressive as p increased, and at a particular value of p, high values of q produced the higher strain; the value of p seems to be the dominant effect. The shear strain was always positive, because of the form of the equation used to calculate this parameter, which for

triaxial test conditions is:

$$\varepsilon_p = \frac{2}{3}(\varepsilon_{p_1} - \varepsilon_{p_3}) \qquad (A.5)$$

The results show that as p increased ε_p decreased and as q increased ε_p increases; each effect appearing to be similar.

It was found that by plotting the volumetric strain after a specific length of time, for all stress conditions, against $(p_m)^2/q_r$, a unique relationship was obtained. Such a plot is shown in Figure A.6 for the volumetric strain after 10^3 seconds. The parameter p_m is the mean value of p, shown in Figure 9.3, and is a realistic representation of the level of p occurring in the triaxial test, where constant confining pressure was used, and is half the value of p (p_r) used to specify stress conditions throughout the text. The parameter q_r is the dynamic deviator stress and is the same in all cases as the value of q used to specify stress conditions. It was found that a line approximating to the best fit line through the experimental points had the following equation:

$$v_p(\%) = -2 + \log_{10}(p_m^2/q_r) \qquad (A.6)$$

It should be noted that only one of the points shown on Figure A.6 is from the tensile test results. The permanent volumetric strain from these tests was always tensile and approached high values very quickly. Also, $(p_m)^2/q_r$ will be positive and small, resulting in the curve being asymptotic to the volumetric strain axis. Therefore, equation (A.6) only approximates the expected behaviour of the material.

Extension of the results from Figures A.1 to A.5 to produce plots such as Figure A.6 for elapsed times of 10^2, 10^4 and 10^5 seconds resulted in a family of curves which could be approximated by the following equation:

$$v_p(\%) = (-2 + \log_{10}(p_m^2/q_r)) \cdot (\log_{10} t)/3 \qquad (A.7)$$

where, t is the total elapsed time in seconds. These curves are shown in Figure A.7. Hence, a predicted value of the permanent volumetric strain, for most stress conditions and elapsed times up to 10^5 seconds, may be obtained.

The plots of shear strain versus (p_m/q_r) for a specific elapsed time, did not result in such well defined relationships as were obtained with the volumetric strain plots, as may be seen from Figure A.8 which shows the results after 10^3 seconds. However, as with the volumetric strain results, it was found that the family of curves for the range of elapsed time from 10^2 to 10^5 seconds, could be approximated by the following equation:

$$\varepsilon_p(\%) = (1/(p_m/q_r + (p_m/q_r)^2)).\ (\log_{10} t) - 1)/2 \qquad (A.8)$$

Hence, predicted values of permanent shear strain may also be obtained. For the cases where p_m is tensile (negative), the value of (p_m/q_r) can be assumed to be positive without incurring large errors, since these tensile values of p_m are generally very small.

Prediction of permanent strains in the DBM for pavement 1

Calculations to predict the principal permanent strains, after an elapsed time of 10^4 seconds, were carried out in the manner described at the beginning of this section for the first six elements of rows 1 and 6 shown in Figure 8.5, which shows the DEFPAV finite element network for pavement 1. The calculations are presented in Table A.1, overleaf.

It may be seen from the Table that the two predictions of permanent shear strain ε_p and ε_p', differ considerably for the six elements in row 1, which are at the surface of the pavement. This is probably because the constant of proportionality relating each of the three pairs of principal resilient and permanent strains will be different, viz,

TABLE A.1 CALCULATION OF PERMANENT STRAINS AFTER 10^4 SECONDS

Row No.	Element No.	p_r kN/m^2	q_r kN/m^2	p_m^2/q_r kN/m^2	p_m/q_r	ε_{r_1} %	ε_{r_2} %	ε_{r_3} %	v_r %	v_p %	k	ε_{p_1} %	ε_{p_2} %	ε_{p_3} %	ε_p %	ε_p' %
1	1	979	630	380	.78	.0299	.0282	-.0233	.0348	.7800	22.4	.6700	.6300	-.5200	1.0600	.7900
	2	915	550	381	.83	.0283	.0273	-.0209	.0347	.7800	22.5	.6370	.6150	-.4700	.9800	.7300
	3	822	528	320	.78	.0305	.0261	-.0226	.0340	.6800	20.0	.6100	.5200	-.4500	1.0600	.6400
	4	722	586	222	.62	.0379	.0253	-.0301	.0331	.4600	13.9	.5270	.3500	-.4200	1.5100	.5800
	5	553	677	113	.41	.0514	.0253	-.0461	.0306	.600	2.0	.1030	.0506	-.8122	2.6000	.1160
	6	385	555	67	.35	.0501	.0259	-.0493	.0267	-.2400	-9.0	-.4500	-.2330	.4440	3.1400	.5740
6	1	-111	235	13.11	-.24	.1313	-.0880	-.0880	-.0447	-1.1700	26.2	3.4400	-2.3000	-2.3000	3.4000	3.8150
	2	-106	232	12.11	-.23	.1219	-.0773	-.0842	-.0396	-1.2000	30.3	3.7000	-2.3400	-2.5500	3.6000	4.0900
	3	-101	226	11.3	-.22	.1102	-.0662	-.0792	-.0352	-1.2300	34.9	3.8500	-2.3100	-2.7600	3.8000	4.2500
	4	98	218	11.0	.22	.1008	-.0577	-.0754	-.0323	-1.2500	38.7	3.9000	-2.2300	-2.9200	3.8000	4.3200
	5	95	212	10.6	.22	.0937	-.0507	-.0728	-.0298	-1.2800	43.0	4.0300	-2.1800	-3.1300	3.8000	4.4800
	6	92	204	10.4	.22	.0859	-.0442	-.0697	-.0280	-1.3000	46.4	3.9900	-2.0500	-3.2300	3.8000	4.4600

p_r and q_r are the dynamic levels of p and q predicted by DEFPAV.

p_m is the mean level of $p = p_r/2$

ε_{r_1}, ε_{r_2}, ε_{r_3} are the principal resilient strains.

v_r is the resilient volumetric strain.

v_p is the permanent volumetric strain, predicted from equation (A.6)

k $= v_p/v_r$

ε_{p_1}, ε_{p_2}, ε_{p_3} are the principal permanent strains, predicted from equations (A.1)

ε_p is the predicted permanent shear strain, from equation (A.8)

ε_p' is the predicted permanent shear strain from equation (A.4)

rewriting equations (A.1):

$$\varepsilon_{p_1} = k_1 \varepsilon_{r_1}$$

$$\varepsilon_{p_2} = k_2 \varepsilon_{r_2} \qquad \text{(A.9)}$$

$$\varepsilon_{p_3} = k_3 \varepsilon_{r_3}$$

It appears that the assumption, that the constant is the same for all three cases, may not result in large errors in ε_p when the values of v_r and v_p are of the same sign and v_p is large, since the discrepancies between ε_p and ε_p' for row 6 are all less than 20 per cent. However, when v_p is small or when v_r and v_p are of opposite signs the discrepancies are very large (greater than 90 per cent of ε_p for element 5, row 1), which is understandable since the method of calculation results in ε_{p_1}, ε_{p_2} and ε_{p_3} being of opposite sign to the corresponding resilient strains, which seems intuitively incorrect.

It may be possible to employ an iterative correction technique to the calculation procedure such that the three constants k_1, k_2 and k_3 would be evolved and the values ε_p and ε_p' approached agreement. However, this would be computationally difficult and time has not permitted investigation of such an approach.

The calculation of the vertical permanent strains using Mohr's circle are straightforward, and the method is not presented here. Table A.2 presents the results of the calculations, excluding those for elements 4, 5 and 6 of row 1 where the predicted principal permanent strain were considered grossly inaccurate. It may be seen that the calculated values of ε_{vp} at the top of the DBM layer are tensile, disagreeing with the measurements which approached a high compressive value at this location. At the bottom of the layer, the predicted values are approximately half of those measured after 10^5 passes

TABLE A.2 RESULTS OF VERTICAL PERMANENT STRAIN CALCULATIONS

Row	Element	Predicted ε_{vp} %
1	1	-.48
	2	-.40
	3	-.29
6	1	3.43
	2	3.68
	3	3.79
	4	3.81
	5	3.90
	6	3.77

(corresponding approximately to a total loading time of 10^4 seconds at the centre of the distribution). Also, the value of ε_{vp} is virtually the same in each element, indicating that the model to predict volumetric strain overpredicts at low stress levels, although it does describe the behaviour of the test specimens adequately.

CONCLUDING REMARKS

The method has potential provided an iterative procedure can be developed to give three values of principal permanent strain such that calculated values of shear strain agree with predicted ones from the models of specimen behaviour in the characterisation tests.

Clearly, the modelling of the permanent strain behaviour should be examined more closely. Possibly the most accurate solution would be to model the radial strain behaviour of the specimens and then combine predictions of this and the vertical strain to give volumetric and shear strains. This would not be as convenient as the use of a unique equation,

but accurate modelling is of prime importance.

It is interesting to note that although a detailed and accurate study of the volumetric strains has not been possible, for the whole network of pavement 1, it seems probable from the predicted stress levels (DEFPAV) that for most locations this would be tensile in the DBM, and compressive in the Keuper marl. This suggests that an over-:all increase in volume of the DBM may have been expected, but this was not detected by the in-situ measurements. The surface measure-:ments of the rut profile showed a significant decrease in volume of the whole pavement, but neither the strain coil measurements or slab thickness measurements were comprehensive enough to indicate whether certain parts of the DBM had undergone tensile volumetric strain. Similarly the in-situ instrumentation was not sufficient to ascertain the pattern of volumetric strain in the subgrade.

At the present time, the best assumption for obtaining predicted vertical permanent strains appears to be the simple one, adopted herein, that it is equivalent to the major permanent strain measured in the triaxial test.

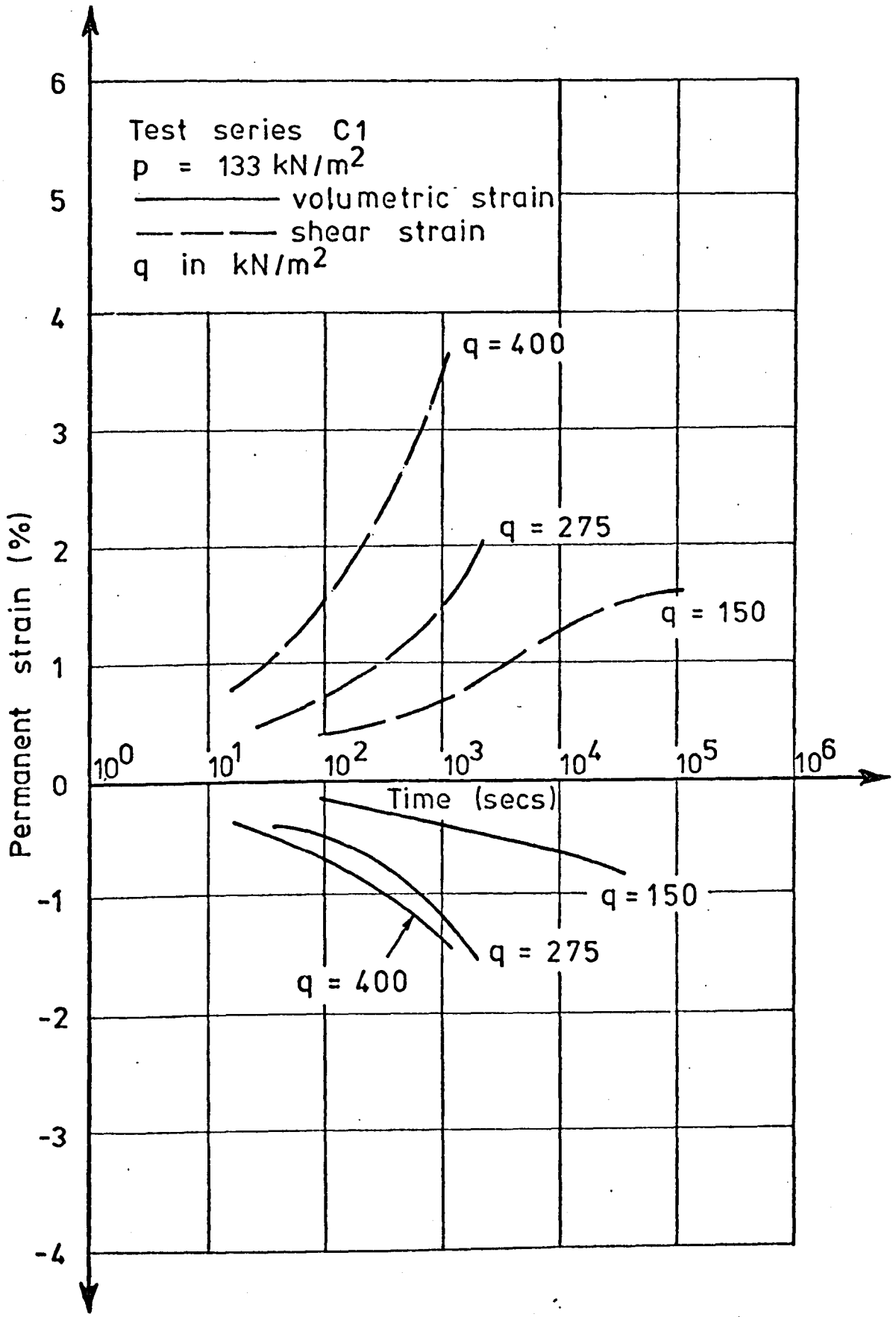

FIG. A1 THE EFFECT OF q ON THE PERMANENT STRAIN RESPONSE OF DBM,

p = 133 kN/m²

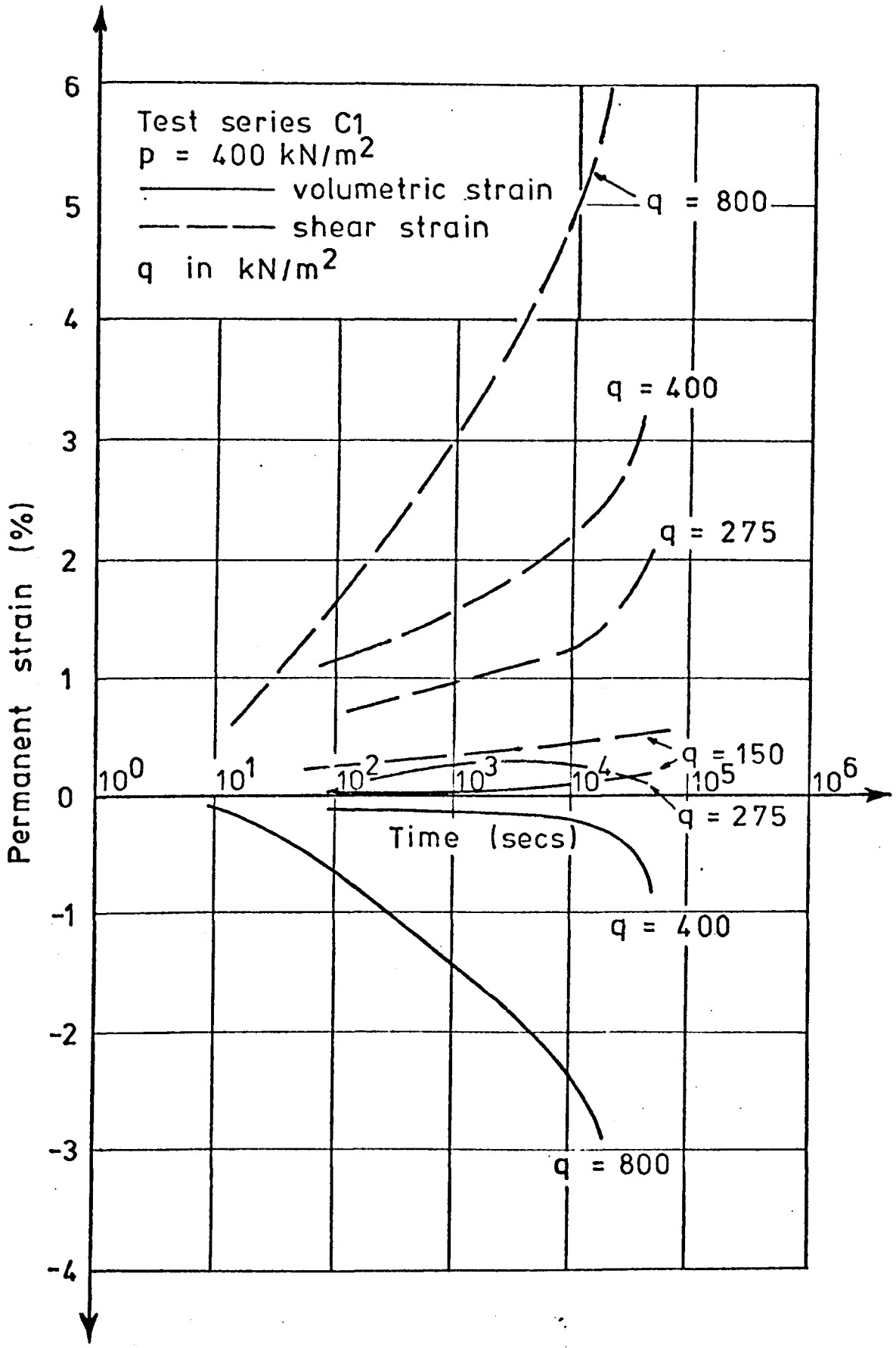

FIG. A2 THE EFFECT OF q ON THE PERMANENT STRAIN RESPONSE OF DBM,

p = 400 kN/m^2

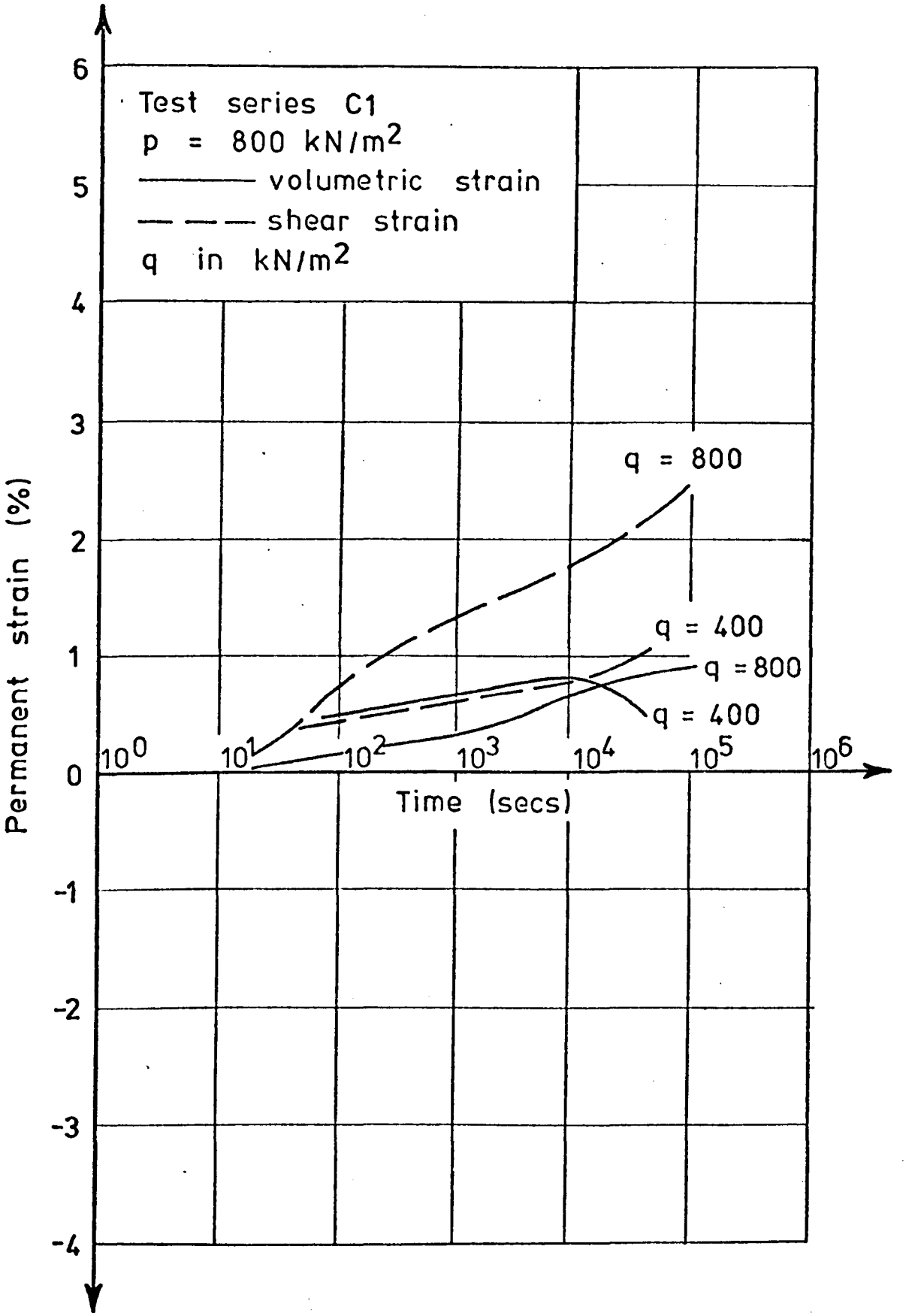

FIG. A3 THE EFFECT OF q ON THE PERMANENT STRAIN RESPONSE OF DBM,

p = 800 kN/m^2

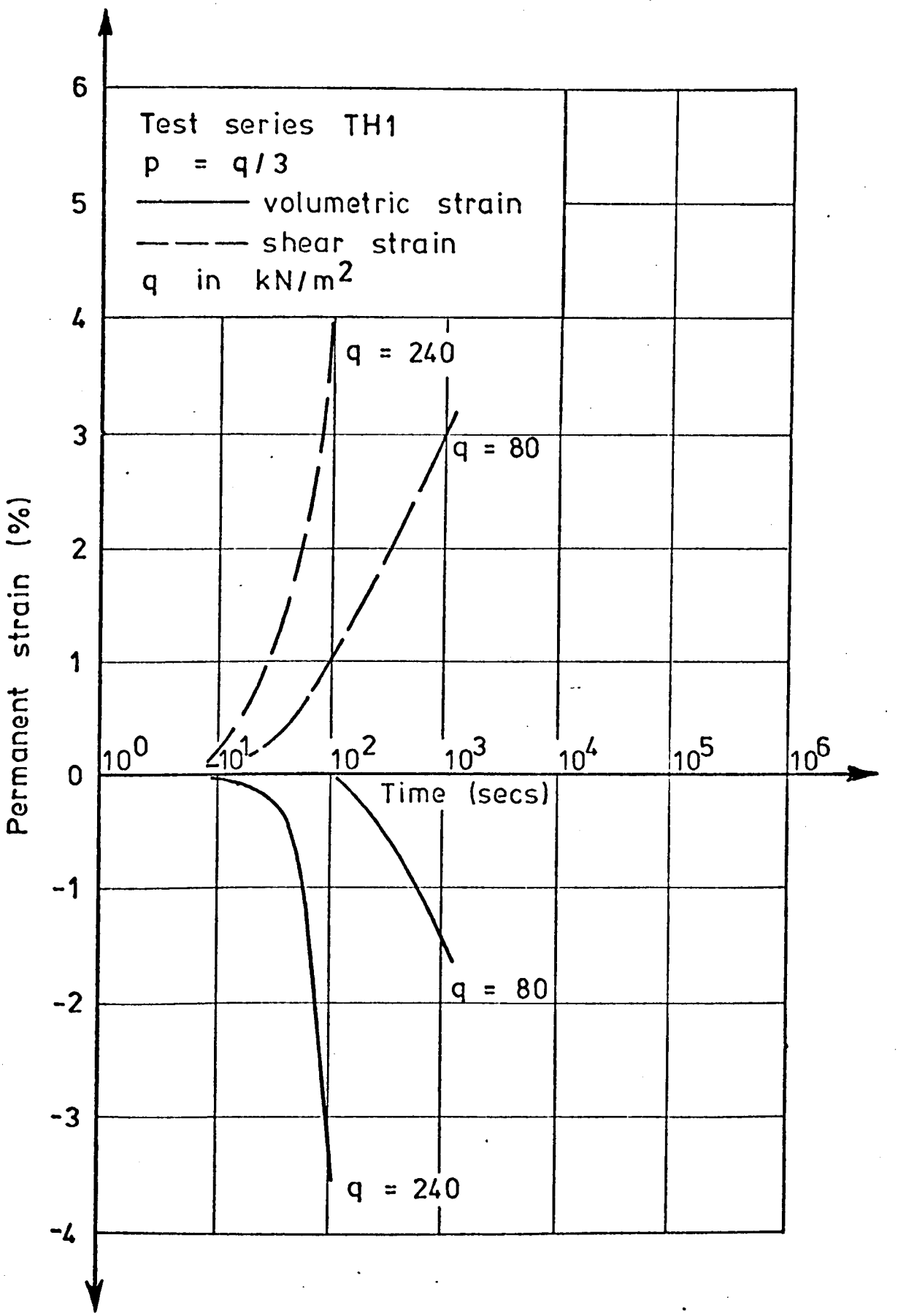

FIG. A4 THE EFFECT OF q ON THE PERMANENT STRAIN RESPONSE OF DBM,

p = q/3

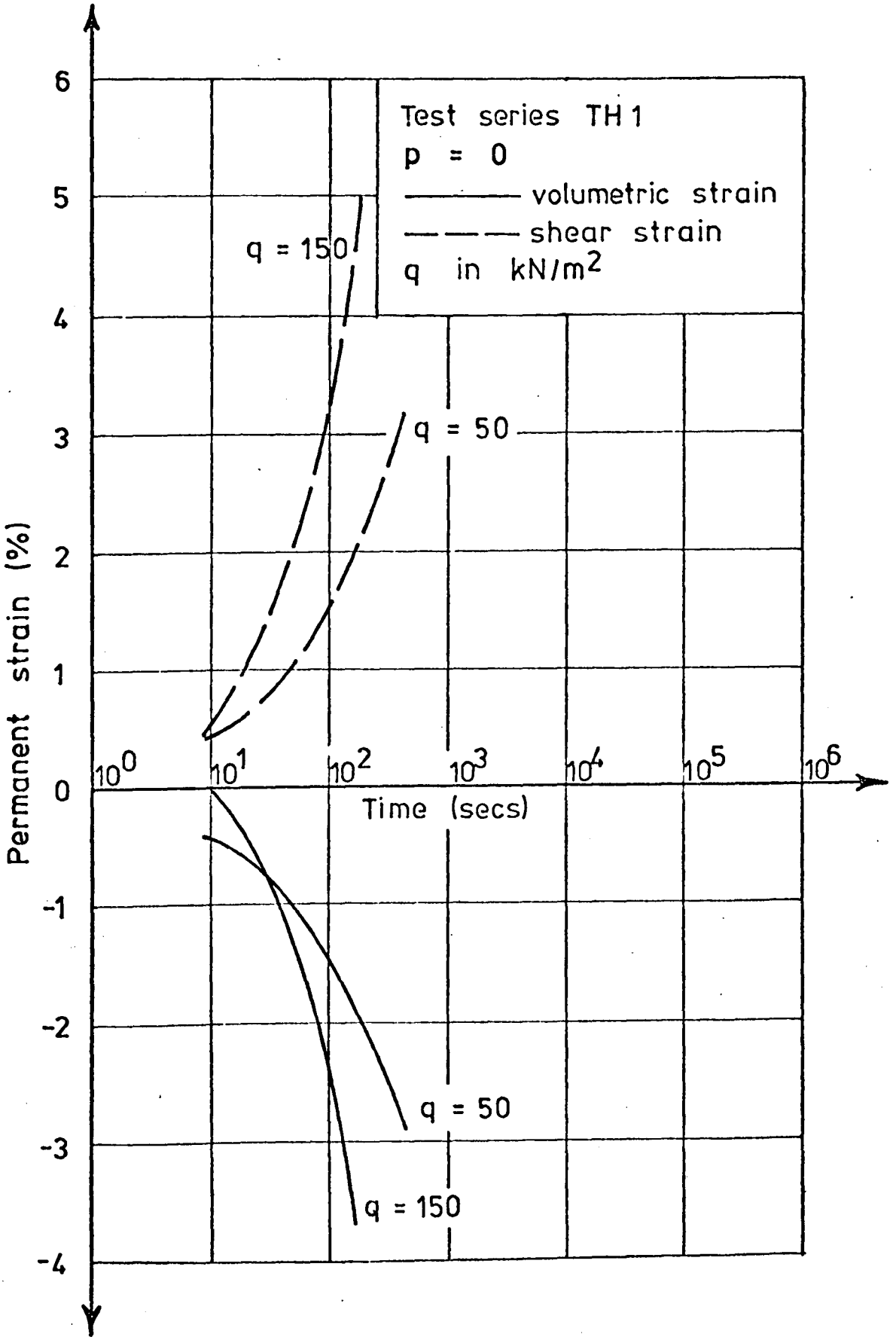

FIG. A5 THE EFFECT OF q ON THE PERMANENT STRAIN RESPONSE OF DBM,

p = 0

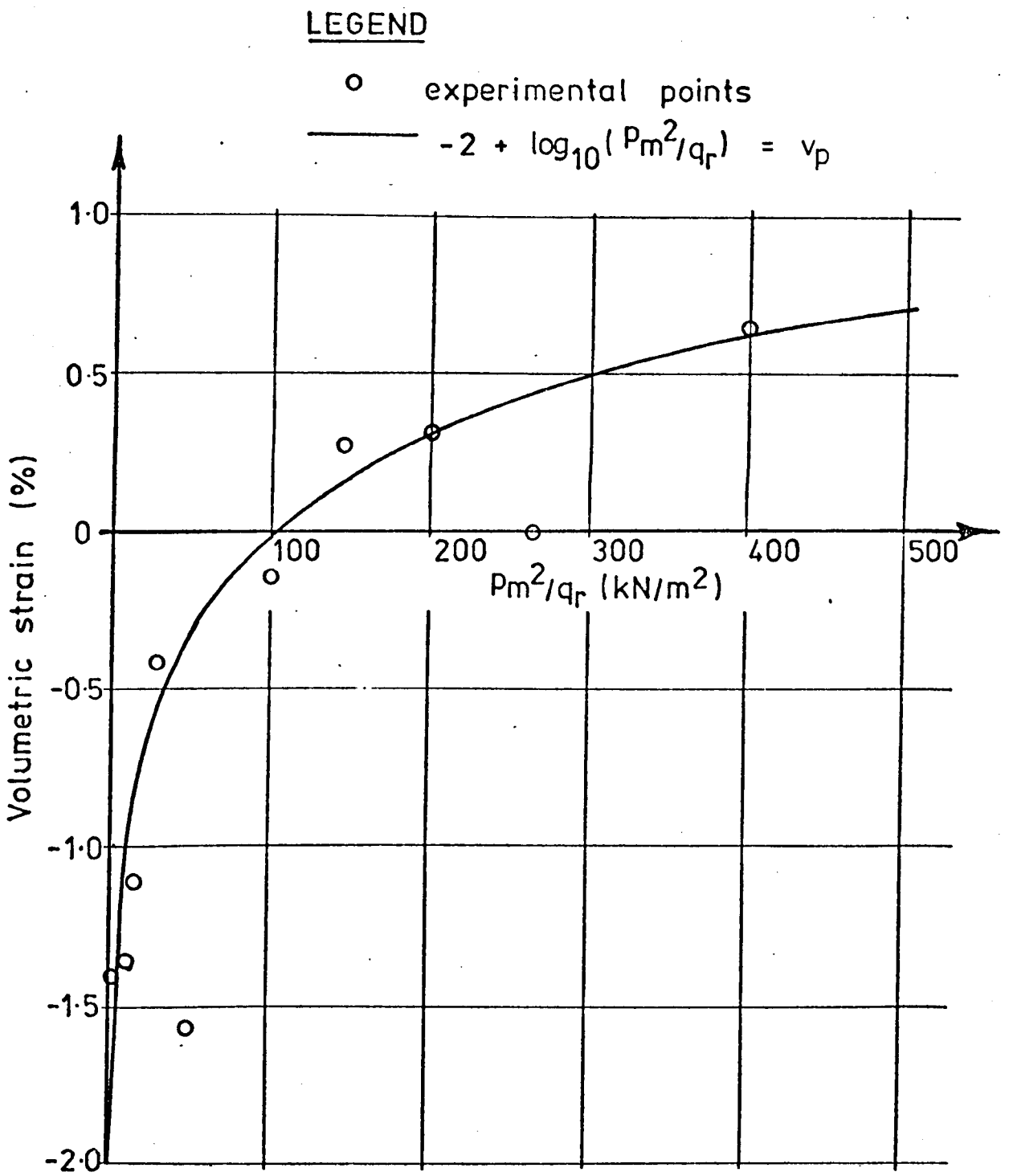

FIG. A6 VOLUMETRIC STRAIN VERSUS p_m^2/q_r AFTER 10^3 SECONDS

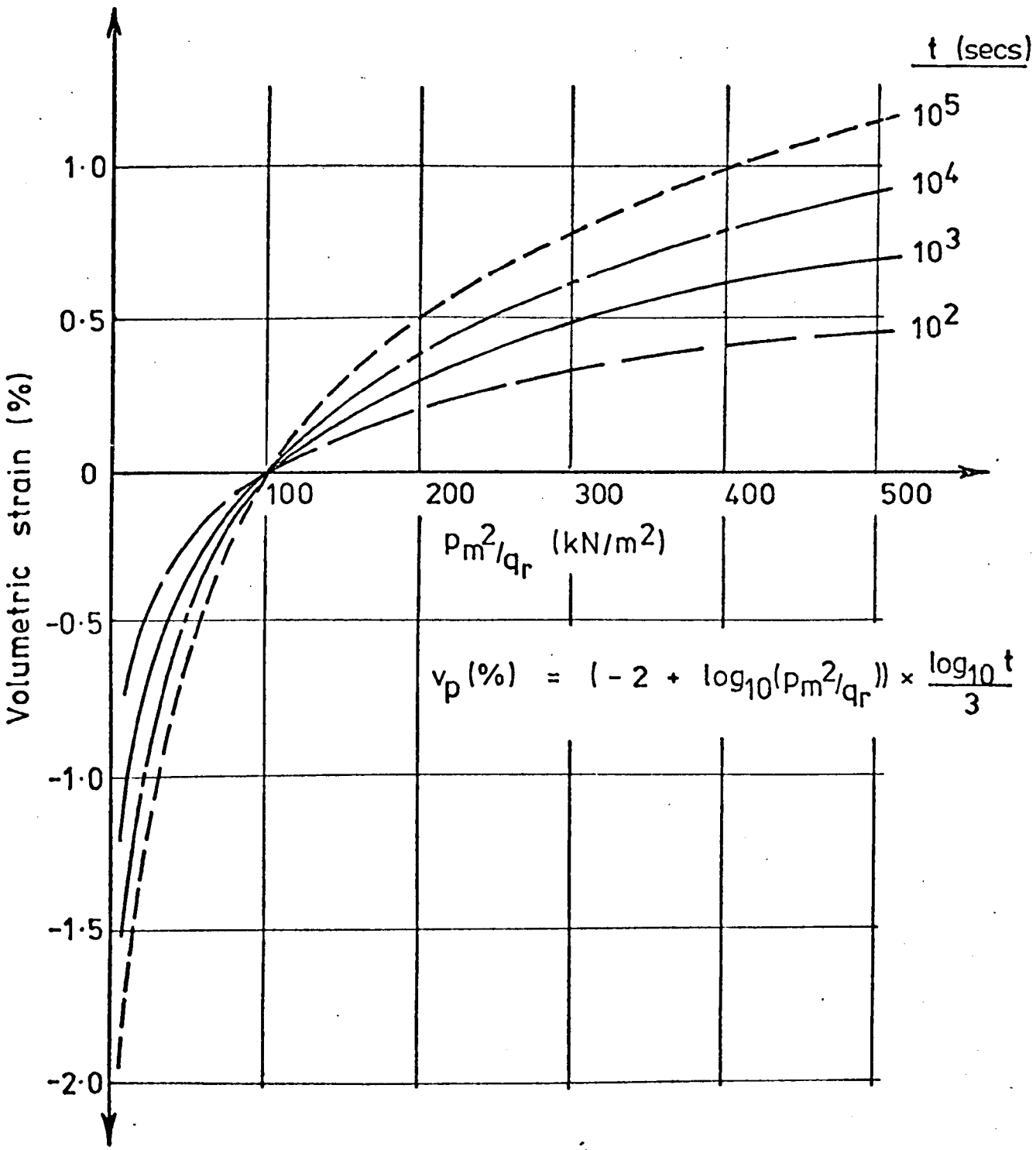

FIG. A7 IDEALISED VOLUMETRIC STRAIN BEHAVIOUR

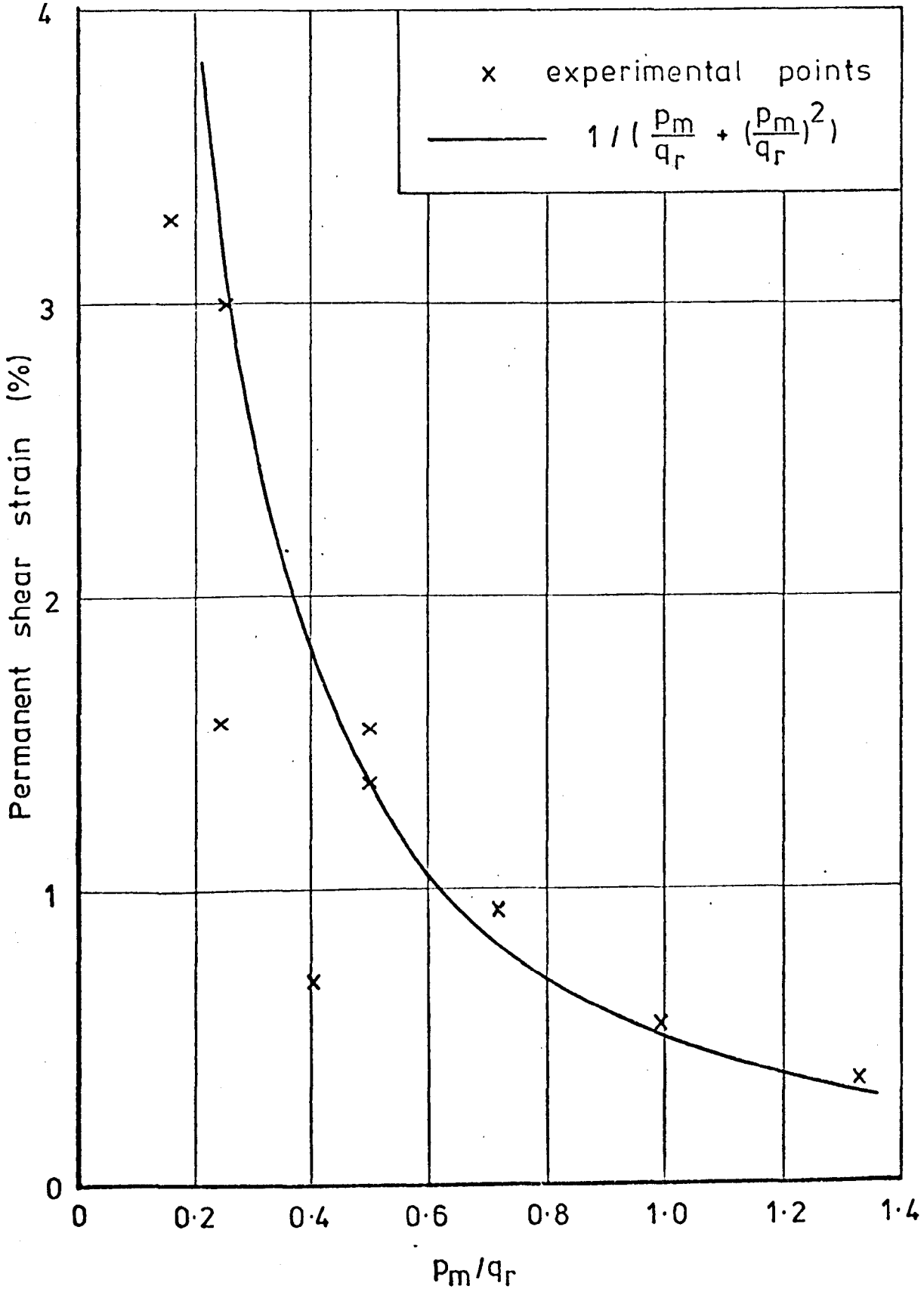

FIG. A8 PERMANENT SHEAR STRAIN VERSUS p_m/q_r AFTER 10^3 SECONDS